MSc Thesis

Development of a method for the determination of preload in High Strength Friction Grip Connections of existing structures

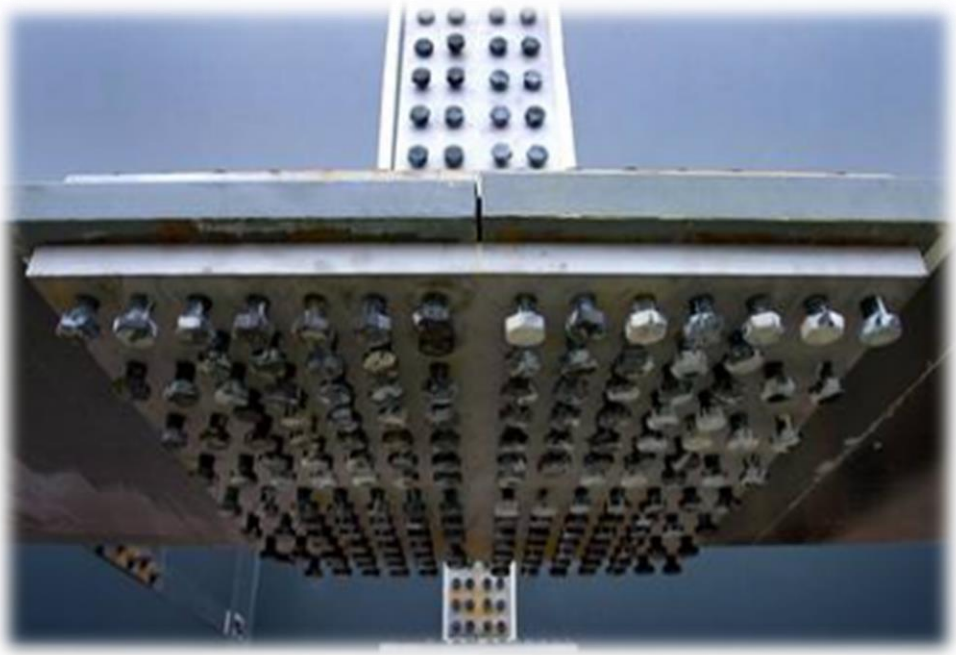

Konstantinos Chondrogiannis

2017

MSc Civil Engineering

TU Delft
Technische Universiteit Delft

Master Thesis 2017

"Development of a method for the determination of preload in High Strength Friction Grip Connections"

Konstantinos Chondrogiannis

Committee

Prof. M. Veljkovic

Ir. P.A. de Vries

Dr. Ir. Y. Yang

Delft University of Technology

Civil Engineering faculty

Department of Structural Engineering

Section of Steel and Composite Structures

Abstract

The aim of this thesis is to investigate the feasibility of determining the preload in bolts in High Strength Friction Grip Conections and performing in situ measurements. The magnitude of the preload is important for the behavior of High Strength Friction Grip Connections, as it defines the fatigue life of the connection and limits the displacement of the joint. For this reason, it is important knowing the preload at any point during the service life of the connection. This thesis first analyses the causes that may lead to an insufficient initial preload and the factors which may result in a preload loss over time. Then, the state of the art in the determination of preload in High Strength Friction Grip Connections is reviewed and the strain gauge method is tested to define the potential of this method on performing in situ measurements, for two reasons: 1) so far, the in situ tests with this method were not possible, because of a complicated installation procedure. For the tests presented in this thesis, a new type of strain gauges (BTMC strain gauges) is used, which simplifies the installation procedure and 2) the strain gauge method is less affected by factors which govern the in situ measurements. This is done by imitating the in situ conditions in the lab and determining the uncertainty interval of this method. Then, this method is tested on a connection of an existing structure. The results show that it is possible to do in situ measurements with the strain gauge method. It is also shown that the best way to determine the force with a maximum accuracy is by conducting time consuming calibration tests. Therefore, in the last part of this thesis four approaches are suggested, which aim to reduce the number of calibration tests, without loosing much of the accuracy in the estimation of the force.

Aknowledgments

I would like to thank Ir. P. A. de Vries for his continuous support throughout all the stages of this project. His advice has been vital for progressing efficiently through all the steps of my thesis. His recommendations on the theoretical and experimental part helped me produce a detailed connection between theory and experimental results. Also his assistance on procedural matters was indispensable for completing this thesis.

Moreover, I would like to thank Prof. Milan Veljkovic for giving me the opportunity to work on this topic. I am grateful for every advice and guidance in each one of our meetings. Thank you for your interest on my research and the engineering way of thinking that you tried to communicate with me.

Furthermore, I feel thankful for the assistance of Dr. Ir. Y. Yang during this period, his comments and suggestions, his advice on our meetings.

I would also like to thank the staff of Stevinlab, at Delft University of Technology, for the assistance with the experimental setup.

Finally, I would like to thank my friends and especially Stavros, Natalia and Giorgos for their assistance and my family for their encouragement, patience and mental support.

Konstantinos Chondrogiannis

Dedicated to my father and my uncle Stamatis

Contents

List of Figures in Main Part

List of Tables in Main Part

Abbreviations

Latin capital letters

$F_{s,Rd}$	slip resistance	[kN]
$F_{p,C}$	minimum required preload	[kN]
A_s	tensile threaded area of the bolt	[mm^2]
T	torque	[Nm]
P	pitch of the threads	[mm]
D_0	outer diameter of the nut	[mm]
E	Young's modulus	[GPa]
V	coefficient of variation	[-]
$V_{in/out}$	input/output voltage	[V]
L_{eff}	effective length	[mm]
GF	gage factor	[-]
R	resistance	[Ω]
CF	calibration factor	[kN/microstrain]
A_{cor}	corrected net cross section area	[mm^2]
A_{net}	net cross section area	[mm^2]
Y	electrical admittance	[1/Ω]
C	acoustoelastic constant	[-]

Latin small letters

k_s	factor considering shape and size of the hole	[-]
f_{ub}	ultimate tensile strength	[N/mm^2]
r_t	effective contact radius of the threads	[mm]
r_n	effective radius of contact between nut and plate	[mm]
d_h	the diameter of the bolt hole	[mm]
d	shank diameter	[mm]
l_c	clamping length	[mm]
v	ultrasound velocity	[m/sec]
v_0	ultrasound velocity (zero stress)	[m/sec]

f_n	resonance frequency	[kHz]
d_{nom}	nominal diameter	[mm]
d_{min}	minimum nominal diameter	[mm]
d_{max}	maximum nominal diameter	[mm]

Greek small letters

μ	slip factor	[-]
γ_M	partial safety factor	[-]
μ_t	coefficient of friction between nut and bolt threads	[-]
β	half angle of the threads	[degrees]
μ_n	coefficient of friction between nut and plate	[-]
ε	strain	[-]
σ	stress	[N/mm^2]
ΔL	elongation	[mm]

INTRODUCTION

Preloaded bolts are used in connections, if the joint is subjected to load reversals, vibrations or the displacements should be limited. The behavior of such connections depends on the magnitude of the preload. A preload lower than the minimum required preload will lead to excesive deformations or fatigue failure of the connection. Considering also that the spread in the initially applied preload, which results from most of the tightening methods, may lead to overtightening of the bolts or not achieving the required prelod and that the preload of the bolts decreases with time, it is necessary knowing the residual preload of the bolts at any point during the service life of a connection.

The purpose of this thesis is to investigate the feasibility of performing in situ measurements for the determination of the preload in HSFG connections, using a new type of strain gauges. This is done by initially imitating in situ conditions in the lab (preliminary tests) and then testing the strain gauges on a connection of an existing structure.

Before discussing the in situ measurements, the importance of preloaded bolts in High Strength Friction Grip Connections is explained in chapter one. The second chapter is reffered to the reasons that lead to a spread in the initial preload and the factors which cause preload loss are mentioned. In chapter three, the state of the art is discussed and in chapter four the results of the preliminary tests are presented. Chapters five, six are about the in situ measurements. The conclusion of the research is mentioned in chapter seven.

1. HIGH STRENGTH FRICTION GRIP CONNECTIONS

According to EN 1993-1-8 article 2.6, when a joint loaded in shear is subjected to impact or significant vibration or reversal of shear load and deformations should be limited, preloaded bolts should be used. For this reason, firstly the behavior of a joint loaded in shear will be described in order to see why preloaded bolts are beneficial for this type of joint.

When a joint is loaded in shear, the forces are transferred by bearing of the plates against the shank of the bolt and consequently they are transferred by shear in the shank of the bolt, as shown in Fig. 1.1.

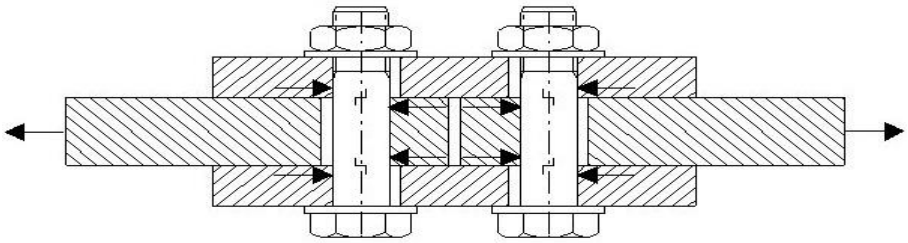

Figure 1.1: Joint loaded in shear, non preloaded bolts [17]

There are some consequences resulting from this action. The load is introduced by the shank of the bolt in a very concentrated way leading to a high stress concentration at the hole of the plate, which can cause a fatigue crack at that location. Furthermore, if the joint is subjected to a variable shear which changes sign, large displacements will occur repeatedly due to the clearance between the hole and the shank of the bolt and the variable shear may also cause failure in the shank of the bolt at the shear plane.

By preloading the bolts by using High Strength Friction Grip Bolts, a clamping pressure occurs between the connected plates which enables load to be transferred by frictional resistance, as shown in Fig. 1.2.

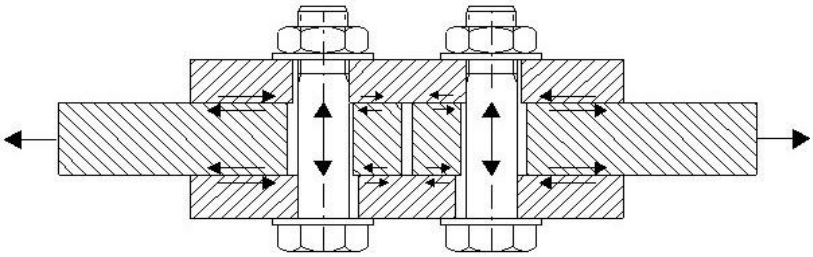

Figure 1.2: High Strength Friction Grip Connection [17]

This results in a much less concentrated load transfer at the hole, because the load transfer by friction takes place over the whole area, where compressive stresses are present due to the bolt preloading. Therefore, at the hole the load has already been transferred, which results in a much lower stress concentration at that location compared to the case in which non preloaded bolts are used, as shown in Fig. 1.3.

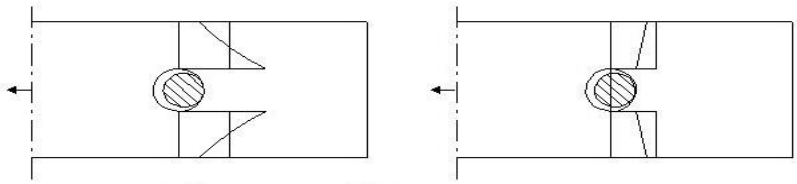

Figure 1.3: Stress concentration at the hole for non preloaded bolts (at the left) and preloaded bolts at the right

Then, fatigue cracking in the shank of bolt is avoided and due to the low stress concentration at the hole, fatigue cracking occurs in the gross section of the plates where the contact pressure is not high enough to prevent slip between the plates, resulting in crack initiation by fretting, as shown in Fig. 1.4.

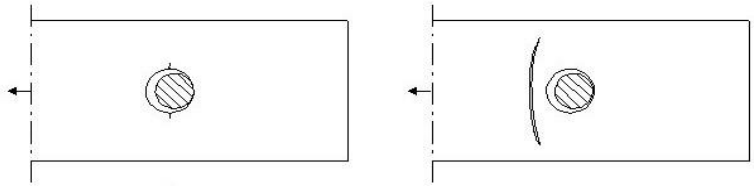

Figure 1.4: Possible crack location for non preloaded bolts (at the left) and preloaded bolts (at the right)

This is also shown by EN 1993-1-9 prescriptions regarding preloaded and non preloaded bolts. For conventional bolts, the bolt is governing the fatigue life and has fatigue category 100. In case of preloaded bolts, the bolts will not fail under fatigue loading provided that an adequate preload has been applied. Furthermore, for non preloaded bolts the fatigue strength of the plates should be calculated for the net cross section and the detail category 112. For preloaded bolts, the plates fall into the same category, however since failure does not occur in the net cross section, the gross cross section of the plate is used to calculate fatigue stress.

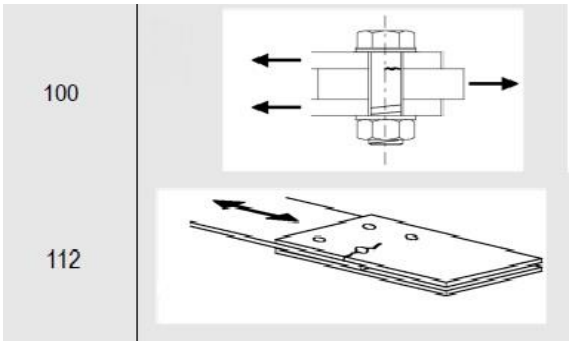

Figure 1.5: Fatigue classification according to EN 1993-1-9. Top: conventional bolts, bottom: preloaded bolts

Additionally, connections with preloaded bolts can be used when the joint is subjected to a variable load which changes sign, because the friction between the plates limits the displacement in the joint.

Based on this, two categories of preloaded bolts are distinguished: a) Category B and b) Category C. The difference between the two categories is that for Category B connections, slip will not occur under service loads and for Category C connections, slip is not acceptable under any circumstances. However, in actual practice the connections slip only marginally and fail when the slip is equal to 0.15 mm. Failure by slip means that the displacement is so large that the connection becomes more of a bearing type. For this reason, the applied preload level is of high importance for the slip resistance of the connection, as shown by eq. 1.1.

$$F_{s,Rd} = \frac{k_s \cdot n \cdot \mu}{\gamma_M} \cdot F_{p,C} \quad (1.1)$$

where, $F_{s,Rd}$ is the slip resistance, k_s is a factor considering shape and size of the hole, n is the number of friction surfaces, μ is the slip factor, γ_M is the partial safety factor and $F_{p,C} = 0.7 \cdot f_{ub} \cdot A_s$ is the design preload for preloaded bolts with f_{ub} the ultimate tensile strength of the bolt and A_s the tensile threaded area of the bolt. Therefore, a higher applied preload increases the slip resistance of the connection, reducing the displacement, as shown in Fig. 1.6.

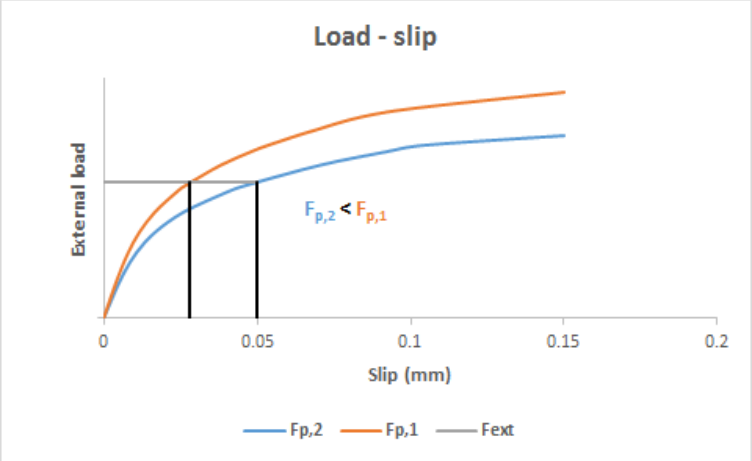

Figure 1.6: External load – slip curve for different preload levels

Consequently, applying sufficient preload is of high importance for High Strength Friction Grip Connections.

Based on the abovementioned, it is important to know the preload at three different times:

- Initial preload: the tension created in a bolt when it is first tightened.
- Residual preload: the tension remaining in a bolt at the end of the assembly process, after all bolts have been tightened.
- The tension in a bolt in service.

The most important is the tension in the bolts while they are in service. However, the initial preload is the preload which is most directly controlled and it usually determines the residual and in-service conditions. Correct initial preload is therefore essential.

2. INITIAL PRELOAD AND PRELOAD LOSS

Based on EN 1090-2, the bolts should be preloaded to the level:

$$F_{p,C} = 0.7 f_{ub} A_s \tag{2.1}$$

One of the major problems with the use of bolted joints is the precision, with regard to achieving an accurate preload, of the bolt tightening method selected. When a bolt is tightened, the nut is rotated with respect to the bolt, stretching the bolt and resulting in preload. There are several ways to control the rotation of the nut. The most common ways are by measuring the torque which is applied, measuring the angle of rotation of the nut or a combination of these. In the following sections the four most common tightening methods are analyzed. Furthermore, in section 2.2 the factors that result in short and long term loss of preload are discussed and their influence on the magnitude of preload loss according to the literature survey is presented.

2.1 Tightening methods

2.1.1 Torque method

Since a bolt is designed to be tightened by twisting the nut with respect to the head, the most convenient way to do this is by applying a torque. This method is called torque control method and experience and theoretical analysis say that there is usually a linear relationship between the torque applied to a fastener and the preload developed in a given fastener:

$$T = C \cdot F_{p,C} \tag{2.2}$$

where, T is the torque, $F_{p,C}$ is the preload force.

A number of equations have been derived that attempt to define the constant C. The following equation has been proposed by Motosh [8]:

$$T = F_{p,C}\left(\frac{P}{2\pi} + \frac{\mu_t r_t}{\cos\beta} + \mu_n r_n\right) \tag{2.3}$$

where, T is the torque applied to the fastener, $F_{p,C}$ is the preload created in the fastener, P is the pitch of the threads, μ_t is the coefficient of friction between nut and bolt threads, r_t is the effective contact radius of the threads, β is the half angle of the threads, μ_n is the coefficient of friction between the face of the nut and the upper surface of the joint and r_n is the effective radius of contact between the nut and joint surface.

Eq. 2.3 shows that the input torque is resisted by three reaction torques. These are as follows: the reaction produced by the inclined plane action of nut threads on bolt threads, which is the only component that ends up as preload in the bolt, the reaction torque created by frictional restraint between nut and bolt threads and the reaction torque created by frictional restraint between the face of the nut and the washer or joint. These force reactions affect the amount of initial preload we get when we tighten a fastener. The most influencing factors are the friction components.

If these components are determined based on a typical bolt's dimensions, for example an M20, assume coefficients of friction μ_t = 0.15, μ_n = 0.15 and a preload force F = 1000 N, it is

concluded that each 1000 N of tension produce 0.40 Nm of bolt stretch reaction torque, 1.84 Nm of reaction torque from thread friction and 1.99 Nm of reaction torque from friction under the nut. The total torque is 4.23 Nm. Therefore, as shown in Fig. 2.1 only a 9% of the input torque results in bolt tension, a 44% is lost due to friction between the threads and a 47% is lost due to friction between the nut and the plate or the washer.

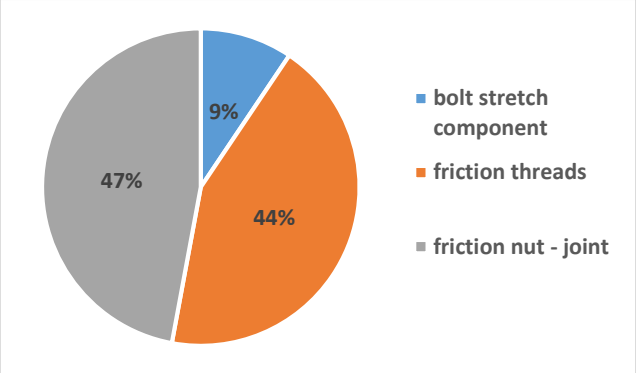

Figure 2.1: Reaction torques which oppose the input torque

If it is assumed that the coefficient of friction between the nut and the joint is 10% greater than what was initially assumed $\mu_n = 0.165$, then the required input torque to overcome nut joint friction increases from 1.99 Nm to 2.19 Nm, 52% of the total input torque. So, in order to produce the same tension of 1000 N, the input torque has to increase by 5%. However, this is not possible because the operator has no way of telling that this set of parts is absorbing more torque between nut and joint. Furthermore, that extra 5% will not come from the thread friction component, unless the coefficient of friction at that point decreases somehow to offset the other increase. Therefore, the only ''source'' of that extra torque is the bolt stretch component. The corresponding resisting torque will decrease from 9% to 4%, which results in loss of tension equal to 55%. Therefore, a variation of 10% in friction coefficient can cause a 55% loss in the resulting preload. Likewise, a 10% increase in friction between threads of bolt and nut will lead to a loss of pretension equal to 53%.

Generally, a variation of 10% in friction coefficient is very common. The coefficient of friction is very difficult to control and impossible to predict. There are almost 40 variables that affect the friction seen in a threaded fastener. These include things as: hardness of all parts, surface finishes, type of materials, speed with which the nut is tightened, fit between threads, presence or absence of washers, the temperature of the lubricants involved etc [1]. But, apart from friction coefficient, there are also some other variables that affect the torque - preload relationship. These factors are geometry, as shown in eq. 2.3, the operator and tool accuracy and strain energy losses. A part of the input work may end up as strain energy losses due to bolt twist, a bent shank or nut deformation. In one extreme case, for example, if the threads gall and seize, the input torque produces just torsional strain and no preload at all. In that case the input energy does not result in heat due to friction losses but strain energy. Therefore, strain energy losses is another factor that affect the torque – preload relationship.

In Fig. 2.2, the influence on the preload force of the most important variables in the torque – preload relationship is presented, based on eq. 2.3. As shown, the biggest influence is caused by variations in friction coefficients, whereas the pitch of the threads has the lowest influence.

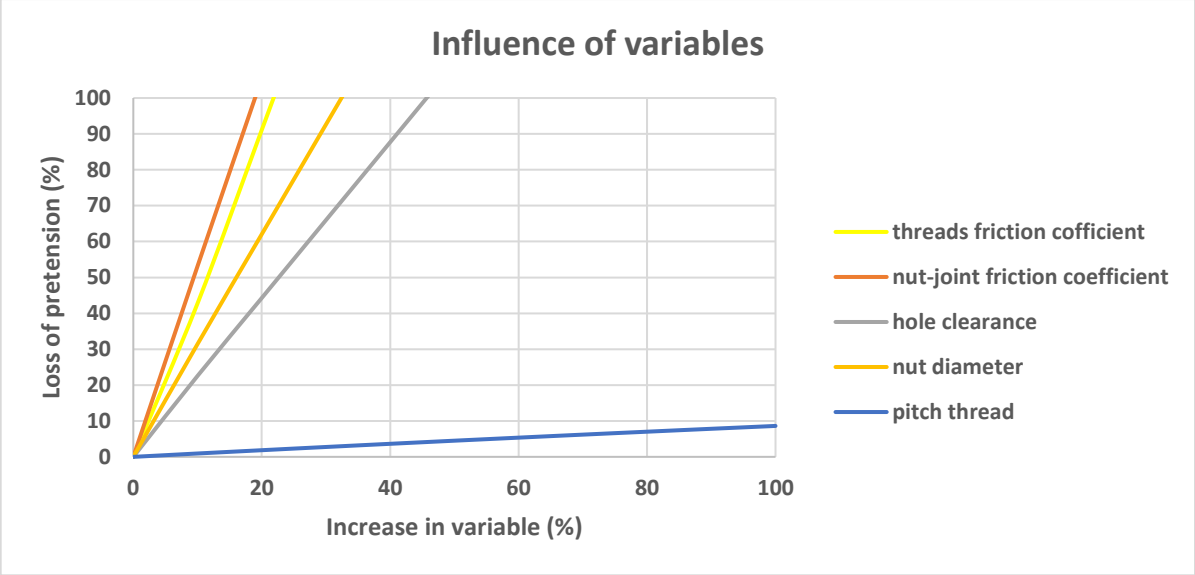

Figure 2.2: Influence of variables on preload

The influence of these variables on the preload force is also shown by looking to the determination of nut factor k. The nut factor k is an experimental constant which summarizes anything and everything that affects the relationship between torque and preload, including friction, torsion, bending, plastic deformation of threads and any other factor. It is measured by experimentally applying a torque and measuring the achieved preload and it is defined as:

$$k = \frac{T}{F_{p,C} \cdot d} \tag{2.4}$$

where, T is the torque applied to the fastener, $F_{p,C}$ is the preload created in the fastener and d is bolt's diameter.

The influence of these variables on the k factor is shown in Fig. 2.3. Bickford determined the value of the nut factor for bolts in their as received state, without thread coating [1]. He did that based on the nut factors determined for a large number of such bolts with different dimensions and from different joints . The results are shown in Fig. 2.3.

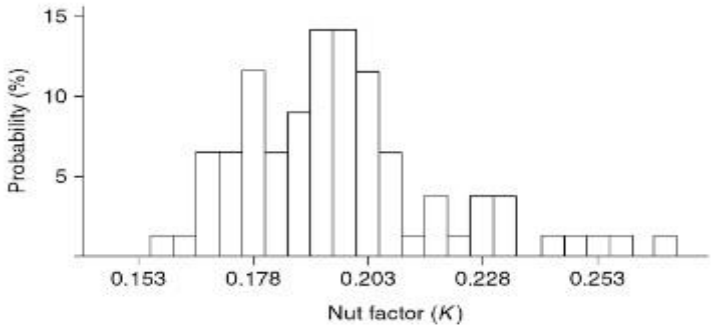

Figure 2.3: Histogram of k values reported for as – received bolts from a large number of sources [1]

Based on Fig. 2.3, the scatter in the k factor is 25%. This scatter is caused by things like different friction conditions between the nuts and the joint surfaces, different hole clearances, operator's errors, tool accuracy etc.

Therefore, all these factors can cause a high scatter in the resulting preload. This means that in order to ensure that the minimum required preload will be achieved, a sufficiently high target preload should be chosen, considering the variation in k factor. According to the report "Evaluation Tightening Preloaded Bolt Assemblies according to EN 1090-2" any target preload for a variation in the k factor 10%, results in a very high spread in the preload, leading to a high probability of overtightening or not achieving the minimum required preload. For a variation in the k factor 6% and a target preload $0.8 \cdot f_{ub} \cdot A_s$, the reliability of achieving the minimum required preload of $0.7 \cdot f_{ub} \cdot A_s$ is 94.8% and the reliability of surpassing a top value of $0.9 \cdot f_{ub} \cdot A_s$ and overtightening the bolt is 5.2%, whereas the prescribed values according to EN 1090 are 95% and 5%, respectively. In this case, the resulting spread with a 95% reliability is 25%, as shown in Fig. 2.4, leading to a low risk of overtightening a bolt.

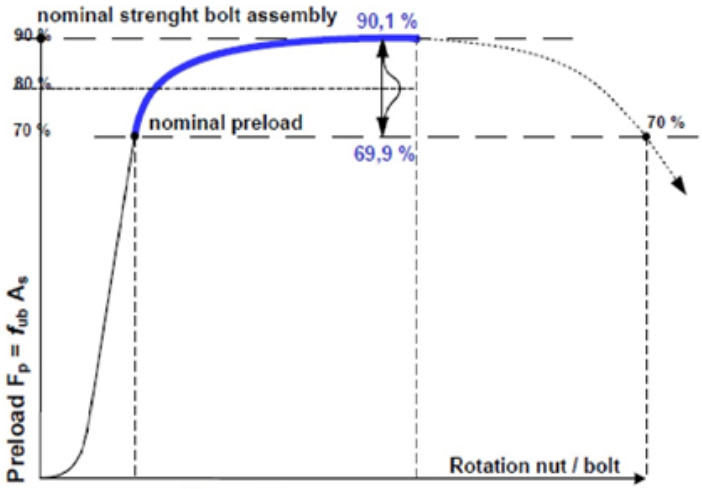

Figure 2.4: Distribution of preloads in torque method for variation in k factor 6%

2.1.2 Turn of the nut method

The second method is the turn of the nut method. This method is based on a predetermined rotation of the nut to achieve the desired preload force. Normally, a predetermined rotation results in a certain elongation of the bolt, which leads to the desired preload. However, there are some factors that may affect the turn – preload relationship.

The turn of the nut method starts by applying the first few turns of the nut which produce no preload at all, because the nut has not yet been run down against joint members and they are therefore not yet involved. This situation is shown in Fig. 2.5a. When the nut starts to pull joint members together, some tension is produced in the bolt and this process is called snugging, as suggested by Fig. 2.5b. After the joint has been snugged, all bolts and joint members start to deform simultaneously. Preload now starts to build more rapidly in the bolt, following a straight line, as shown in Fig. 2.5c [1].

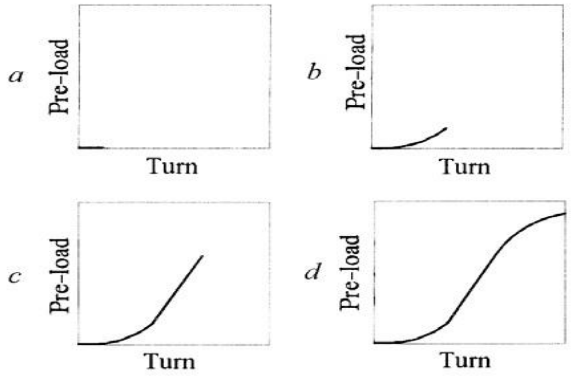

Figure 2.5: Step-by-step build-up of pre-load [1]

However, in practice it is not that simple. The problem arises during the snugging process, when the tension in the bolt starts increasing. A high portion of that tension is absorbed by the joint and the bolt sees only a small increase in preload. However, the amount of that tension may vary from bolt to bolt and from joint to joint. This depends on several factors like bent washers or not perfectly flat joint members. If the plates are not flat and parallel and the worker has not paid attention closing the gaps between the plates, then there is a high risk of not reaching the required preload level. Furthermore, the uncertainty in the rotation of the nut or any difference in the actual dimensions of the bolts may lead to a scatter in the resulting preload for a certain degree of rotation. These are shown in Fig. 2.6.

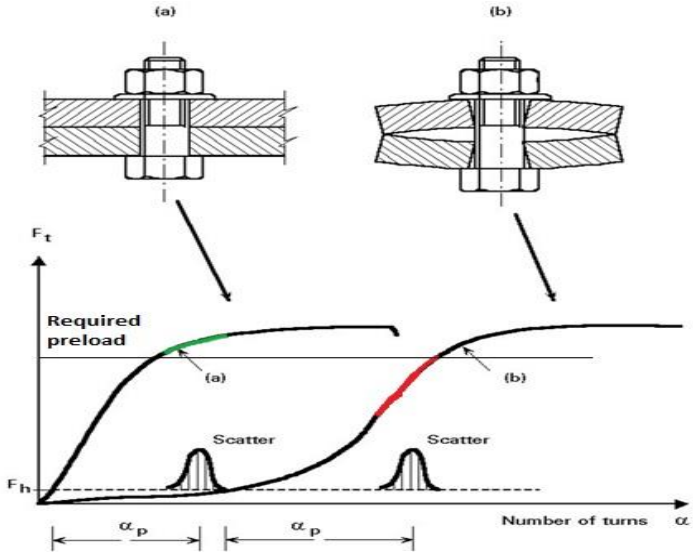

Figure 2.6: Effect of non parallel and flat plates on the resulting preload [17]

2.1.3 Combined method

In this method the torque method and the turn of the nut method are combined. The nut is first snugged with a torque to 75% of the full preload. The nut is then turned further by a predetermined angle which stretches the bolt past its yield point. This method is the most advantageous compared to the other two.

The first reason is that the torque used in the first step of the combined method is better in compensating for start-up variables, like the closing of the gaps between the plates, even for a high variation in the k factor. According to EN 14399-3 the k factor can vary between $0.10 \leq k \leq 0.16$. In order to determine the torque required to reach a preload of $75\%F_{p,C} = 0.525 \cdot f_{ub} \cdot A_s$

in the first step, a k factor equal to 0.13 may be assumed, according to EN 1090-2 art 8.5.4, resulting in a torque M = $0.13 \cdot d \cdot 0.525 \cdot f_{ub} \cdot A_s$. In this case, if the actual k factor is 0.16, this torque would lead to a bottom preload equal to $0.13/0.16 \cdot 0.525 \cdot f_{ub} \cdot A_s = 0.43 f_{ub} A_s$ and if the actual k factor is 0.10, the resulting top preload would be $0.13/0.10 \cdot 0.525 \cdot f_{ub} \cdot A_s = 0.68 f_{ub} A_s$. Therefore, the resulting preload range is high enough to snug fit the plates and low enough in order to avoid overtightening of the bolt.

The second reason is that by rotating the nut by 90˚ (or more/less, depending on the clamping length) in the second step of the combined method, independently of the preload value achieved in the first step, the bolt is preloaded to a value somewhere on its plastic region. The reason is that the spread in the preload in the first step creates a small difference in the rotation on the elastic part of the preload – rotation curve. Therefore, a further rotation by 90˚ will take the bolt on its plastic region, as shown in Fig. 2.7.

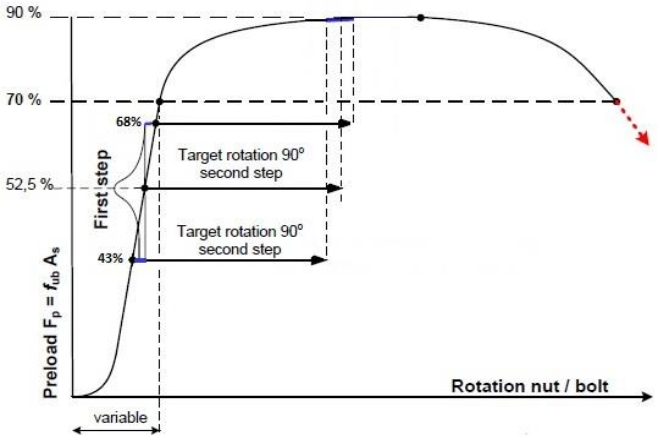

Figure 2.7: Preload – rotation curve for the combined method

2.1.4 Direct Tension Indicators (DTI)

The interest in a guaranteed minimum preload has led the structural steel industry to adopt several new types of fasteners which improve the chances that the fasteners will be pre-loaded properly and make it easier to inspect previously tightened fasteners for minimum tension. These fasteners are formally classified as fasteners which allow “direct tension indicator tightening”.

The most common type of direct tension indicator (DTI) at the present time is a washer with “bumps” on its upper surface, as shown in Fig. 2.8. A DTI washer is interposed between the head of the bolt and the surface of the joint and it works as a mechanical load cell. As the nut is tightened, the arch-like protrusions are compressed and yield plastically at a predetermined pressure, which is proportional to the tension in the bolt, reducing the gap between the head of the bolt and the washer. A feeler gage is used to measure this gap. When the gap has been reduced below a preselected maximum value, the tightening process is stopped.

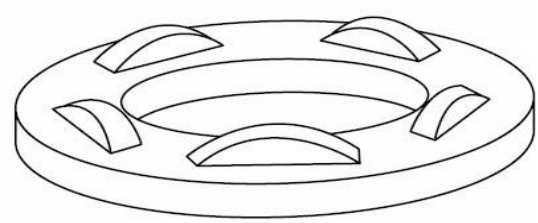

Figure 2.8: Direct Tension Indicator (DTI) [1]

However, a direct tension indicating washer is affected by the geometrical tolerances of the connection, like the actual size of the head of the bolt, which affects the resulting pressure on the protrusions. Several studies have been made to evaluate the accuracy with which the DTI washer controls initial preload in a fastener, resulting in a spread at the minimum required preload level, which varies from ±5% to ±12% [13].

2.1.5 Discussion

In conclusion, apart from the combined method, the other three methods may result in a high scatter in the initial preload, increasing the danger of overtightening or not achieving the required preload and making any estimation on the residual preload of the bolts at some point in the future difficult. For this reason, it is also important to know what mechanisms can lead to preload loss. This is explained in the following section.

2.2 Loss of preload

Loss of preload is important for all the reasons mentioned in chapter 1 and it can lead to an early failure of the connection, depending on the amount of loss and on the value of the initial preload. Loss of preload is basically divided into two stages, as schematically shown in Fig. 2.9.

a) The short-term relaxation, which appears within the first days after tightening the bolts and b) long term relaxation, which is developed during the life time of the bolt and it is mainly caused by the action of the external load.

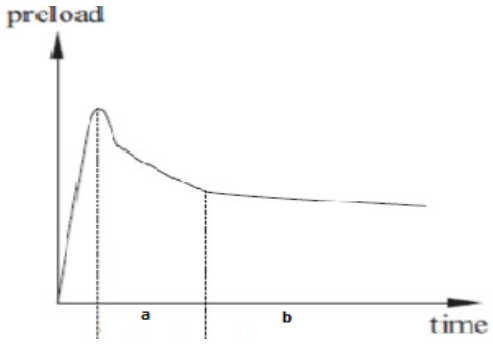

Figure 2.9: Time dependent development of preload [2]

2.2.1 Short term loss of preload

In general, short term losses are caused by elastic interactions and short term relaxation.

Elastic interactions between bolts are caused when a bolt is tightened and it partially compresses the other joint members. When nearby bolts are tightened later, they further compress the joint in this region. The contraction of the plate material that occurs, allows the first bolt to lose preload. However, an appropriate tightening sequence can reduce the effect

of elastic interactions. Generally, the amount of the elastic interaction depends on the size of the joint, the distance between the bolts and the stiffness of the bolts [15].

Short term relaxation occurs in a bolted joint because something has been loaded past its yield point and will creep. This can be a component, such as a bolt or a gasket or the first threads in a nut.

Embedment

The most common cause of short term relaxation is embedment. The surfaces of the threads in the nut, the bolt and the faying surfaces of structural members are never perfectly flat. They consist of a series of asperities, as shown in Fig 2.10. When such parts are first loaded, they contact each other only through high spots on the material surfaces. Since initial contact areas are relatively small, the material at the contact points cannot stand the pressures. In case of bolt or nut threads, plastic deformation occurs until enough of the total thread surface has been involved in sharing the load. The same thing happens in the faying surfaces, which results in a reduction of the grip length and a decrease of pretension [1].

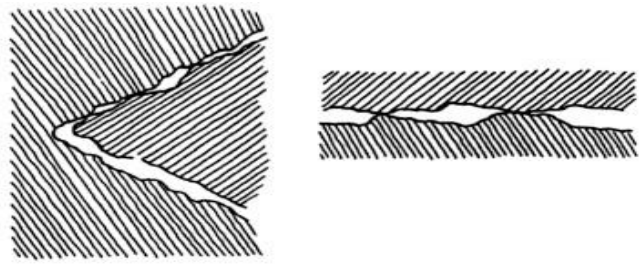

Figure 2.10: High spots on thread and plate contact surfaces [1]

Embedment of coating surfaces

The problem of loss of pretension force has been examined various times with respect to the type of coating for various types of bolts [2], [3], [4], [5]. It has been shown that the amount of embedment depends on the coating system and in uncoated connections the preload is reduced too. Furthermore, loss of preload increases with the thickness of coating layer and the number of coated surfaces, as there are more high spots to embed and settle in together. This was confirmed by tests which were performed by Yang and DeWolf. The results are shown in Fig. 2.11.

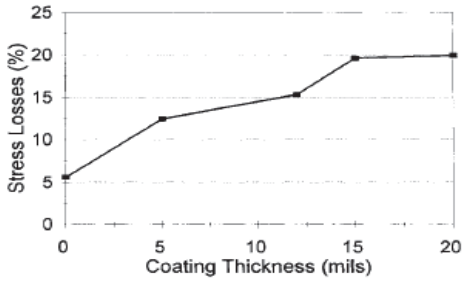

Figure 2.11: Loss of bolt stress versus coating thickness [5]

Embedment of the coating surfaces occurs not only between the plates, but also between the head of the bolt and the plate or the nut and the plate. However, in this case the embedment is higher, because the pressure between the plates is lower due to the effect of load spread, as shown in Fig. 2.12 [14].

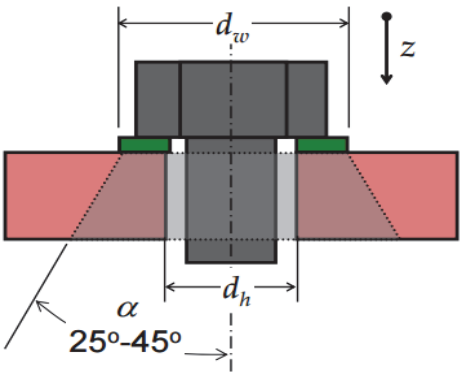

Figure 2.12: Pressure reduction due to load spread [14]

Moreover, losses are more important in case of thin plates in a connection where creeping of the coating has a relatively greater influence. Generally, hard coatings like epoxy-zinc and epoxy-iron mica and polyurethane systems, lead to good results. Soft coatings, like alkyd, are pushed out of the connection and lead to a higher loss of preload [3].

Embedment of the threads

When a bolt is first loaded, it exerts extremely high surface pressures on its threads. Thread dimensions have been selected to support these high loads, but only if a significant percentage of the total thread surfaces shares that load. Bolts with higher $l_{clamping}/d$ ratios relax by a smaller percentage, as the total embedment relaxation is the same for a given initial preload, but the embedment will be a different percentage of the total length of the bolt.

Furthermore, poor thread engagement, as shown in Fig. 2.13, can lead to a plastic deformation of the threads. If the bolt is undersized, or the nut oversized, thread contact areas will be less than those planned by the designer, and substantial plastic deformation may occur. Moreover, if parts are softer than intended by the designer, (perhaps because of improper heat treatment or incorrect material) they may creep and relax substantially, even if the geometry is correct and loads are normal [1].

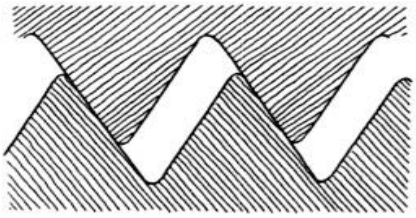

Figure 2.13: Poor thread engagement [1]

Other factors that cause embedment of the threads and joint

Other factors that may cause a short-term relaxation are the oversized or undersized holes and the non-perpendicular nuts or bolt heads. In case of oversized holes there is too little contact between nut and joint surface or between bolt head and joint surface. Unless a washer is used to distribute contact pressures and limit contact stresses, the head or the nut will embed itself in the joint surfaces, as shown in Fig. 2.14, which results in a reduction of the grip length of the bolt.

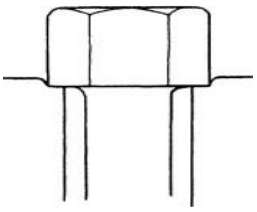

Figure 2.14: Oversized holes [1]

Undersized holes, like the one in Fig. 2.15, can also lead to a loss of preload, because the edge of the hole will break down under initial contact pressures, resulting even in loss of the elongation of the bolt, since such effects are usually large compared to the amount by which the bolt was stretched when it was initially tightened.

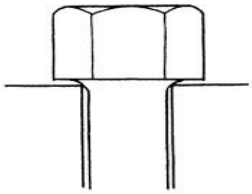

Figure 2.15: Undersized holes [1]

Furthermore, the contact faces of nuts and bolt heads are never exactly perpendicular to the axis of the threads or the axis of the bolt hole. This means that only a portion of the contact surface of the nut or bolt head is loaded when we first tighten the fastener. These abnormally loaded surfaces will creep until enough additional contact area has been involved to reduce contact pressures and stabilize the joint.

Tightening speed also affects the amount of relaxation that takes place in a joint. A high tightening speed can also increase the relaxation, because in that case bolts will not have time to settle in together during the tightening process. However, this problem is dealt with tightening in steps to give bolts time to relax.

It is considered that most of the short-term relaxation (mainly caused by embedment) takes place within 12 days after tightening, during which bolt forces decrease asymptotically [1]. This time interval is dependent on the type of coating used. It has been reported that for surfaces coated with zinc rich primer or alkyd, the preload force was nearly stable after the first 12 hours, whereas for galvanized coated surfaces the preload force was stabilized after 12 days. The total loss varies between 7% for uncoated surfaces and 20% for coated surfaces of the initial pretension, for normal holes and structural steel (depending on coating surface and number of coated surfaces) [2], [3], [4], [5]. The difference in losses between connections with slotted holes and normal holes is not great and represents about 1% of the initial pretension [6].

2.2.2 Long term loss of preload

Long term losses describe the reduction of residual preload over the life time of the connection under static or cyclic loads. This, on the one hand depends on the relaxation of the bolt and the clamping package and on the lateral contraction under external tensile loads, on the other hand on the self-loosening of the bolt, which is provoked by dynamic loads acting on the structure.

When a load is transferred by a connection, the bolt forces are affected by two phenomena [6]. First, in plane stresses are accompanied by transversal strains which tend to decrease or increase the grip length under tensile or compressive stresses respectively. Second, the shear force is resisted by the deformation and yielding of opposite asperities of the plates, that define contact. These deformations are accompanied by an inward normal plastic displacement that reduces the grip length and leads to loss of preload.

Long term loss under static loading

The influence of a static load on a connection with pretensioned bolts has been examined by C. Heistermann. It was found that an external static load does not increase the loss of pretension significantly. The long-term loss under a constant external tensile load is not affected by the load magnitude and the relative loss of pretension is asymptotical. It was found that for specimen with three Tension Control Bolts (M30) used in a lap joint, subjected to 60% and 80% of the ultimate resistance for 4 months, which are grit-blasted with steel grit and an inorganic two component ethyl silicate zinc rich paint as a coating, the relative loss of pretension under static loading was on average below 4% (after 15 weeks) [7]. This loss was caused mainly due to the lateral contraction of the clamping package and also due to the yielding of the opposite asperities between the plates, which take the external force. The yielding is expected to be higher for the part of the plates which is close to the external bolts, since these bolts carry most of the external force. This was confirmed by the tests, by observing higher loss of preload for the leading bolts of the connection.

Another test included double shear lap joints, where the plates were bolted together by a group of three lockbolts. The plate surfaces in these experiments were all galvanized. The bolts were left for 12 hours to measure the loss of pretension due to short-term relaxation and it was found that the average loss of the pretension force was 23% of the force they had after tightening was completed. Then, a gradually increasing tensile force was applied on the specimen. During the test, the bolts also lost some of their pretension. Based on the maximum bolt forces when the bolts were tightened, the bolts lost on average 2% of their forces until the maximum applied load was reached. This means that the forces in the bolts were more or less stable during load application [4].

Long term losses under cyclic loading caused by embedment

Cyclic loading is the main cause of self-loosening of a preloaded bolt. However, first we will see the influence of cyclic loading on a connection in which self-loosening is excluded. The losses will therefore be attributed to embedment of coating surfaces.

Friede tested single bolted connections with standard bolts and different coating systems. The coating systems which were used were epoxy iron mica and polyurethane as a cover with epoxy zinc as a primer, epoxy iron mica and polyurethane as a cover and intermediate coating layer with epoxy zinc as a primer and two connections with alkyd of different thickness. One of the connections was uncoated. The plates of the connection were fixed in a testing machine and a cyclic deformation between the plates was applied. Self-loosening was avoided by a weld spot. The connections were left for 2 days to allow for short term relaxation. Then, the preload was measured over the load cycles. The preload was reduced due to slippage in the contact pairs, which led to embedment of the asperities. Based on the bolt forces after the

short-term relaxation occurred, the uncoated connections had the smallest reduction of preload force, which was about 40%. For thin and hard coating systems, the reduction was almost 60% and for thicker and hard coating systems the loss was 80%. For the connections with thin and soft coating systems (alkyd), the preload loss after the short-term relaxation was 50%, whereas for the thick and soft systems the loss was 75% [3].

The influence of cyclic load on a connection with pretensioned bolts has been examined by C. Heistermann [4]. Double shear lap joints were tested, where the plates were bolted together by a group of three Huck BobTail lockbolt, which have a high vibration resistance and thus self-loosening can be excluded. Therefore, the loss of preload is attributed to the embedment of the coating surface. The plate surfaces in these experiments were all galvanized. Galvanized steel is a very hard coating system, which means that the expected preload loss will be low. Indeed, the bolts lost on average a 5% of the force they had after the short term losses.

Long term losses under cyclic loading caused by self-loosening

When a dynamic load is acting on a connection, cyclic loading induces micro settlements in the thread of a bolt shank. A bolt will not loosen unless the friction forces existing between the external threads of the bolt and the internal threads of a nut are either reduced or eliminated by some external mechanism acting on the bolt and joint, which causes these micro settlements. This mechanism is generated when a relative movement occurs between the mating threads, because the transverse force acting on the joint is larger than the frictional resisting force generated by bolt's preload.

Under small transverse joint movements, the fastener will initially bend, rather than suffering slip between the head of the bolt and the surface of the plate. As the movement increases, the friction between the threads and between the head and the surface is overcome. The amount of movement to cause surface slip is referred to as critical slip. Surface slip is critical for self-loosening to occur. This is shown in Fig. 2.16.

However, the value of the critical slip is dependent upon several factors: the key ones include the preload, the fastener diameter and the bearing face friction value. Many researchers confirmed this by performing tests and using finite element models to derive a relation between the value of critical slip and the preload force. In case of a single lap joint the critical slip is determined based on eq. 2.5 [3].

$$a = \frac{F_V \cdot l_c^3 \cdot \mu}{12 \cdot \mathrm{EI}} \tag{2.5}$$

Where, F_V is the preload, l_c is the clamping length, μ is the slip factor and EI is the bending stiffness of the bolt.

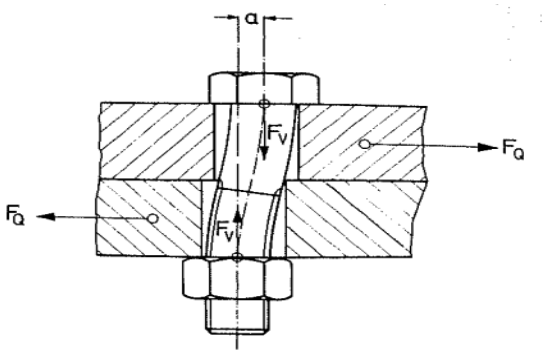

Figure 2.16: Lap joint with transversal deformation [3]

When the critical slip value is reached, the bolt's threads plunge into the nut's threads. Then, a normal force is acting on the surface of the threads. Due to the inclination of the threads with respect to the bolt axis, this force has two components, one perpendicular and the other parallel to the bolt axis. The force which is parallel to the bolt axis is the one that causes the preload. The force perpendicular to the bolt axis generates the torque to the nut. This force has a component tangential to the thread surface, which causes the relative slide between the threads. The bolt and nut threads slide relatively when the bolt moves laterally and if it does not slide back when the bolt comes to its normal position, the slide is not recovered in the load cycle [16]. This results in self-loosening. These forces are shown in Fig. 2.17.

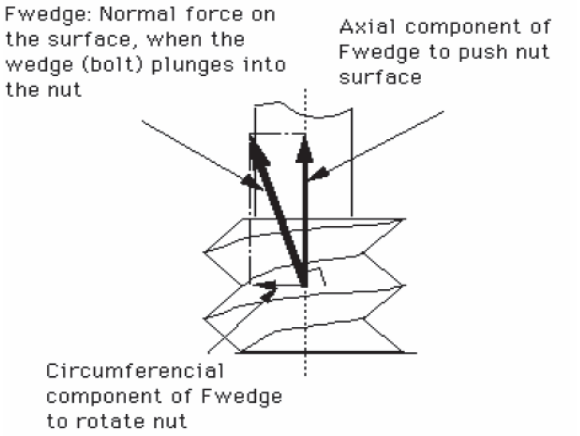

Figure 2.17: The mechanism of the nut rotation [16]

A bolted joint, properly designed so that the clamp force from the bolts is sufficient to prevent transverse movement between the joint plates, will not come loose.

Friede performed several tests to assess self-loosening. Single bolted lap joints were tested for various $l_{clamping}$/d ratios and the tests were run displacement controlled. Loss of preload can be traced back on a combination of embedding and self-loosening.

Friede found that below a certain clamping length all the preload was lost even for a low number of cycles. But, even higher clamping lengths led to a significant loss of the preload. However, for these clamping lengths, no slippage of the bolt/nut was measured, which means that self-loosening did not occur and the loss was caused by embedment. Furthermore, for the tests with a low displacement almost no self-loosening occurred, whereas for higher displacements the loss of preload due to self-loosening increased [3].

2.2.3 Discussion

As discussed, there are several mechanisms which result in loss of the initially applied preload. The loss of preload based on these mechanisms varies, depending on factors like the number of plates in the connection or the coating surfaces, but also on factors difficult to predict and control like the size of the holes, etc. Furthermore, the importance of a correct initial preload to avoid self-loosening was discussed. All these factors that result in loss of preload, combined with the application of the initial preload lead to the problem statement.

2.3 Conclusion: Problem statement

In summary, most of the tightening methods result in a spread in the initial preload, increasing the danger of overtightening the bolts or not achieving the required preload. Furthermore, loss of preload can lead to a preload lower than the minimum required preload level. Therefore, considering the importance of a sufficiently high preload in HSFG connections which was discussed in chapter 1, it is clear that it is necessary knowing the preload during the lifetime of the connection. Normally, the only way to deal with preload loss is to retighten the bolts periodically, which leads to high maintenance costs. Consequently, the development of a method that determines the preload is essential, as it will contribute to improve safety, reduce the maintenance costs and eventually give extended life time predictions of a connection. In the next chapter the state of the art is presented and in chapters 4, 5 the feasibility of performing in situ measurements with the strain gauge method is analyzed, by imitating in situ conditions in the lab and testing the method on a connection of an existing structure.

3. STATE OF THE ART

In the previous chapter, the importance of knowing the preload of bolts used in High Strength Friction Grip Connections was analyzed. Nowadays, there are several techniques which offer the possibility to determine the preload of the bolts, like the conventional ultrasound method, the velocity ratio method, the mechanical resonance frequency shift method, the piezoelectric active sensing method and the strain gauge method. In this chapter, the factors that affect the measurements and the suitability of these methods to perform in situ measurements are discussed.

3.1 Ultrasound method

3.1.1 Theory

The principle on which this technique is based, is the measurement of the elongation of a preloaded bolt by measuring its length before and after the application of the preload. The instrument measures the Time Of Flight (TOF) of an ultrasound wave to travel from the head to the bottom of a bolt and back to the head, after its reflection on the bottom. Then, the ultrasonic length is obtained by multiplying the TOF by half the material velocity. The ultrasound wave is emitted by an ultrasound transducer which is placed on the head of the bolt, coupled with the bolt by a thin film of a viscous liquid, which permits transmission of ultrasound across the interface. The difference between the final ultrasonic length under load and the initial ultrasonic length under no-load condition, is referred to as the ultrasonic stretch ΔL.

The preload is:

$$F = \sigma \cdot A = E \cdot \varepsilon \cdot A = \frac{AE}{L_{eff}} \Delta L \tag{3.1}$$

where, A is the cross section area, E is Young's modulus and L_{eff} is the effective length of the bolt. However, measuring the ultrasonic length or stretch of a bolt is not easy, as there are many factors that affect the measurement. These factors are analyzed in the following sections.

3.1.2 Stress

Bolt's ultrasonic length increases when the bolt is loaded under a tensile load. However, this is caused not only because of the elongation of the bolt, but also because the stress in the bolt causes a reduction of the velocity of the ultrasound wave. This is known as acoustoelastic effect [20]. Furthermore, the stress distribution along the axis of a bolt is not uniform, as shown in Fig. 3.1, which means that areas of the bolt with higher stress, result in a higher reduction of the ultrasound wave velocity.

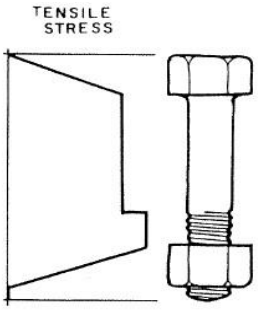

Figure 3.1: Tensile stress along the axis of a bolt [19]

Considering that the acoustoelastic constant of the rail steel, which has a chemical composition similar to the carbon steel, is equal to $C_L = {dv/v}/{\varepsilon}$ = -2.38 [18] and assuming that for zero external load no stress is present in the bolt, then the error in the ultrasonic stretch for a bolt M24 with a clamping length of 80 mm is close to 240%. Therefore, the extra (ultrasonic) stretch caused by the acoustoelastic effect due to the reduction of the ultrasound velocity, is almost 2.5 times higher than the actual stretch of the bolt. This means that the only way to deal with such a high error is to determine the acoustoelastic constant of the bolt or perform calibration. Generally, the firms which provide the ultrasound equipment used for this method, offer the possibility of compensation for these stress related effects, by giving a procedure for the determination of a correction stress factor. This correction factor results actually in the acoustoelastic constant of the material, $\text{correction factor} = 1/(1-C_L)$. The procedure provided with the Norbar USM-3 Ultrasonic Bolt Meter operation manual is presented in Appendix A [40].

3.1.3 Residual stress

The stress caused in a bolt because of the external load is not the only stress that affects the ultrasound velocity. Residual stress also affects the ultrasound velocity. If the ultrasound wave experiences the same profile of residual stresses in the stressed and unstressed state of a bolt, their influence on the ultrasonic stretch is cancelled, since they are present in both the stressed and unstressed state of a bolt. However, if the transducer is placed on a different position on the head of the bolt, when (for example) the measurement in the stressed state is taken, the ultrasound wave will experience a different residual stress profile, resulting in an error in the force. However, it is not possible to know the residual stress profile that the ultrasound waves will experience in the bolt. Compressive or tensile residual stress, the direction of the residual stress with respect to the propagation of the wave in the bolt are some factors, which influence the estimation of the force. Egle et al. estimated the acoustoelastic coefficients for longitudinal waves propagating parallel or perpendicular to compressive or tensile stresses [18]. The results are shown in Table A1 in Appendix A. In a bolt the average residual stress level is low and significant residual stress concentrations exist at the threads, head to body fillet etc. Trying to simplify the problem, in order to estimate the error, it is assumed that only the threaded part is subjected to a uniform residual stress distribution and for the rest of the bolt no stress is present. As shown in Table A1, the highest influence on the velocity of the waves is when the stress (compressive or tensile) is parallel to the propagation of the longitudinal waves. Based on this pessimistic case, the results shown in Fig. 3.2 are obtained.

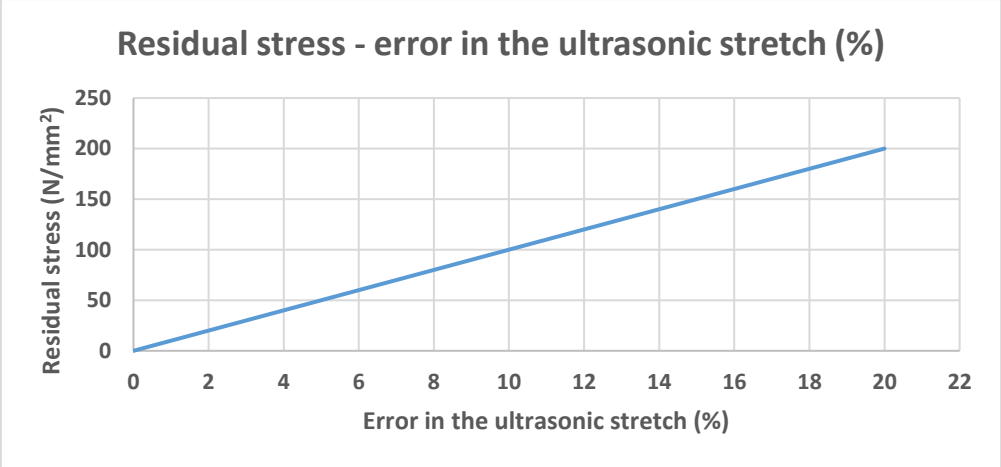

Figure 3.2: Error in the ultrasonic stretch (%) vs residual stress

As shown in Fig. 3.2, even for a low difference in the residual stress profile experienced by the ultrasound wave, the error in the force is quite high. Therefore, it is important to avoid any motions of the transducer on the head of the bolt. It has to be noted that this is a pessimistic estimation, considering that the residual stresses are present everywhere in the path of the wave along the threaded part of the bolt and that they are characterized by a direction with the highest influence on the ultrasound wave.

3.1.4 Temperature

Temperature also affects the ultrasonic stretch. The length of a bolt increases linearly with increasing temperature within certain limits and the velocity of an ultrasound wave decreases linearly with increasing temperature. If the temperature is the same for the measurement in the stressed and unstressed state, then the ultrasonic stretch is not influenced. However, if there is a temperature change between the two measurements, the ultrasonic stretch is affected. It has been estimated that for carbon steel, the velocity of a longitudinal ultrasound wave decreases linearly with increasing temperature with a rate 0.80 $\frac{m/sec}{^{\circ}C}$ [2]. Based on a thermal expansion coefficient for carbon steel equal to $1.08 \cdot 10^{-5}$ mm/mm˚C, the error in the ultrasonic stretch at a load level of 250 kN, for a temperature increase of 0.5 ˚C is 3%. The graph between the error in the ultrasonic stretch and temperature increase is shown in Fig. A1 in Appendix A. As shown, even for a low temperature change the error in the ultrasonic stretch is high, which means that in case of in situ measurements, a continuous and accurate temperature measurement is required in order to compensate for temperature related effects. As mentioned for the stress influence, the ultrasound equipment offers the possibility of compensating for the temperature related effects. The procedure described in the Norbar USM-3 Ultrasonic Bolt Meter operation manual is presented in Appendix A [40].

3.1.5 Couplant

One more source of error in the determination of the ultrasonic stretch is the couplant which is added between the head of the bolt and the transducer. Couplant's thickness may vary, depending on the pressure on the transducer and the amount of couplant, resulting in error in the ultrasonic measurements. For example, a bolt M24 (l_c = 80 mm) which is preloaded to a level close to the minimum required preload, is characterized by a stretch equal to 0.2746 mm. A variation in couplant's thickness equal to 12 μm can result in an error in the ultrasonic stretch equal to 5%. Therefore, the couplant may have a quite high influence on the measurements.

Recently, a new type of bolt was developed based on Permanent Mounted Transducer System Technology (PMTS). These bolts are ordinary bolts, with the only difference that there is a permanently mounted durable thin-film transducer on the top of the head of these bolts, which diminishes handling and coupling errors, since there is a direct contact of the transducer with the head of the bolt, without using couplant. Since the transducer is a real part of these bolts, every bolt has its own transducer, offering compensation for temperature related effects, based on the material of that particular bolt. According to the literature the accuracy of this method is ±3%, compared to the accuracy of ±30% of the conventional handheld transudcers [42].

3.1.6 Other factors that affect the measurements

So far, the error in the determination of the ultrasonic stretch is discussed. However, the purpose of the ultrasound tests is to determine the force and not the stretch. In order to do that, the model described by eq. 3.1 is used. However, this requires an accurate determination of the effective length of the bolt, Young's modulus and the ultrasound wave velocity. And even if the uncertainty in Young's modulus value (5%) is considered acceptable, it is not possible to reach the same conclusion about the effective length. There are several models that describe the effective length of a bolt, but these models do not apply on all the bolt sizes, since the actual effective length of a bolt depends on factors like the clamping length and the length of the bolt. In practice, the uncertainty in the effective length of the bolt is high, therefore the resulting error in the force could be very high. All these uncertainties are dealt with calibration.

Another important factor that may affect the measurements is the surface of the bolt. In order to emit and receive an ultrasound wave, the bolt must have a flat surface for the transducer to contact. The opposite end of the bolt should also have a parallel surface to reflect the ultrasound back to the transducer. Furthermore, a flat and smooth surface is very important to proper coupling of the transducer, otherwise the transducer may not achieve proper contact.

Finally, another point of interest is the accuracy of the measurement of the ultrasonic length. Since the change in the length between the stressed and unstressed state of the bolt is very low, it is required to measure the length to the nearest 0.001 mm. This is shown in Fig. 3.3, where an error equal to 2% in the stretch, results in an error in the force equal to 6%.

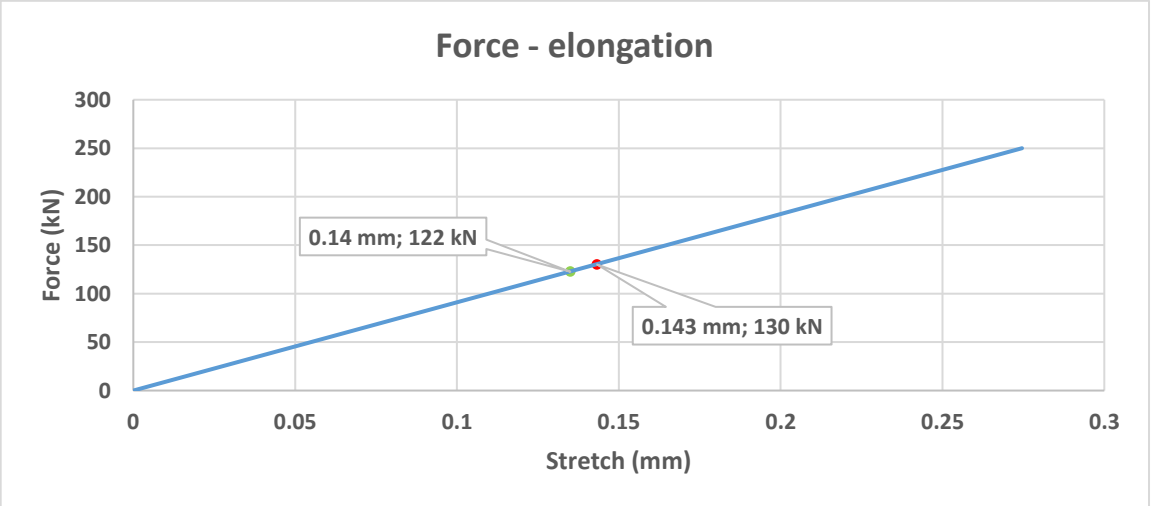

Figure 3.3: Force – elongation for M24, l_c = 80 mm

In terms of TOF, this means that it is necessary to resolve 2·0.001 mm / 5890000 (mm/sec) = $3.4 \cdot 10^{-10}$ sec. This requires a high sampling rate 1 sample/($3.4 \cdot 10^{-10}$ sec) = $3 \cdot 10^{9}$ Hz or 3 GHz, which increases the cost of the equipment.

3.1.7 Discussion

Based on the abovementioned, the conventional ultrasound method is sensitive to factors which may have a big influence on the in-situ measurements, like temperature variations between the measurements or environmental noise. Furthermore, attention must be paid to the contact of the transducer with the head of the bolt, which requires flat and parallel surfaces, to the pressure applied on the transducer, which may cause variation in couplant's thickness and to the location of the transducer on the head, when the measurements in the stressed and unstresses state are taken. All these make the in-situ application of this method difficult. Finally, compensation for temperature or stress related effects requires determination of a correction factor and in order to overcome the uncertainty in the effective length of the bolt or the ultrasound wave velocity, calibration is required. All these result in a time consuming process.

3.2 Velocity ratio method

3.2.1 Theory

As it is mentioned in the previous section, the conventional ultrasound method is based on measurements in the stressed and unstressed state of the bolt, which means that it is required to loosen the nut in order to obtain a measurement under zero force. In order to avoid loosening of the bolt, a new method was developed, which relates the ratio of times of flight of a transverse and a longitudinal wave with the applied force.

$$\frac{t_T^\sigma}{t_L^\sigma} = \frac{v_L^0}{v_T^0}\left[1 - \frac{L_{eff}}{L}(C_T - C_L)\frac{F}{A_{eff}}\right] \tag{3.2}$$

where, C_T and C_L are the acoustoelastic constants for longitudinal and transverse waves, respectively, L_{eff} is the effective length of the bolt, A_{eff} is the effective cross section area of the bolt, v_L^0 and v_T^0 is the longitudinal and transverse wave velocity for the unstressed state, respectively and L is the length of the bolt.

The force – ratio of TOFs is presented in Fig. 3.4 for a bolt M24 with a clamping length of 80 mm. Based on that graph, it is observed that a small change in the ratio of times of flight results in a big change in the force F. For example, a change of 0.03% in the ratio of times of flight can result in a change in force F equal to 10%. As shown in Fig. 3.4, it is important to measure the TOF of the longitudinal wave with an accuracy of 10^{-9} sec ($2 \cdot 10^{-9}$ sec for a round trip), which means that the requirement for a high sampling rate ($1/(2 \cdot 10^{-9}$ sec) = 500 MHz) described in the previous section for the conventional ultrasound method, applies here too. The measurement of the TOF of the longitudinal wave is critical, because of its higher velocity (double than the velocity of shear wave), which means that smaller changes in the TOF occur, at a given load level. In the following sections, the factors which affect the measurement of the ratio of TOFs will be analyzed.

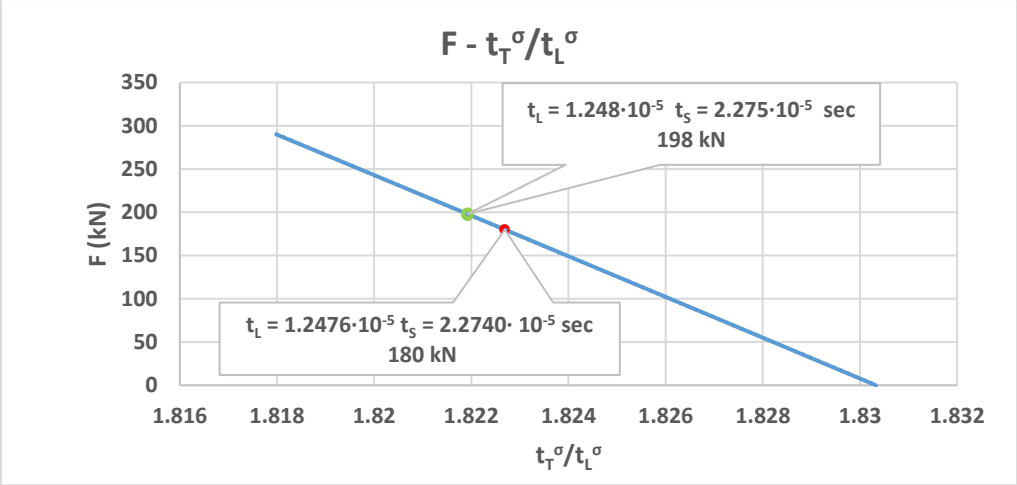

Figure 3.4: Theoretical force – ratio of TOFs

3.2.2 Residual stress

The velocity ratio method relates the ratio of TOFs with the difference in the acoustoelastic coefficients to determine the force on the bolt. Any stress, apart from the stress caused by the preload, results in an error in the ratio of TOFs. Therefore, in this section the influence of the residual stress will be examined.

In contrast to the conventional ultrasound method, in which the influence of the residual stresses is cancelled if the ultrasound wave experiences the same residual stress profile in the stressed and unstressed state of the bolt, the velocity ratio method has no way of cancelling the effect of the residual stress. Although it is expected that the influence of the residual stress in the ratio of TOFs will be limited, since both the nominator and the denominator are affected in the same way, the resulting error in the ratio of TOFs and the estimated force will depend on the different influence of the acoustoelastic effect on the longitudinal and transverse waves.

As shown in Table A1, the highest influence on the velocity of the waves is when the stress (compressive or tensile) is parallel to the propagation of the longitudinal and transverse waves. Based on this pessimistic case and based on the assumptions mentioned in section 3.1.3, the error in the force due to residual stress is shown in Fig. 3.5.

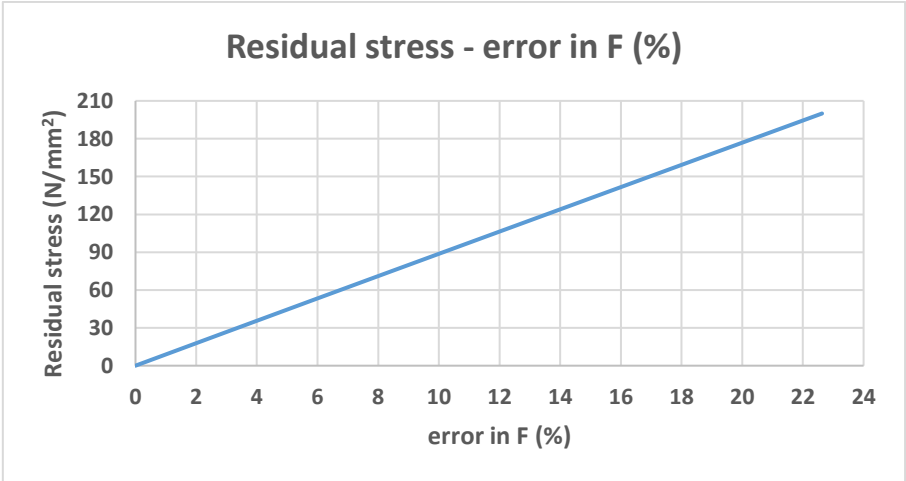

Figure 3.5: Residual stress influence on preload force F

As shown, the residual stresses can have a quite high influence on the estimated force, depending on their magnitude. The error presented in x axis, is the average difference of the estimated force from the theoretical actual force, which is calculated for the working loads of a preloaded bolt (140 – 300 kN). However, this is a pessimistic estimation, considering that the residual stresses are present along the threaded part of the bolt in the path of the waves and that they are characterized by a direction with the highest influence on the ultrasound waves.

3.2.3 Temperature

As it is already mentioned, anything that results in a different TOF, apart from the stress caused by the preload, leads to an error in the estimation of the force. At the reference temperature of 21 ˚C the ultrasound velocity is equal to $v_{0,L}$ =5890 m/sec and $v_{o,T}$ = 3218 m/sec at the no stress state. When the temperature increases over or drops under that temperature, causes a reduction or a rise in the ultrasound velocity, excluding the reduction which is caused due to the stress. The same applies if calibration is performed at a certain temperature and the measurements of TOFs are done in a different temperature. This result in an error in the estimated force. For example, temperature increase causes thermal stresses, which result in an elongation of the bolt. Furthermore, a rise of the temperature results in a reduction of the ultrasound velocity. In order to estimate the influence of temperature variations, the thermal expansion coefficient of carbon steel equal to $1.08 \cdot 10^{-5}$ mm/mm˚C is considered. Furthermore, based on literature, the velocity of longitudinal and transverse ultrasound waves decreases linearly with increasing temperature, with a rate of 0.80 $\frac{m/sec}{^\circ C}$ and 0.44 $\frac{m/sec}{^\circ C}$ respectively [19]. The average error for different preload levels (between 100 – 300 kN) is 0.1% for a 10 ˚C temperature increase, as shown in Fig. A2 in Appendix A. The influence of temperature on the force, estimated by the velocity ratio method is much lower compared to the conventional ultrasound method. This is reasonable, because the ratio of TOFs remains more or less constant, since both the nominator and denominator increase. The influence is much lower here compared to the influence of the residual stresses, because the influence of temperature on longitudinal wave velocity is 1.8 times higher than that on the transverse wave velocity, whereas the influence of residual stresses on longitudinal wave velocity is almost 9.5 times higher than that on transverse wave velocity.

Another point of interest is when temperature variations take place between the longitudinal and transverse wave measurements. This can happen if measurements are not taken at the same time. Such a temperature change can have a quite big influence on the measurements. For example, an increase of just 0.5 ˚C when the longitudinal wave measurements are taken, can lead to an average error in the preload force equal to 1.8%, as shown in Fig. A3 in Appendix A. It is therefore important to check the temperature before any measurement is taken.

Techniques like the one that is based on mode conversion of ultrasound waves can diminish this error. Generally, it is possible to obtain measurements for simultaneous generation of longitudinal and transverse waves. Several researchers used transverse waves generated by electromagnetic acoustic transducers (EMAT). The transverse wave is obliquely incident to the bolt head and then it is transmitted in the bolt as a pair of longitudinal and transverse waves due to mode conversion [21]. In that case, both waves experience the same temperature.

3.2.4 Influence of couplant

The couplant can also affect the ultrasonic measurements. Variations in couplant's thickness between the measurements or between calibration and periodic monitoring of a bolt, introduce a change in ultrasonic measurements.

Yasui estimated the influence of couplant's thickness, using a transducer which excites and receives simultaneously longitudinal and shear waves, using a viscous couplant at the transducer – bolt head interface [22]. He performed calibration tests on two different types of bolt. A short bolt with a length equal to 28 mm and a longer bolt with a length equal to 55 mm. At each load step he attached and removed the transducer 20 times. He found that the relative change of the ratio at a specific load step was 2.9% for a long bolt and 28.4% for a shorter one, which is reasonable because couplant thickness variations will have a bigger influence in case of a shorter time of flight. However, the error caused by the couplant's thickness can be diminished by using an EMAT transducer which needs no couplant when attached on bolt head [21].

3.2.5 Other factors influencing the time ratio preload relationship

Determination of the force based on the model described by eq. 3.2 requires not only an accurate measurement of the ratio of TOFs, but also an accurate estimation of constants like the acoustoelastic coefficients or the zero stress velocities. Furthermore, an accurate determination of the effective length is needed. Given that there is a high uncertainty in the way that a bolt is stressed, the only way to deal with these uncertainties is to perform calibration.

Additionally, the requirement for parallel and smooth surfaces, which allow the reflection of the ultrasound waves, applies here too.

3.2.6 Discussion

As discussed, the main advantage of this method is that it does not require untightening of the bolt. However, in order to do that, it is necessary to know accurately many constants, which define the relationship between the ratio of TOFs and the force. Furthermore, this method has no way of cancelling the effect of residual stresses on the measurement of the ratio of TOFs, which means that even if all the constants are determined accurately, the resulting force is characterized by a certain degree of error. Therefore, calibration is necessary, if maximum accuracy is required, which means that untightening of the bolt cannot be avoided. But even in this case, there are several factors which may affect the measurements. Any change in the position of the transducer on the head of the bolt between calibration and periodic monitoring of a bolt, may lead to an error, because the waves will experience a different residual stress profile. The same applies for the influence of the couplant, as any variations in the thickness affect the resulting force. The influence of temperature variations is almost negligible, if there is no change in the temperature between the measurement of the TOF of the longitudinal and ultrasound wave. Finally, the requirement of a very accurate measurement of TOF makes the application of this method in situ challenging, as the environment interference can cause noise and distort the measurements.

3.4 Mechanical Resonance Frequency Shift Method

3.4.1 Theory

Mechanical Resonance Frequency Shift Method is one more method which measures the applied stress based on acoustoelastic effect. In the previous method TOFs were measured.

Now, number of cycles per second are measured, in other words frequencies. A transducer is placed on the head of the bolt and generates a band of ultrasonic frequencies. Assuming that complete reflection occurs at the flat and parallel ends of the bolt, the transducer receives the reflected waves looking for that particular frequency which has resonated within the bolt. This will be that frequency which sees the length of the bolt as an exact multiple of its wavelength. The acoustic resonant frequencies are given by:

$$f_n = \frac{nv}{L} \tag{3.3}$$

where, n is a harmonic integer, v is the velocity of acoustic waves and L/2 is the length of the bolt.

When a stress is applied to the sample, both L and v change, resulting in a change in the resonant frequency. Therefore, based on eq. 3.3, the relationship between change in resonant frequency and load is:

$$\Delta f_n = -f_n \frac{L_{eff}}{L}\left(C_L + \frac{1}{E}\right)\frac{F}{A} \tag{3.4}$$

where, L_{eff} is the effective length, C_L is the acoustoelastic constant for longitudinal wave, E is Young's modulus, A is the cross section area.

The theoretical resonant frequencies of a bolt M24 with l_c = 80 mm are on the order of 25kHz. Since the order of the magnitude of the resonant frequencies is known, the transducer generates a range of frequencies of several kHz. The resonant frequency is recognized in the frequency response spectrum, because it is characterized by high amplitude (voltage) vibrations. Therefore, in contrast to the conventional ultrasound method and the velocity ratio method, which require a very accurate measurement of TOFs, in the Mechanical Resonance Frequency Shift method, it is sufficient that the sampling rate is such to reconstruct the input signal in a way that provides information about the amplitude of the vibrations. Based on the Nyquist frequency, this frequency can be over 100 kHz, on the order of some kHz or even MHz (the higher the sampling frequency, the better the resolution), which is lower than that of the other two acoustoelastic effect methods, but still quite high. In the following sections, the factors that affect the measurement of the frequency are presented.

3.4.2 Temperature

Temperature increase can cause thermal stresses, which result in an elongation of the bolt. Furthermore, a rise of the temperature results in a reduction of the ultrasound velocity. Both result in a reduction in the resonant frequency. If the temperature of the bolt is constant between stressed and unstressed readings, then no error is introduced in the preload force. However, if there is a change, the error depends on the temperature increase. As shown in Fig. A4 small variations in temperature, like these that take place in the short time when a bolt is tightened, do not influence much the force. For example, a temperature increase of 0.5 ˚C in the stressed state will result in an error in the force equal to 1.3%. However, if maximum accuracy is required, it is important checking the temperature before a measurement is taken.

Josi and Pathare developed a method based on phase detection to track the frequency shift of the mechanical resonance of the bolt [25]. A Voltage Controlled Oscillator (VCO) is used to emit signals of various frequencies and a phase detector compares the phase of the transmitted signal to that of the received signal. When their phase difference is zero resonance occurs and the VCO locks onto the resonant frequency. A temperature increase however causes a change in the phase of the signal. In that case a variable phase shifter is used which introduces a phase shift to the input signal in such a manner as to compensate for effects of temperature variations, provided that the relation between temperature variation and phase shift is known. It is therefore possible to keep the frequency constant even if the mechanical resonant frequency varies with the ambient temperature.

3.4.3 Residual stress

Residual stresses can affect the frequency and result in an error in the preload force. However, since the difference between the resonance frequencies in the stressed and unstressed state is measured, the influence of residual stresses will be the same for both measurements, provided that the transducer is placed on the same location on the head of the bolt on the stressed and unstressed state. Therefore, in that case it is possible to neglect their influence. However, if this is not the case, the position of the transducer on the head of the bolt plays a very important role, because it can introduce an error caused by the difference in residual stresses experienced by the wave in the unstressed and stressed state. In this case and making all the assumptions discussed in section 3.1.3, the average influence of residual stresses on the preload force (for loads between 140 – 300 kN) is presented in Fig. 3.6.

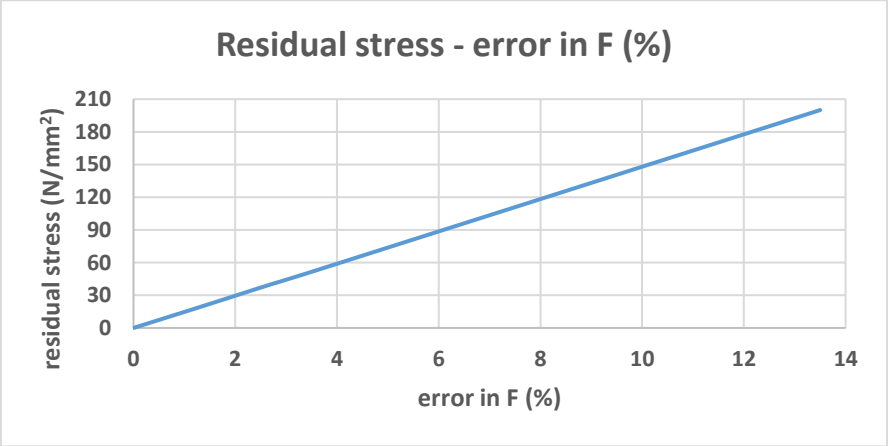

Figure 3.6: Influence of residual stress on preload

3.4.4 Influence of couplant

The couplant used to bond the transducer on the head of the bolt can affect the measurements. Changes in couplant's thickness between the unstressed and stressed readings can introduce an error in the preload force. For example, a 12μm variation in couplant's thickness leads to an error in the force equal to 1.6%, lower than that in the conventional ultrasound method.

3.4.5 Other factors influencing the estimated force

As shown in eq. 3.4, even if we measure accurately the resonance frequencies, it is required to determine the acoustoelastic constant, the effective length and Young's modulus. However, their uncertainties and especially the uncertainty in the effective length can introduce a high error in the preload force. Therefore, in order to reduce these uncertainties

calibration is performed. Furthermore, it is required that the surfaces of the bolt are flat and parallel so that reflection of the ultrasound wave can occur.

3.4.6 Discussion

The Mechanical Resonance Shift Method is a method based on the acoustoelastic effect, which relates the difference in the resonance frequencies in the unstressed and stressed state with the applied stress on a bolt. Compared to the conventional ultrasound method (which is the other method which includes measurements in the stressed and unstressed state of the bolt), it is less affected by temperature variations between the measurements. Provided that the transducer is placed on the same position for the stressed and unstressed measurements, the Mechanical Resonance Shift Method allows measurement of the frequencies by ignoring the influence of residual stresses. If not, the Mechanical Resonance Shift Method is less affected by residual stresses compared to the conventional ultrasound method. Flat and parallel surfaces are requirements for all the methods, whereas the influence of the couplant is lower for the Mechanical Resonance Shift Method. The required sampling rate is high, but lower compared to the other two methods, because it is easier working in the frequency domain than in the time domain. Finally, the instrument required for the application of this method, is not easy to be used in situ.

3.5. Piezoelectric Active Sensing Method

3.5.1 Theory

All surfaces are rough to different degrees and as a result, the contact between surfaces is restricted to discrete areas at the tips of the surface asperities, as shown in Fig. 3.7. In this respect, all bolted joints also develop partial contact at their imperfect interfaces. The applied torque on the bolt may change interfacial characteristics like true contact area. Once the interfacial characteristics changes are obtained, the tightness of the bolted connections can be determined.

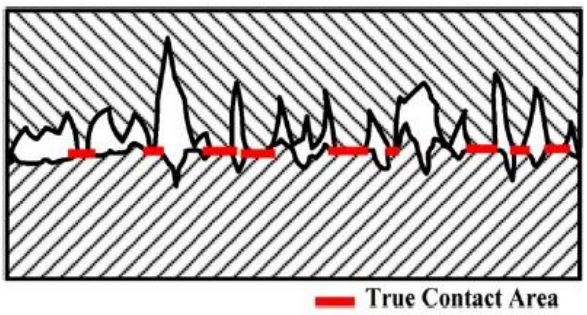

Figure 3.7: Microscopic view of imperfect interfaces [26]

The behavior of fastening the bolted joints can be regarded as imposing higher contact pressure at the imperfect interfaces. At these imperfect interfaces, a fraction of the nominal contact area, defined as a true contact area, is generated as shown in Fig. 3.7. The true contact area is known to be smaller than the nominal contact area. This true contact area varies with the contact pressure.

According to the sinusoidal surface model and the classic Hertz contact theory, the true contact area A_t and the contact pressure P have following relationship [26]:

$$A_t \propto C\sqrt{P} \tag{3.5}$$

where C is a constant.

Therefore, by increasing the fastening torque, the true contact area will increase and the wave will propagate across the interface with less energy loss. Two pieces of PZT (lead zirconate titanate) are bonded to the different sides of the interface as an actuator and a sensor, as shown in Fig. 3.8. PZT1, as an actuator, generates an ultrasonic wave that propagates across the interface, and then the signal is captured by PZT2, as a sensor. Propagating waves are the means of power transmission. As illustrated in Fig. 3.8, incoming waves are split into transmitted and lost waves at the microcontact interface. The transmitted wave energy is proportional to the true contact area, which is affected by the surface force generated by the bolt.

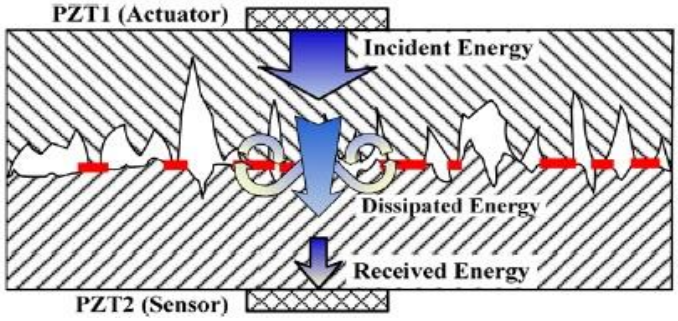

Figure 3.8: Energy transmission at the microcontact interface [26]

The active sensing method is based on the emission of a signal and measures the transient response of the structure with the aid of the PZT ceramics that enable actuating and sensing. For the received digital signal, after appropriate simplification, the signal energy can be expressed in the discrete time domain [t_s, t_f] as follows:

$$E_s = \frac{1}{f_s} \sum_{t=t_s}^{t_f} V^2[t] \tag{3.6}$$

where, V[t] and f_s denote the discrete sensor signal and its sampling frequency, respectively.

Therefore, by measuring the signal voltage of the received wave, the tightening of the connection can be evaluated.

3.5.2 Factors that affect the measurements

The relationship between the applied force or pressure between the plates and the true contact area between the plates, which is proportional to the transmitted energy requires calibration, based on eq. 3.5. Hence, it is important to know what factors may change the measured energy.

As mentioned, the transmitted energy increases with the increase of clamping force, because of the increase of the true contact area. Therefore, anything that happens in the contact area between the plates affects the amount of the transmitted energy. When the bolts in a connection are tightened, some of the asperities that define contact between the plates are plastically deformed and the true contact area reaches a maximum, even if the preload force on the bolts is increasing. In that case, the transmitted energy remains constant.

This was confirmed by Liu et al. who performed tests on four single bolted specimen with different dimensions and roughness by increasing the torque stepwise and measuring the transmitted energy. The characteristics of the specimen are shown in Table A2 in Appendix A. Experimental results for different fastening force levels are shown in Fig. 3.9.

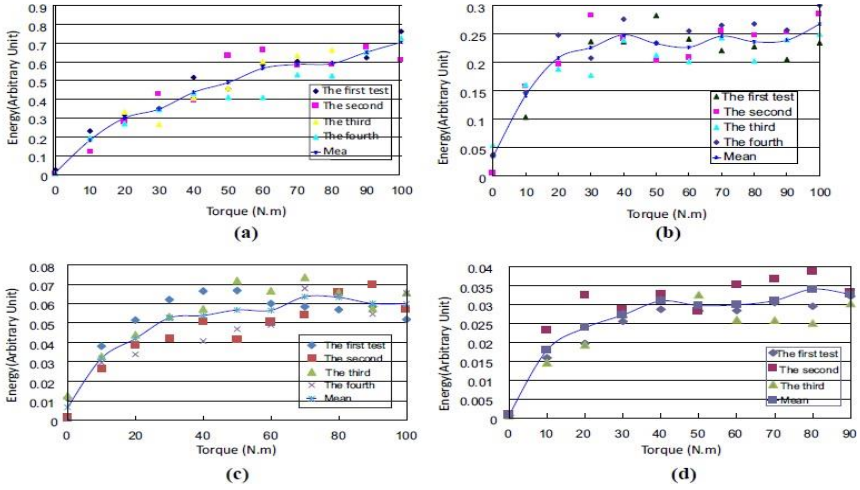

Figure 3.9: Transmitted energy trend in specimen 1, 2, 3, 4 [27]

It is clear that with increase of the torque level, the received signal energy also increases. However, the energy level achieves a constant over a certain torque level. This means that the maximum pressure below which the true contact area is proportional to the applied pressure is surpassed resulting in a maximum true contact area between the asperities and embedment of the plates during the tightening process. When this energy level is reached, the bolt is preloaded to a certain level resulting in a certain pressure between the plates. If saturation of the energy occurs at a preload level lower than the minimum required, then it is not possible to know if the bolt is preloaded over the minimum required preload. If saturation occurs at a preload level higher than the minimum required preload, then it is possible to know, based on calibration, that the bolt is preloaded at least to the force corresponding to the transmitted energy during saturation, which is over the $F_{p,C}$. Therefore, it is possible to evaluate the preload condition of a bolt during the tighteting procedure, but it has to be taken into account that since anything that happens in the contact area between the platets affects the measurements, factors like the surface roughness could change the amount of transmitted energy. Indeed, for specimen 1 and 2 (Fig. 3.9a and 3.9b) whose only difference is surface roughness, as shown in Table A2, there is a big difference in the transmitted energy values. For specimen 2 (Fig. 3.9b), which is characterized by a lower roughness than specimen 1 (Fig. 3.9a), the transmitted energy is lower and saturation of the energy occurs at a lower torque level. Therefore, for plates with a specific roughness, it is possible to know how much transmitted energy leads to a certain preload. If in situ measurements are performed with this method and the influence of neighboring already tightened bolts on the measurements is taken into account, then it is possible to estimate the preload applied on a bolt during the tightening procedure.

However, this method is suitable for estimation of the preload only during the tightening process. In case that the purpose of the test is to evaluate the tightness during the service life of the connection, given that the preload – transmitted energy (pressure) relationship is known, the embedment which takes place at the plates as a result of tightening the bolt, will

result in misleading conclusions, because the plastic (permanent) deformation of the asperities will not change the transmitted energy much, even if the pressure between the plates drops.

3.5.3. Discussion

The piezoelectric active sensing method is a method that evaluates the tightening of bolts by measuring the transmitted energy, which is proportional to pressure through the true contact area of the plates. The roughness of the plates, the distance from the neighboring bolts are some factors that affect the measurements. However, this method is suitable only for real time monitoring during the tightening process, as the embedment of the plates will affect the measurements obtained in case of periodic monitoring.

3.6. Strain Gauge Method

3.6.1 Theory

The most common method to measure the strain of a bolt is with a strain gauge. The strain gauge is glued in the shank of a bolt, as shown in Fig. 3.11 and it consists of a very fine wire arranged in a grid pattern, as shown in Fig. 3.10 [36], [37]. The grid pattern maximizes the amount of metallic wire subject to strain in the parallel direction. The cross-sectional area of the grid is minimized to reduce the effect of shear strain and Poisson strain. The grid is bonded to a thin backing, called the carrier, which is attached directly in the shank of the bolt. Therefore, the strain experienced by the bolt is transferred directly to the strain gauge, which responds with a linear change in electrical resistance. Strain gauges are available commercially with nominal resistance values from 30 to 3,000 Ω, with 120, 350, and 1,000 Ω being the most common values [36].

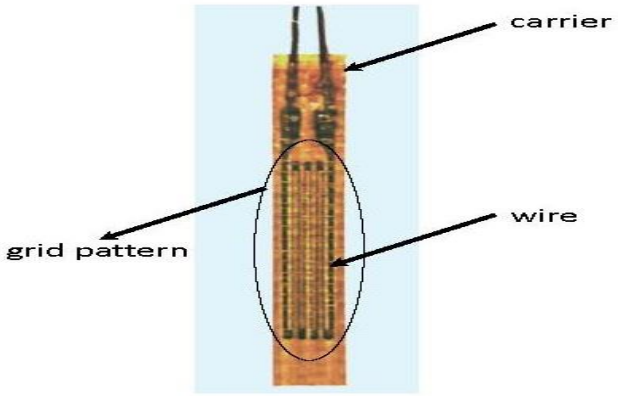

Figure 3.10: BTM strain gauge [37]

Figure 3.11: Strain gauge embedded [37]

Therefore, if the relationship between the change in strain and the change in resistance is known, it is possible to determine the strain applied on a bolt and then the force. A fundamental parameter of the strain gauge is its sensitivity to strain, expressed quantitatively as the gage factor (GF). Gage factor is defined as the ratio of fractional change in electrical resistance to the fractional change in length (strain) [36]:

$$GF = \frac{\frac{\Delta R}{R}}{\frac{\Delta L}{L}} = \frac{\Delta R}{R \cdot \varepsilon} \tag{3.7}$$

where ε is the strain, R is the electrical resistance of the wire, ΔR is the change of electrical resistance.

In practice, strain measurements rarely involve quantities larger than a few millistrain (εx10^{-3}). Therefore, to measure the strain requires accurate measurement of very small changes in resistance. These very small changes in electrical resistance are measured by using a Wheatstone bridge. As shown in Fig. 3.12, a supply voltage is supplied across the bridge, which contains four resistors and the output voltage is measured across the legs in the middle of the bridge. The output voltage is given by eq. 3.8.

$$V_o = V_s \frac{R_3 R_1 - R_4 R_2}{(R_2 + R_3)(R_1 + R_4)} \tag{3.8}$$

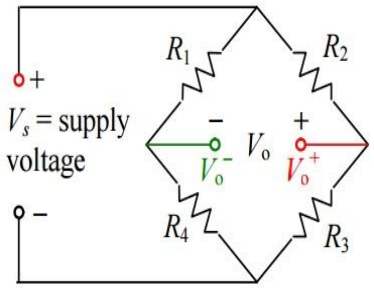

Figure 3.12: Wheatstone bridge

When the strain is obtained the force can be determined based on eq. 3.9:

$$F = A_{net} E \cdot \varepsilon \tag{3.9}$$

where, A_{net} is the net cross section are, E is Young's modulus and ε is the measured strain. In the following section, the factors that affect the measurements are discussed.

3.6.2 Factors that affect the measurements

Temperature variations is the most serious error source in the practice of strain measurement with a strain gauge. Provided that the strain gauge is installed successfully in the shank of the bolt, in addition to the desired measurement signal indicating strain, the strain gauge also produces a temperature – dependent measurement signal, which may result in an apparent strain, giving an error in the strain gauge measurement. There are four effects that may cause this error:

- Thermal expansion of the bolt

- Temperature – dependent change in the strain gauge resistance
- Thermal expansion of the strain gauge measuring grid foil
- Temperature response of the connection wires

For a typical strain gauge attached to a steel test material, the apparent strain as a function of the temperature is shown in Fig. 3.13.

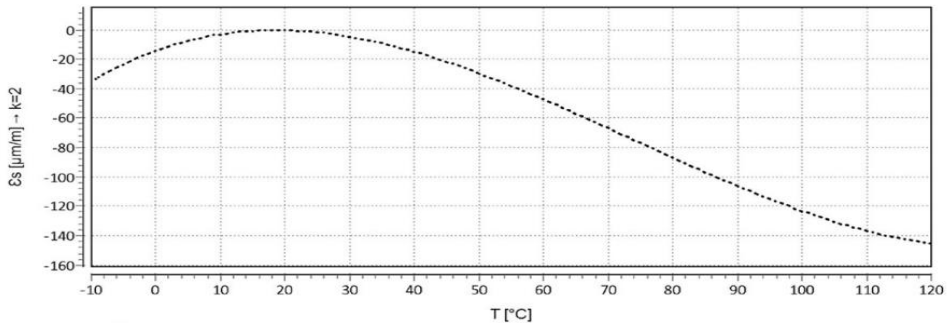

Figure 3.13: Apparent strain vs temperature [39]

As shown in Fig. 3.13, for temperature variations close to room temperature, the apparent strain is very low. For lower and higher temperature, the apparent strain increases, which results in an increase of the error in the strain.

However, there is a way to compensate for temperature related effects. As discussed in section 3.6.1, the change in the electrical resistance is measured by using a Wheatstone bridge. Based on Fig. 3.12, when the electrical resistance of the four resistors is the same, the bridge is balanced and $V_o = 0$. However, when at least one of the electrical resistances changes, it results in a $V_o \neq 0$ and this resistor is called active resistor. Therefore, by measuring the output voltage, it is possible to determine the change in the resistance of the strain gauge/resistor due to a change in the strain. Depending on the type of the Wheatstone bridge configuration which is used, there are three types of strain gauge configurations: quarter bridge, half bridge and full bridge. Quarter bridge includes one active resistor/strain gauge, half bridge includes two active resistors and full bridge includes four active resistors. The temperature variations affect the electrical resistance of the resistors, which means that if a quarter bridge is used the electrical resistance of the one and only active resistor will change because of temperature variations, resulting in an error. However, when four active resistors are used in a full Wheatstone bridge configuration, all the resistors change their resistance in the same proportion, thus cancelling the effects of temperature change.

3.6.3 Bolt strain gauges series BTMC

Measuring the preload force of a bolt by using strain gauges is an old technique. However, the installation of a strain gauge was not always an easy process. In order to glue the strain gauge in a bolt, a specific type of adhesive was used. The hardening of this adhesive required the bolt to be subjected under a specific vacuum treatment, to ensure that no air was left inside the adhesive and afterwards, the bolt had to be given a heat treatment to allow for curing of the adhesive. Recently, in order to facilitate the installation of a strain gauge, a new type of adhesive was created, called CN adhesive, which can harden by taking up water from the environment. The amount of water required to cure the CN adhesive is included in the upper part of the strain gauge, making the installation procedure easier and faster.

3.6.4 Discussion

The strain gauge method offers the possibility of determination of the force in the bolt by measuring the strain in the shank. It requires a time consuming installation process, however the development of a new type of adhesive can simplify it. The strain gauge measurements are affected by temperature variations, but the use of a full Wheatstone bridge is a simple way to diminish their influence. The feasibility of performing in situ measurements with the strain gauge method is further discussed in chapters 4 and 5.

3.7. Conclusion

In this chapter, five methods and their potential on performing in situ measurements for the determination of the preload of High Strength Friction Grip Connections was discussed. In the following table, the influence of several factors on the measurements, the duration of the installation procedure and the required material constants which should be determined if calibration is not performed, are described. The active sensing method is not included, since this method is not suitable to determine the residual preload of the bolts, because of the influence of the embedment of the plates on the measurements.

Table 3.1: General description of influencing factors and requirements for the measurements

	Installation process	Temperature compensation	Residual Stress influence	Couplant influence	Smooth/flat surface	Material Constants, L_{eff}	Environmental noise influence
Conventional Ultrasound Method	short	requires tests	no, for no motions of the transducer	yes	yes	C_L, E, L_{eff}	high
Velocity Ratio Method	short	requires tests	yes	yes	yes	C_L , C_T, E, L_{eff}	high
Mechanical Resonance Frequency Shift Method	short	requires tests	no, for no motions of the transducer	yes	yes	C_L, E, L_{eff}	lower
Strain Gauge Method	time consuming	Wheatstone bridge	no	no	no	E, d	no

As shown in Table 3.1, all the acoustoelastic effect methods, which are sensitive to temperature variations, require tests to compensate for the temperature related effects. All these methods are influenced by variations in couplant's thickness and residual stresses, require smooth and flat surfaces and they are affected by the environmental noise. If calibration is not performed, then the determination of numerous material constants and the effective length of the bolt is required, which is characterized by a high uncertainty. However, the installation process is short and simple.

The strain gauge method requires a time consuming installation, but it is affected only by temperature variations. However, in contrast to the acoustoelastic methods which require tests to determine the influence of temperature on the measurements, the temperature influence on the strain gauge measurements can be easily compensated for by using a full Wheatstone bridge. Determination of the force based on the model is much easier with the strain gauge method, because it requires measurement only of the shank's diameter and an assumption on Young's modulus value, instead of measurement of numerous complicated material constants. Finally, this method is not affected by noise or residual stresses.

In conclusion, the acoustoelastic effect methods are mainly affected by factors which are governing the in situ measurements (temperature, noise) or factors difficult to control, like couplant's thickness variations, which make any estimation on the accuracy of these methods difficult. Compensation for temperature or stress effects requires time consuming tests. The strain gauge method offers a quite simple compensation for temperature variations and the new type of strain gauges simplifies the installation process. Therefore, given that a strain gauge is properly installed in the shank of the bolt, it is possible to determine accurately the force. The feasibility of performing in situ measurements with this method is discussed in chapters 4 and 5.

4. STRAIN GAUGE METHOD AND PRELIMINARY TESTS

The principle on which the operation of the strain gauge is based was described in section 3.6. The next step is to test the feasibility of this method to perform in situ measurements. Many researchers have claimed that it is not possible to perform in situ meaurements with the strain gauge method. So, in this chapter the results of the preliminary tests, performed in the lab with the new type of strain gauges (series BTMC), which makes the installation process simple, as described in section 3.6.3, are presented. The purpose of these tests was to imitate the in situ conditions. For this reason, four bolts were tested: B1 (installation of a strain gauge in a vertical bolt), B2 (installation of a strain gauge in an already tightened vertical bolt), B3 (installation of a strain gauge in a horizontal bolt) and B4 (influence of drilling oil on the strain gauge measurements). All strain gauges were calibrated to obtain the relationship between the strain in the bolt and the force on the bolt. The calibration tests were repeated three times to determine the variation of the calibration factor of the same bolt. Then, the experimental strain was compared with the theoretical strain, which was determined based on the actual shank diameter, the nominal dimensions and three values of Young's modulus, to obtain their influence on the determination of the strain. In the next section, the installation of a strain gauge in the shank of a bolt is described.

4.1 Installation of the strain gauge

In order to measure the strain of a bolt, which is subjected to a tensile load, the strain gauge is installed and glued in the shank of the bolt. Therefore, it is very important that the strain gauge be properly placed into the bolt, so that the strain is accurately transferred from the bolt, through the adhesive and strain gauge backing, to the wire itself. So, in this section the installation procedure of a strain gauge in the shank of the bolt is described. The same installation procedure was followed for all the bolts which were tested for the preliminary tests.

As reported in the manual, the gauge has to be embedded into a hole of 2 mm diameter, drilled at the center of the bolt head with CN adhesive in a depth of 40 mm, as shown in Fig. 4.6. The dimensions of the strain gauge used are shown in Table 4.1 and Fig. 4.5 [37].

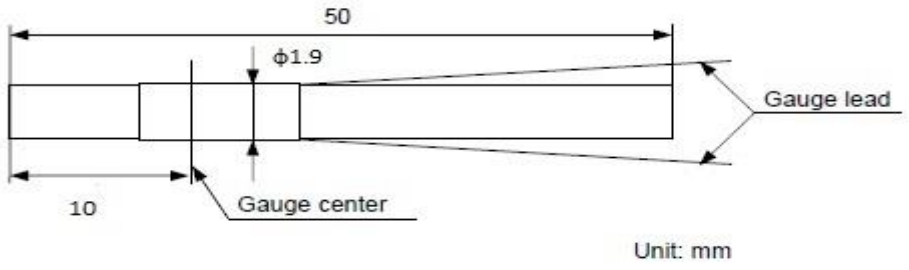

Figure 4.1: Dimensions of BTMC strain gauge [37]

Table 4.1: Dimensions of BTMC strain gauge [37]

Type	Gauge length (mm)	Gauge center position (mm)	Backing diameter (mm)
BTMC-3-D20-006LE	3	10	ϕ1.9

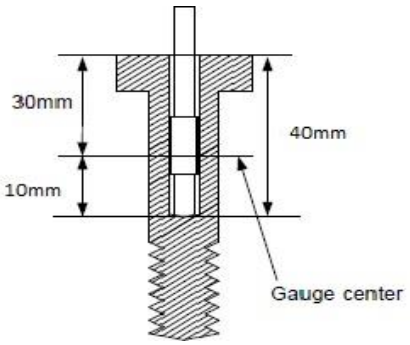

Figure 4.2: Installation depth of BTMC strain gauge

So, the first step is to drill a 2 mm diameter straight hole on the head of the bolt. In order to ensure that the hole will be straight and drilled in the center of the head of the bolt, a hexagonal steel die is used as a guide, with a hole drilled in the center of its upper side, designed in such a way to fit on the head of the bolt, as shown in Fig. 4.7.

Figure 4.3: Hexagonal steel die on the head of the bolt

Then, the hexagonal die was clamped on the head of the bolt in order to prevent any movement during the drilling of the hole by using a hex wrench key, as shown in Fig. 4.4.

Figure 4.4: Clamping of the hexagonal die on the head of the bolt

After the hexagonal die is clamped on the head of the bolt, the drilling process begins. To drill the hole, a drill is used and two drill bits of different length, as shown in Fig. 4.5. The shorter one is used in the beginning of the drilling process, because it is stiffer and it can withstand higher pressure compared to the longer one. The longer one is used to increase the depth of the hole. In order to make sure that the required depth of 40 mm, according to the technical specifications is not surpassed, a piece of tape is placed on the drill bit at the required length, as shown in Fig. 4.6.

Figure 4.5: Drill and drilling bits used in drilling process

Figure 4.6: Drilling bit with a tape at the length of 40 mm

As the drilling progresses, it is possible to see steel dust pieces coming out of the hole, which is a sign that the depth of the hole grows, as shown in Fig. 4.7. After the whole length of the short drilling bit is in the hole, the drilling process continues with the longer one, as shown in Fig. 4.8.

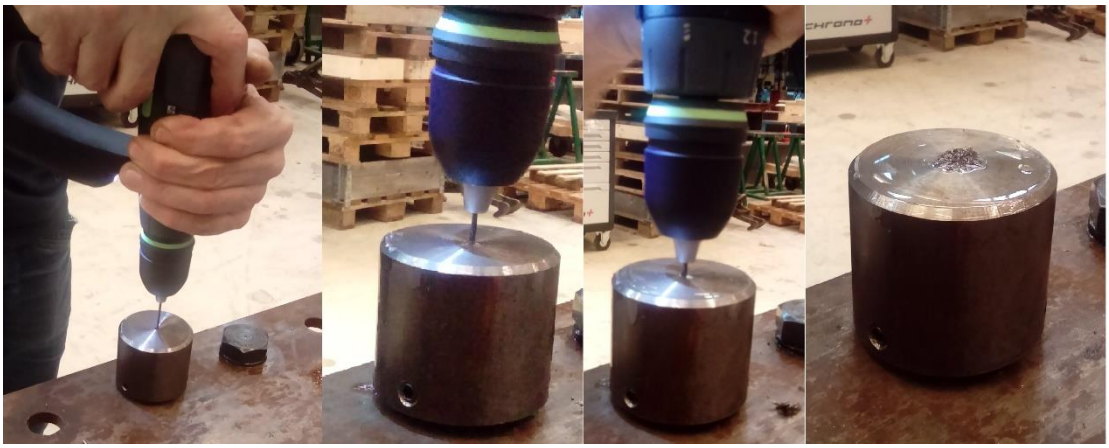

Figure 4.7: Drilling process with the short drill bit

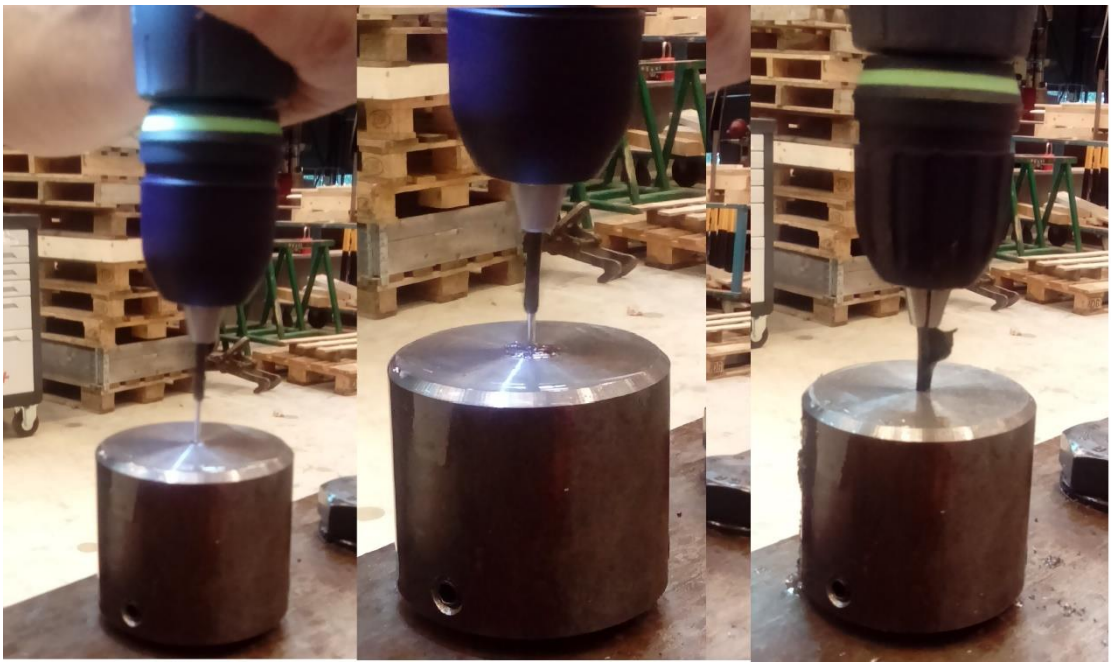

Figure 4.8: Drilling process with the long drill bit

After the required depth is reached, the drill and the hexagonal die are removed. The hole on the head of the bolt is shown in Fig. 4.9.

Figure 4.9: Hole on the head of the bolt

After the drilling of the hole (and before the installation of the strain gauge), the hole had to be cleaned. A solvent was poured into the hole using a syringe to wash out dust. To remove remainders in the hole, a solvent-dampened tissue was used which was rolled on a drill bit. Then, the remaining solvent in the inner hole was removed with a clean tissue. The removal of the solvent is of high importance, because if solvent or dust remain in the hole, curing failure of adhesive may occur. After that, the head of the bolt was cleaned.

Now that the hole is cleaned, as shown in Fig. 4.10, the installation of the strain gauge can begin. In Fig. 4.11 the strain gauge and the gauge wires, which transfer the changes in the electrical resistance of the strain gauge due to strain to the terminal are shown.

Figure 4.10: Strain gauge hole

Figure 4.11: BTMC strain gauge

In the next step the adhesive is injected in the hole by a syringe, as shown in Fig. 4.12.

Figure 4.12: CN adhesive

Immediately after filling the adhesive into the hole, the gauge was inserted until the bottom of the gauge hit the bottom of the hole. The strain gauge is being held from its upper part by a tweezer and installed with attention in the hole in such a way that the wires stay out of the hole in order to be connected later with the terminal, as shown in Fig. 4.13.

Figure 4.13: Installation of the strain gauge

Then, the bolt was kept calm in upright position at room temperature for 24 hours to allow for curing of the adhesive. After the adhesive was cured, the pipe extruded from the hole was

cut. After cutting the pipe, a connecting terminal was installed and connected to the gauge lead and an instrumentation lead wire was connected to the terminal.

4.2 Test setup

A BTMC strain gauge with a resistance of 120 Ω was installed in the shank of the bolts (B1, B2, B3, B4). M24 bolts were used of a quality class 10.9. The bolts were lubricated and they were placed in a Skidmore – Wilhelm device with a clamping length of 50 mm. Washers of 4 mm thickness were used.

The Skidmore – Willhelm instrument is shown in Fig. 4.14, 4.15. The instrument consists of hydraulic cylinder with a hole through the middle. The bolts runs through the hole and the nut and the washers are added and the bolt is tightened. This raises the pressure in the cylinder and a calibrated pressure gauge interprets the increase in pressure in terms of clamping force.

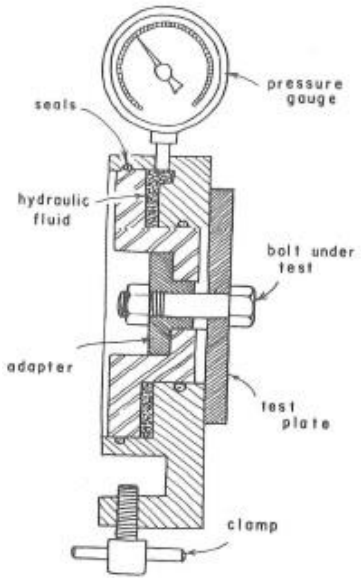

Figure 4.14: Skidmore – Wilhelm instrument [1]

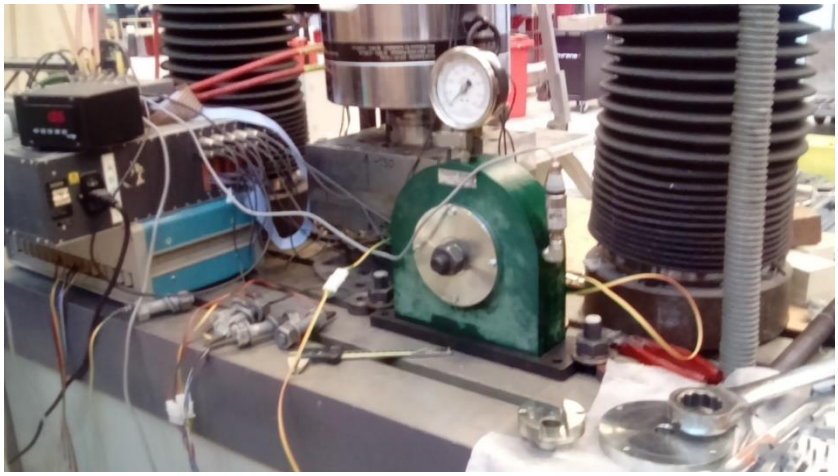

Figure 4.15: Skidmore – Wilhelm device

Then the bolt was tightened using a pneumatic tightening device, as shown in Fig. 4.16. The force applied on the bolt was shown on a screen connected to the tensile force instrument, as shown in Fig. 4.17. For each loading step, the strain gauge measured the strain, which was shown on the screen of an amplifier, as shown in Fig. 4.18. The strain gauge was connected

with a quarter bridge configuration, as the test was performed indoors, where no temperature variation is expected.

Figure 4.16: Pneumatic tightening device

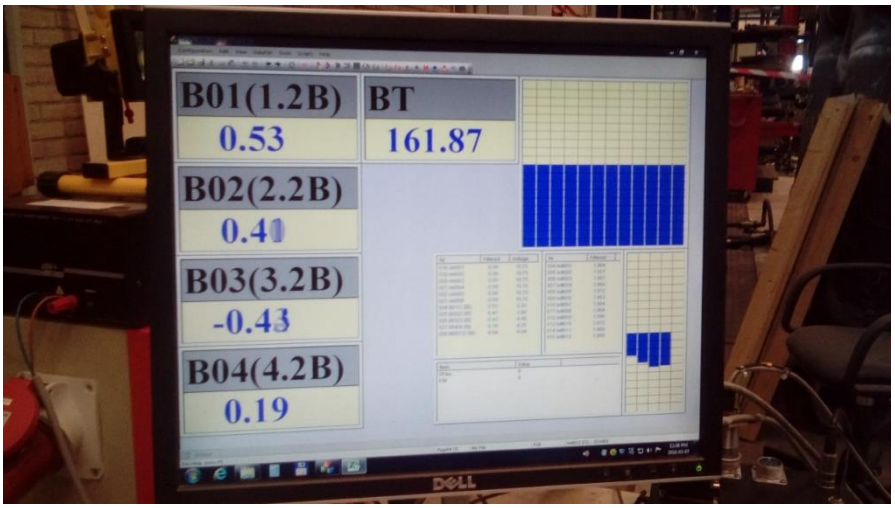

Figure 4.17: Force applied on the bolt

Figure 4.18: PEEKEL amplifier

4.3 Preliminary tests

As it is already mentioned, the purpose of the tests is to imitate the in situ conditions by installing a strain gauge in a vertical bolt (B1), in an already tightened bolt (B2), in a horizontal

bolt (B3), because in this case there is a danger of flowing out of the adhesive, before the hardening is completed. Bolts B1, B2, B3 are shown in Fig. 4.19, 4.20 and 4.21, respectively.

Figure 4.19: M24 bolt (B1) with implanted strain gauge

Figure 4.20: M24 bolt (B2) in tensile force instrument

Figure 4.21: Bolt B3 with implanted strain gauge

Furthermore, in preparation for the in situ measurements, several practical issues were considered. The most important was about possible problems that may arise during the drilling of the bolt, because of the environmental conditions. Therefore, in order to make drilling of the bolt easier, it was decided that drilling oil should be used. However, this may affect the gluing of the strain gauge in the hole, especially in case that the hole is not cleaned sufficiently. Subsequently this may affect the measurements. Therefore, it is necessary to test

the influence of drilling oil on the strain gauge measurements and modify the cleaning procedure of the hole, in order to ensure that no remainder of the drilling oil is left (B4).

Regarding the installation of bolt B4, the same procedure described in section 4.1 is followed, with the only difference that drilling oil is used in order to facilitate the drilling of the hole. After the hexagonal die has been clamped on the head of the bolt, some drilling oil is injected into the hole of the hexagonal die until it reaches the surface of the head of the bolt, as shown in Fig. 4.22. Then, the drilling process begins, as described in section 4.1. During the drilling process more oil is added in the hole to facilitate the process.

Figure 4.22: Injection of drilling oil

After the drilling of the hole is completed, the next step is to clean the hole. This is done in two ways. The first way is to inject a solvent with a syringe to wash out the dust. The second way, is to use an air driven machine which blows in the hole through the needle of a syringe, as shown in Fig. 4.23. The needle is inserted into the hole and by blowing high pressure air the remaining solvent, oil and dust are removed, as shown in Fig 4.24.

Figure 4.23: Air driven machine

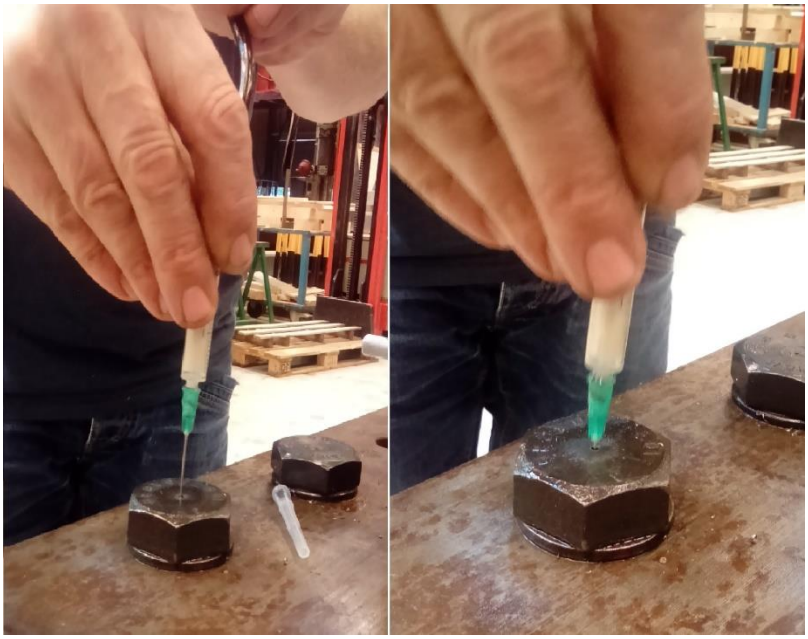

Figure 4.24: Cleaning the hole with the air driven machine

Then, the strain gauge is installed in the shank of the bolt and it is left for 24 hours to allow hardening of the adhesive. The installation procedure is completed.

After the strain gauges were installed in the shank of the bolts, calibration was performed to derive the relationship between the force applied on the bolt and the strain in the shank of the bolt. Calibration is needed in order to derive the unique relationship for each bolt, between the force and the strain, taking into account the actual position of the strain gauge in the shank of the bolt, the actual dimensions of the bolt, Young's modulus etc. Therefore, calibration is a way to guarantee the accuracy with which the strain gauge can measure the force on the bolt. The calibration was repeated three times to account for relaxation effects of the bolts. Each time the bolts were tightened gradually to a maximum tensile force approximately equal to the bolt preloading force given by the Eurocode ($F_{p,C} = 0.7 \cdot f_{ub} \cdot A_s$). This force is approximately 240 kN for M24 bolts. Then, they were untightened gradually back to zero force. For each calibration line, the slope was derived, which is called calibration factor (the ratio between the force on the bolt and the strain in the shank of the bolt). The comparison of the three calibration factors of each bolt, will show the uncertainty of the method.

Then, the theoretical strain for each load step was determined based on the actual diameter of the bolt, the nominal dimension, dimensional toleraces and E = 200 , 210, 220 GPa to check the experimental data and obtain the influence of these assumptions on the difference between the theoretical and experimental strain.

4.4 Results

The calibration lines of all strain gauges were drawn according to linear least squares and they can be found in Appendix B. The calibration line of bolt B1, which was derived from the first test is shown in Fig. 4.25 and the calibration factors of all the strain gauges are shown in Table 4.2.

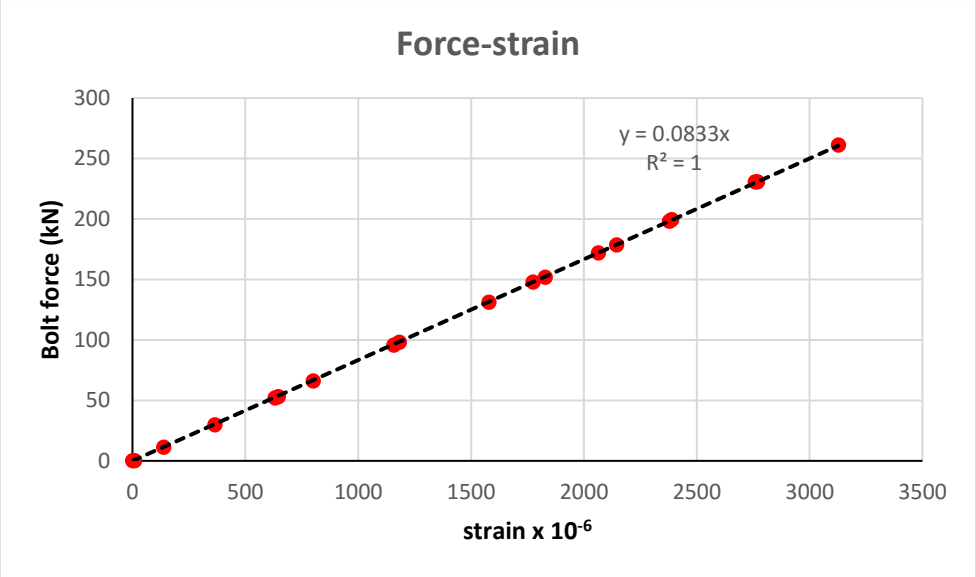

Figure 4.25: Force-strain diagram obtained for the first test (B1)

Table 4.2: Calibration factors of B1, B2, B3, B4

B1			
	Test 1	**Test 2**	**Test 3**
calibration factor	0.0833	0.0836	0.0837
B2			
calibration factor	0.0847	0.0845	0.0848
B3			
calibration factor	0.0868	0.0869	0.0867
B4			
calibration factor	0.0917	0.0894	0.0892

The values of coefficients of determination R^2 were between 0.9998 and 1 for all strain gauges. The high values of coefficient of determination R^2 indicate that there is a high strength of linear association between the applied force F and the measured strain ε. The difference of calibration factors of the same bolt is very low and it is characterized by a coefficient of variation equal to 0.25%, 0.18%, 0.12%, 1.5% for bolt B1, B2, B3 and B4, respectively. The difference of calibration factors of different bolts is much higher, but it is reasonable as these four bolts do not come from the same batch and they are also characterized by different actual dimensions or different position of the strain gauge in the shank of the bolt.

Regarding bolt B2 (installation of a strain gauge in a vertical tightened bolt), after the hardening of the adhesive was completed and before calibration is performed, a torque wrench was used to loosen the tightened bolt. The measurement of the strain gauge was shown on the screen of the strain gauge amplifier. Before loosening the bolt, the measured strain was $11 \cdot 10^{-6}$ and after loosening the bolt, the measured strain was $1776 \cdot 10^{-6}$, so the total change of strain was $1765 \cdot 10^{-6}$. The residual preload of bolt B2 was determined based on the actual and nominal dimensions and E = 210 ± 10 GPa. Based on the strain gauge measurement, the resulting stress is:

$$\sigma = \mathrm{E} \cdot \varepsilon = 210000 \cdot 1765 \cdot 10^{-6} = 371 \ \mathrm{N/mm^2}$$

with an uncertainty because of Young's modulus variations:

$$\Delta\sigma = \varepsilon \cdot \Delta\mathrm{E} = 1765 \cdot 10^{-6} \cdot 10000 = 17.65 N/mm^2 .$$

The actual diameter of the shank of B2 was measured, at the location where the strain gauge was installed. Based on these and the nominal dimensions and $\mathrm{A_{net}} = \pi \frac{\mathrm{d}^2}{4} - \pi \frac{2^2}{4}$, the following are obtained:

d_{nom} = 24 mm

The net cross section area is A_{net} = 449.25 mm^2.

The force is F = σ · A_{net} = 371 · 449.25 = 167 ± 8 kN

d_{max} = 24.84 mm

The net cross section area is A_{net} = 481.47 mm^2.

The force is F = σ · A_{net} = 371 · 481.47 = 179 ± 8 kN

d_{min} = 23.16 mm

The net cross section area is A_{net} = 418.13 mm^2.

The force is F = σ · A_{net} = 371 · 418.13 = 155 ± 8 kN

Then, the actual diameter of bolt B2 was measured and it was found equal to 23.22 mm. The force based on the actual diameter is:

d_{actual} = 23.22 mm

The net cross section area is A_{net} = 420.32 mm^2.

The force is F = σ · A_{net} = 371 · 449.25 = 156 ± 8 kN

Therefore, it was shown, that it is possible to determine the force on a bolt without performing calibration. The spread in the resulting force for determination based on the nominal dimensions is 12%, whereas the spread for determination based on the actual diameter is 5%.

These were also confirmed by comparing the strain gauge strain with the theoretical strain based on the actual, nominal dimensions and E = 210 ± 10 GPa for all bolts. The theoretical strain for each calibration test is presented in Appendix B. It was found that for determination of the theoretical strain based on the actual diameters of the bolts, the average difference from the strain gauge strain varies from 2% to 12% (depending on the assumption on E modulus), leading to a spread equal to 5% and that for determination based on the nominal dimensions the average lowest difference and the average highest difference is 1% and 23%, respectively, resulting in a spread equal to 11%.

4.5 Conclusion

In chapter 4, the feasibility of performing in situ measurements with the strain gauge method was examined, by imitating the in situ conditions in the lab. A strain gauge was successfully installed in a vertical untightened bolt, showing by performing calibration, that there is a linear

relationship between the applied force on the bolt and the strain gauge measurement in the shank of the bolt. Furthermore, it was shown that a strain gauge can also measure the strain of an already tightened bolt. Regarding the installation procedure, it was shown that a strain gauge can be successfully installed in a horizontal bolt and the use of drilling oil which facilitates the drilling of the bolt has no effect on the measurements. The calibration of each strain gauge was repeated three times, showing a maximum measured variation in the calibration factor equal to 1.5%. All calibration lines were characterized by a high degree of linearity and the difference observed for calibration lines of different bolts, is considered reasonable due to differences in the material, the actual dimensions of these bolts and the actual position of the strain gauge in the shank.

Furthermore, the influence of the nominal dimensions, dimensional tolerances and Young's modulus assumption on the determination of the force was examined, by comparing the experimental with the theoretical strain. This comparison leads to the conclusion that there is a high influence of the nominal dimensions and Young's modulus assumption, on the theoretical strain, resulting in a maximum difference equal to 23% from the strain gauge strain. This will be further examined in chapter 6.

5. IN SITU MEASUREMENTS – ANALYSIS OF THE RESULTS

After the strain gauge method is tested under laboratory conditions and seems to be an efficient way of determining the preload force on a bolt, this method is going to be tested under actual practice conditions. After having asked permission from Ministry of Infrastructure and the authority which is responsible for the design, construction, management and maintenance of the main infrastructure facilities in the Netherlands, the Rijkswaterstraat, the Middachterbrug bridge was chosen to perform the in-situ measurements. Middachterbrug was built in 1974, and for this reason it was considered important to know the residual preload in one of its connections. The bridge and the tested connection, which is a bottom flange connection of an inverted T beam are shown in Fig. 5.1 and 5.2. The in-situ measurements were completed within three days. The strain gauges were installed in the shank of the bolts and the bolts with a strain gauge in their shank were loosened to determine the residual strain and then they were replaced by new bolts. In this chapter, the procedure which was followed in situ and in the lab, in order to convert the strain gauge measurements to force, is described. Furthermore, the initial preload is estimated based on the tests which were performed in the lab and it is compared with the expected (theoretical) values. Lastly, two ways of achieving the estimated initial preload are discussed.

Figure 5.1: Middachterbrug

Figure 5.2: The tested connection

5.1 The connection

A bottom flange connection of an inverted T beam is tested. Based on the design plans, the connection consists of two cover plates of 26 mm thickness, a main plate with a thickness

equal to 32 mm and two washers with a thickness of 4 mm, resulting in a clamping length equal to 92 mm, as shown in Fig. 5.3. 84 bolts M24 of a grade 10.9 and a nominal length of 120 mm hold the plates together. In Fig. 5.4 the dimensions of the connection are shown.

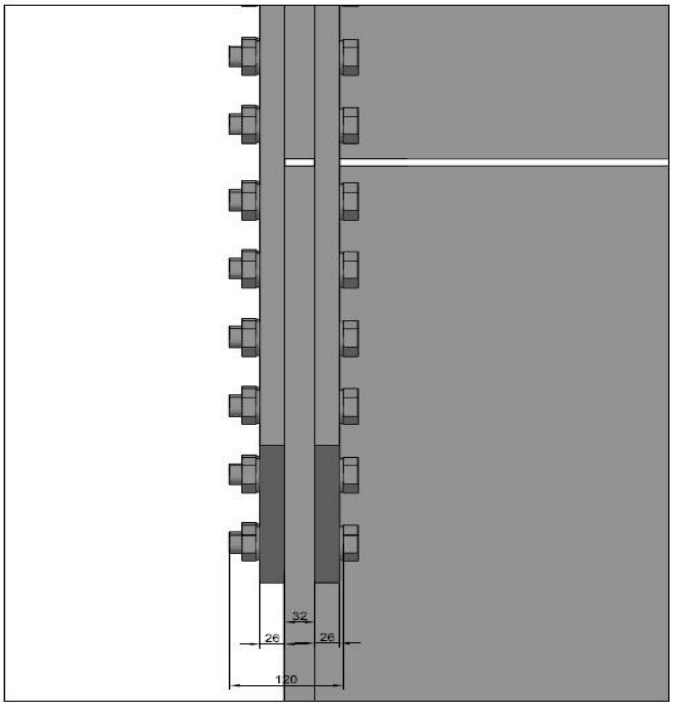

Figure 5.3: Side view of the tested connection

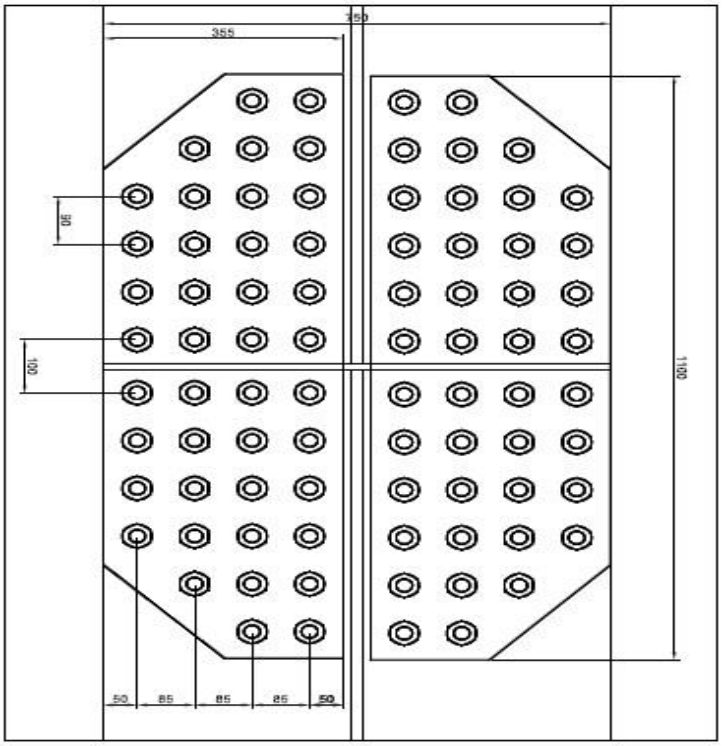

Figure 5.4: Plan view of the tested connection

5.2 Procedure

Sixteen strain gauges were used for the in situ measurements. Therefore, 16 bolts had to be chosen in a way that the measurements could provide us with as much information as possible about the residual preload of these bolts. The strain gauges are going to be installed in the shank of the bolts and then the bolts will be loosened to obtain the change of the strain in the shank of the bolts. Then, the tested bolts will be replaced by new bolts, which will be tightened by the combined method. Based on these measurements the residual preload of the bolts will be determined based on calibration of the implanted strain gauges.

The next step is to choose the 16 bolts out of the 84 bolts in the connection. The only information about the bolts of the connection is that they were tightened by the torque or the combined method. Therefore, based on the fact that all the bolts were tightened by the same method and that the bolts of each quadrant were subjected to the same external load, the preload loss of each bolt in each quadrant will be similar to that of the counterpart bolts located at the other quadrants. For example, each of the two bolts of the top line of bolts in the upper left quadrant, is expected to have the same losses as each of the top line bolts that belong to the upper right quadrant or the bottom line bolts of the lower left and right quadrants. Therefore, if the residual preload of each bolt in one quadrant and the residual preload of their counterparts in the other quadrants is known, it will be possible to reach a conclusion about the scatter in the initial preload applied on these bolts. For this reason, it was decided to test four bolts in one quadrant and their counterparts in the other three quadrants.

The next step is to choose these 4 bolts out of the 16 bolts in each quadrant. There are two questions that need to be answered: first, what is the relationship between the residual preload of bolts of the same vertical row. In order to give an answer to that question, two bolts in the same vertical row of bolts were tested.

The second question is about the influence of tightening a bolt on the neighboring bolts. It is expected that the tightening of a bolt will result in a loss of preload of the adjacent bolts. Since four bolts were tested in each quadrant and each of these bolts was replaced by a new bolt which was tightened by the combined method, it was important to know how the tightening of each new bolt influences the other bolts. This information could be obtained by preloading a new bolt and looking at how it affects the strain gauge signal of the other bolts. Therefore, in each quadrant a different tightening sequence was chosen, in a way that in the end of the process the influence of tightening of each new bolt on the other bolts is known. In Fig. 5.5 the tested bolts and their numbering is presented. For example, if the first bolt which is replaced in the upper left quadrant is bolt A3, the influence of tightening a new bolt (the replacement of A3) on bolts A1, A2 and A4 is recorded. Then, we continue with bolt A2. However, its influence on bolt A3 cannot be measured, since the new bolt A3 does not have an implanted strain gauge. We can see that influence by choosing to loosen first bolt B2 (in the upper right quadrant), replace it with a new bolt and record its influence on bolt B2, B1, B4 and so on for the rest of the bolts in all quadrants.

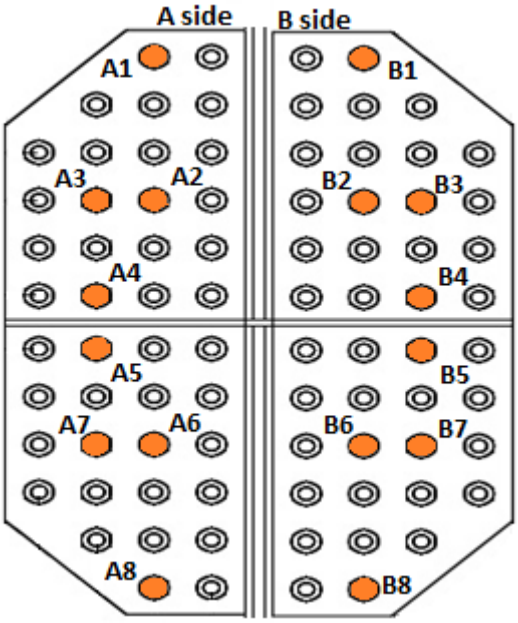

Figure 5.5: Tested bolts and their numbering

The in situ measurements started on October 31 and were completed on November 2. On the first and second day, the strain gauges were installed in the bolts and on the third and last day the bolts were loosened and the measurements were obtained.

In order to drill a hole in the head of the bolts to install the strain gauges, the painting layer had to be removed with the tool shown in Fig. 5.6. Then a hole was drilled in the head of the bolts. Drilling oil was used, which made the drilling process easier. Then, the hole was cleaned by injecting a solvent with a syringe to wash out the dust. At the second stage of the cleaning process, the air driven machine shown in Fig. 5.7 was used, which blew in the hole through the needle of a syringe in order to remove any remaining dust or drilling oil, as described in chapter 4.

Figure 5.6: Paint removal tool

Figure 5.7: Air driven machine

After having injected the adhesive in the hole, the strain gauges were inserted in the shank. Then, the bolts were left for 48 hours to allow hardening of the glue. Some of the strain gauges were installed in the second day, so the time for hardening of the glue was 24 hours. The gauge leads were connected with the wire connectors. In Fig. 5.8, 5.9, 5.10 the bolts after the installation of the strain gauges are shown.

Figure 5.8: Bolts after the installation of the strain gauges

Figure 5.9: Bolt after the installation of the strain gauge

Figure 5.10: The connection after the installation of the strain gauges

On the third day, the strain gauges were connected with the terminal, using a full Wheatstone bridge configuration, which cancels the effects of temperature variation, as it is already explained in the previous chapter. For the in situ measurements the full Wheatstone bridge shown in Fig. 5.11 was used with three resistors responding only on changes because of temperature variations and it was attached on the head of the bolt so that the three resistors experience the same temperature varations as the fourth resistor/strain gauge which was inserted in the shank of the bolt.

Figure 5.11: Full Wheatstone bridge

Therefore, by using a full Wheatstone bridge configuration, the error due to temperature variations is avoided. Furthermore, the readings were in voltage, which means that they must be converted into microstrain based on the gage factor k (ratio between change in resistance and strain) which is given by the manufacturer of the strain gauges.

The measurements started by loosening the nut of the first bolt with a hydraulic torque wrench by holding the head of the bolt stationary with another wrench, as shown in Fig. 5.12. When the nut was completely loosened the resulting voltage signal was received in a laptop which was connected with the terminal, as shown in Fig. 5.13, 5.14.

Figure 5.12: Loosening the nut with a hydraulic torque wrench

Figure 5.13: Loosened bolts connected with the terminal

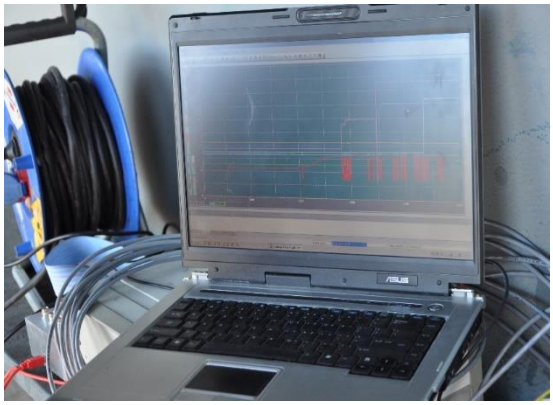

Figure 5.14: Voltage signals of the strain gauges

After the bolt with the implanted strain gauge was loosened, a new bolt was tightened with a hydraulic torque wrench by the combined method. In Fig. 5.15 the marked nuts and bolts are shown, to check whether the nuts were rotated 90 degrees. Before the new bolt was tightened, the surface of the plate near the hole was ground to remove any layers which would result in a non-perpendicularity between the plate surface and the bolt axis, as shown in Fig. 5.16.

Figure 5.15: Marked nuts, bolts after the combined method was applied

Figure 5.16: Grinding of the plate surface

Figure 5.17: New bolt tightened on the connection

This procedure was repeated for all the bolts of the connection. In Fig. 5.18 one of the sides of the connection with the new bolts is shown and in Fig. 5.19 the removed bolts with the implanted strain gauges are shown, which were taken to the lab to perform calibration.

Figure 5.18: One side of the connection after the measurements

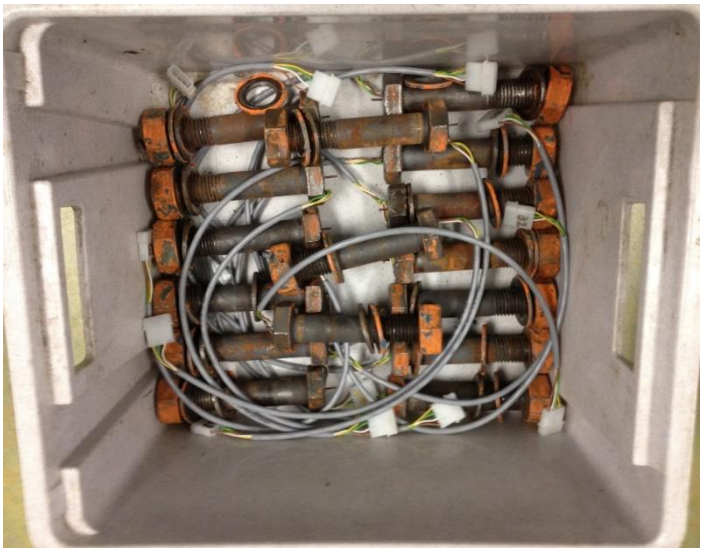

Figure 5.19: Bolts removed from the connection

5.3 Results

The measurements were obtained in voltage. In Fig. 5.20, the results obtained for bolts B2, B3 are shown. As shown in Fig. 5.20, the voltage signal of the strain gauges is constant until the moment of the untightening of the bolts, where a jump occurs. The residual strain of the bolts is the difference in voltage between the moment before and after untightening, so it is actually the height of the jumps in the graphs.

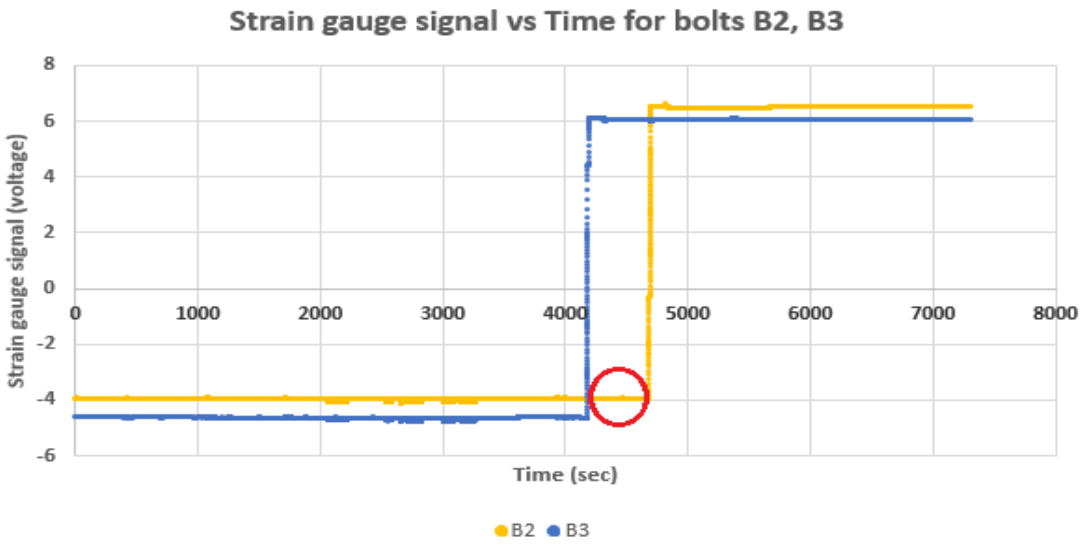

Figure 5.20: Strain gauge signals for bolts B2, B3.

Furthermore, the tightening of the new bolts did not influence the preload of the neighboring bolts. For example, as shown in Fig. 5.20, when bolt B3 was loosened and the new bolt was tightened by the combined method, the strain gauge signal of bolt B2 (located next to B3, as shown in Fig. 5.5) was not influenced (the red circle). The same was observed for the rest of the bolts. Therefore, there was no influence of elastic interactions. In a new connection, tightening of a bolt will influence the preload of neighboring bolts. However, this bridge was built in 1974. In an old connection a chemical bonding has been created between the plates, which make the plates homogeneous and does not allow them to deform under the force introduced by the new bolts, which is of a magnitude similar to the initial preload applied on the original bolts. Therefore, the same tightening sequence was followed for all the quadrants of the connection.

Furthermore, it has to be noted that some of the strain gauges did not work. The strain gauge of bolts A3, B5 gave unreliable readings, so they were excluded from the measurements. Bolt B8 was accidentally loosened before connected with the terminal. Therefore, bolts A3, B5 and B8 were excluded from the measurements. The strain gauge signals of all bolts can be found in Appendix C, Fig. C1 and C2.

In Tables 5.1, 5.2 the difference between the voltage before and after the untightening of the bolts is presented.

Table 5.1: Difference in voltage for A side's bolts

Bolts	Voltage
A1	10.01
A2	10.34
A3	-
A4	11.06
A5	10.82
A6	11.20
A7	6.50
A8	11.60

Table 5.2: Difference in voltage for B side's bolts

Bolts	Voltage
B1	10.71
B2	10.46
B3	10.91
B4	10.93
B5	-
B6	11.36
B7	9.50
B8	-

5.4 Elaboration of the results

5.4.1 Conversion of voltage to microstrain

The first step is to convert the voltage into strain. The relationship between the input, output voltage (in mV) and the relative change of the resistance for a Wheatstone bridge is given by eq. 5.1.

$$\frac{V_{output}}{V_{input}} = \frac{1}{4}\frac{\Delta R}{R} \tag{5.1}$$

And the relationship between the relative change in resistance and the strainis given by eq. 5.2.

$$k = \frac{\Delta R / R}{\varepsilon} \tag{5.2}$$

Based on eq. 5.1 and eq. 5.2 the following formula is obtained:

$$\varepsilon = \frac{4V_{output}}{kV_{input}} \tag{5.3}$$

For an unbalanced Wheatstone bridge and an input voltage of 6 V, the output voltage is 10 mV. The strain gauge factor k is given by the manufacturer and it is equal to 2.06. This results in a strain $\varepsilon = 3.23624 \cdot 10^{-3}$ / 10 mV of output voltage. Therefore, the voltage values should be multiplied by $3.23624 \cdot 10^{-3} \cdot 10^{6} / 10 = 323.624$ microstrain/mV to give microstrain. The resulting strain based on Tables 5.1, 5.2 is presented in Tables 5.3, 5.4.

Table 5.3: Converted values of microstrain for A series

Bolts	strain x 10^{-6}
A1	3239
A2	3346
A3	-
A4	3579
A5	3502
A6	3625
A7	2104
A8	3754

Table 5.4: Converted values of microstrain for B series

Bolts	strain x 10^{-6}
B1	3466
B2	3385
B3	3531
B4	3537
B5	-
B6	3676
B7	3074
B8	-

5.4.2 Calibration and determination of residual preload

The next step is to perform calibration of the bolts taken from the bridge, in order to determine the residual preload. The bolts with the implanted strain gauges were loaded up to the voltage value obtained when they were loosened in the connection, to determine the preload corresponding to that voltage value. The forces were not determined based on the best fit line, which results from calibration, because most of the calibration lines are not perfectly straight lines. Calibration was performed on the Universal Testing Machine (UTM) shown in Fig. 5.21. The calibration lines of the bolts are presented in the Appendix C (Fig. C3 – C15). In Tables 5.4, 5.5 the calibration factors of the strain gauges are presented, for bolts loaded up to the force, which corresponds to the voltage value obtained when the bolts were loosened.

Figure 5.21: Universal Testing Machine during calibration

Table 5.4: Calibration factors of A series

Bolt	Calibration factor	R^2
A1	0.0889	0.9988
A2	0.0985	0.9999
A4	0.0917	0.9999
A5	0.0931	0.9999
A6	0.0919	0.9999
A7	0.0908	0.9999
A8	0.0914	0.9999

Table 5.5: Calibration factors of B series

Bolt	Calibration factor	R^2
B1	0.0897	0.9999
B2	0.0899	0.9996
B3	0.0899	0.9999
B4	0.0895	0.9997
B6	0.0876	0.9989
B7	0.0898	0.9999

The bolts taken from the connection come from the same batch of bolts, therefore it is expected that their calibration factors will be more or less the same. The difference between calibration factors observed in Tables 5.4, 5.5 is mainly caused by the different actual diameters of these bolts and the difference in the actual position of the strain gauges in the

shank of the bolts. Furthermore, it has to be taken into account that differences in the calibration factors are also caused by different degree of non linearity of these lines.

Based on what is already mentoned, the residual preload of the bolts is presented in Tables 5.6 and 5.7.

Table 5.6: Residual preload for A series

Bolts	Force (kN)
A1	280
A2	328
A3	-
A4	337
A5	326
A6	330
A7	189
A8	342

Table 5.7: Residual preload for B series

Bolts	Force (kN)
B1	308
B2	299
B3	317
B4	313
B5	-
B6	320
B7	271
B8	-

5.4.3 Discussion

In Fig. 5.22, 5.23 the residual preload of the bolts is presented, which is compared with the minimum required preload for a M24, $F_{p,C} = 0.7 \cdot f_{ub} \cdot A_s = 0.7 \cdot 1000 \cdot 353 = 247$ kN. As shown, all bolts apart from bolt A7 are characterized by a high residual preload, higher than the minimum required preload.

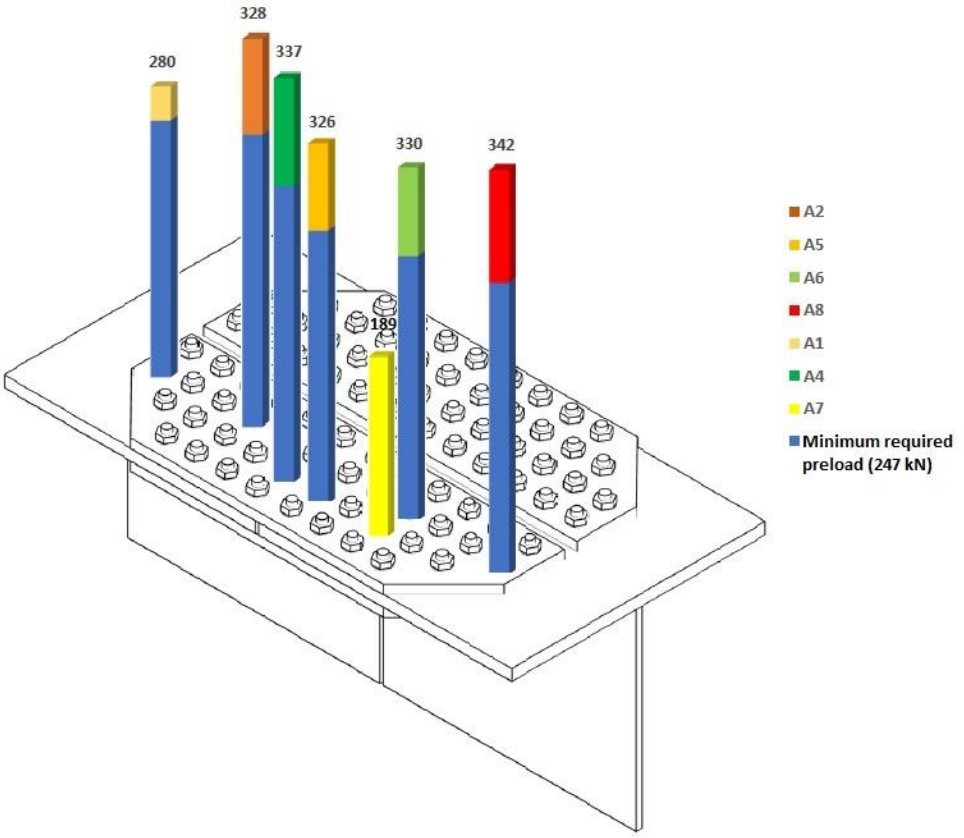

Figure 5.22: Residual preload of A series bolts based on calibration

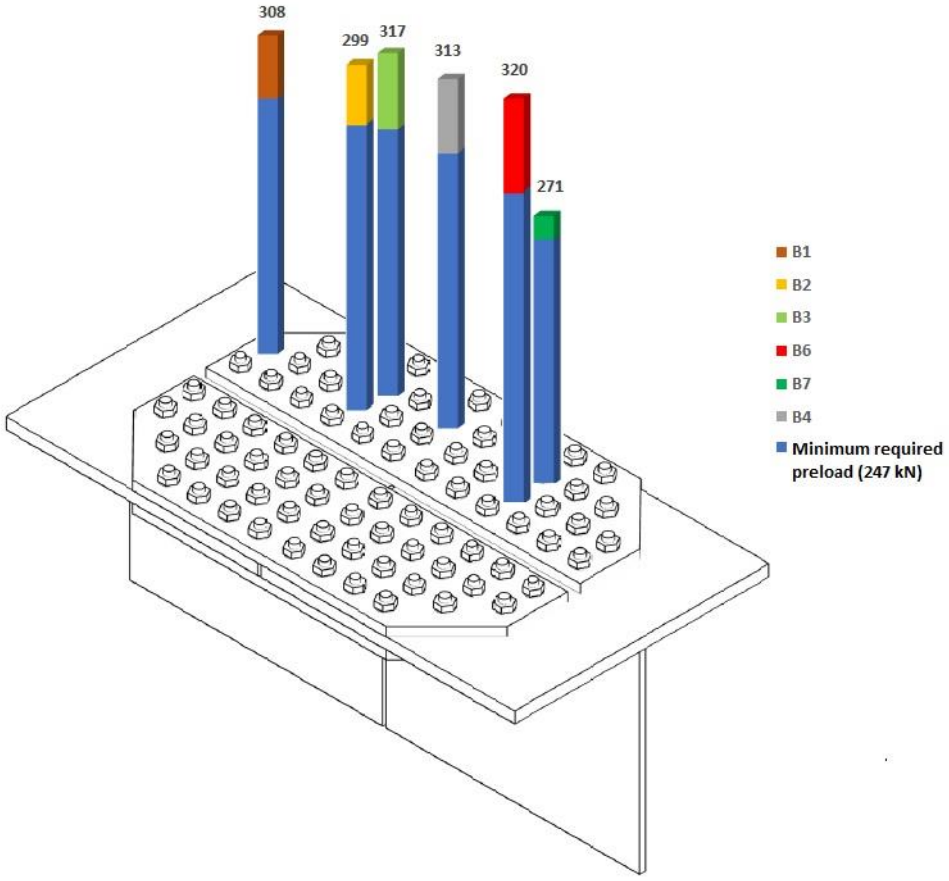

Figure 5.23: Residual preload of B series bolts based on calibration

Bolt A7 has a much lower preload compared to the other bolts. Considering the fact that during the in-situ measurements that bolt was the only bolt which was stuck in the hole and loaded in bearing, two conclusions can be derived. First, that independently of the tightening method which was used, the bolt was not preloaded sufficiently or that this bolt was over tightened, which resulted in yielding of the threads, which made the bolt incapable of sustaining the applied preload. For these reasons, this bolt was excluded from the analysis, since it is not representative of the preload condition of the bolts of the connection.

Regarding the mechanism that caused the preload loss, independently of the method which was used to apply the initial preload, two cases are distinguished:

1. The preload loss of the bolts is dependent on the location of the bolts. The external bolts carry most of the external load and for this reason they are characterized by a higher loss of preload compared to the inner bolts.
2. The location of the bolts is not critical and all bolts lost the same portion of their initial preload.

Considering that the connection consists of a large number of bolts and that the residual preload of these bolts is high, which means that their initial preload was even higher, it is concluded that the design resistance is much higher than the design force, which results in a low utilization ratio. Therefore, it can be said that almost no slip occured in the interface between the plates. Therefore, the location of the bolts is not critical and since the quality of the surface of the plates is the same everywhere, it can be said that the preload loss is the same for all bolts. Furthermore, the high residual preload determined for almost all the bolts makes it very probable that some bolts were overtightened during the installation in the connection. For this reason, material testing was performed, in order to determine the actual ultimate strength of the bolts.

5.5 Material testing

After the determination of a high residual preload, the bolts were subjected to a tensile test in order to determine their actual ultimate tensile strength and distinguish the bolts which were overtightened from the rest. The test was performed on the UTM, which was modified for safety reasons as shown in Fig. 5.24, in order to avoid any injury because of the explosion of the threaded part of the bolt. The bolt failure occurred, as it was expected, in the threaded part, as shown in Fig. 5.25, 5.26. The broken threaded part was characterized by the typical full-slant fracture surface, which indicates a high tensile load, as shown in Fig. 5.27. The material testing was displacement controlled with a rate of 0.01 mm/sec. The load displacement curves are presented in Appendix C (Fig. C16 – C30). The maximum load applied on the bolts is shown in Tables 5.8 and 5.9.

Figure 5.24: UTM for material testing of the bolts

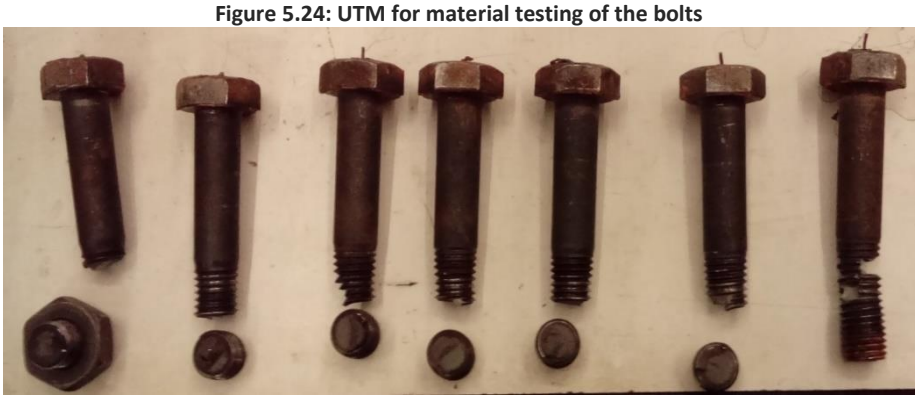

Figure 5.25: Broken bolts (A series)

Figure 5.26: Broken bolts (B series)

Figure 5.27: Fracture surface

Table 5.8: Maximum force in material testing (A series)

Bolts	Maximum force (kN)
A1	376
A2	388
A3	358
A4	364
A5	385
A6	394
A7	-
A8	395

Table 5.9: Maximum force in material testing (B series)

Bolts	Maximum force (kN)
B1	365
B2	368
B3	373
B4	351
B5	363
B6	387
B7	385
B8	343

5.5.1 Discussion

After examination of the threads of the bolts, it was observed that the threads of some bolts were damaged. This was an indication that these bolts were probably preloaded beyond their actual ultimate tensile strength, during the tightening procedure in the connection. Therefore, the maximum force determined in material testing was lower than their actual ultimate tensile strength. Therefore, it was attemted to identify these bolts. Bolt A1 is a typical example, as shown in Fig. 5.28. Pictures of the rest of the bolts can be found in Appendix D.

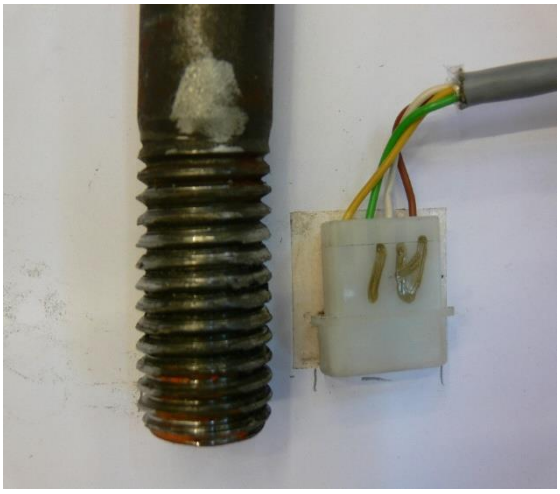

Figure 5.28: Threads of bolt A1

Apart from the calibration in the UTM, it was attempted to calibrate the strain gauges in the Skidmore – Wilhelm instrument. However, because of the damaged threads of some bolts, it was very difficult to tighten these bolts up to the force corresponding to the voltage value obtained by the in situ measurements. Therefore, these results are not presented and only the results obtained by the UTM were used to determine the residual preload. However, during calibration in the Skidmore – Wilhelm instrument, an incorrect clamping length was accidentally used and for this reason it was important to distinguish the damage in the threads caused by the incorrect clamping length from the damage in the threads caused by the initial tightening of the bolts in the connection. Eventually, this was easy to be done, because the clamping length used during calibration in the Skidmore – Wilhelm instrument was 84 mm instead of the original clamping length of 92 mm used in the connection. Therefore, the damage because of the incorrect clamping length in the Skidmore – Wilhelm instrument is expected to be found at the upper part of the threaded area, whereas the damage because of overtightening during the installation of the bolt on the connection is expected to be found at a lower location.

However, during the examination of the threads of the bolts, it was observed that the location of the damage caused by the initial tightening of these bolts was not in agreement with the clamping length of 92 mm which was used according to the design plans. The location of the damaged threads implied a lower clamping length than that of 92 mm. This was confirmed by the fact that the part of the threads which is extended below the nut was painted after the installation of the bolts in the connection, as shown in Fig. 5.29. Therefore, considering the length of the painted part of the threads and the length of the nut, it was concluded that a lower clamping length, approximately equal to 88 mm was used, which is in agreement with the location of the damaged threads. In Fig. 5.30, the location of the nut at the threads is shown, with the first thread engaged by the nut being damaged.

Figure 5.29: The painted extended part of the bolts below the nut

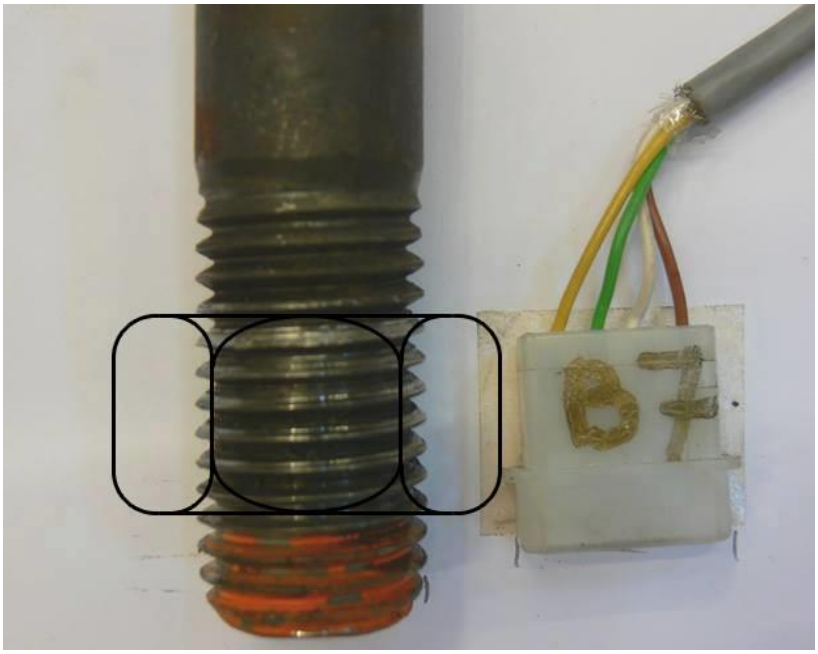

Figure 5.30: Location of the nut at the threads

Then, the two types of damage were distinguished for all the bolts. Indeed, this is confirmed by comparing the pictures of bolts B8 and B1 and observing carefully their threads, which are damaged at two different locations. Bolt B8 was not calibrated, because it was loosened before connected with the terminal and Fig. D8 shows the condition of the threads in the as received state from the connection, where a damaged thread in the middle of the threaded part is shown. Bolt B1 (Fig. D1) was calibrated in the Skidmore – Wilhelm instrument to the highest force compared to the rest of the bolts (315 kN) and it is the only bolt which has a damaged thread on the upper part of the threaded part.

The condition of the threads of the bolts was not the only criterion to judge on whether the maximum force determined in the material testing is the actual ultimate tensile strength or not. Based on force – displacement curves, the length of the plastic region of the bolts was also considered. These values are shown in Table 5.10. The bolts with damaged threads and small plastic region were considered as overtightened and thus the maximum force determined in the material testing was lower than the actual ultimate tensile strength.

Bolt A3 is excluded from the determination of the actual ultimate strength because this bolt comes from a different batch of bolts. Furthermore, bolt A7 is also not included because it broke during calibration in the Skidmore – Wilhelm instrument. Bolt A7 broke at 280 kN, because of an incorrect clamping length in the Skidmore – Wilhelm instrument and because it was overtightened during the installation in the connection, which is confirmed by its highly damaged threads.

Table 5.10: Length of plastic region (mm)

Bolts	plastic displacement (mm)
A1	3.64
A2	2.86
A4	2.21
A5	2.41
A6	2.86
A8	2.08
B1	5.59
B2	4.36
B3	4.68
B4	4.81
B5	5.4
B6	4.03
B7	4.94
B8	4.55

Based on these, the pictures of the threads of the bolts shown in Appendix D and based on Table 5.10, the following are concluded:

Bolt B1 is characterized by the longest plastic region. The threads are in a quite good condition, excluding the damage at the upper part of the threaded area caused by calibration in Skidmore – Wilhelm instrument up to 315 kN. Since there is no sign of damaged threads due to overtightening during the installation of the bolt on the connection and the force of 315 kN is not high enough to take the bolt beyond its ultimate tensile strength, it is concluded that the value of the maximum force determined in material testing (365 kN) is the actual ultimate tensile strength of the bolt.

Bolts B2, B3, B5, B6 are also characterized by a long plastic region and threads of a quite good condition, therefore the maximum force determined in material testing was considered the same with the ultimate tensile strength.

Bolt's B4 threads are in a good condition but the maximum force determined in material testing (351 kN) is much lower compared to the ultimate tensile strength of the other bolts and therefore it is considered that this bolt was tightened beyond its ultimate tensile strength.

Bolt's B7 threads are more damaged compared to bolts B1, B2, B3, B5 and the bolt is characterized by a quite long yield plateau and a high maximum force. The damaged threads which imply that the bolt was probably overtightened are probably caused by the fact that bolt B7 was accidentaly tightened to 358 kN, before loosening the nut, without adding lubricant to the threads. Therefore the maximum force is considered equal to the ultimate tensile strength.

The condition of the threads of bolt B8 is a bit worse than that of bolt B7. Even if it has a quite long yield plateau the maximum force obtained by material testing was quite low (343 kN) and it was considered that this bolt was tightened beyond the ultimate tensile strength. Therefore, the maximum force determined in material testing is considered lower than the actual tensile strength.

Bolts A2, A5, A6 and A8 are characterized by a shorter plastic displacement, but their threads are in a good condition. Furthermore, the maximum force determined in material testing (388, 385, 394, 395 kN respectively) was high enough to consider it as a good approximation of the actual ultimate tensile strength. Therefore, the results of material testing are considered equal to the ultimate tensile strength of these bolts.

Bolts' A1 and A4 threads are in a bad condition and in combination with their short plastic region, they are considered as tightened beyond their ultimate tensile strength. Therefore, these bolts are excluded from the determination of the ultimate tensile strength.

In conclusion, 30% of the tested bolts were overtightened. The ultimate tensile strength of the rest of the bolts is presented in Table 5.11.

Table 5.11: Ultimate tensile strength

Bolts	Ultimate tensile strength (kN)
A2	388
A5	385
A6	394
A8	395
B1	365
B2	368
B3	373
B5	363
B6	387
B7	385
average	380
scatter (%)	3.15

5.6 Loss of preload

5.6.1 Expected loss of preload (based on theory)

As discussed in section 2.2, the preload loss depends on factors like, the number of the coated surfaces, the thickness of the plates and the coating system. Considering that no information is available for the coating system, the expected loss of preload will be estimated based on the guide values of embedding, which are given by VDI 2230 as a function of the average roughness height of the coating system for HSFG connections, as shown in Table 5.12.

Table 5.12: Guide values for amount of embedding of bolts, nuts and clamped parts made of steel [41]

Average roughness height R_Z according to DIN 4768	Guide values for amount of embedding in µm		
	in the thread	per head or nut bearing area	per inner interface
< 10 µm	3	3	2
10 µm up to < 40 µm	3	4.5	2.5
40 µm up to < 160 µm	3	6.5	3.5

The bolt stiffness is determined based on Hooke's law. The shank of the bolt and the threaded part are considered as two serial springs with stiffness k_s, k_t.

$$k_{bolt} = \frac{k_t \cdot k_s}{k_t + k_s} \tag{5.4}$$

$$\text{with } k_t = \frac{A_t E}{L_t}, \; k_s = \frac{A_s E}{L_s} \tag{5.5}$$

where, E is Young's modulus, A_t is the threaded area, A_s is the shank cross section area, L_t the length of the threaded part included in the clamping length and L_s the length of the shank.

The deformation of the plates can be calculated using Hooke's Law. The stressed area is dependent on the distance from the plate surface due to stress spreading, as shown in Fig. 5.31. Considering that angle α is equal to 30˚, that all the clamped members have the same elastic modulus and that the clamped members are frusta spreading from the bolt head and nut to the midpoint of the grip, the stiffness of the clamping package is given by eq 5.6 [14].

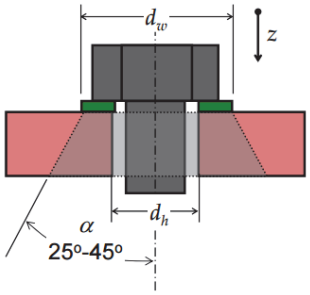

Figure 5.31: Stress spreading under the head and the nut [14]

$$k_{clamped} = \frac{\pi E d \tan(\alpha)}{2 \cdot \ln\left[\frac{\left(d_w - d_h + l_c \cdot \tan(\alpha)\right)\left(d_w + d_h\right)}{\left(d_w + d_h + l_c \cdot \tan(\alpha)\right)\left(d_w - d_h\right)}\right]} \tag{5.6}$$

where, d is the bolt's diameter, α = 30˚, d_w is the washer diameter, d_h the hole diameter and l_c the clamping thickness.

Then, the preload loss due to embedment is given by eq. 5.7.

$$F_Z = f_Z \frac{k_{bolt} \cdot k_{clamped}}{k_{bolt} + k_{clamped}} \tag{5.7}$$

where, f_Z is the deformation due to embedment given by Table 5.8.

Based on eq. 5.4, 5.5, 5.6 k_{bolt} = 1055098 N/mm and $k_{clamped}$ = 6301859 N/mm. Considering that embedment occurs at the locations shown in Fig. 5.32 and making the most pessimistic estimation about the expected amount of embedment, based on Table 5.12, the expected preload loss is estimated equal to 27 kN.

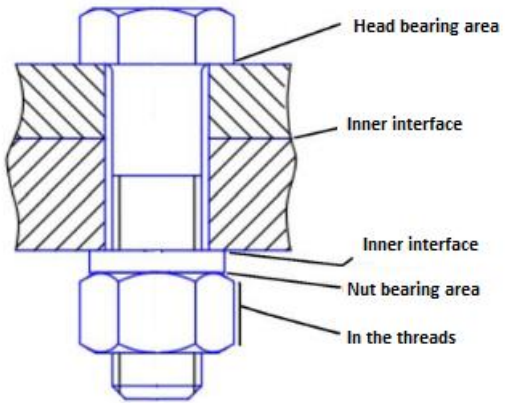

Figure 5.32: Locations where embedment can occur

In Table 5.13, the expected (theoretical) initial preload is presented, based on Fig. 5.22, 5.23, on an expected preload loss equal to 27 kN and considering that all the bolts lost the same amount of preload, for the reason discussed in section 5.4.3.

Table 5.13: Expected (theoretical) initial preload

Bolts	Expected initial preload (kN)
A2	355
A5	353
A6	357
A8	369
A1	307
A4	364
B1	335
B2	326
B3	344
B6	347
B7	298
B4	340

In Fig. 5.33, the preload loss is presented in terms of elastic deformation for bolt B1 and the plates. As shown, 1 μm of embedment results in 0.87 μm of loss of elongation of the bolt and 0.13 μm of elastic deformation of the plates, which is reasonable as the stiffness of the clamping package is 6 times higher than that of the bolt.

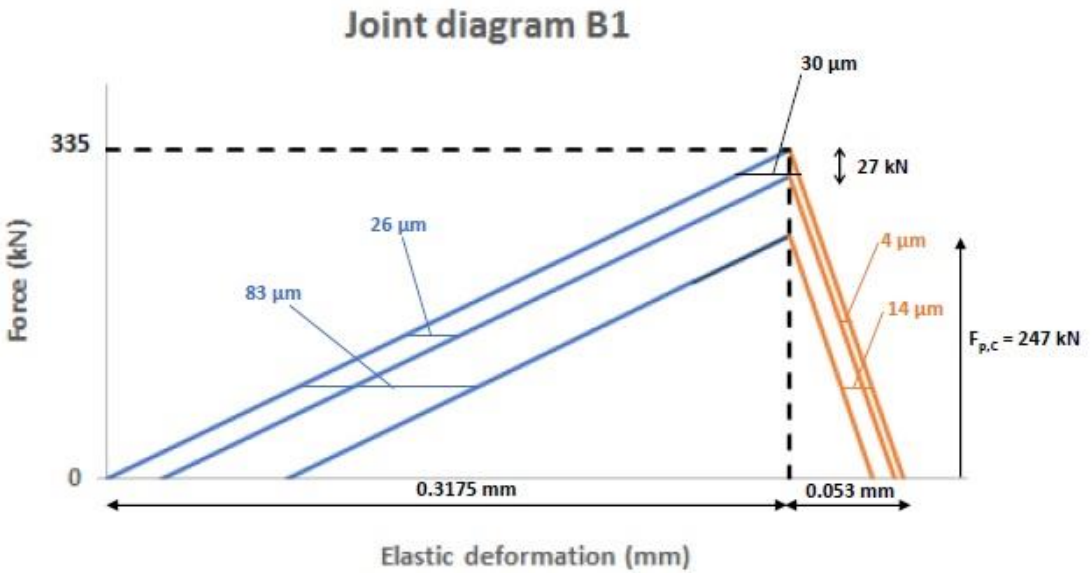

Figure 5.33: Joint diagram based on expected preload loss for B1

5.6.2 Estimated loss of preload (based on the tests)

It is possible to estimate the initial preload and the preload loss by taking advantage of the information provided by the overtightened bolts. This can be done by looking at the maximum force determined in material testing for these bolts. As shown in Fig. 5.34, a bolt with an ultimate tensile strength represented by point A, which is tightened up to point B (beyond ultimate tensile strength), will deform based on line (BD), when a portion of the initial preload is lost. When this bolt is loaded in material testing, a maximum force represented by point C is determined, which is close enough to the initial preload force (point B).

In our case, there are three bolts which can provide us with this information, as shown in Table 5.14. It is possible to estimate the preload loss by assuming that the initial preload is approximately equal to the maximum force. The actual loss will be a bit higher, but this is a simplification to see if the hypothesis of the same losses for all bolts is true. In this case, it can be said that bolt A1 is exluded, because it lost a much higher portion of its initial preload compared to the other bolts, which is reasonable as its threads are completely damaged, which means that it could hardly sustain the initial preload. The residual preload of bolts A4 and B4 is 337 and 313 kN, with a maximum force 364 and 351 kN, which leads to a loss equal to 27 and 38 kN, respectively, which means that these bolts lost approximately the same amount of their initial preload.

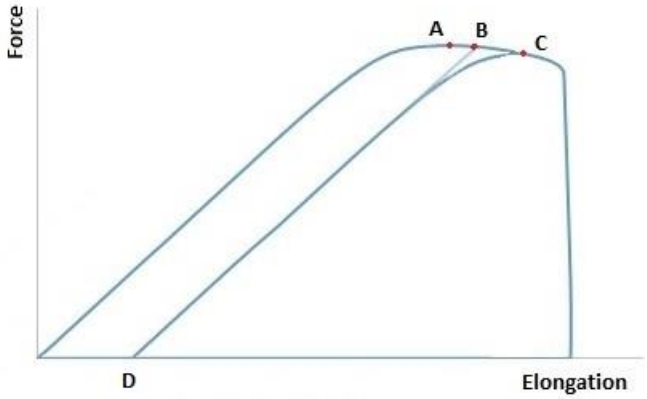

Figure 5.34: Force – elongation graph

Table 5.14: Bolts tightened beyond the ultimate tensile strength

Bolts	Maximum force (kN)	Residual preload (kN)	Approximate preload loss (kN)
A1	376	280	96
A4	364	337	27
B4	351	313	38

As it is already mentioned, it is considered that the bolt lost the same amount of preload. Therefore and in order to estimate the initial preload, the preload loss is considered as the average of 27 kN and 38 kN, since there only two overtightened bolts, which can provide us with this information. The difference between the initial preload (point C) and the maximum force (point B) was estimated graphically and it can be considered equal to 10 kN. Therefore, the preload loss will be considered equal to 10 + 32 = 42 kN for the rest of the bolts. Based on this and based on the residual preload presented in Fig. 5.22 and 5.23, the initial preload of the rest of the (tested) bolts is presented in Table 5.15.

Table 5.15: Estimated initial preload as a portion of F_{ult}

Bolts	Estimated initial preload	
A1	386	-
A2	370	$0.954F_{ult}$
A4	374	-
A5	368	$0.956F_{ult}$
A6	372	$0.944F_{ult}$
A8	384	$0.972F_{ult}$
B1	350	$0.959F_{ult}$
B2	341	$0.927F_{ult}$
B3	359	$0.962F_{ult}$
B4	361	-
B6	362	$0.935F_{ult}$
B7	313	$0.813F_{ult}$

In Fig. 5.35 the joint diagram of bolt B1 is presented, based on the estimated preload loss, which results in a plastic deformation because of embedment equal to 46.4 μm.

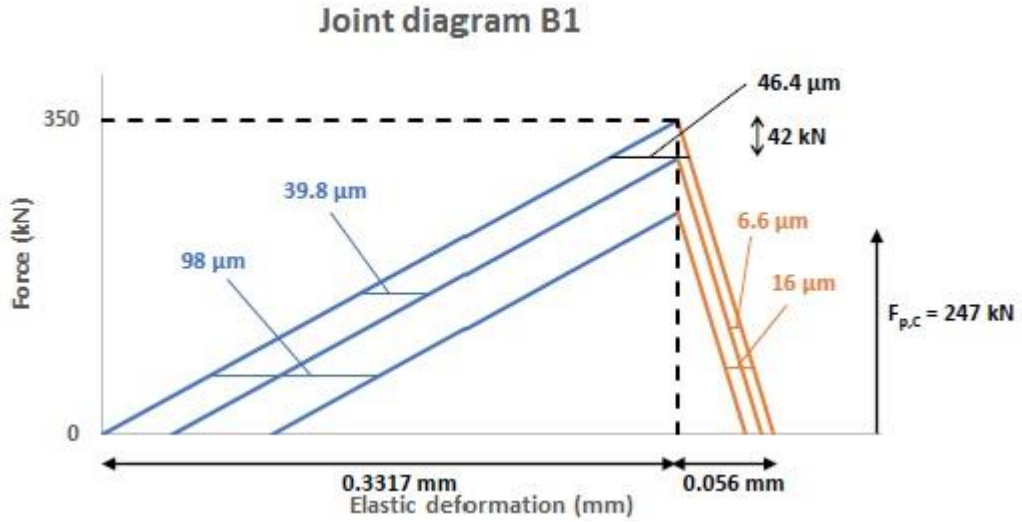

Figure 5.35: Joint diagram based on estimated preload loss for B1

5.6.3 Comparison between expected and theoretical initial preload

In Table 5.16 the theoretical and estimated initial preload is presented.

Table 5.16: Expected and estimated initial preload

Bolts	Expected initial preload (kN)	Estimated initial preload (kN)
A2	355	370
A5	353	368
A6	357	372
A8	369	384
A1	307	386
A4	364	374
B1	335	350
B2	326	341
B3	344	359
B6	347	362
B7	298	313
B4	340	361

As discussed in sections 5.6.1, 5.6.2, the theoretical preload loss was considered equal to 27 kN and the estimated preload loss equal to 42 kN. It has to be noted that several assumptions were made in order to determine the theoretical loss, like the same Young's modulus for the bolt and the clamped parts, the effective length of the bolt and the angle of spread of the stress between the plates. Furthermore, no information was available about the coating system of the plates of the connection and the preload loss was estimated based on a high average roughness of the plates. The influence of the elastic interactions was ignored, considering that the bolts were tightened following an appropriate tightening sequence, which minimized preload variations due to elastic interactions. Lastly, the suggested values of embedment in Table 5.12 were derived based on tests with bolts preloaded to a force close to the minimum required preload $F_{p,C}$. As discussed, the bolts of the connection under

examination are characterized by a much higher preload, which leads to the conclusion that a higher pressure at the locations where embedment occurs, would result in a preload loss higher than 27 kN.

5.7 Discussion about the tightening methods

As discussed in the previous sections, the bolts are characterized by a high residual preload, which leads to the conclusion that some of them were overtightened. Overtightening a bolt is a dangerous situation, which results in damage of the threads and makes the bolt incapable of sustaining the initially applied preload and it also leads to a lower preload. For that particular connection overtightening did not have any visible consequences. Nevertheless, from an engineering point of view, it would be interesting to discuss the causes that led to a high initial preload. It is expected that this was caused because of low friction in the threads of the bolts. Since it is unknown whether the torque method or the combined method was used to apply the initial preload, in the following sections 5.7.1 and 5.7.2, two scenarios are distinguished: tightening by 1) the torque method and 2) the combined method. In the end the feasibility of achieving the initial preload shown in Table 5.15, Fig. 5.36, 5.37 is discussed.

5.7.1 Torque method

In Fig. 5.36 and 5.37 the estimated initial preload of the tested bolts is presented. The only available information about the tightening procedure of these bolts, is that according to the design plans, a torque equal to 1100 Nm and a k factor equal to 0.177 were used in order to achieve the minimum required preload of $0.7f_{ub}A_s$. This torque and k factor result in a preload force $F = \frac{T}{k \cdot d} = \frac{1100}{0.177 \cdot 24} = 259 \text{ kN}$. According to theory, depending on the variation of the k factor, the preload which results from the torque method is characterized by a certain spread, which is the case here. The k factor value used here is relatively high, which means that bolts with a low friction coefficient at the threads were overtightened resulting in the damaged threads shown in the pictures in Appendix D.

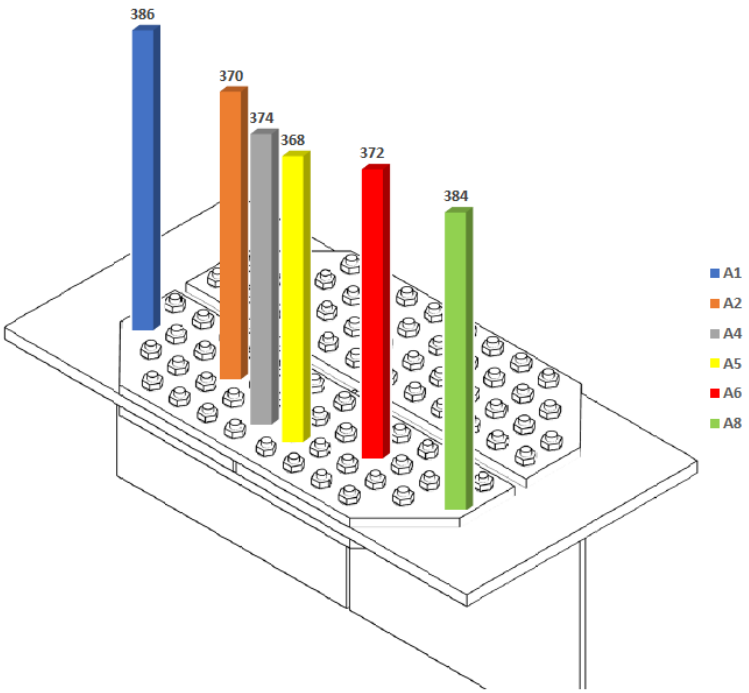

Figure 5.36: Estimated initial preload (A series)

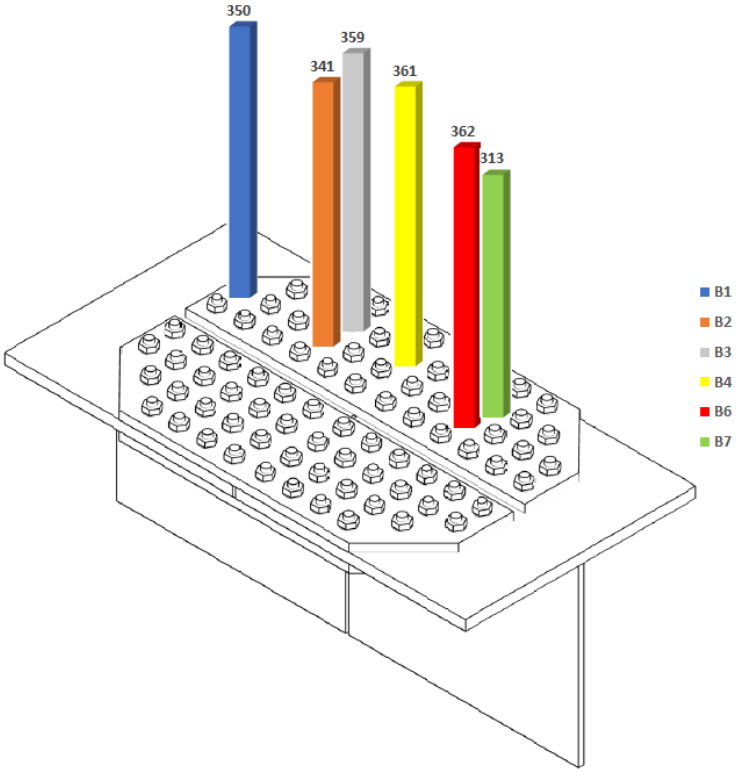

Figure 5.37: Estimated initial preload (B series)

Taking into consideration the torque (T = 1100 Nm) and the estimated initial preload values, it is possible to estimate the values of the k factor for each bolt. For the determination of k factor's values, the initial preload of bolts A1, A4, A7, B4 is ignored, because these bolts were tightened beyond their ultimate tensile strength. $k_{estimated}$ factor's values are shown in Table 5.17.

Table 5.17: Estimated k factor values

Bolts	Initial preload (kN)	T (Nm)	$k_{estimeated}$
A2	370	1100	0.124
A5	368	1100	0.125
A6	372	1100	0.123
A8	384	1100	0.119
B1	350	1100	0.131
B2	341	1100	0.134
B3	359	1100	0.128
B6	362	1100	0.127
B7	313	1100	0.146
		mean	**0.129**
		standard deviation	**0.008**

Therefore, the k_{factor} is estimated as 1.5 times lower than the one which was assumed to tighten the bolts (0.177). The maximum and minimum values of the preload are shown in Table 5.18.

Table 5.18: Estimated initial preload of untested bolts

F = T/dk	$k_{est,max}$	k_{est}	$k_{est,min}$
	0.137	0.129	0.121
$F_{initial}$	335	355	379
$F_{residual}$	293	313	337

Considering that the bolts of the connection, which come from the same batch of bolts have an average ultimate tensile strength equal to 380 kN with a scatter of 3.15%, as shown in Table 5.11, then the mean value of the estimated initial preload as a portion of the average ultimate tensile strength is 355/380 = 0.934.

Since the scatter in the strength of the bolt affects the scatter in the initial preload and both scatters are known, it is possible to determine the scatter in the initial preload due to the rest of the factors that result in the torque method scatter (friction coefficient, dimensional tolerances etc). The determination of the scatter is based on the following formula:

$$\text{total scatter} = \sqrt{(\text{tensile strength scatter})^2 + (\text{rest factors that result in torque method scatter})^2}$$

The results are shown in Table 5.19.

Table 5.19: Estimated torque method scatter

total scatter (%)	7
scatter in tensile strength (%)	3
scatter because of torque method uncertainties (%)	6

Therefore, the variation of the initial preload as a portion of the average ultimate tensile strength is shown in Table 5.20.

Table 5.20: Estimated initial preload as a portion of the ultimate tensile strength

	minimum	**mean**	**maximum**
initial preload	$0.878F_{ult}$	$0.934F_{ult}$	$0.990F_{ult}$

However, the actual value of k factor is probably lower than the one determined in Table 5.18, because the bolts which were tightened beyond the ultimate tensile strength were not taken into account. These bolts are characterized by a lower k factor and for this reason the minimum and maximum values shown in Table 5.18 would be higher. In our case, 5 out of 15 bolts were tightened beyond the ultimate tensile strength.

Therefore, the assumption of the torque method explains the spread in the residual preload and leads to an indication of a low k factor, which implies highly lubricated threads. In section 5.7.2 the combined method will be considered as the method of applying the preload.

5.7.2 Combined method

In case that the combined method was used, the torque T = 1100 Nm is the torque used for the first step of the combined method. In this section, the suitability of that torque will be investigated, to achieve the initial preload shown in Table 5.15 and Fig. 5.36, 5.37.

According to EN 14399, when the combined method is used, the k factor should be $0.10 \leq k \leq 0.16$. Furthermore, the bolts should be preloaded for the first step to the value of 75% of $0.7f_{ub}A_s = 0.525f_{ub}A_s$, according to article 8.5.3 of EN 1090-2 and for the determination of the torque applied for the first step the k factor can be considered equal to 0.13, according to EN 1090-2 article 8.5.4. This would result in a bottom preload value of $0.13/0.16 \times 0.525f_{ub}A_s = 0.43f_{ub}A_s$ and a top value of $0.13/0.10 \times 0.525f_{ub}A_s = 0.68f_{ub}A_s$. Then, by rotating the nut by 90˚ the bolt is preloaded to a level close to its yield strength, in the worst case higher than $0.7F_{pC}A_s$.

In our case, in Fig. 5.38, the resulting preload from the first step is shown, by applying a torque T = 1100 Nm for $0.10 \leq k \leq 0.16$.

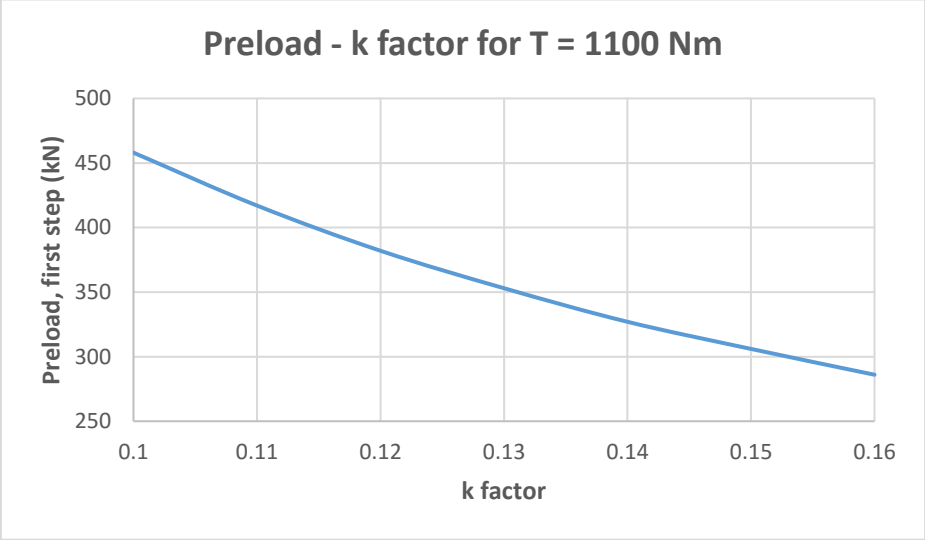

Figure 5.38: Preload (first step) – k factor for T = 1100 Nm

As shown in Fig. 5.38 any value of the k factor lower than 0.125 would lead to fracture of the bolt before the prescribed rotation of the nut in the second step and any value of k factor between 0.125 and 0.15 is high enough to cause fracture of the bolt during the rotation of the nut in the second step. For a k factor between 0.15 and 0.16 and a torque T = 1100 Nm, the resulting preload in the first step of the combined method is shown in Table 5.45.

Table 5.45: Resulting preload in the first step of the combined method

	k	
Bolts	**0.15**	**0.16**
A2	$0.789F_{ult}$	$0.737F_{ult}$
A5	$0.795F_{ult}$	$0.743F_{ult}$
A6	$0.777F_{ult}$	$0.726F_{ult}$
A8	$0.775F_{ult}$	$0.724F_{ult}$
B1	$0.838F_{ult}$	$0.784F_{ult}$
B2	$0.832F_{ult}$	$0.777F_{ult}$
B3	$0.820F_{ult}$	$0.767F_{ult}$
B5	$0.843F_{ult}$	$0.788F_{ult}$
B6	$0.791F_{ult}$	$0.739F_{ult}$
B7	$0.795F_{ult}$	$0.743F_{ult}$

These values are higher than the top value of the preload force in the first step of the combined method prescribed by EN 1090-2. This means that it is very probable that after the rotation of the nut in the second step most of the bolts were overtightened. However, this does not explain the relatively low initial preload of bolt B7, which is $0.813F_{ult}$. The preload achieved in the first step of the combined method is $0.795F_{ult} – 0.743F_{ult}$, which is quite high to result in a final preload equal to $0.813F_{ult}$ by rotating the nut.

5.7.3 Conclusion

In sections 5.7.1 and 5.7.2 both the torque and the combined method were considered as tightening methods of the bolts of that connection.

The bolts of the connection were preloaded based on a high value of k factor (k = 0.177), which was used to determine the torque, which is required in order to preload the bolts over the minimum required preload of $0.7f_{ub}A_s$, which in combination with the low values of the actual k factor (it was estimated as k = 0.129) resulted in high values of initial preload and overtightening of some of the bolts.

On the other hand, the in situ measurements make highly impossible that the bolts of the connection were tightened by the combined method. In this case, the torque mentioned in the design plans (T = 1100 Nm) is the torque used for the first step of the combined method. For typical and ordinary values of k factor ($0.10 \leq k \leq 0.16$) this means that the preload achieved after the first step of the combined method is, in the worst case, that high that leads to breaking of almost all the bolts and in the best case it is high enough in order to lead to overtightening of almost all the bolts. Furthermore, these values of k factor and the torque which was used do not explain the scatter found in the residual preload values. The use of the combined method could be possible only for values of the k factor around 0.20, which implies very badly lubricated bolts. This could also explain the damage in the threads of most of the bolts.

Since such values of the k factor are not realistic, it was concluded that the torque method was used to tighten the bolts of that connection. A possible explanation for the high initial

preload which was measured, is that more lubricant than what was required was applied on the threads of the bolts, which led to low values of k factor.

5.8 Conclusion

In this chapter the procedure and the results of the in situ measurements were presented and discussed. It was shown that it is possible to perform in situ measurements with the strain gauge method. However, two strain gauges out of the sixteen gave unreliable readings and they were excluded from the measurements. The residual forces were determined based on calibration of the implanted strain gauges and the bolts were loaded up to the force corresponding to the voltage value obtained by the in situ measurements. The best fit line of calibration data points was not used, since calibration lines are not perfectly straight lines and thus this could result in an error. Apart from the calibration procedure, the forces were also determined based on the force – strain gauge measurement data points, which were obtained by material testing. The difference in the force was not more than 2%. Furthermore, the preload loss of the tested bolts was estimated and compared with the theoretical preload loss. It was found that the theoretical loss is lower than the estimated loss, however the uncertainty regarding the properties of the coating system has to be taken into account and also the high initial/residual preload of the bolts, which could have led to a higher (than what is expected) degree of embedment. Lastly, the tightening method which was used to preload the bolts was discussed, leading to the conclusion that the bolts of the connection were tightened by the torque method. In this chapter, the forces were determined based on calibration of the strain gauges, which offers the maximum accuracy. In the following chapter four approaches to estimate the preload without performing calibration of all bolts, are discussed.

6 IN SITU MEASUREMENTS – WAYS OF ESTIMATION OF THE FORCE

In the previous chapter, the determination of the preload force was made based on calibration of all the implanted strain gauges. The bolts were calibrated up to the force which results from the voltage value obtained by the in situ measurements. This is the most accurate way of determining the preload, but it is also a very time-consuming process. For this reason, in this chapter, alternative ways of determination of the preload force are discussed. The preload values which result from each approach are compared with the "true" calibration forces shown in Tables 5.6, 5.7 leading to an engineering assessment about the accuracy of each approach. It has to be noted that the error values which are presented in the following sections, are related with the geometric characteristics, distribution of bolts' diameters of that particular connection. To generalize and validate them, further investigation on more connections is necessary. A basic assumption for all the approaches presented in this chapter is that the strain gauges are properly installed in the shank of the bolts.

6.1 Estimation of the preload based on the model (1st approach)

The 1st approach is about the determination of the force based on a model. Based on theory the relationship between force and strain is:

$$F = \sigma \mathrm{A} \Leftrightarrow F = E\varepsilon \mathrm{A} = \mathrm{AE}\varepsilon \tag{6.1}$$

where A is the net cross section area, E is Young's modulus and ε is the measured strain.

Therefore, if the residual strain is known, then the residual preload can be determined. In this section the residual preload is determined for the actual diameter of the shank, the lowest and maximum boundaries of the nominal dimensions and for Young's modulus equal to 200, 210, 220 GPa.

The diameters in the shank of the bolts taken from the connection are presented in Tables E1 and E2 in Appendix E. Each bolt's diameter was measured at three different locations, as shown in Fig. 6.1. Then, the bolt was turned 90 degrees and three more measurements, at the same locations, were taken. The diameters shown in Tables E1 and E2 are the mean values of the measurements. The mean values were compared with the two measurements taken at Location B, which is approximately representing the position of the strain gauge in the shank of the bolt. Mean values which are characterized by a high deviation from the measurements taken at Location B, are corrected based on these two measurements. The net cross section area is equal to $A = \frac{\pi}{4}\left(d^2 - 2^2\right)$ considering that the hole which was drilled on the head of the bolts has a diameter of 2 mm.

The estimated forces based on the model and their difference from the calibration forces are presented in Tables E3 - E20 in Appendix E.

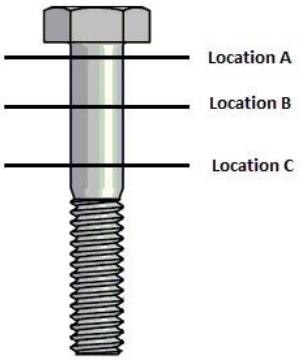

Figure 6.1: Diameter's measurement locations

6.1.1 Discussion

As shown, the error between model forces and calibration forces varies depending on the assumption on Young's modulus and also on the use of the actual or nominal dimensions of the bolts. The average, maximum and minimum values of error determined for different values of Young's modulus and actual or nominal dimensions are summarized in Fig. 6.2 and Table 6.1.

Table 6.1: Error in determination of model forces

Error (%) between F_{model} and $F_{calibration}$	average error (%)	maximum error (%)	minimum error (%)
Model-d_{actual} (E = 210)	2.76	4.08	1.43
Model-d_{max} (E = 210)	12.05	15.9	8.21
Model-d_{min} (E = 210)	3.07	6.03	0.1
Model-d_{actual} (E = 220)	6.58	9.3	3.86
Model-d_{max} (E = 220)	17.39	21.42	13.36
Model-d_{min} (E = 220)	3.43	5.33	1.53
Model-d_{actual} (E = 200)	3.11	5.68	0.54
Model-d_{max} (E = 200)	6.62	10.28	2.96
Model-d_{min} (E = 200)	7.35	10.54	4.17

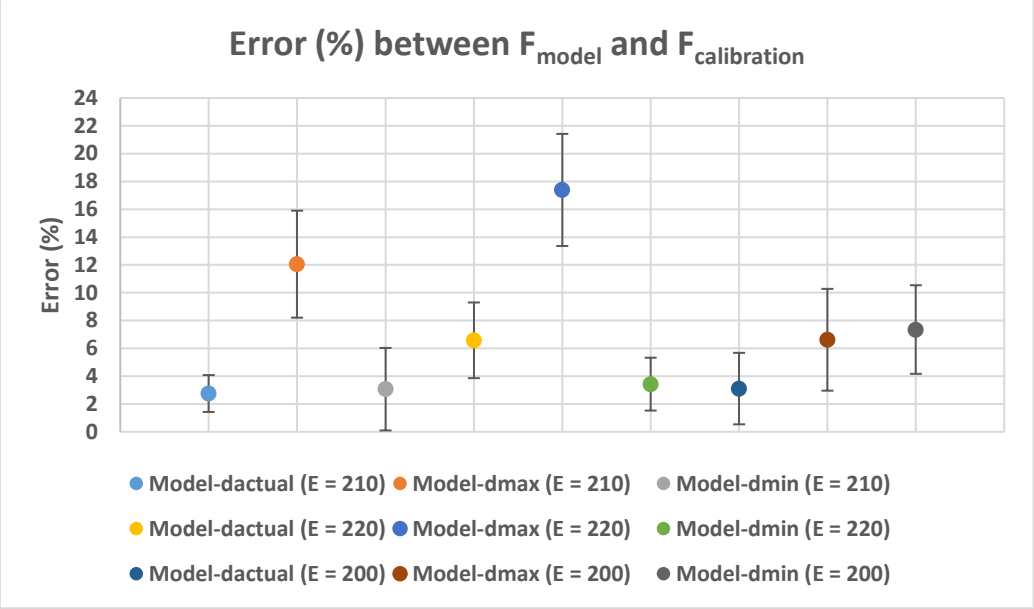

Figure 6.2: Error in determination of model forces

For the bolts of that particular connection and considering the actual dimensions of the bolts, the maximum error which was determined was 9.3%. The error increases to 21.42% for determination of the forces based on the dimensional tolerances. These errors are derived based on the highest boundary of Young's modulus and the nominal dimensions, therefore it is known that the forces are overestimated. For that particular connection in which all bolts have diameters between the lowest boundary of the nominal dimensions (23.16 mm) and the nominal diameter of 24 mm, it is reasonable to expect an overestimation of the residual preload for determination of the residual preload based on the highest boundary of the nominal dimensions. However, for bolts with an actual diameter between the nominal diameter and the highest boundary of the nominal dimensions (24.84 mm), the determination of the residual preload based on the lowest boundary of the nominal dimensions would lead to an underestimation of the residual preload. Therefore, if the results presented in this section are generalized, it is possible to say that for the most pessimistic estimation of the residual preload based on the lowest boundary of the nominal dimensions, the error between the estimated and true force can lead to an underestimation of the calibration force of a similar or even higher magnitude, as in the case presented in this section, depending on the value of the actual diameter. Therefore, this method offers the possibility of knowing whether the force is underestimated or overestimated, but the high error can result in misleading conclusions about the preload condition of the bolts.

The next step is to reduce that error by eliminating or reducing the effect of Young's modulus on the determination of the preload force. This can be done by obtaining information about Young's modulus by calibrating one of the bolts of the connection, considering that all the bolts come from the same batch. The procedure and the results are presented in the next section.

6.2 Estimation of the force based on one calibration line corrected based on the actual diameters (2nd approach)

The bolts in a connection come from the same batch of bolts, which means that they are made of the same material with the same Young's modulus. The calibration of a bolt results in a line which describes the relationship between the force and the strain. The slope of that line is

called calibration factor. Based on the model, the calibration factor is equal to the product of the net cross section area and Young's modulus, EA. As shown in Tables E3, E4, E9, E10, E15, E16 in Appendix E, this product is more or less constant and it can be said that the small difference between the products of different bolts are caused mainly by differences in bolts' diameters. In Table 6.2 the difference between the calibration factors (experimental) and the EA product (theoretical) of two bolts is presented.

Table 6.2: EA and calibration factors' difference

difference between theoretical/experimental calibration factor of bolts A7 and Ai, Bi (%)		A1	A2	A4	A5	A6	A7	A8	B1	B2	B3	B4	B6	B7
A7	theoretical	1.69	-1.85	-0.08	-1.62	-0.51	-	-0.08	0.75	0.26	0.59	0.71	1.69	0.68
	experimental	2.09	-8.48	-0.99	-2.53	-1.21		-0.77	1.21	0.99	0.99	1.43	3.52	1.1

As shown in Table 6.2, the difference between the difference of the EA product of two bolts and their calibration factors is low in most cases. In some cases in which that difference is higher, it is caused by a not accurate measurement of the diameter or a not straight calibration line or because of assumptions made in the derivation of the product EA. For example, the product EA is derived based on the assumption that the strain gauge is located at the position in the shank where the diameter was measured. The calibration factor considers the actual position of the strain gauge.

Furthermore, it is important to note that this procedure requires a thorough examination of the calibration lines, in order to exclude the parts of the lines which are not perfectly linear. For example, bolt's A2 original calibration line is shown in Fig. C4 in Appendix C. It is obvious that at around 60-80 kN a jump occurs in the line. Furthermore, the calibration factor of that line is much higher compared to the calibration factors of the rest of the bolts, which implies that the line is not representing the elastic region of the force – strain graph accurately. For this reason, it was decided to exclude the part over 60 kN and draw the line up to the level of 60 kN, as shown in Fig. F2 in Appendix F. The (corrected) calibration lines used for the determination of the preload force are presented in Appendix F (Fig. F1 – F13). For the determination of these calibration lines, only the loading path obtained by the calibration procedure was taken into account and it was compared with the unloading path, since it is expected that the loading and unloading path of the calibration line of the same bolt will be the same.

The results presented in Table 6.4 confirm that the difference between the calibration lines of different bolts (of the same batch) is caused mainly by the difference in their actual diameter.

Therefore, if the calibration line of one bolt is obtained, then it would be possible to determine the residual preload of the other bolts by correcting it based on their diameter.

For example, if the calibration line of bolt A1 based on the model is $F_{A1} = \left(EA_{A1}\right)\varepsilon$, then the residual preload of the rest of the bolts is determined as:

$$F_i = \left(EA_{A1}\right)\frac{A_i}{A_{A1}}\varepsilon \text{ with } i = A2...A8 \text{ , } B1...B8 \tag{6.2}$$

In the Tables F14 – F26 in Appendix F, the residual preload is determined based on eq. 6.2 based on the calibration line of each bolt.

6.2.1 Discussion

The error between the model and calibration forces is presented in the following figures, where the horizontal right axis represents the bolts based on which the model forces were determined.

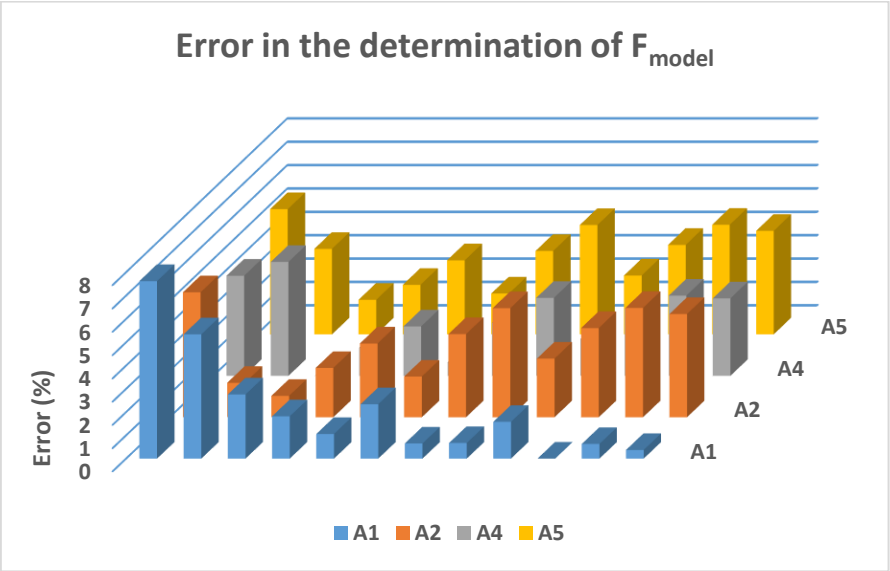

Figure 6.3: Error between model – calibration forces for model forces based on calibration of A1, A2, A4, A5

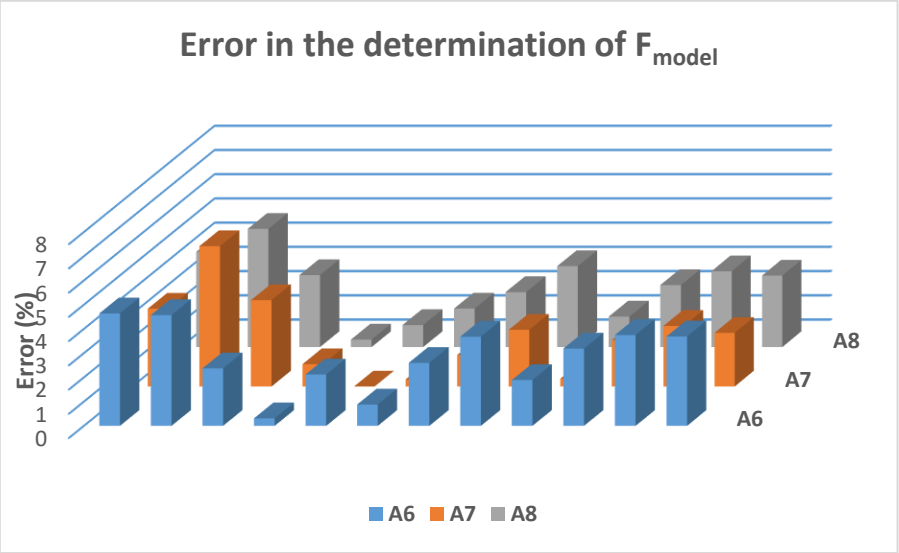

Figure 6.4: Error between model – calibration forces for model forces based on calibration of A6, A7, A8

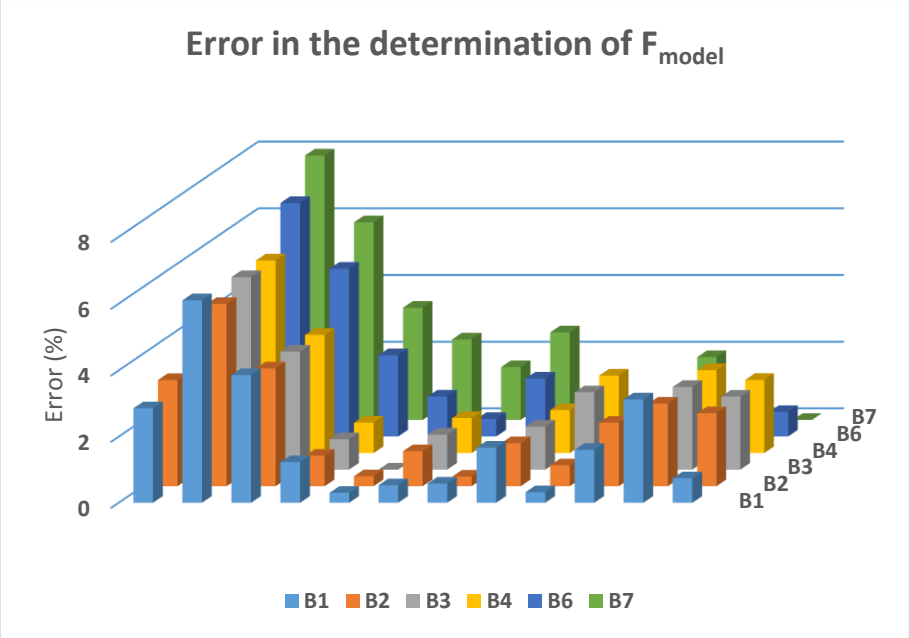

Figure 6.5: Error between model – calibration forces for model forces based on calibration of B1, B2, B3, B4, B6, B7

As shown in the tables and figures for most of the bolts the difference between model and calibration forces is very low, resulting in an average error of 2.36% with a standard deviation of 1.72%, which leads to a maximum error of 4.08% and a minimum error of 0.64%. Generally, that difference depends on two factors: 1) the "quality" of the calibration line based on which the determination of the model force is done and how accurately does the model fits to the line, since the procedure presented in this section is a combination between the model presented in section 6.1 and the calibration lines of the bolts. 2)The accuracy of the diameter measurement. Therefore, before the determination of the model force based on a calibration line, it is required to ensure a good "quality" of the calibration line and to measure bolts' diameters as accurate as possible.

6.3 Estimation of the force based on one calibration line (3rd approach)

As it is described in section 6.2, the modified model derived from calibration line of one bolt is based on the assumption that since the bolts come from the same batch, their Young's modulus is the same and therefore, the difference between the calibration factors is caused mainly by the difference in the net cross section area. If this difference is quite low, then it could be possible to ignore the actual diameter of the bolts and derive the residual preload based on the calibration line of one bolt, without being corrected based on the actual diameter. In Tables F27 – F39 in Appendix F, the residual preload is estimated based on calibration lines of all bolts, as presented in Appendix F (Fig. F1 – F13).

6.3.1 Discussion

The error between the estimated and calibration forces is presented in the following figures, where the horizontal right axis represents the bolts of which the calibration lines were used to determine the residual forces.

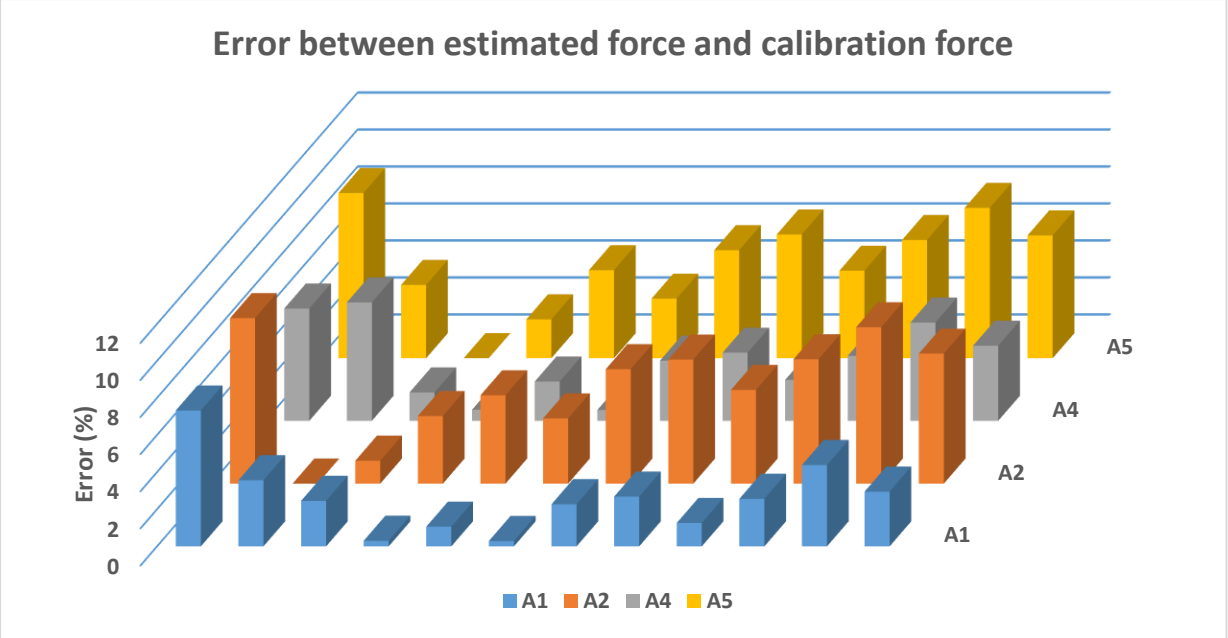

Figure 6.6: Error between estimated – calibration forces for forces based on calibration of A1, A2, A4, A5

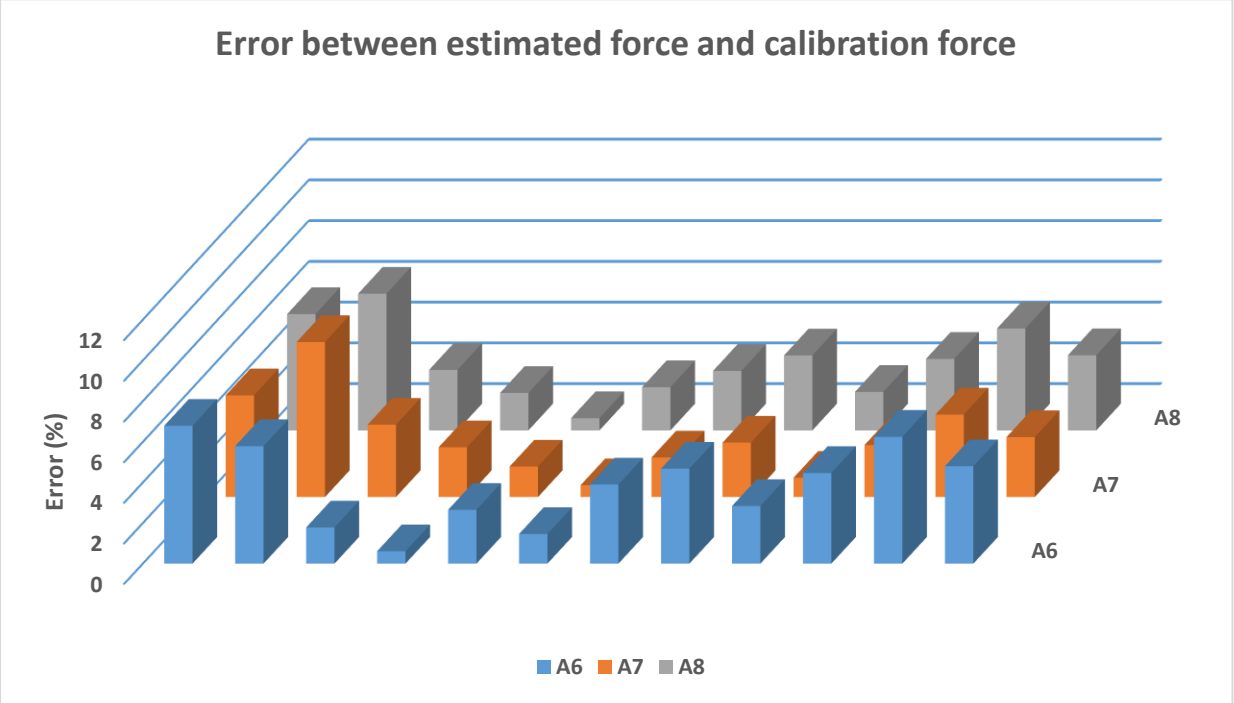

Figure 6.7: Error between estimated – calibration forces for forces based on calibration of A6, A7, A8

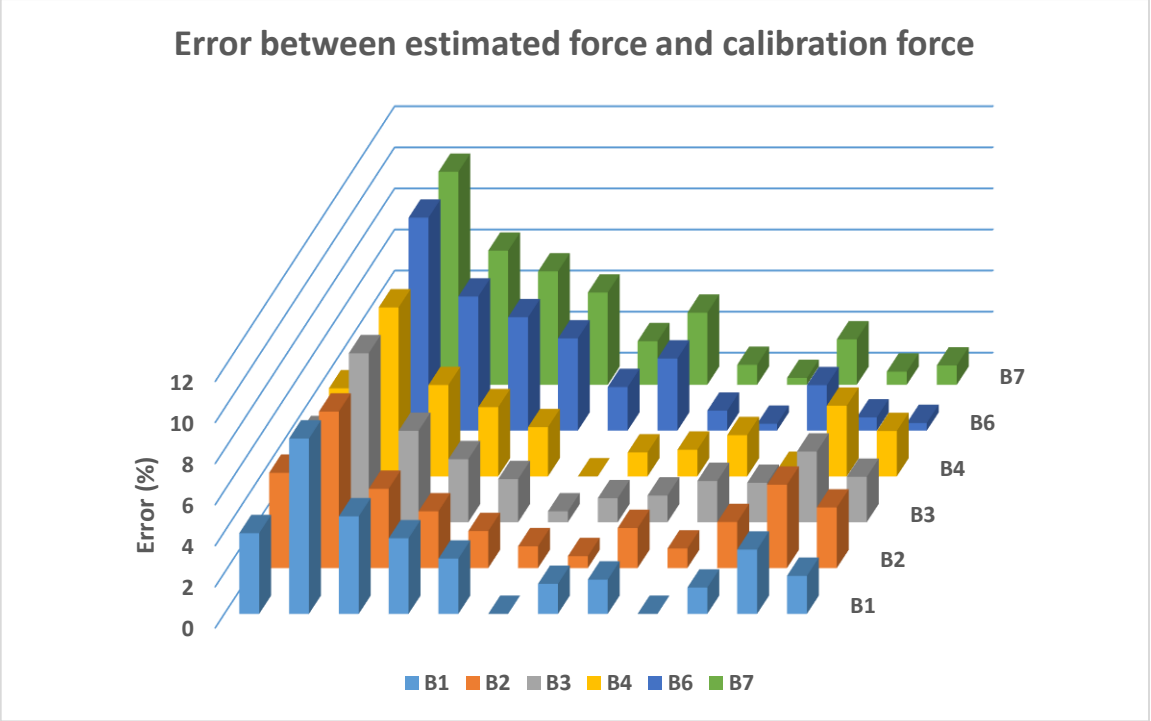

Figure 6.8: Error between estimated – calibration forces for forces based on calibration of B1, B2, B3, B4, B6, B7

The average difference between calibration and model forces is 3.4% with a standard deviation of 2.36%, resulting in a maximum error of 5.76% and a minimum error of 1.04%. The average error is slightly higher compared to the approach presented in section 6.2. The biggest difference between model and calibration forces is observed for determination of the forces based on the calibration line of bolts A2, A5, A6, as shown in Fig. 6.6, 6.7, 6.8, because these bolts are characterized by the largest diameters among the bolts of the connection. Generally, the difference between estimated and calibration forces depends mainly on the difference between the diameter of the bolt of which the calibration line is used and the diameter of the bolt of which the preload force is asked.

It would be possible to correct the calibration lines of bolts with diameters close to the highest and lowest boundary of the range of diameters of the bolts of the connection, if the mean value of the diameters of the bolts of the connection was known. Considering that the diameters of the bolts are normally distributed and that most of the diameters of the bolts are close to the mean value, it would be possible to correct the calibration factors (the slope of calibration lines) of the calibration lines which are used to determine the forces, based on that mean value. Therefore, if the diameter of the bolt of which the calibration line is used to determine the forces is close to the highest or lowest boundary of the range of diameters of the bolts of the connection, it could be corrected based on the mean value of the diameters and therefore reduce the error in the force of most of the bolts. If the diameter of the bolt of which the calibration line is used to determine the forces is close to the mean value of the diameters of the bolts of the connection, then this correction will not have any influence on the resulting forces. However, such information about the mean value of the bolts is not provided.

The only available information about bolts which come from the same batch is that the maximum coefficient of variation of their diameters is 0.005, as mentioned in the background report to Eurocode 3 “Common unified rules for steel structures”. Therefore, what is possible

is to correct the calibration factor of the bolt of which the calibration line is used to determine the forces to a lower value, based on the coefficient of variation, by assuming that the diameter of the bolt is close to the highest boundary of the range of diameters of the bolts of the connection. This would result in an underestimation of the preload force, which is on the safe side. The procedure is described in detail in section 6.4.

6.4 Estimation of the force based on correction of calibration factors (4th approach)

In this section the procedure for the correction of the calibration factors is described. The influence of two corrections on the estimated force and the influence of the variation in bolts' diameters on the estimated force are discussed.

6.4.1 Estimation of the force based on correction of calibration factors (correction A)

As mentioned, based on the background report to Eurocode 3 "Common unified rules for steel structures" the coefficient of variation of bolts which come from the same batch is maximum 0.005. In order to verify that information, the coefficient of variation of the bolts taken from the connection was determined and it was found equal to 0.005. Furthermore, the diameters of thirty bolts from the lab were measured and their coefficient of variation was determined equal to 0.0007.

If a bolt B_i with a diameter d_i is taken from the connection in order to perform calibration, then the calibration line is described by eq. 6.3.

$$F_i = CF_i \cdot \varepsilon \tag{6.3}$$

where, CF_i is the calibration factor, ε is the strain and F_i is the force.

The only available information about the diameters of the bolts of the connection is that their coefficient of variation is not more than 0.005, which means that s = 0.005·m, where s is the standard deviation and m is the mean value. Three cases are distinguished:

1) If d_i is close to the highest boundary of the range of the diameters of the bolts of the connection, then a good estimation of the mean value would be $d_{cor} = d_i - 0.005 \cdot m$. This would lead in a reduction of the error in the forces of most of the bolts.

2) If d_i is close to the mean value of the diameters of the bolts of the connection and the same correction is used ($d_{cor} = d_i - 0.005 \cdot m$), then this would increase the error in the resulting force of most of the bolts compared to the case in which no correction is applied, but this error is still lower than that determined based on the model described in section 6.2. Furthermore, since the calibration factor is corrected to a lower value, the preload force of most of the bolts is underestimated and is on the safe side.

3) If d_i is close to the lowest boundary of the range of the diameters of the bolts of the connection and the same correction $d_{cor} = d_i - 0.005 \cdot m$ is applied, the estimated force is again on the safe side and the error in the force increases slightly.

For these reasons we can assume that the diameter of the bolt d_i is close to the highest boundary of the range of the diameters of the bolts. In the best case (1) the error of the estimated forces of most of the bolts will be reduced and in the worst case (2, 3) the estimated force will be on the safe side and the error will slightly increase, but it will be lower than that determined based on the model in section 6.1.

Since the mean value m is not known, it is possible to apply this correction by considering m = d_i. The difference will not be high, because 0.005·mean value = 0.005·23.67 = 0.118 mm and considering the dimensional tolerances of the bolts, the correction varies from 0.005·23.16 = 0.116 ≈ 0.12 mm to 0.005·24.84 = 0.124 ≈ 0.12 mm. Therefore, the correction can be considered equal to 0.12 mm or 0.005·d_i.

The estimated force is decribed by eq. 6.4.

$$F_i = \frac{CF_i}{A_i} A_{cor} \tag{6.4}$$

where, $A_{cor} = \frac{\pi d_{cor}^2}{4} - A_{hole}$ and $A_i = \frac{\pi d_i^2}{4} - A_{hole}$.

The results are presented in Tables F40 – F52 in Appendix F. The negative error means that the estimated force is higher than the calibration force, therefore a positive error means underestimation of the preload force.

The resulting average error in the preload force based on the corrected calibration lines is 3.25% with a standard deviation of 2.44%, resulting in a maximum error of 5.69% and a minimum error of 0.81%., which is slightly lower compared to the case in which the forces are determined based on the original calibration line of one bolt. Furthermore, the average error in the underestimated forces is 3.67%, with a standard deviation of 0.97%, which leads to a maximum error equal to 4.64% and a minimum error equal to 2.7% and the average error in the overestimated forces is 2.21% associated by a maximum error of 3.59% and a minimum error of 0.83%. This means that the force which is determined based on this approach may be either 4.64% lower than the actual force or 3.59% higher than the actual force. Therefore, by applying this correction it is achieved to define the lowest (in case of underestimation) and highest boundary (in case of overestimation) of the error.

As shown in Tables F40 – F52, for determination of the forces based on the calibration lines of bolts A2 and A5 which are characterized by the highest diameters among the bolts of the connection, the error in the estimated force reduces for almost all the bolts. Determination of the forces based on calibration lines of bolts A4, A7, A8, B1, B2, B3, B4, B7 which are characterized by diameters close to the average value of 23.67 mm, results in forces with a very low error for the bolts with diameters between the lowest boundary and the mean value and for bolts with diameters between the mean value and the highest boundary the error increases a bit, but the estimation is on the safe side, because the estimated force is lower than the calibration force. Finally, for determination of the force based on the calibration line of bolts with diameters close to the lowest boundary the error of all the bolts increases a bit (bolts B6 and B7), but the estimation of the force is on the safe side.

6.4.2 Estimation of the force based on correction of calibration factors (correction B)

As mentioned before, by applying a correction and reducing the diameter of the bolt by 0.5%, it is possible to define the lowest and highest boundary of the error. Therefore, if the diameter is reduced by 3·0.5% = 1.5%, a more underestimated force will be derived. The results are shown in Tables F53 – F65 in Appendix F.

The average error which results from the determination of the preload force based on correction A and B is shown in Table 6.3 and Fig. 6.9. At the left side of Fig. 6.9 the error which results from correction A is presented and at the right side the error which results from correction B is shown. Each coloured dot represents the average error and the bars represent the maximum and minimum values of that error.

Table 6.3: Error (%) resulting from correction A and B

Error (%) in te estimated force for the two approaches based on the correction of one calibration line		average error (%)	maximum error (%)	minimum error (%)
Correction A (reduction of diameters by 0.5%)	total error (%)	3.25	5.69	0.81
	Error in underestimated forces (%)	3.67	4.67	2.7
	Error in overestimated forces (%)	2.21	3.59	0.83
Correction B (reduction of diameters by 1.5%)	total error (%)	3.52	6.50	0.54
	Error in underestimated forces (%)	3.93	4.77	3.09
	Error in overestimated forces (%)	1.23	2.16	0.30

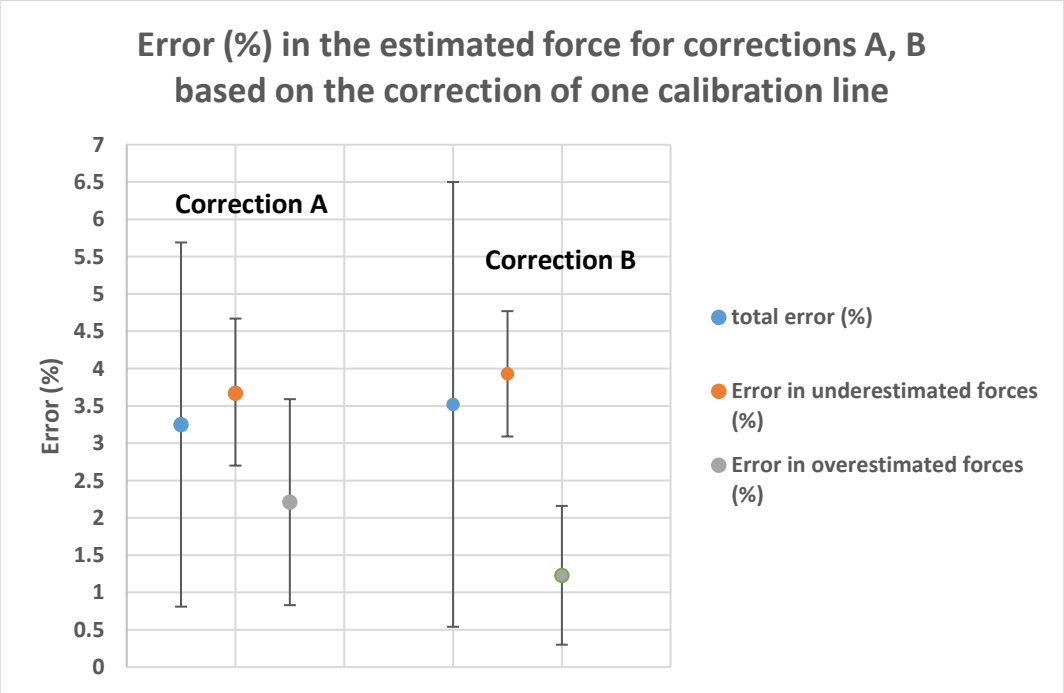

Figure 6.9: Error (%) resulting from correction A and B

As shown, the total average error, which describes how far or how close are the estimated forces from the actual value of the force, increases slightly, because of the higher reduction of the diameter of the bolt which is calibrated. Therefore, the new calibration factor describes less accurately the original calibration factors of the majority of the bolts, the bolts with

diameters close to the average diameter. Furthermore, the error in the overestimated force, which describes how much higher is a force which is overestimated than the actual value of the force, drops by almost 1.4%. The error in the underestimated force, which describes how lower is the underestimated force compared to the actual force, increases slightly. For that particular group of bolts with that specific variation, this small increase is caused because, as shown in Fig. 6.10, it is assumed that bolts' diameters follow a normal distribution, but most of the bolts are characterized by diameters which are between the lowest boundary of the diameters' distribution and the average value. Therefore, an even higher reduction of the diameter of the bolt which is calibrated, does not affect much the lowest boundary of the estimated force.

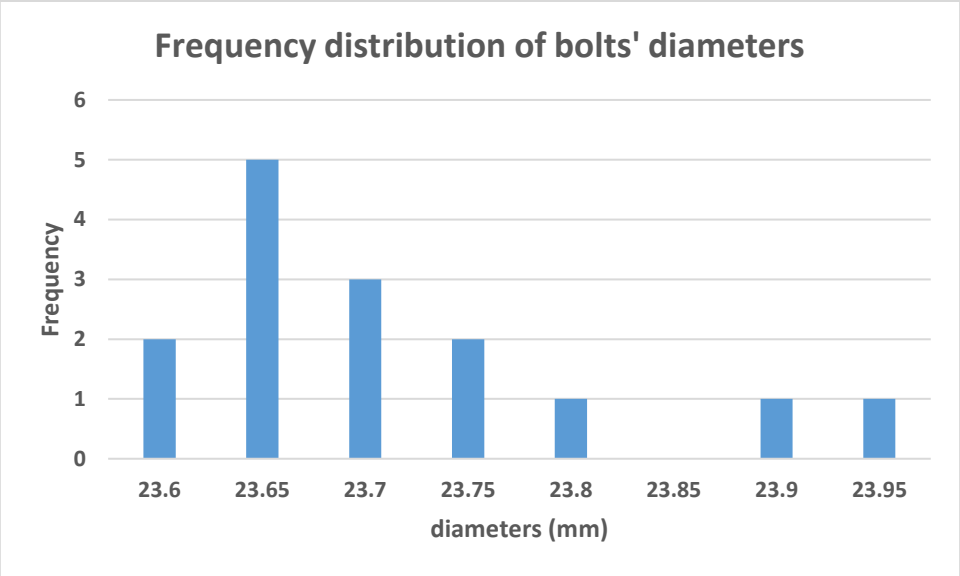

Figure 6.10: Frequency distribution of bolts' diameters

6.4.3 Influence of various corrections on the estimated force

As shown in sections 6.4.1, 6.4.2, by correcting the calibration line assuming a maximum variation in bolts' diameters equal to 0.005, it is possible to "control" the highest and the lowest boundary of the estimated force. Depending on the purpose of the in situ measurements that are performed, a different correction can be applied, resulting in a different degree of underestimation or overestimation of the force. The resulting maximum error in the underestimated and overestimated force is shown in Fig. 6.11 and Table F79 in Appendix F, for various corrections of a calibration factor. The coloured dots represent the actual force and the bars at the positive and negative side of the vertical axis represent the error for each correction, for an overestimated or underestimated force, respectively. For example, if the correction $-3 \cdot 0.005 d_i$, represented by the yellow dot, is applied, it means that if the resulting force is overestimated, then the maximum error of that force is 2.1%. Likewise, if the resulting force is underestimated, then the maximum error of that force is 4.8%.

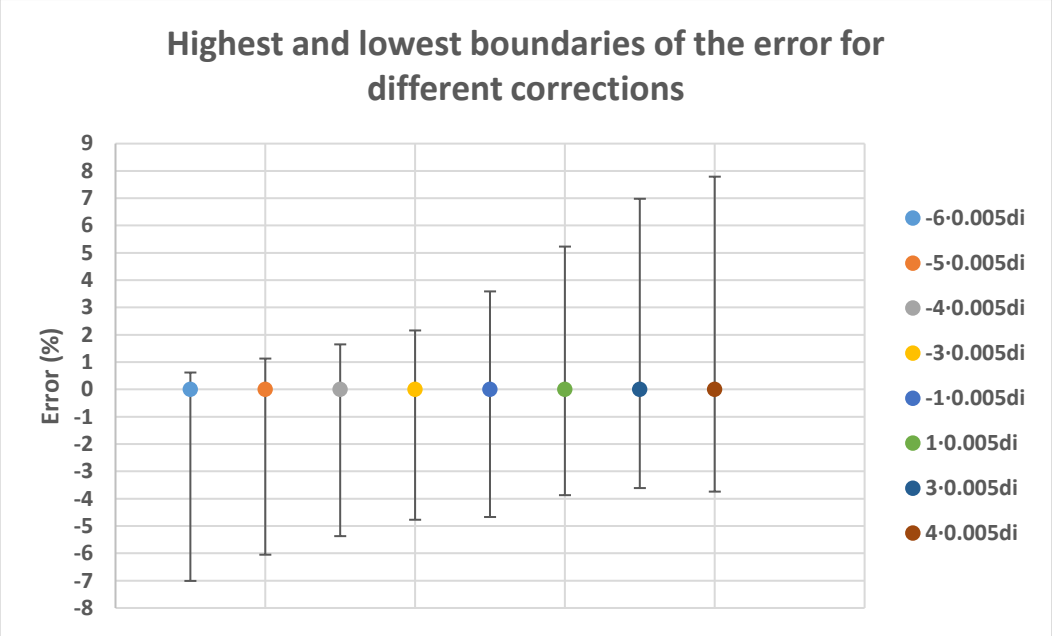

Figure 6.11: Influence of different corrections on the highest and lowest boundaries of the estimated force

As shown, a different correction results in a different error in the underestimated/overestimated force. Therefore, by applying a correction in that way, it is possible to know whether the resulting force is underestimated or overestimated. However, the disadvantage of this approach is that the accuracy of the estimation drops. For example, for a correction $d_{cor} = d_i - 6 \cdot 0.005 d_i$ it is possible to ignore the error in the overestimated force, because it is very low. Therefore, it is known that the force is underestimated with a maximum error of 7%.

These boundaries are typical for diameters with a variation equal to 0.005 and for the distribution of the bolts of that particular connection. As shown in Fig. 6.42, the distribution of these bolts resembles a positively skewed normal distribution. In other connections the bolts may resemble a normal distribution or even a negatively skewed normal distribution and for this reason these boundaries should be tested for different distributions.

6.4.4 Estimation of the force based on the mean diameter

Now that the average error in the determination of the preload force based on the calibration line of one bolt corrected based on the variation of bolts' diameters is known, it would be interesting to see what would be the error in the force, if the calibration lines of the bolts were corrected based on the average diameter of the group of bolts.

The calibration lines of all the bolts taken from the connection are corrected based on the average diameter, which is equal to 23.67 mm. The results are presented in Tables F66 – F78 in Appendix F.

The average error in the preload force for correction of the calibration lines based on the average value of bolts' diameters is 3.09% with a standard deviation of 2.02%, resulting in a maximum error of 5.11% and a minimum error of 1.07%.

Comparing the correction based on the average diameter with the correction based on the variation of bolts' diameters, it is observed that it is possible to achieve the accuracy of the first by applying the second approach. For example, the maximum average error in the estimated force resulting from the second approach can reach 5.69% (correction A), 0.6%

higher than the maximum error resulting from the method which is based on the correction according to the average diameter. However, the benefit of correcting based on the variation is that depending on the correction which is applied, it is possible to "control" the boundaries of the estimated force and know whether the estimated force is higher or lower than the actual force.

6.4.5 Influence of the actual coefficient of variation on the estimated force

In section 6.4, a process of correcting the calibration lines of the bolts based on the variation of the diameters was presented. This correction is based on the fact that the maximum coefficient of variation of bolts of the connection is 0.005. Indeed, the coefficient of variation of the bolts of that particular connection is 0.005. This brings up the question, what would be the influence on the error of the determined forces, if the actual coefficient of variation of the bolts of a connection is different than 0.005? The answer is given by considering that the connection which is under consideration consists of four quadrants and at each quadrant four bolts were tested. It is expected that the variation of the diameters of the bolts will not be the same at each quadrant. For some quadrants it might be higher than 0.005 and for other quadrants it might be lower than 0.005. Therefore, in this section the influence of the correction, based on an assumed coefficient of variation 0.005, on the error of the forces will be examined, as a function of the actual variation at each quadrant.

The diameters of the bolts of the first quadrant are characterized by a coefficient of variation 0.009, of the second quadrant 0.004, of the third quadrant 0.001 and of the fourth quadrant 0.003. The forces based on the correction of the calibration factor have been estimated in section 6.4 and in Tables F40 - F65 in Appendix F. The resulting error per quadrant is presented in the following tables. The second row in these tables presents the bolts of which the calibration lines were used and corrected to determine the preload and the fist column presents the bolts of which the preload was determined. In this section, a correction based on $-1 \cdot 0.005 d_i$ (correction A) and $-3 \cdot 0.005 d_i$ (correction B) only will be considered.

Table 6.4: Error (%) in the force for determination of the preload based on the corrected calibration lines of the bolts of the 1st quadrant

1st quadrant (c.o.v = 0.009)								
	Correction A				**Correction B**			
Bolts	**A1**	**A2**	**A3**	**A4**	**A1**	**A2**	**A3**	**A4**
A1	-	8.23	-	4.45	-	-5.71	-	-2.86
A2	-7.86	-	-	0.89	10.06	-	-	9.15
A3	-	-	-	-	-	-	-	-
A4	-5	7.32	-	-	6.53	2.97	-	-
average error (%)	**5.63**				**6.22**			
maximum error (%)	**8.42**				**9.24**			
minimum error (%)	**2.84**				**3.20**			

Table 6.5: Error (%) in the force for determination of the preload based on the corrected calibration lines of the bolts of the 2nd quadrant

2nd quadrant (c.o.v = 0.004)								
	Correction A				Correction B			
Bolts	**A5**	**A6**	**A7**	**A8**	**A5**	**A6**	**A7**	**A8**
A5	-	1.84	3.68	2.76	-	3.68	5.52	4.6
A6	-1.2	-	2.69	1.8	0.9	-	4.49	3.59
A7	-3.7	-1.59	-	-1.06	-1.59	0	-	1.06
A8	-2.34	-0.29	1.46	-	-0.29	1.75	3.51	-
average error (%)	**2.03**				**2.58**			
maximum error (%)	**3.07**				**4.44**			
minimum error (%)	**0.99**				**0.72**			

Table 6.6: Error (%) in the force for determination of the preload based on the corrected calibration lines of the bolts of the 3rd quadrant

3rd quadrant (c.o.v = 0.001)								
	Correction A				Correctioin B			
Bolts	**B1**	**B2**	**B3**	**B4**	**B1**	**B2**	**B3**	**B4**
B1	-	-0.97	-0.32	-0.32	-	0.97	1.62	1.62
B2	-0.67	-	-1	-1	1.34	-	1	1
B3	0.95	0	-	0.63	3.15	2.21	-	2.84
B4	-0.32	-1.28	-0.64	-	1.6	0.64	1.28	-
average error (%)	**0.68**				**1.61**			
maximum error (%)	**1.06**				**2.38**			
minimum error (%)	**0.3**				**0.84**			

Table 6.7: Error (%) in the force for determination of the preload based on the corrected calibration lines of the bolts of the 4th quadrant

4th quadrant (c.o.v = 0.003)								
	Correction A				Correction B			
Bolts	**B5**	**B6**	**B7**	**B8**	**B5**	**B6**	**B7**	**B8**
B5	-	-	-	-	-	-	-	-
B6	-	-	0	-	-	-	2.19	-
B7	-	1.48	-	-	-	3.32	-	-
B8	-	-	-	-	-	-	-	-
average error (%)	**0.74**				**2.76**			
maximum error (%)	**1.79**				**3.56**			
minimum error (%)	**0.31**				**1.96**			

The results are summarized in Fig. 6.12. The coloured dots represent the average total error and the bars the maximum and minimum values. It is obvious that the higher the coefficient of variation in the diameters of the bolts of a connection is, the higher the resulting error in the estimated force becomes, for both approaches. The highest error is observed for a coefficient of variation equal to 0.009. However, it has to be noted that according to the background report to Eurocode 3 "Common unified rules for steel structures", the maximum value of the coefficient of variation which has been observed for bolts of the same connection is 0.005 and this was also confirmed by measuring the diameters of bolts found in the lab. Finding lower error for lower coefficient of variation is reasonable, because a low coefficient of variation means that bolts' diameters are close to each other. Therefore, any correction applied, will correct the diameter of the bolt to a new value, close enough to the diameters of the other bolts. Furthermore, the second approach leads to a slightly higher error than the first approach, because of the higher reduction of the calibration factor.

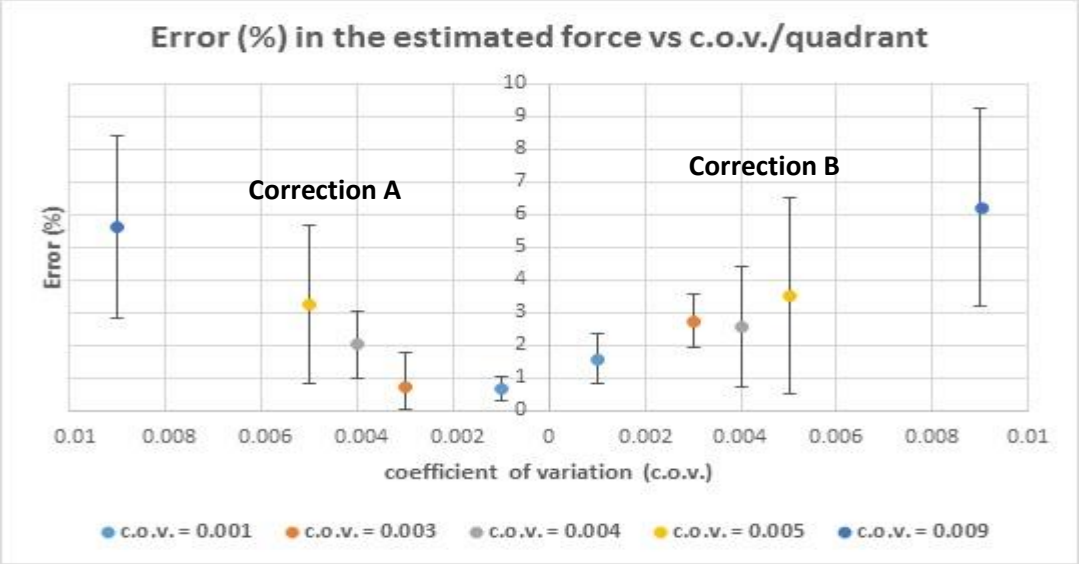

Figure 6.12: Error (%) in the determination of the preload force vs c.o.v.

It is already shown that the error in the underestimated force increases and the error in the overestimated force drops, when correction B is applied. In Fig. 6.13, it is shown that the same occurs for different variations in the diameters of the bolts. Furthermore, the lower the coefficient of variation is, the lower the error in the underestimated and overestimated force becomes, for both approaches. Therefore, it can be said that a variation in bolts' diameters equal to 0.005 can lead to the highest error for both the underestimated and overestimated force.

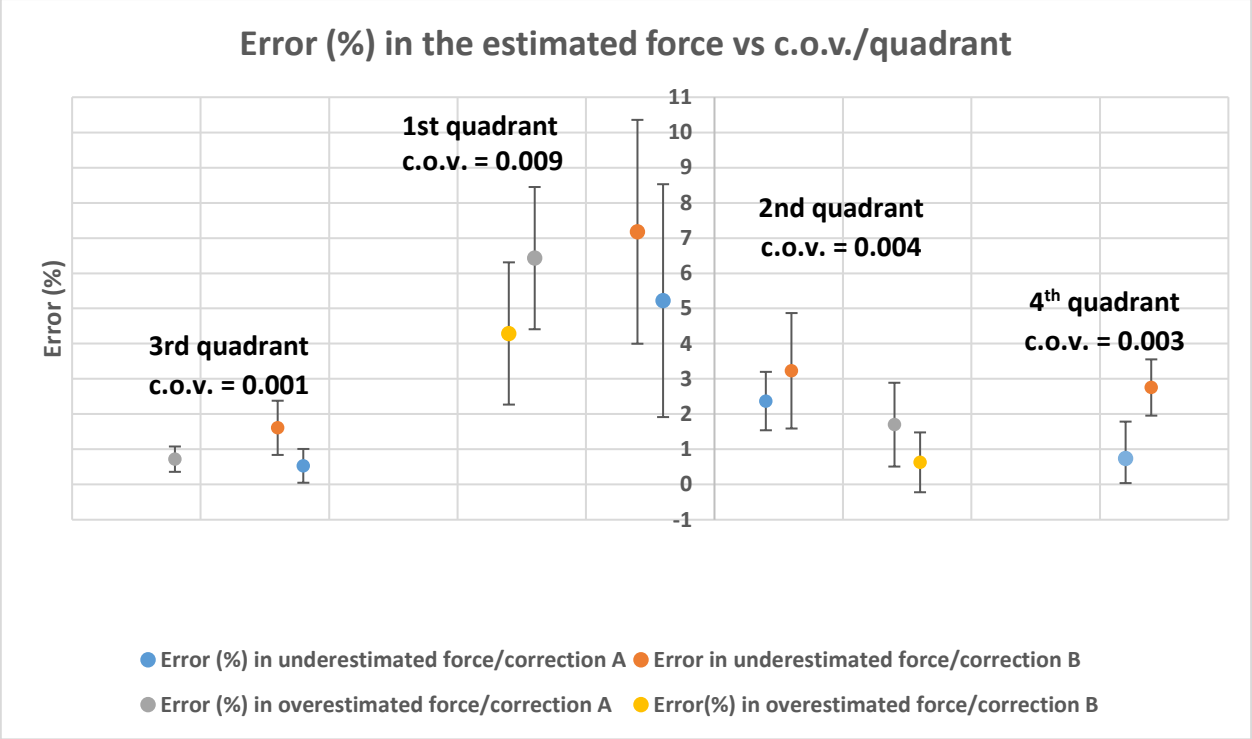

Figure 6.13: Error (%) in the under/overestimated force for each quadrant

6.5 Acceptability of the error resulting from the different approaches

In the last four sections, four ways of determining the preload were discussed, aiming to reduce the time which is required to calibrate all bolts and achieve the maximum accuracy. Each approach results in a different error. Therefore, it is important to know whether the error resulting from each approach can lead to a safe conclusion about the preload condition of the bolts of a connection.

The answer to the question what error can be considered as acceptable is not unique. It depends on the purpose of the in situ measurements. If the aim is to check whether the residual preload is higher than the minimum required preload, even the original model based on the dimensional toleranes may be enough, if the most pessimistic estimation is higher than the $0.7f_{ub}A_s$, which implies that the actual residual preload is much higher than the estimated. If not, then a more accurate estimation is needed like the one which is based on the original model and measurement of the diameters of the bolts. Therefore, the acceptability of the error depends on the purpose of the measurements and also on the magnitude of the estimated residual preload.

However, if a detailed analysis is required, which includes estimation of the mechanism that led to the preload loss, then a high accuracy is required, because in this case, it might be necessary to distinguish the difference in the preload force of bolts at different locations on the connection.

Therefore, the purpose of the measurements is the basic criterion based on which the most appropriate approach for the determination of the preload force is chosen.

6.6 Conclusion

In this chapter four approaches of determination of the preload force and the resulting error was discussed. The purpose of these approaches is to reduce the time which is required to

calibrate all bolts. In Fig. 6.14 the accuracy of these approaches is presented. The coloured dots represent the average total error and the bars the maximum and minimum boundaries of that error.

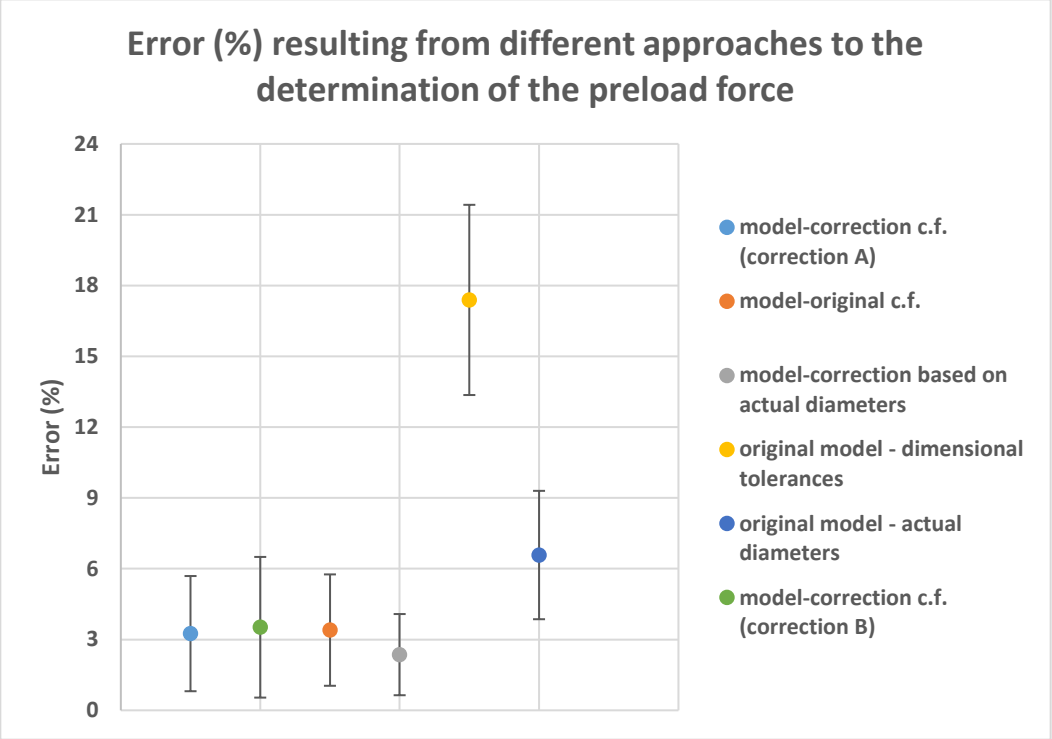

Figure 6.14: Error (%) and its boundaries for the five methods of estimation of the force

Therefore, there are five different ways in total, to estimate the force:

1) Calibration of all bolts. This approach results in the maximum accuracy, however it is the most time consuming way of determination of the force.

2a) Based on the original model without knowing the actual diameters: Considering that F = AE·ε, the force is estimated for different values of Young's modulus and based on the dimensional tolerances. This approach requires the least amount of work, but it results in the highest error.

2b) Based on the original model with known actual diameters: What is mentioned in 2a) applies here too, with the only difference that the actual diameters of all the bolts are known.

3) Based on a combination between the model and one calibration line. The slope of that line is considered equal to the product EA_{net}. Therefore, by calibrating one bolt the uncertainty of Young's modulus diminishes, since all the bolts of the connection come from the same lot. Then, the calibration line is corrected based on the actual diameter of each bolt. In that case, the calibration of one bolt and the measurement of the diameters of all the bolts are required.

4) Based on the calibration line of one bolt. The difference between the calibration lines of the bolts of the connection is caused mainly by the difference in their diameters. Therefore, if the variation in the diameters is low, this will result in a low error in the estimated force. This approach requires the calibration of one bolt, without measurement of the diameters. The error increases compared to the third way of approach.

5)Lastly, the fifth approach is based on the calibration of one bolt and the correction of its calibration factor based on the variation in the diameters of the bolts of the connection. Depending on the correction which is applied, it is possible to underestimate or overestimate the force. Therefore, this approach is advantageous compared to approaches 3) and 4), because it offers the possibility of knowing whether the estimated force is higher or lower than the actual force, but with a lower accuracy. The same is offered by approaches 2a) and 2b) (for an estimation of the force based on the lowest boundaries of E modulus and d_{nom}), however, the accuracy of approach 5) is higher. Therefore, this method gives the possibility, not to improve the accuracy, but to "control" the degree of the underestimation or overestimation of the force. This method requires the calibration of one bolt and measurement of its diameter.

The error of the approaches presented in this chapter is representative for the bolts of that particular connection, which are characterized by a certain geometry and distribution of their diameters. Therefore, in order to generalize the conclusions discussed in this chapter, more tests are needed on connections with bolts of different geometrical characteristics and diameters' distribution.

The acceptability of the error resulting from each approach depends on the purpose of the measurements.

7 CONCLUSION

Considering the importance of knowing the preload of bolts in HSFG connections, the following conclusions can be derived about the feasibility of determining the preload of the bolts.

1. It is possible to determine the residual preload of bolts in HSFG connections (under actual practice conditions) using the strain gauge method, given that the strain gauges are properly installed in the bolts. The installation of a strain gauge is a time consuming process. In this report a new type of strain gauges is mentioned, which simplifies the installation procedure. The strain gauge method was tested under laboratory conditions by imitating the in situ conditions and under actual practice conditions by testing the connection of an existing structure. The maximum measured variation in the forces is 1.5%. Temperature variations may affect the strain gauge measurements, but a way to compensate for temperature related effects is presented in this report. It has to be noted that two out of the sixteen strain gauges used for the in situ measurements gave unreliable readings.

2. If maximum accuracy is required, then time consuming calibration tests are neccessary. However, in this report four approaches and an engineering assessment on the difference of the estimated force resulting from each approach from the calibration force, was presented. These approaches aim to reduce the number of calibration tests. The obtained error presented for these ways of estimating the preload, was based on the calibration lines, geometrical characteristics and the distribution of the bolts' diameters, for the bolts of that particular connection. To generalize and validate them, further investigation on more connections is necessary.

3. Compared with other methods which offer the possibility of determining the preload of bolts in HSFG, the strain gauge method is the most beneficial method. In contrast to these methods, the strain gauge method is not affected by factors which govern the in situ measurements and it offers a simple compensation for these effects and also it is not affected by unpredictable variables like couplant's thickness.

References

[1] J.H. Bickford, Introduction to the Design and Behavior of Bolted Joints, third edition.

[2] Christine Heistermann, Resistance of Friction Connections with Open Slotted Holes in Towers for Wind Turbines, Doctoral Thesis, Lulea University of Technology, November 2014.

[3] Friede R., Lange, J.: "Loss of preload in bolted connections due to embedding and self loosening", Proc. Stability and ductility of steel structures (SDSS'Rio 2010), pp. 287 – 293, Rio de Janeiro, Brazil, 2010.

[4] Christine Heistermann, Behaviour of Pretensioned Bolts in Friction Connections, Licentiate Thesis, Lulea University of Technology, June 2011.

[5] John T. DeWolf, Jun Yang, Relaxation in high-strength bolted connections with galvanized steel, Connecticut Transportation Institute, 2000.

[6] Wylliam Husson, Friction Connections with Slotted Holes for Wind Towers, Licentiate Thesis, Lulea University of Technology, November 2008.

[7] C. Heistermann, M. Veljkovic, R. Simões, C. Rebelo, L. Simões da Silva, Design of slip resistant lap joints with long open slotted holes, Journal of Constructional Steel Research 82 (2013) 223-233, January 2013.

[8] N. Motosh, Development of Design Charts for Bolts Preloaded up to the Plastic Range,

J. Eng. Ind., doi:10.1115/1.3439041, pages 858-861 (1976).

[9] Struik, J.H.A. and Fisher J.W., Bolt Tension Control with a Direct Tension Indicator, AISC Engineering Journal, vol. 10, no. 1, pp. 1–5 (1973).

[10] Prof. Ir. Jacques Berenbak, EN 1090-2 "Technical requirements for steel structures" for 95% reliability EN1990, June 2012.

[11] Nederlandse norm NEN-EN 14399-4 (en). High-strength structural bolting assemblies for preloading - Part 4: System HV - Hexagon bolt and nut assemblies, April 2005.

[12] Yoon-Si Lee, Brent Phares, Tim Brockman, Jessica Rooney, High Strength Bolt Tightening and Verification Techniques, Journal of Civil Engineering and Architecture Research, Vol. 3, No. 8, pp. 1605-1617, August 2016.

[13] John H. A. Struik, Abayomi O. Oyeledun and John W. Fisher, Bolt Tension Control with a Direct Tension Indicator, AISC Engineering Journal, pp. 1-5, 1973.

[14] Culpepper M., Elements of Mechanical design, MIT OpenCourseWare, https://ocw.mit.edu/courses/mechanical-engineering/2-72-elements-of-mechanical-design-spring-2009/lecture-notes/MIT2_72s09_lec10.pdf, 2009.

[15] Davet George, Why Do Gasketed Joints Leak?, http:// www. solonmfg.com / springs /pdfs /JointLeaksLoRez.pdf, Solon Manufacturing Company.

[16] Shoji, Y., & Sawa, T., Analytical Research on Mechanism of Bolt Loosening due to Lateral Loads, Pressure Vessels and Piping Division Conference, Denver, (pp. 1-7), 2005.

[17] ESDEP, Connections with Preloaded Bolts.

[18] D. M. Egle and D. E. Bray, Measurement of acoustoelastic and third-order elastic constants for rail steel, School of Aerospace, Mechanical and Nuclear Engineering, University of Oklahoma, Norman, Oklahoma 73069, 15 May 1976.

[19] Pham Van Thanh, Pham Thi Tuyet Nhung, Luong Thi Minh Thuy, Nguyen Hoa Nhai, Effect of Temperature on Ultrasonic Velocities, Attenuations, Reflection and Transmission Coefficients between Motor Oil and Carbon Steel Estimated by Pulse-echo Technique of Ultrasonic Testing Method, Faculty of Physics, VNU University of Science, 03 October 2015.

[20] Nohyu Kim, Minsung Hong, N.Kim and M.Hong, Measurement of axial stress using mode converted ultrasound, NDT and E International, vol. 42, no. 3, pp. 164–169, 2009.

[21] Xu Ding, Xinjun Wu, Yugang Wang, Bolt axial stress measurement based on a mode-converted ultrasound method using an electromagnetic acoustic transducer, Ultrasonics 54, pp. 914-920, 2014.

[22] Hajime Yasui, Koichiro Kawashima, Acoustoelastic measurement of bolt axial load with velocity ratio method, in: 15th World Conference on Non-Destructive Testing, Rome, 2000.

[23] Salim Chaki, Gilles Corneloup, Ivan Lillamand, Henri Walaszek, Combination of longitudinal and transverse ultrasonic waves for in situ control of the tightening of bolts, Journal of Pressure Vessel Technology, Vol. 129, pp. 383-389, August 2007.

[24] Joseph S. Heyman, A CW Ultrasonic Bolt Strain Monitor, Experimental Mechanics 17, pp. 183-187, 1977.

[25] S. G. Joshi, R. G. Pathare, Ultrasonic instrument for measuring bolt stress, Ultrasonics, pp. 270-274, November 1984.

[26] Tao Wang, Gangbing Song, Zhigang Wang, Yourong Li, Proof-of-concept study of monitoring bolt connection status using a piezoelectric based active sensing method, Smart Materials and Structures, vol. 22, no. 8, Article ID 087001, 2013.

[27] Shaopeng Liu, Yourong Li, Tao Wang, Yi Luo, A piezoelectric active sensing method for detection of bolt load loss, Sensor Review, vol. 34, pp. 337-342, 2014.

[28] M. B. Marshall, R. Lewis, T. Howard, and H. Brunskill, Ultrasonic measurement of self-loosening in bolted joints, Proceedings of the Institution of Mechanical Engineers C, vol. 226, no. 7, pp. 1869–1884, 2012.

[29] D. Doyle, A. Zagrai, B. Arritt, and H. Cakan, Damage detection in bolted space structures, Journal of Intelligent Material Systems and Structures, vol. 21, no. 3, pp. 251–264, 2010.

[30]Shahruddin Mahzan, Hatem Mostafa Elwalwal, Muheieddin Meftah Farag Elghanudi, Viability of applying mechanical impedance based structural health monitoring for pipeline: a review, ARPN Journal of Engineering and Applied Sciences, vol. 11, no. 14, July 2016.

[31] Sun, F., Chaudhry, Z., Liang, C., and Rogers, C. A., Truss structure integrity identification using PZT sensor-actuator, J. Intelligent Mat. Sys. and Struct. 6, pp. 134–139, 1995.

[32] Gyuhae Park, Harley H. Cudney, Daniel J. Inman, Impedance – based health monitoring of civil structural components, Journal of Infrastructure Systems, pp. 153 – 160, December 2000.

[33] G. Park and C. R. Farrar, Impedance Methods for Damage Detection and Sensor Validation, Encyclopedia of Structural Health Monitoring, edited by C. Boller, F.K. Chang and Y. Fujino, ISBN: 978-0-470-05822-0, John Wiley & Sons Ltd, Chichester, UK, 2009.

[34] Fabricio G. Baptista, Danilo E. Budoya, Vinicius A. D. de Almeida, Jose Alfredo C. Ulson, An Experimental Study on the Effect of Temperature on Piezoelectric Sensors for Impedance-Based Structural Health Monitoring, Sensors, pp. 1208-1227, 2014.

[35] Park, G., Kabeya, K., Cudney, H., Inman, D. J., Impedance based structural health monitoring for temperature varying applications, JSME Int. J., 42, pp. 249–258, 1999.

[36] National Instruments Measurement Fundamentals series, publish date 4 November 2014.

[37] Installation manual of TML BTMC bolt strain gauges.

[38] Nederlandse norm NEN-EN 14399-4 (en). High-strength structural bolting assemblies for preloading - Part 4: System HV - Hexagon bolt and nut assemblies, April 2005.

[39] Temperature Compensation for Strain Gauges, Theory and Practical Implementation, https://www.hbm.com/en/3977/tips-and-tricks-temperature-compensation-for-strain-gauges/.

[40] Norbar USM – 3, Ultrasonic Bolt Meter, Operation and reference manual, ver. 2.0.

[41] VDI 2230 Part 1, Systematic calculation of high duty bolted joints, 2003.

[42] Frank Scheuch, Ron Baker, PMTS – Technology Permanent Mounted Transducer System presentation, Intellifast Fastener Technology, 2011.

APPENDIX A

Determining sonic stress factor by measuring length

Following are steps for determining the Sonic Stress Factor for bolts of a specific bolt material and specific geometry by measurement of the actual change in bolt length.

Required Equipment:

- A laboratory or room in which the temperature can be maintained from 66° to 70° F (19°- 21°C).
- A means of applying load to the bolt. Ideally this would be a tensile load machine, capable of measuring the applied load to within 100 lbs. However, since the actual value of the applied load is not used in calculating the stress factor, any means of applying an approximate load to the bolt will suffice. This includes tightening the bolt against a fixture that simulates the actual joint. A mechanical means of traceable measurement of the physical length of the sample fasteners at various tensile loads to an accuracy of plus or minus 0.0001 inch. Examples of such devices include the following
  - Length measurement function of sophisticated tensile test machine
  - Mechanical or electronic height gages
  - Averaged values of length measurement with mechanical and electric micrometers.
- A Norbar USM-3 Ultrasonic Bolt Meter.
- A minimum of three sample bolts which are representative of the bolt type and geometry for which the Sonic Stress Factor is to be determined.

NOTES:

- The Norbar USM-3 must be calibrated, or zeroed, as described in the procedure entitled System Zeroing in the Setup section of the USM-3 Operation.
- The sample bolts must be left to soak in the controlled temperature environment for a period of not less than 24 hours. Care must be taken through out the measurement process to avoid significant change in the bolt temperature due to handling of the sample bolts, or the process of applying load.
- The mechanical apparatus for measurement of length must be calibrated in accord with governing QA procedures. The device should be configured so that minimum handling of the sample bolts will be required during the measurement process.

Determination of the Sonic Stress Factor is accomplish by solving the equation:

$$SonicStressFactor = \frac{\Delta L_{MECHANICAL}}{\Delta L_{ULTRASONIC}} = \frac{L_{MI} - L_{M0}}{L_{UI} - L_{U0}}$$

Where:

$$L_{U0} = UltrasonicLength@ZeroLoad$$
$$L_{M0} = MechanicalLength@ZeroLoad$$
$$L_{UI} = UltrasonicLength@Load$$

$$L_{MI} = MechanicalLength@Load$$

Acquire data as follows:

1. Using the mechanical measuring device, measure and record the Mechanical Length at Zero Load "L_{M0}" for each sample bolt.
2. Using the USM-3 in the Unloaded length measurement mode, measure and record the Ultrasonic Length at Zero Load "L_{U0}" for each sample bolt. NOTE: Ultrasonic measurements will be more easily accomplished, and more accurate, if the transducer remains undisturbed on the bolt through out the loading process.
3. Place the first sample bolt in the loading apparatus.
4. Apply approximately 1/3 of the Maximum load, which is to be placed on the bolt under actual working conditions.
5. Using the mechanical measuring device, measure and record the Mechanical Length at Load 1 "L_{M1}" for the current sample bolt.
6. Using the USM-3 in the Unloaded length measurement mode, measure and record the Ultrasonic Length at Load 1 "L_{U1}"for the current sample bolt.
7. Increase the applied load to approximately 2/3 of the Maximum load, which is to be placed on the bolt under actual working conditions.
8. Using the mechanical measuring device, measure and record the Mechanical Length at Load 2 "L_{M2}" for the current sample bolt.
9. Using the USM-3 in the Unloaded length measurement mode, measure and record the Ultrasonic Length at Load 2 "L_{U2}"for the current sample bolt.
10. Increase the applied load to approximately the Maximum load, which is to be placed on the bolt under actual working conditions.
11. Using the mechanical measuring device, measure and record the Mechanical Length at Load 3 "L_{M3}" for the current sample bolt.
12. Using the USM-3 in the Unloaded length measurement mode, measure and record the Ultrasonic Length at Load 3 "L_{U3}"for the current sample bolt.
13. Repeat steps 4 through 12 for the second and third sample bolt.
14. Calculate the value of the Sonic Stress Factor at each load on each sample bolt.

$$SSF_{B1L1} = \frac{L_{M1} - L_{M0}}{L_{U1} - L_{U0}} \qquad SSF_{B1L2} = \frac{L_{M2} - L_{M0}}{L_{U2} - L_{U0}} \qquad SSF_{B1L3} = \frac{L_{M3} - L_{M0}}{L_{U3} - L_{U0}}$$

AND SO ON FOR EACH SAMPLE BOLT

15. Determine the average value of the Sonic Stress Factor by dividing the sum of all SSF values calculated by the total number of SSF values

Table A1: Acoustoelastic coefficients for longitudinal/transverse waves under compressive/tensile stress [18]

(dv/v)/ε	compressive stress	tensile stress
longitudinal wave // stress	-2.45	-2.38
longitudinal wave | stress	0.27	0.27
transverse wave // stress	-0.27	-0.25
transverse wave | stress	-1.53	-1.5

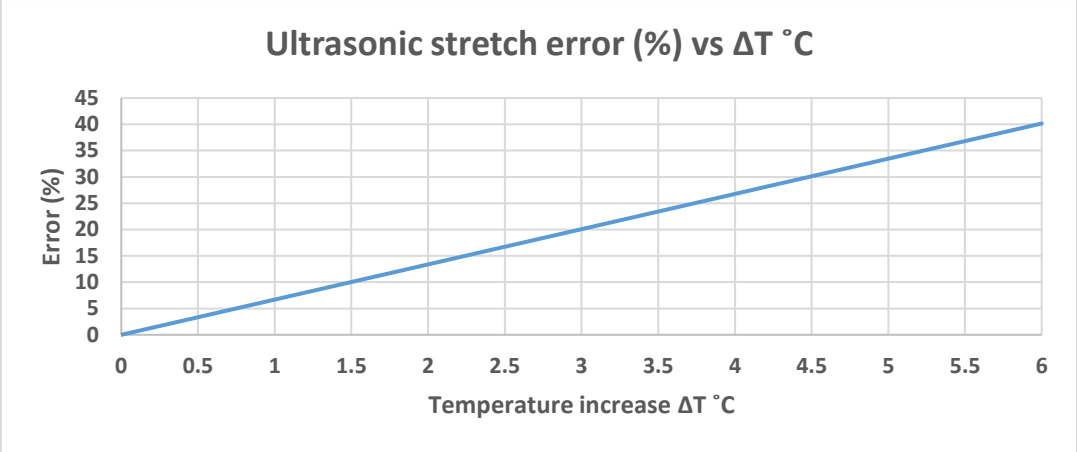

Figure A1: Error (%) in ultrasonic stretch vs temperature increase at 250 kN (conventional ultrasound method)

Determining the Temperature Factor

The following presents the procedure for experimental determination of the Temperature Factor for a bolt made of a specific bolt material and having specific geometry.

Required Equipment.

- A means of varying, and measuring the temperature of the sample bolts between 32° to 212° F (0° to 100° C) to an accuracy of plus or minus 2° F. The device must allow contact of the end of the sample bolt by the ultrasonic transducer of the USM-3.
  Many sophisticate temperature chambers are commercially available, and ideally suited for this function. However, a simple and inexpensive method can be achieved by immersion of the sample bolts in a water bath, which can be heated to boiling or cooled by adding ice. At sea level this will reliably vary the bolt temperature between approximately 212°F and 32° F (100° and 0° C) depending on water purity and atmospheric pressure. By measuring the temperature of the stirred water bath with a precise mercury thermometer, while reading the ultrasonic length of the bolt, accurate calibration points can be obtained.
- A Norbar USM-3 Ultrasonic Stress Meter
- A minimum of three sample bolts, which are representative of the bolt type and geometry for which the Temperature Factor is to be determined.

NOTES:

- The Norbar USM-3 must be calibrated, or zeroed, as described in the procedure entitled System Zeroing in the Setup section of the USM-3 Operation.
- The sample bolts should be left to soak at the measured temperature points for a period of not less than 20 minutes, to insure that temperature is uniform through out the sample.
- If a water bath is used, care must be taken to avoid immersion of the ultrasonic transducer.

Determination of the Temperature Factor is accomplish by solving the equation:

$$TemperatureFactor = \frac{(L_0 - L_T)}{L_T(T_0 - T)} \times 10^6$$

Where:

L_0 = Ultrasonic Length at Beginning Temperature (T_0)
L_T = Ultrasonic Length at Ending Temperature (T)
T_0 = Beginning Temperature
T = Temperature at Present Measurement Point

Acquire data as follows:

1. Stabilize the sample bolt at approximately 32^0 F (0^0 C). If the water bath method is used this is accomplished in a stirred bath of ice and water.
2. Measure and record this minimum temperature as T_0.

3. Using the USM-3 in the "Unloaded Length" measurement mode, measure the ultrasonic length "L_0" of the sample bolt at the above minimum temperature.
4. Increase the temperature of the sample bolt to approximately 68^0 F (20^0 C).
5. Measure and record the exact temperature at this measurement point as T_1.
6. Using the USM-3 in the "Unloaded Length" measurement mode, measure and record the ultrasonic length "L_1" of the sample bolt at temperature T_1.
7. Increase the temperature of the sample bolt to approximately 104° F (40° C).
8. Measure and record the exact temperature at this measurement point as T_2.
9. Using the USM-3 in the "Unloaded Length" measurement mode, measure and record the ultrasonic length "L_2" of the sample bolt at temperature T_2.
10. Increase the temperature of the sample bolt to approximately 140° F (60° C).
11. Measure and record the exact temperature at this measurement point as T_3.
12. Using the USM-3 in the "Unloaded Length" measurement mode, measure and record the ultrasonic length "L_3" of the sample bolt at temperature T_3.
13. Increase the temperature of the sample bolt to approximately 176° F (80° C).
14. Measure and record the exact temperature at this measurement point as T_4.
15. Using the USM-3 in the "Unloaded Length" measurement mode, measure and record the ultrasonic length "L_4" of the sample bolt at temperature T_4.
16. Increase the temperature of the sample bolt to approximately 212° F (100° C).
17. Measure and record the exact temperature at this measurement point as T_5.
18. Using the USM-3 in the "Unloaded Length" measurement mode, measure and record the ultrasonic length "L_5" of the sample bolt at temperature T_5.
19. Repeat steps 1 through 18 for the second and third sample bolt.
20. By solving the above equation calculate the Temperature Factor for each data point on each sample bolt.

$$TF_{B1T1} = \frac{(L_0 - L_1)}{L_1(T_0 - T_1)} \times 10^6 \qquad TF_{B1T2} = \frac{(L_0 - L_2)}{L_2(T_0 - T_2)} \times 10^6$$

AND SO ON FOR EACH SAMPLE BOLT

Determine the average value of the Temperature Factor by dividing the sum of all TF values calculated by the total number of TF values

$$TF_{AVERAGE} = \frac{TF_{B1T1} + TF_{B1T2} + TF_{B1T3} \cdots + TF_{B3T4}}{12}$$

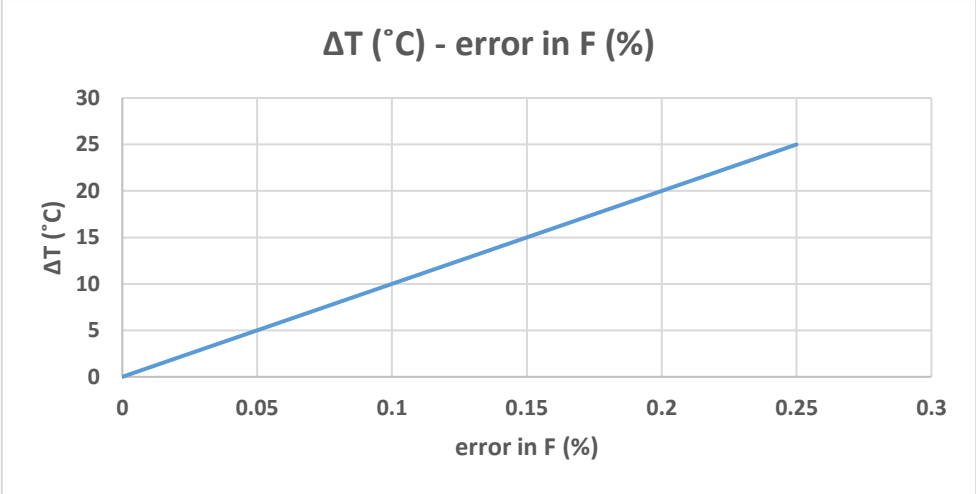

Figure A2: Influence of temperature increase on preload force (velocity ratio method)

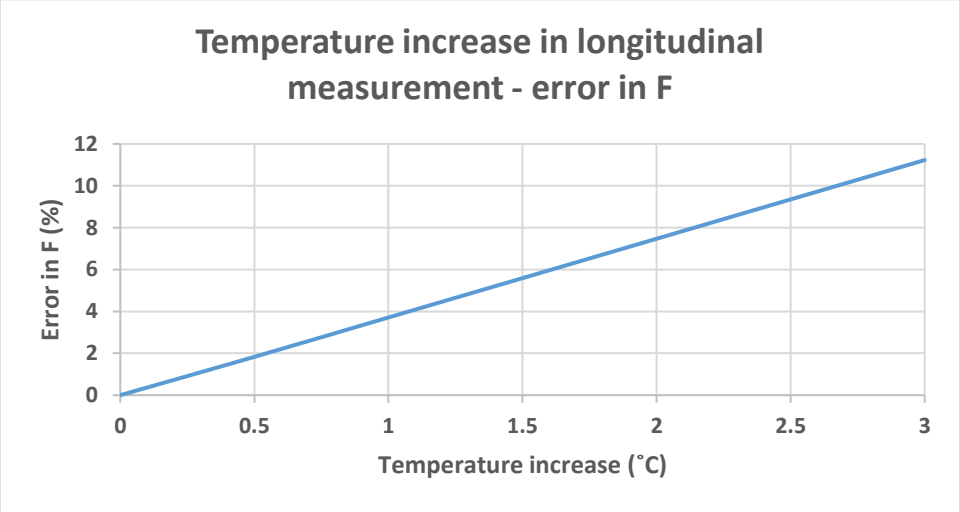

Figure A3: Influence of temperature increase on longitudinal wave measurement (velocity ratio method)

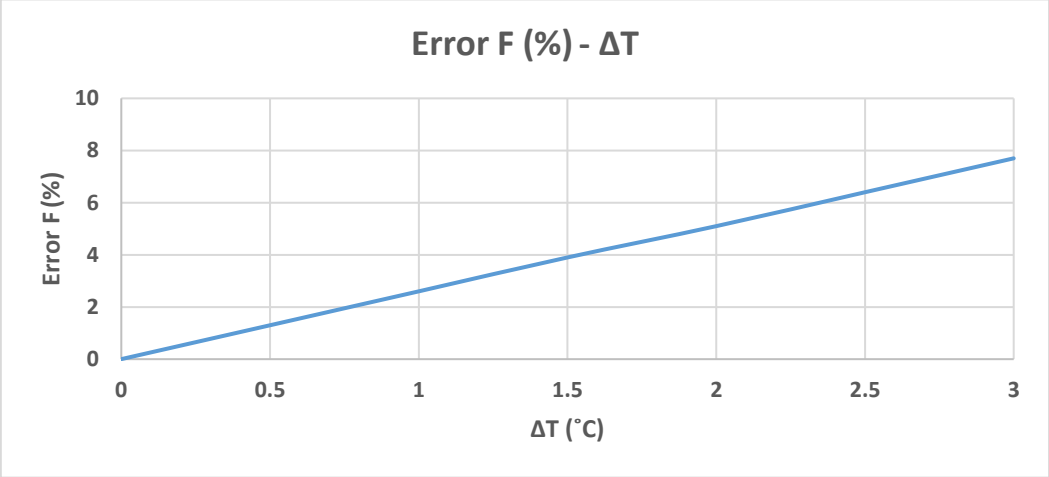

Figure A4: Influence of temperature increase on estimated force (resonance method)

Table A2: Specimen specification [27]

Number	Bolt diameter	Dimension (mm)	Both surfaces (Ra)	Piezoceramic size (mm)
Specimen 1	*M16*	Φ 60 × 10/Φ 60 × 10	1.55/3.49	Φ 6 × 2
Specimen 2	*M16*	Φ 60 × 10/Φ 60 × 10	1.55/2.56	Φ 6 × 2
Specimen 3	*M16*	Φ 60 × 15/Φ 60 × 15	2.53/3.1	5 × 8 × 0.5
Specimen 4	*M10*	100 × 50 × 12/100 × 50 × 12	1.61/1.79	5 × 8 × 0.5

APPENDIX B

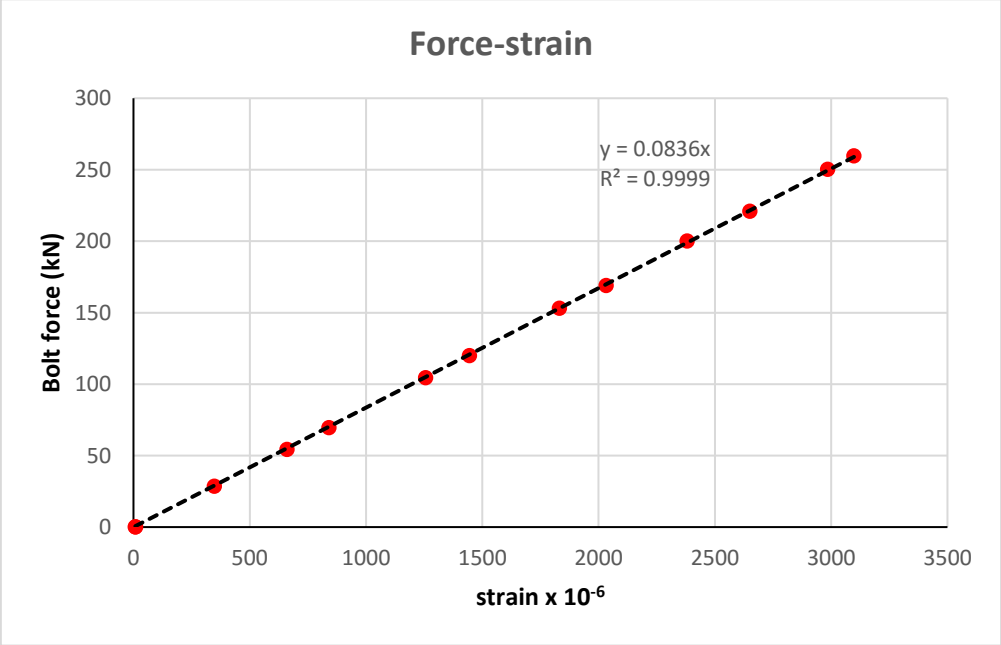

Figure B1: Force-strain diagram obtained for the second test (B1)

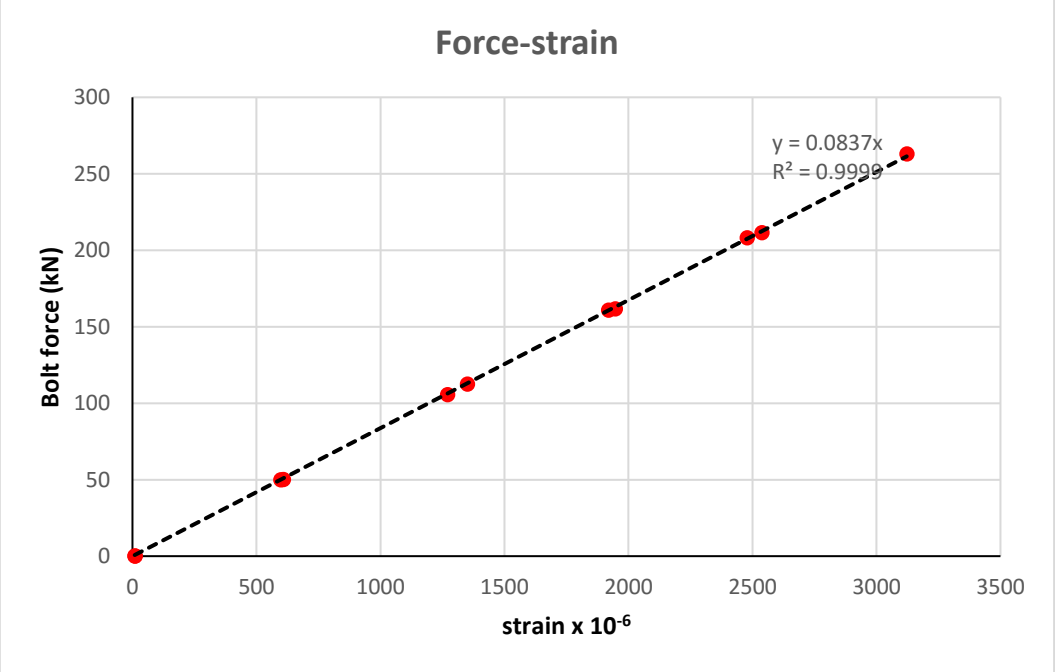

Figure B2: Force-strain diagram obtained for the third test (B1)

Table B1: Theoretical strain derived from the first test (B1) (actual diameter)

strain gauge $\varepsilon x10^{-6}$	F (kN)	σ (N/mm^2)	theoretical $\varepsilon x10^{-6}$	theoretical $\Delta\varepsilon x10^{-6}$	error between theoretical and experimental value (%)	min error(%) E = 200 GPa	max error(%) E = 210 GPa
0	0	0	0	0	-	-	-
138	11	26.03	124	6	11.31	6.25	16.88
365	30	71.00	338	16	7.95	3.04	13.35
645	53	125.44	597	28	7.98	3.07	13.38
800	66	156.21	744	35	7.55	2.66	12.93
1181	98	231.95	1105	53	6.93	2.06	12.27
1578	131	310.05	1476	70	6.88	2.02	12.22
1775	148	350.29	1668	79	6.41	1.58	11.73
2064	172	407.09	1939	92	6.47	1.63	11.80
2144	179	423.66	2017	96	6.27	1.44	11.59
2388	200	473.36	2254	107	5.94	1.12	11.24
2758	231	546.73	2603	124	5.93	1.12	11.23
3127	261	617.74	2942	140	6.30	1.47	11.62
2768	231	546.73	2603	124	6.32	1.49	11.63
2379	198	468.63	2232	106	6.61	1.76	11.94
1828	152	359.75	1713	82	6.71	1.86	12.04
1157	96	227.21	1082	52	6.93	2.07	12.28
631	52	123.07	586	28	7.67	2.77	13.05
8	0	0	0	0	-	-	-

Table B2: Theoretical strain derived from the second test (B1) (actual diameter)

strain gauge $\varepsilon x10^{-6}$	F (kN)	σ (N/mm^2)	theoretical $\varepsilon x10^{-6}$	theoretical $\Delta\varepsilon x10^{-6}$	error between theoretical and experimental value (%)	min error(%) E=200 Gpa	max error(%) E=220 Gpa
8	0	0	0	0	-	-	-
660	54	127.81	609	29	8.44	3.51	13.87
1256	105	248.51	1183	56	6.13	1.31	11.44
1832	153	362.12	1724	82	6.24	1.41	11.55
2380	200	473.36	2254	107	5.59	0.79	10.86
2985	250	591.70	2818	134	5.94	1.12	11.24
3098	260	615.37	2930	140	5.72	0.92	11.01
2651	221	523.06	2491	119	6.43	1.59	11.75
2033	169	399.99	1905	91	6.74	1.88	12.07
1445	120	284.02	1352	64	6.84	1.99	12.18
840	70	165.68	789	38	6.47	1.63	11.80
348	29	68.64	327	16	6.47	1.63	11.80
9	0	0	0	0	-	-	-

Table B3: Theoretical strain derived from the third test (B1) (actual diameter)

strain gauge $\varepsilon x10^{-6}$	F (kN)	σ (N/mm^2)	theoretical $\varepsilon x10^{-6}$	theoretical $\Delta\varepsilon x10^{-6}$	error between theoretical and experimental value (%)	min error(%) E=200 Gpa	max error(%) E=220 Gpa
9	0	0	0	0	-	-	-
608	50	118.34	564	27	7.89	2.99	13.29
1350	113	267.45	1274	61	6.00	1.18	11.30
1919	161	381.06	1815	86	5.76	0.95	11.04
2478	208	492.30	2344	112	5.70	0.90	10.99
3122	263	622.47	2964	141	5.33	0.54	10.59
2538	212	501.76	2389	114	6.22	1.39	11.53
1946	162	383.42	1826	87	6.58	1.74	11.91
1270	106	250.88	1195	57	6.31	1.47	11.62
598	50	118.34	564	27	6.12	1.29	11.42
11	0	0	0	0	-	-	-

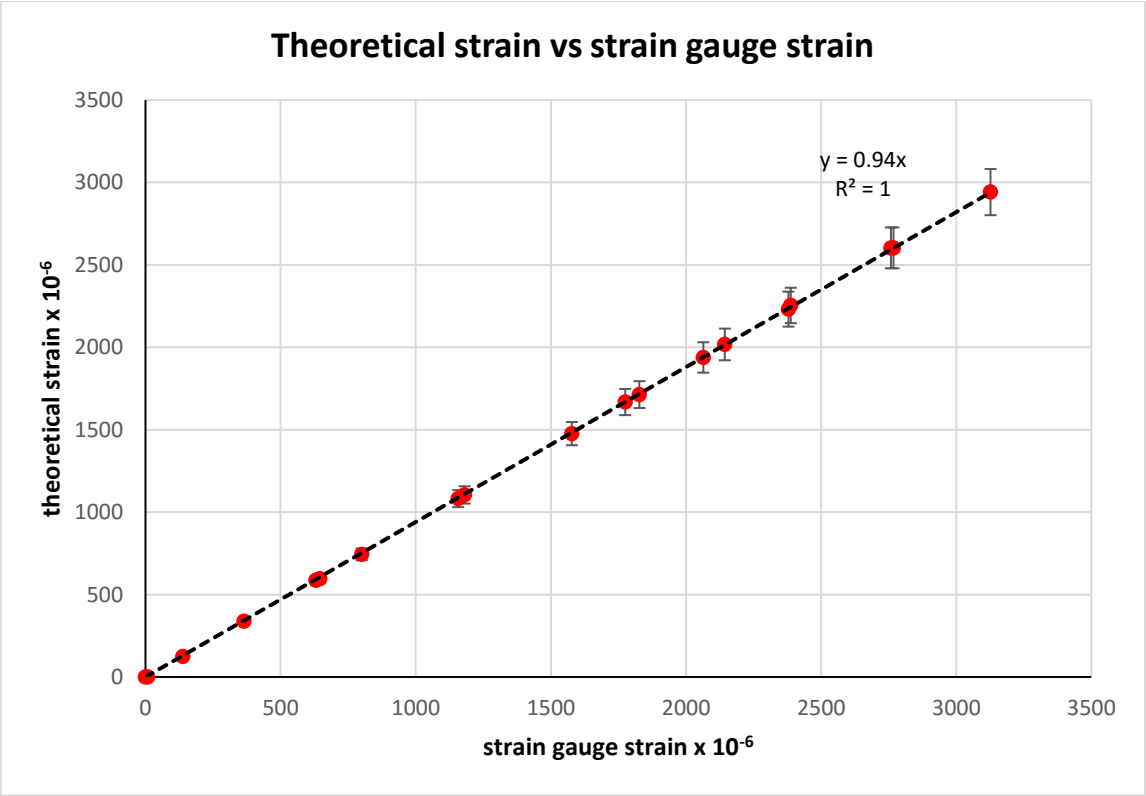

Figure B3: Strain obtained for the first test (B1) (actual diameter)

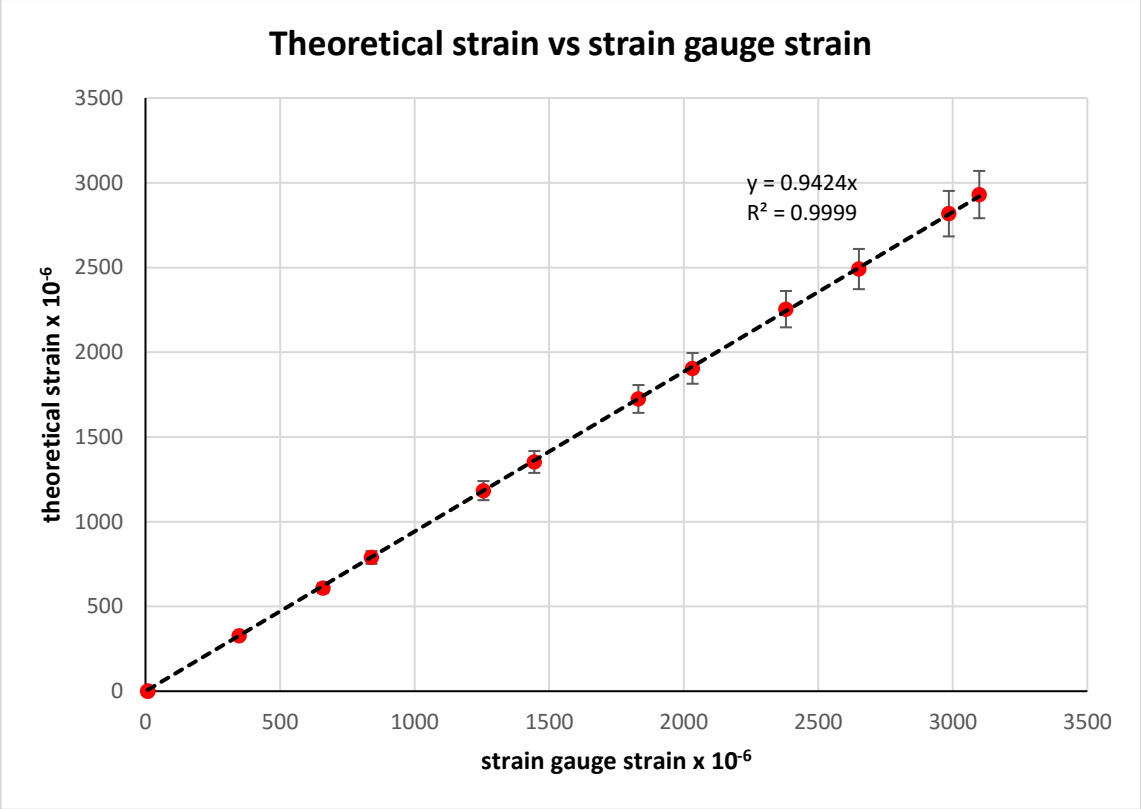

Figure B4: Strain obtained for the second test (B1) (actual diameter)

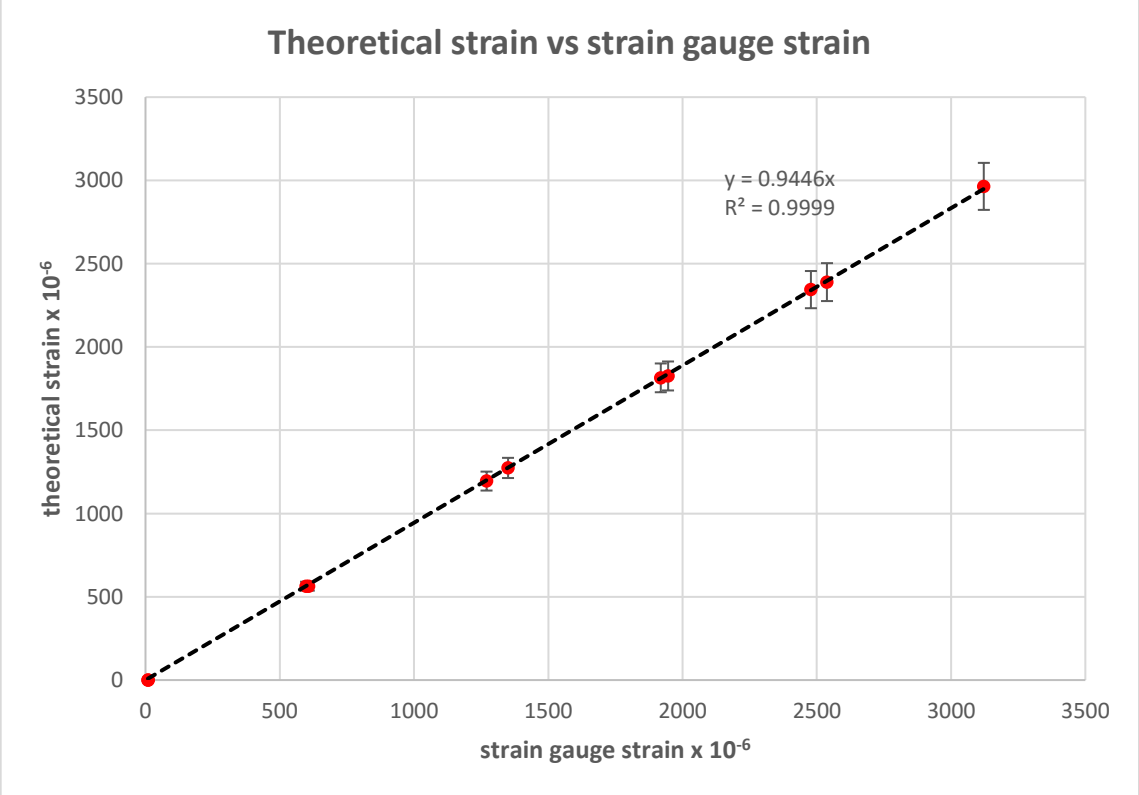

Figure B5: Strain obtained for the third test (B1) (actual diameter)

Table B4: Theoretical strain derived from the first test (B1) (nominal diameter)

strain gauge $\varepsilon x10^{-6}$	F (kN)	σ (N/mm^2)	theoretical $\varepsilon x10^{-6}$	theoretical $\Delta\varepsilon x10^{-6}$	error between theoretical and experimental value (%)	min error(%) E=200 Gpa	max error(%) E=220 Gpa
0	0	0.00	0	0	-	-	-
138	11	24.49	117	6	18.36	12.98	24.27
365	30	66.78	318	15	14.78	9.57	20.52
645	53	117.97	562	27	14.81	9.59	20.55
800	66	146.91	700	33	14.35	9.16	20.07
1181	98	218.14	1039	49	13.69	8.52	19.38
1578	131	291.60	1389	66	13.64	8.48	19.32
1775	148	329.44	1569	75	13.15	8.00	18.80
2064	172	382.86	1823	87	13.21	8.06	18.87
2144	179	398.44	1897	90	13.00	7.86	18.65
2388	200	445.19	2120	101	12.64	7.52	18.28
2758	231	514.19	2449	117	12.64	7.52	18.27
3127	261	580.97	2767	132	13.03	7.89	18.68
2768	231	514.19	2449	117	13.05	7.91	18.70
2379	198	440.74	2099	100	13.35	8.20	19.02
1828	152	338.34	1611	77	13.46	8.30	19.13
1157	96	213.69	1018	48	13.70	8.53	19.39
631	52	115.75	551	26	14.48	9.28	20.20
8	0	0.00	0	0	-	-	-

Table B5: Theoretical strain derived from the second test (B1) (nominal diameter)

strain gauge $\varepsilon x10^{-6}$	F (kN)	σ (N/mm^2)	theoretical $\varepsilon x10^{-6}$	theoretical $\Delta\varepsilon x10^{-6}$	error between theoretical and experimental value (%)	min error(%) E=200 Gpa	max error(%) E=220 Gpa
8	0	0.00	0	0	-	-	-
660	54	120.20	572	27	15.31	10.07	21.07
1256	105	233.72	1113	53	12.85	7.72	18.49
1832	153	340.57	1622	77	12.96	7.83	18.61
2380	200	445.19	2120	101	12.27	7.16	17.88
2985	250	556.49	2650	126	12.64	7.52	18.28
3098	260	578.75	2756	131	12.41	7.30	18.03
2651	221	491.93	2343	112	13.17	8.02	18.83
2033	169	376.18	1791	85	13.49	8.33	19.16
1445	120	267.11	1272	61	13.60	8.44	19.28
840	70	155.82	742	35	13.21	8.06	18.87
348	29	64.55	307	15	13.21	8.06	18.87
9	0	0.00	0	0	-	-	-

Table B6: Theoretical strain derived from the third test (B1) (nominal diameter)

strain gauge $\varepsilon x10^{-6}$	F (kN)	σ (N/mm^2)	theoretical $\varepsilon x10^{-6}$	theoretical $\Delta\varepsilon x10^{-6}$	error between theoretical and experimental value (%)	min error(%) E=200 Gpa	max error(%) E=220 Gpa
9	0	0.00	0	0	-	-	-
608	50	111.30	530	25	14.72	9.51	20.46
1350	113	251.53	1198	57	12.71	7.59	18.34
1919	161	358.38	1707	81	12.45	7.34	18.07
2478	208	463.00	2205	105	12.39	7.29	18.01
3122	263	585.42	2788	133	11.99	6.90	17.59
2538	212	471.90	2247	107	12.94	7.81	18.59
1946	162	360.60	1717	82	13.33	8.18	18.99
1270	106	235.95	1124	54	13.03	7.89	18.68
598	50	111.30	530	25	12.83	7.70	18.47
11	0	0.00	0	0	-	-	-

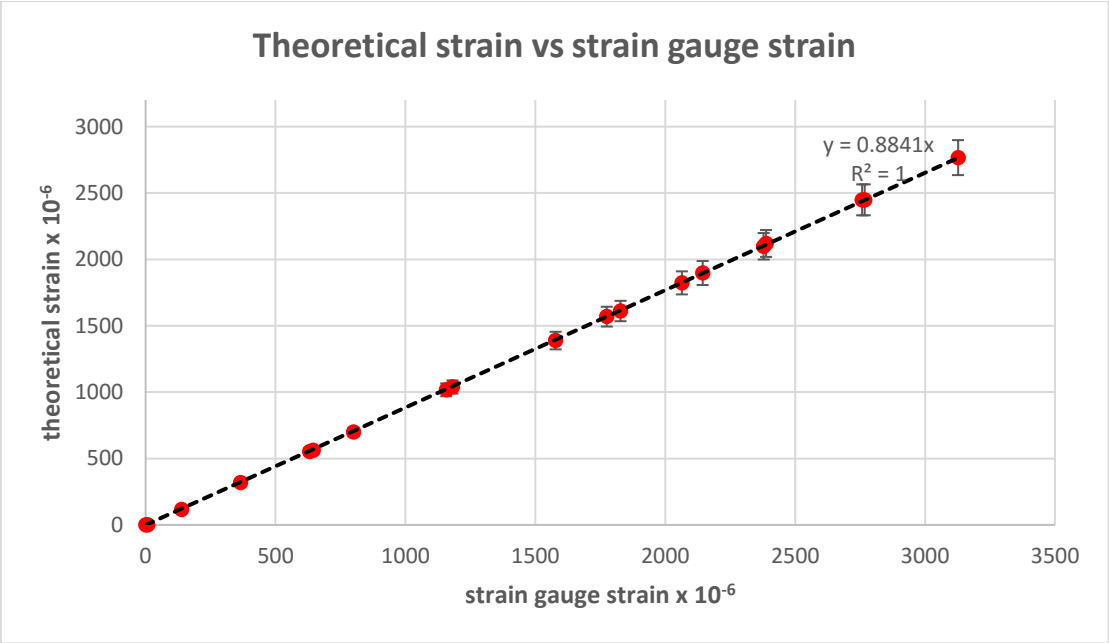

Figure B6: Strain obtained for the first test (B1) (nominal diameter)

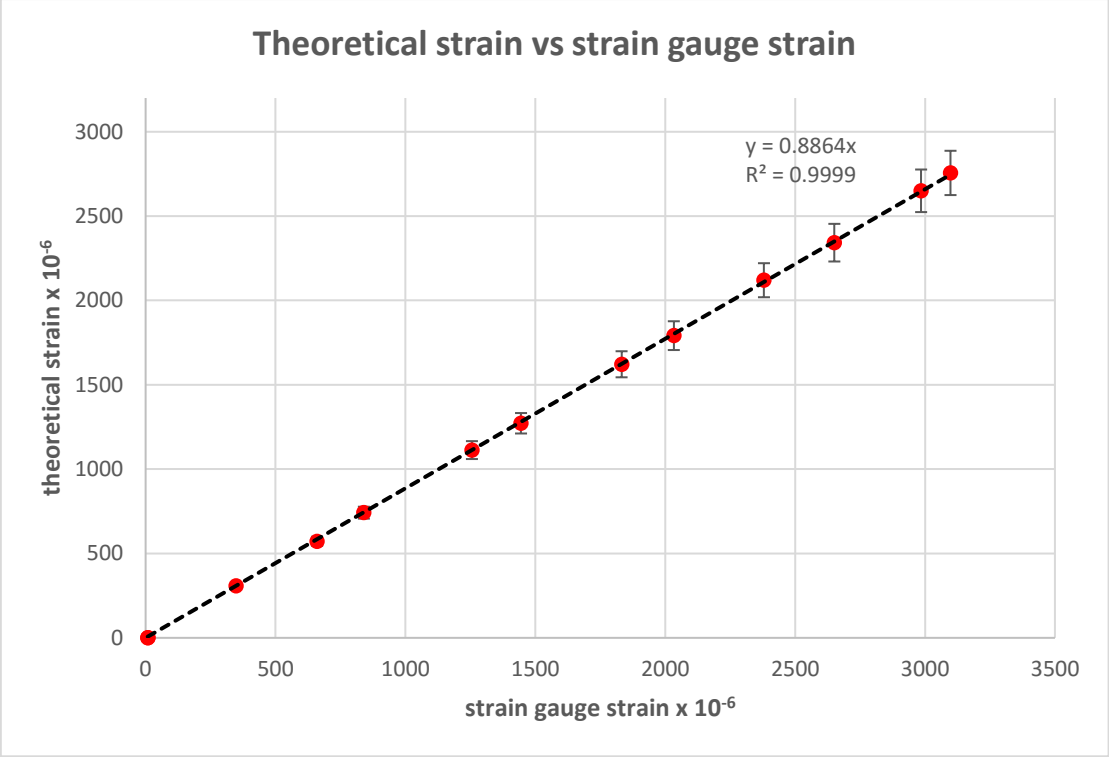

Figure B7: Strain obtained for the second test (B1) (nominal diameter)

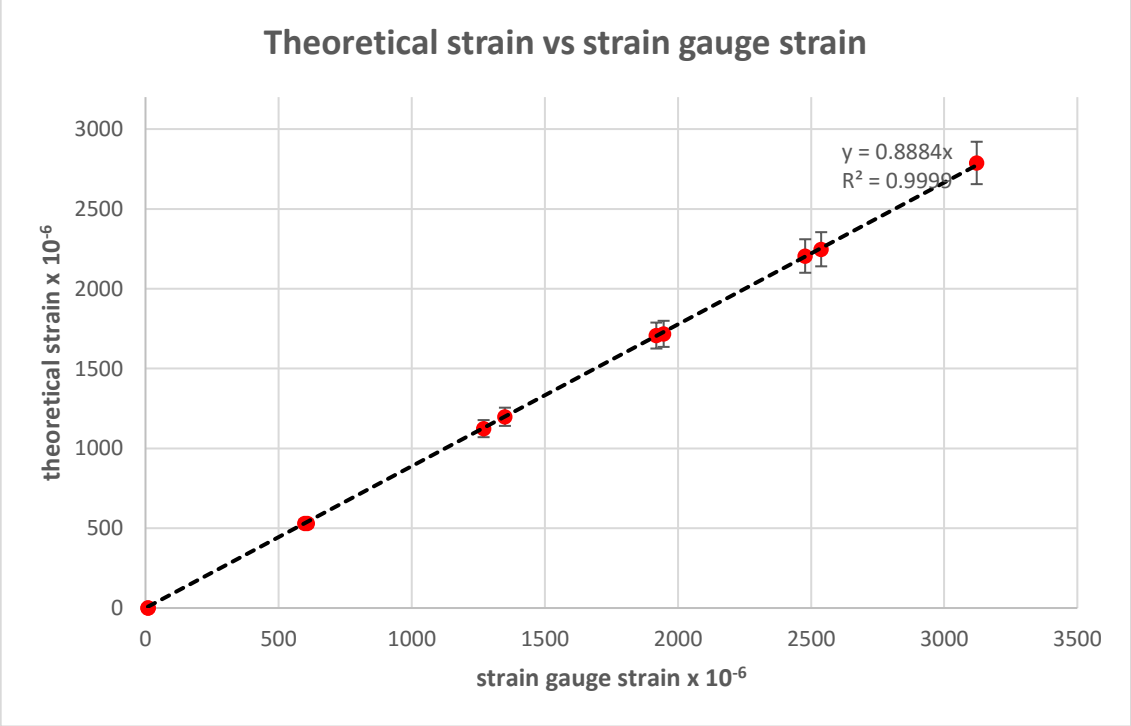

Figure B8: Strain obtained for the third test (B1) (nominal diameter)

Table B7: Theoretical strain derived from the first test (B1) (maximum diameter)

strain gauge $\varepsilon x10^{-6}$	F (kN)	σ (N/mm^2)	theoretical $\varepsilon x10^{-6}$	theoretical $\Delta\varepsilon x10^{-6}$	error between theoretical and experimental value (%)	min error(%) E=200 Gpa	max error(%) E=220 Gpa
0	0	0.00	0	0	-	-	-
138	11	22.85	109	5	26.85	21.08	33.19
365	30	62.31	297	14	23.02	17.42	29.17
645	53	110.08	524	25	23.05	17.45	29.20
800	66	137.08	653	31	22.56	16.99	28.68
1181	98	203.54	969	46	21.85	16.31	27.94
1578	131	272.08	1296	62	21.79	16.26	27.88
1775	148	307.39	1464	70	21.26	15.75	27.33
2064	172	357.24	1701	81	21.33	15.82	27.40
2144	179	371.78	1770	84	21.10	15.60	27.16
2388	200	415.39	1978	94	20.72	15.24	26.76
2758	231	479.78	2285	109	20.72	15.23	26.75
3127	261	542.09	2581	123	21.14	15.63	27.19
2768	231	479.78	2285	109	21.16	15.65	27.21
2379	198	411.24	1958	93	21.48	15.96	27.56
1828	152	315.70	1503	72	21.60	16.07	27.68
1157	96	199.39	949	45	21.86	16.32	27.95
631	52	108.00	514	24	22.69	17.11	28.83
8	0	0.00	0	0	-	-	-

Table B8: Theoretical strain derived from the second test (B1) (maximum diameter)

strain gauge $\varepsilon x10^{-6}$	F (kN)	σ (N/mm^2)	theoretical $\varepsilon x10^{-6}$	theoretical $\Delta\varepsilon x10^{-6}$	error between theoretical and experimental value (%)	min error(%) E=200 Gpa	max error(%) E=220 Gpa
8	0	0.00	0	0	-	-	-
660	54	112.16	534	25	23.58	17.96	29.76
1256	105	218.08	1038	49	20.95	15.45	26.99
1832	153	317.78	1513	72	21.07	15.56	27.12
2380	200	415.39	1978	94	20.32	14.85	26.34
2985	250	519.24	2473	118	20.72	15.24	26.76
3098	260	540.01	2571	122	20.47	15.00	26.50
2651	221	459.01	2186	104	21.28	15.77	27.35
2033	169	351.01	1671	80	21.63	16.10	27.71
1445	120	249.24	1187	57	21.75	16.22	27.84
840	70	145.39	692	33	21.33	15.82	27.40
348	29	60.23	287	14	21.33	15.82	27.40
9	0	0.00	0	0	-	-	-

Table B9: Theoretical strain derived from the third test (B1) (maximum diameter)

strain gauge $\varepsilon x10^{-6}$	F (kN)	σ (N/mm^2)	theoretical $\varepsilon x10^{-6}$	theoretical $\Delta\varepsilon x10^{-6}$	error between theoretical and experimental value (%)	min error(%) E=200 Gpa	max error(%) E=220 Gpa
9	0	0.00	0	0	-	-	-
608	50.2	104.26	496	24	22.46	15.99	30.47
1350	112.5	233.66	1113	53	21.33	15.51	28.00
1919	160.8	333.98	1590	76	20.66	14.98	27.10
2478	208.1	432.22	2058	98	20.40	14.75	26.77
3122	263	546.24	2601	124	20.02	14.70	25.77
2538	211.5	439.28	2092	100	21.33	15.99	27.08
1946	161.7	335.85	1599	76	21.68	16.41	27.29
1270	105.6	219.33	1044	50	21.60	16.47	26.97
598	50	103.85	495	24	20.93	16.16	25.69
11	0	0.00	0	0	-	-	-

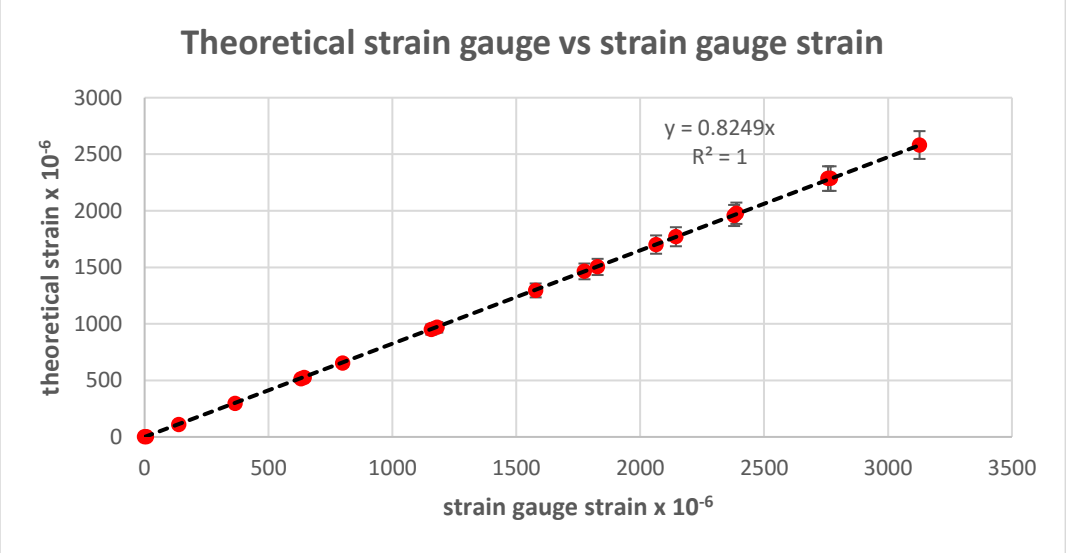

Figure B9: Strain obtained for the first test (B1) (maximum diameter)

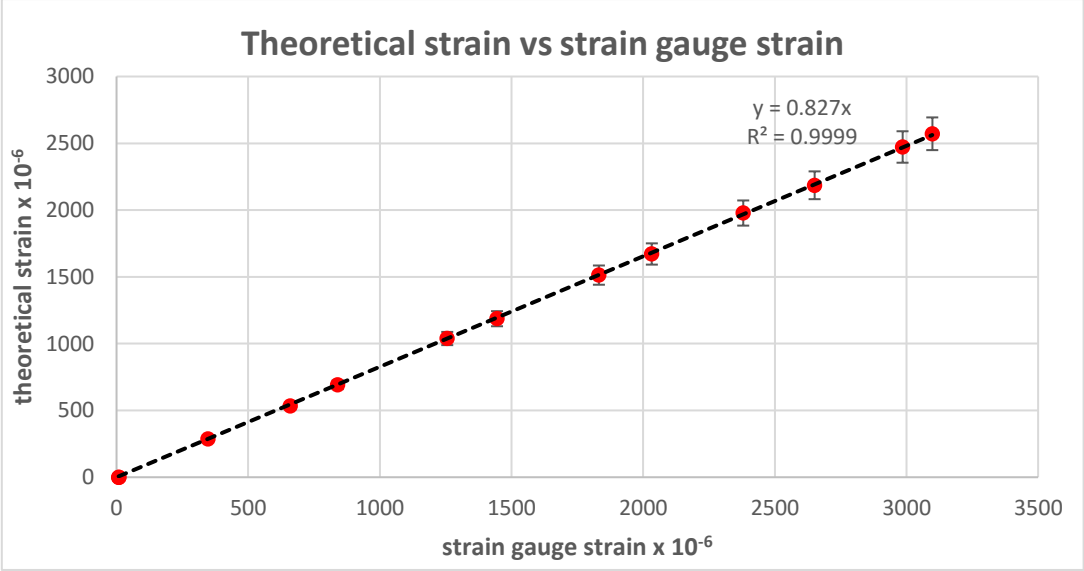

Figure B10: Strain obtained for the second test (B1) (maximum dimeter)

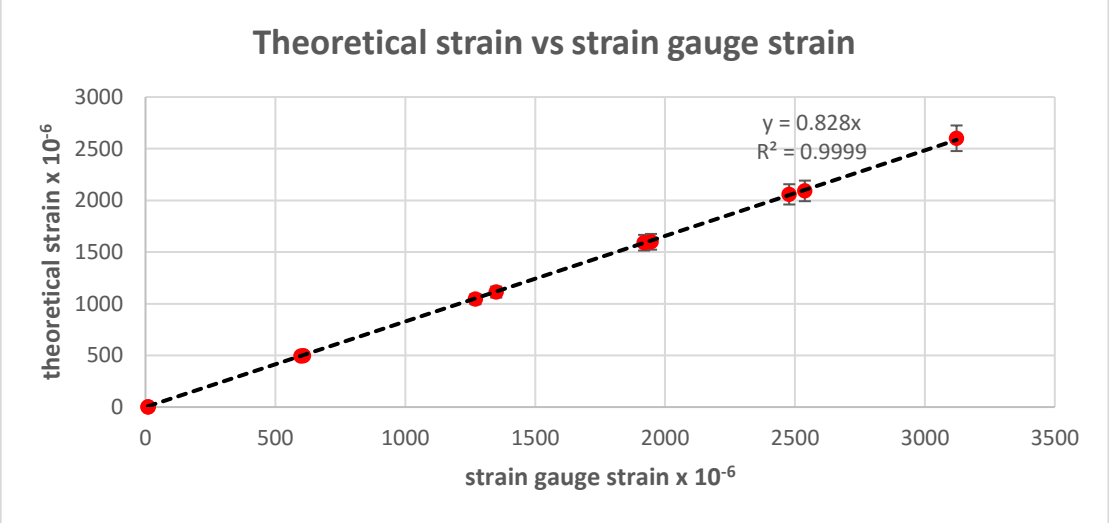

Figure B11: Strain obtained for the third test (B1) (maximum diameter)

Table B10: Theoretical strain derived from the first test (B1) (minimum diameter)

strain gauge $\varepsilon x10^{-6}$	F (kN)	σ (N/mm^2)	theoretical $\varepsilon x10^{-6}$	theoretical $\Delta\varepsilon x10^{-6}$	error between theoretical and experimental value (%)	min error(%) E=200 Gpa	max error(%) E=220 Gpa
0	0	0.00	0	0	-	-	-
138	11	26.31	125	6	10.16	5.15	15.67
365	30	71.75	342	16	6.83	1.98	12.17
645	53	126.75	604	29	6.86	2.00	12.20
800	66	157.85	752	36	6.43	1.60	11.75
1181	98	234.38	1116	53	5.82	1.01	11.11
1578	131	313.30	1492	71	5.77	0.96	11.06
1775	148	353.96	1686	80	5.31	0.52	10.57
2064	172	411.36	1959	93	5.37	0.58	10.64
2144	179	428.10	2039	97	5.17	0.39	10.43
2388	200	478.32	2278	108	4.84	0.08	10.08
2758	231	552.46	2631	125	4.84	0.07	10.08
3127	261	624.21	2972	142	5.20	0.42	10.46
2768	231	552.46	2631	125	5.22	0.43	10.48
2379	198	473.54	2255	107	5.50	0.71	10.78
1828	152	363.52	1731	82	5.60	0.80	10.88
1157	96	229.59	1093	52	5.83	1.02	11.12
631	52	124.36	592	28	6.55	1.71	11.88
8	0	0.00	0	0	-	-	-

Table B11: Theoretical strain derived from the second test (B1) (minimum diameter)

strain gauge $\varepsilon x10^{-6}$	F (kN)	σ (N/mm^2)	theoretical $\varepsilon x10^{-6}$	theoretical $\Delta\varepsilon x10^{-6}$	error between theoretical and experimental value (%)	min error(%) E=200 Gpa	max error(%) E=220 Gpa
8	0	0.00	0	0	-	-	-
660	54	129.15	615	29	7.32	2.44	12.69
1256	105	251.12	1196	57	5.03	0.26	10.29
1832	153	365.91	1742	83	5.14	0.36	10.40
2380	200	478.32	2278	108	4.49	-0.26	9.72
2985	250	597.90	2847	136	4.84	0.08	10.08
3098	260	621.82	2961	141	4.63	-0.13	9.86
2651	221	528.54	2517	120	5.33	0.54	10.60
2033	169	404.18	1925	92	5.63	0.83	10.91
1445	120	286.99	1367	65	5.73	0.93	11.02
840	70	167.41	797	38	5.37	0.58	10.64
348	29	69.36	330	16	5.37	0.58	10.64
9	0	0.00	0	0	-	-	-

Table B12: Theoretical strain derived from the third test (B1) (minimum diameter)

strain gauge $\varepsilon x10^{-6}$	F (kN)	σ (N/mm^2)	theoretical $\varepsilon x10^{-6}$	theoretical $\Delta\varepsilon x10^{-6}$	error between theoretical and experimental value (%)	min error(%) E=200 Gpa	max error(%) E=220 Gpa
9	0	0.00	0	0	-	-	-
608	50	119.58	569	27	6.77	1.92	12.11
1350	113	270.25	1287	61	4.90	0.13	10.15
1919	161	385.05	1834	87	4.66	-0.10	9.89
2478	208	497.45	2369	113	4.61	-0.15	9.84
3122	263	628.99	2995	143	4.23	-0.50	9.45
2538	212	507.02	2414	115	5.12	0.34	10.38
1946	162	387.44	1845	88	5.48	0.68	10.75
1270	106	253.51	1207	57	5.20	0.42	10.46
598	50	119.58	569	27	5.02	0.24	10.27
11	0	0.00	0	0	-	-	-

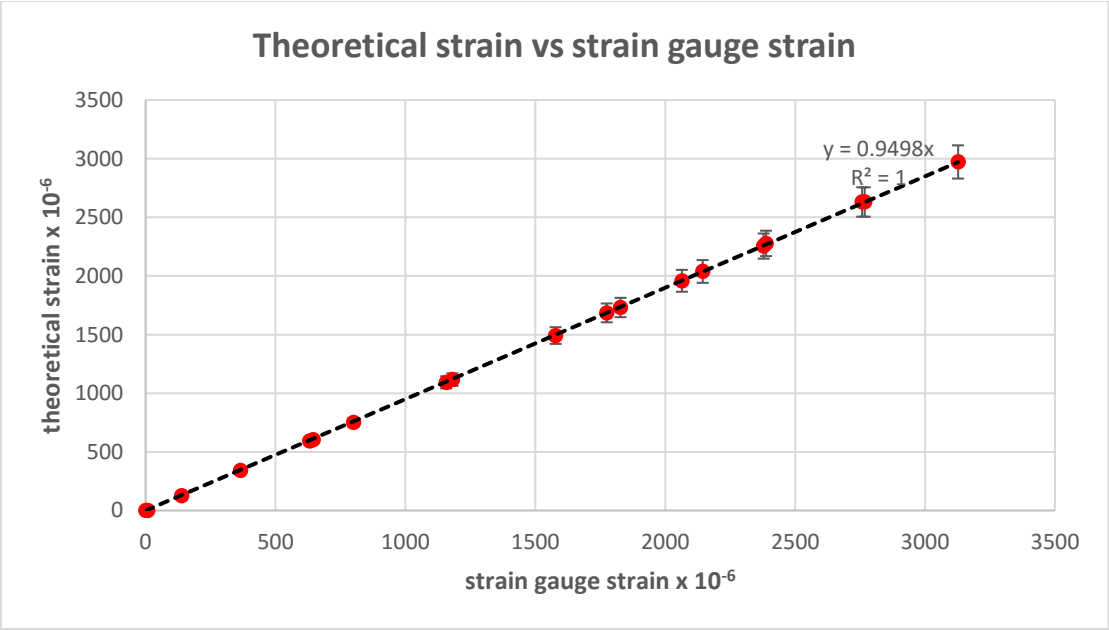

Figure B12: Strain obtained for the first test (B1) (minimum diameter)

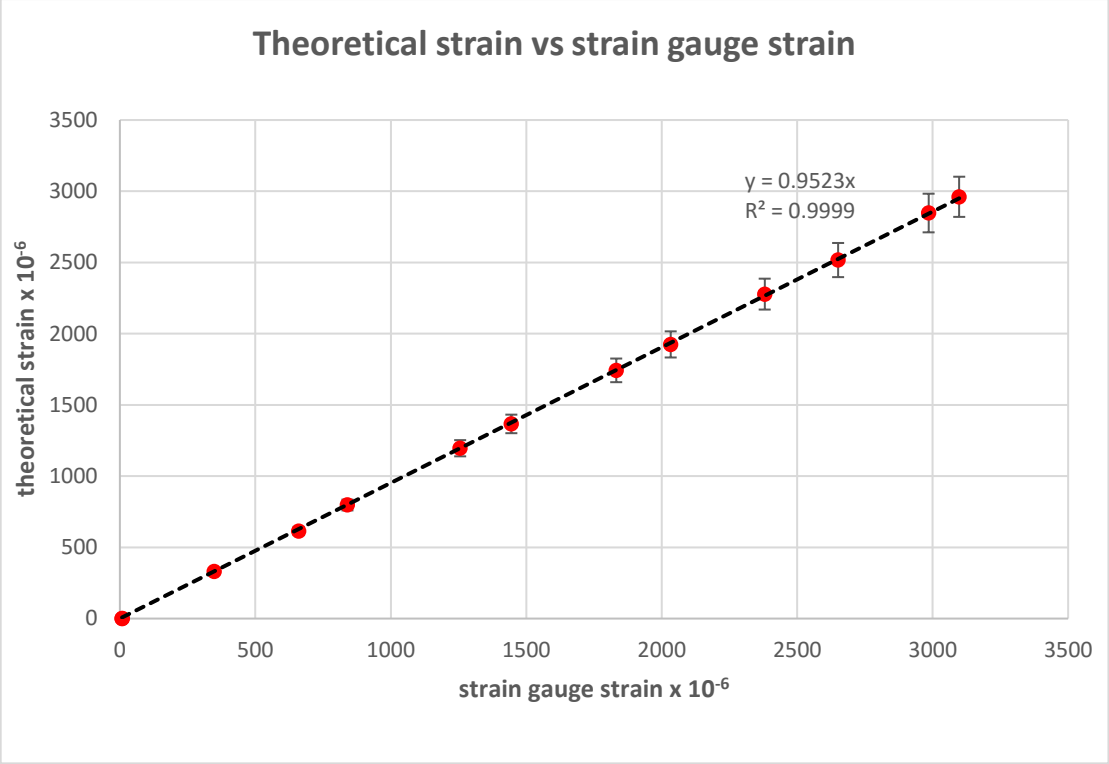

Figure B13: Strain obtained for the second test (B1) (minimum diameter)

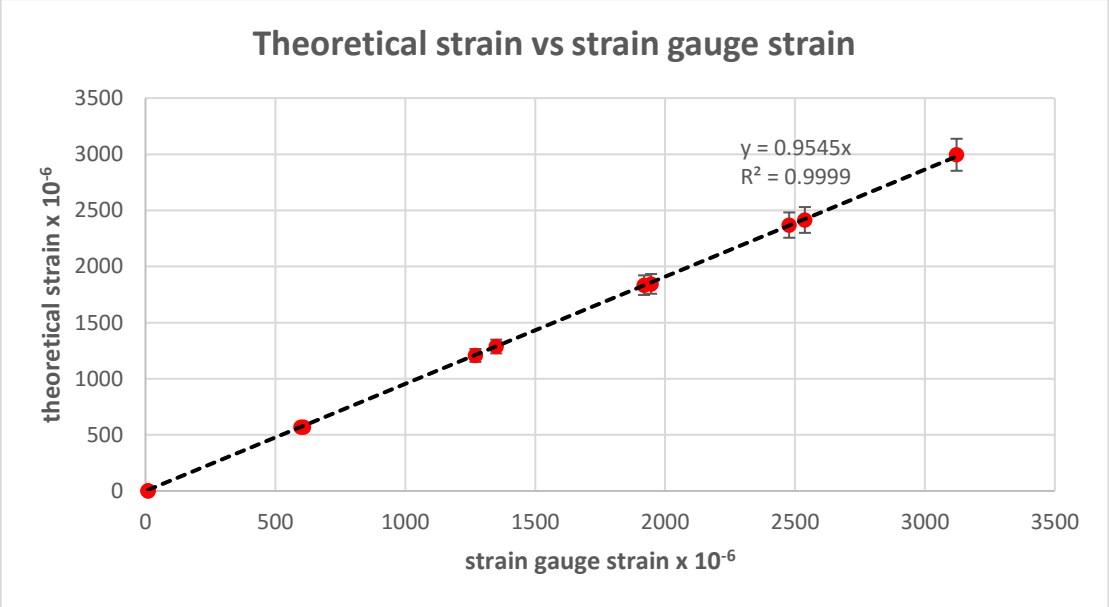

Figure B14: Strain obtained for the third test (B1) (minimum diameter)

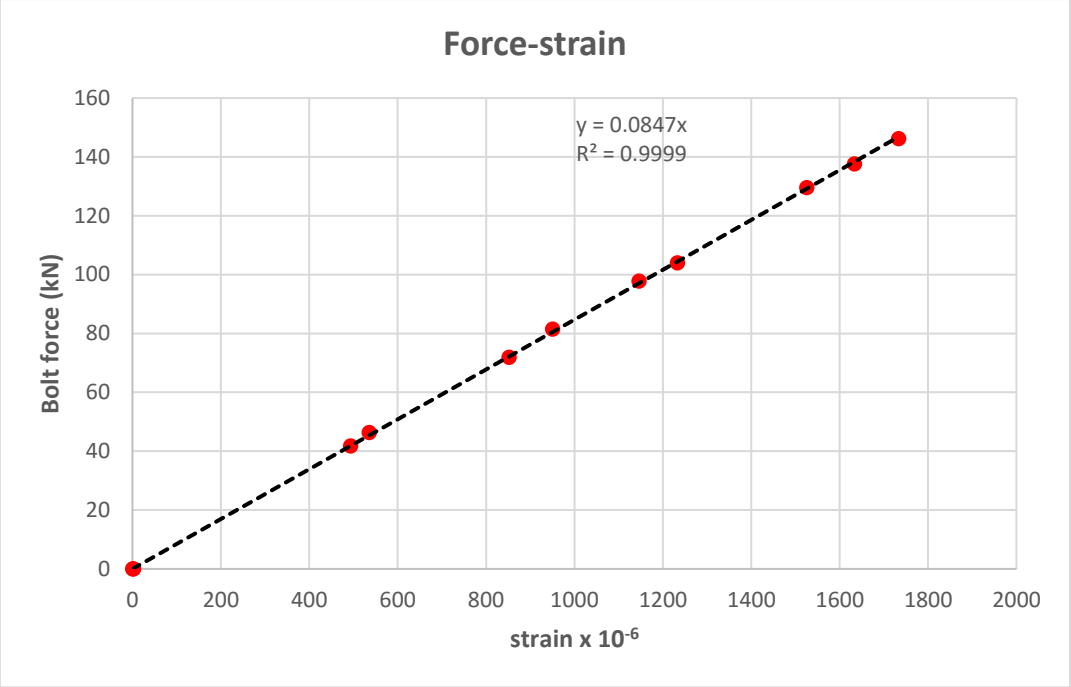

Figure B15: Force-strain diagram obtained for the first test (B2)

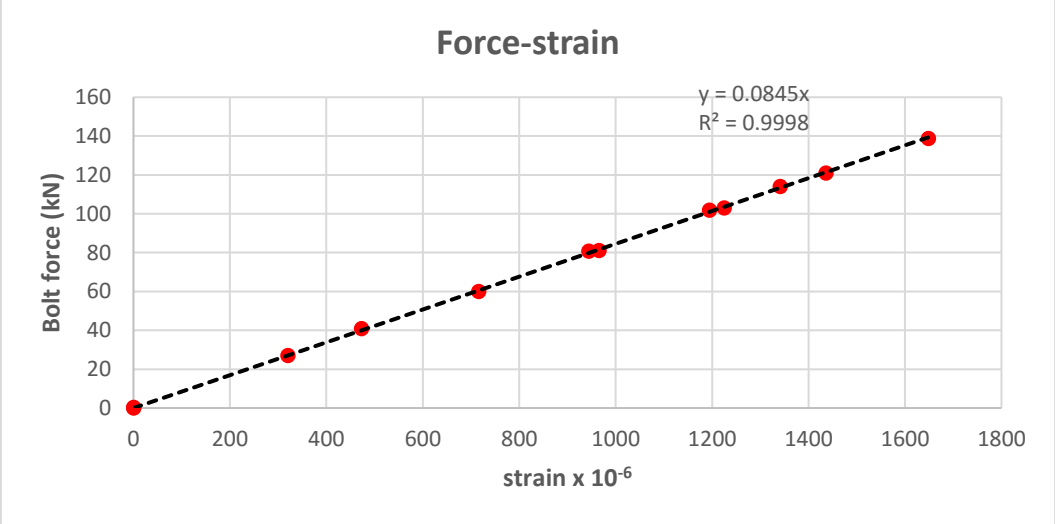

Figure B16: Force-strain diagram obtained for the second test (B2)

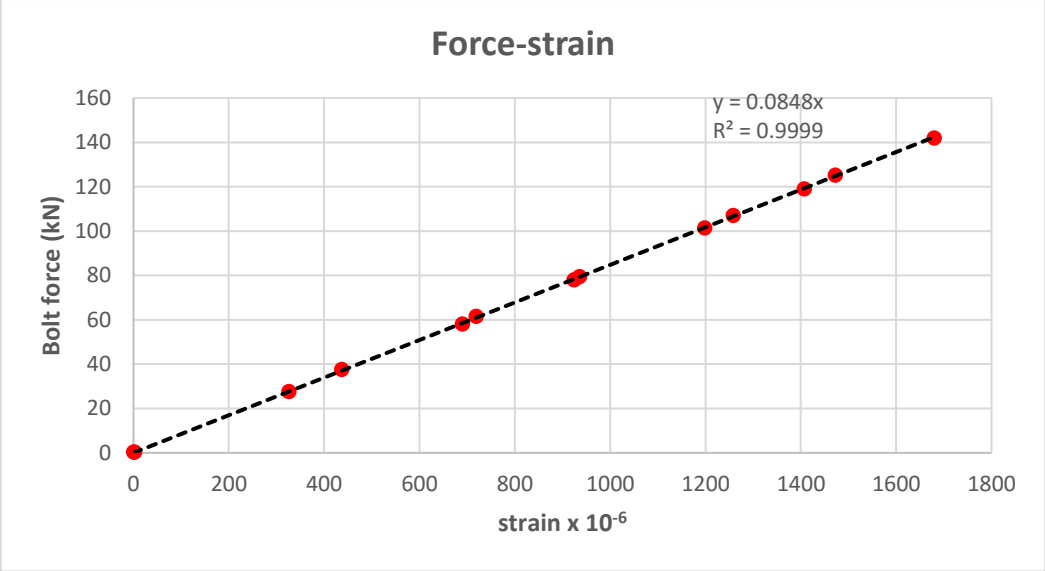

Figure B17: Force-strain diagram obtained for the third test (B2)

Table B13: Theoretical strain derived from the first test (B2) (actual diameter)

strain gauge x 10^{-6}	F (kN)	σ (N/mm^2)	theoretical $\varepsilon x10^{-6}$	theoretical $\Delta\varepsilon x10^{-6}$	error between theoretical and experimental value (%)	min error(%) E = 200 GPa	max error(%) E = 220 GPa
0	0	0.00	0	0	-	-	-
493	42	99.92	476	23	3.61	-1.10	8.79
852	72	171.30	816	39	4.45	-0.30	9.67
1233	104	247.43	1178	56	4.65	-0.11	9.88
1633	138	328.32	1563	74	4.45	-0.30	9.67
1733	146	347.35	1654	79	4.77	0.01	10.01
1525	130	309.29	1473	70	3.54	-1.16	8.72
1146	98	233.16	1110	53	3.22	-1.47	8.38
950	81	192.71	918	44	3.52	-1.18	8.70
535	46	109.44	521	25	2.66	-2.01	7.79
2	0	0.00	0	0	-	-	-

Table B14: Theoretical strain derived from the second test (B2) (actual diameter)

strain gauge x 10^{-6}	F (kN)	σ (N/mm^2)	theoretical $\varepsilon x10^{-6}$	theoretical $\Delta\varepsilon x10^{-6}$	error between theoretical and experimental value (%)	min error(%) E = 200 GPa	max error(%) E = 220 GPa
0	0	0.00	0	0	-	-	-
320	27	64.24	306	15	4.61	-0.14	9.84
716	60	142.75	680	32	5.33	0.54	10.60
965	81	192.71	918	44	5.16	0.38	10.42
1225	103	245.05	1167	56	4.98	0.21	10.23
1436	121	287.88	1371	65	4.75	-0.01	9.99
1648	139	330.70	1575	75	4.65	-0.11	9.88
1341	114	271.22	1292	62	3.83	-0.89	9.02
1194	102	242.67	1156	55	3.32	-1.37	8.49
944	81	192.71	918	44	2.87	-1.81	8.01
473	41	97.54	464	22	1.83	-2.80	6.92
0	0	0.00	0	0	-	-	-

Table B15: Theoretical strain derived from the third test (B2) (actual diameter)

strain gauge x 10^{-6}	F (kN)	σ (N/mm^2)	theoretical $\varepsilon x10^{-6}$	theoretical $\Delta\varepsilon x10^{-6}$	error between theoretical and experimental value (%)	min error(%) E = 200 GPa	max error(%) E = 220 GPa
0	0	0.00	0	0	-	-	-
326	28	66.62	317	15	2.77	-1.90	7.91
690	58	137.99	657	31	5.01	0.23	10.26
924	78	185.57	884	42	4.56	-0.19	9.79
1198	101	240.29	1144	54	4.70	-0.06	9.93
1407	119	283.12	1348	64	4.36	-0.38	9.58
1680	142	337.84	1609	77	4.43	-0.32	9.65
1472	125	297.39	1416	67	3.94	-0.78	9.14
1258	107	254.57	1212	58	3.78	-0.94	8.96
936	80	190.33	906	43	3.27	-1.42	8.44
719	62	147.51	702	33	2.36	-2.29	7.48
437	38	90.41	431	21	1.51	-3.11	6.58
2	0	0.00	0	0	-	-	-

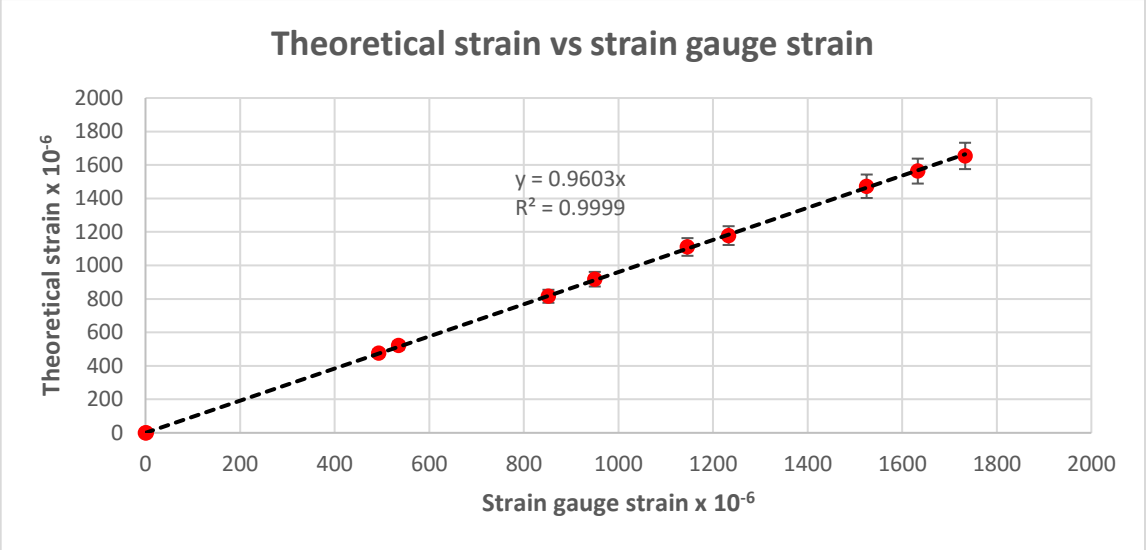

Figure B18: Strain obtained for the first test (B2) (actual diameter)

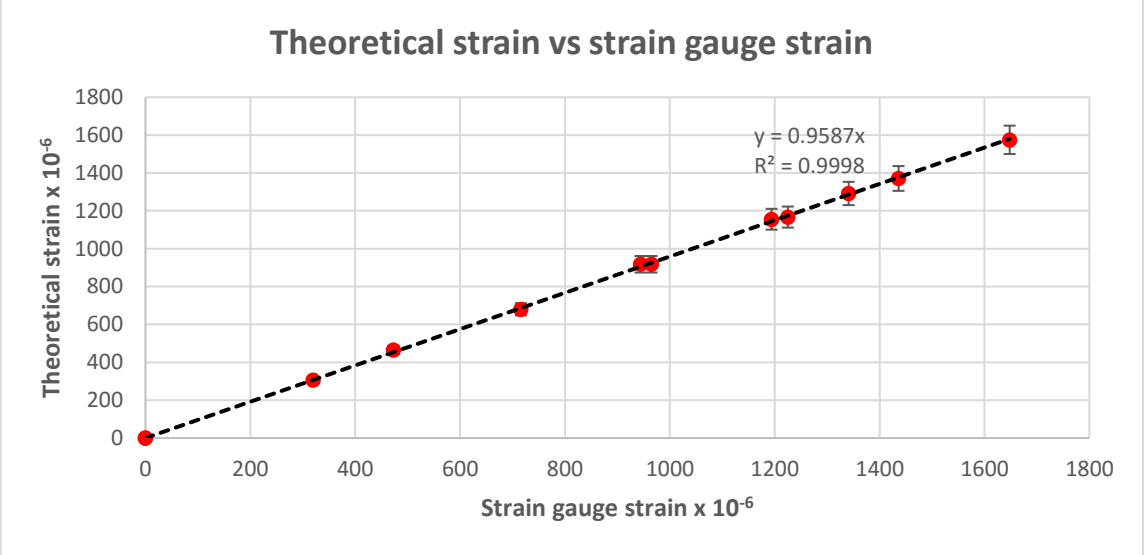

Figure B19: Strain obtained for the second test (B2) (actual diameter)

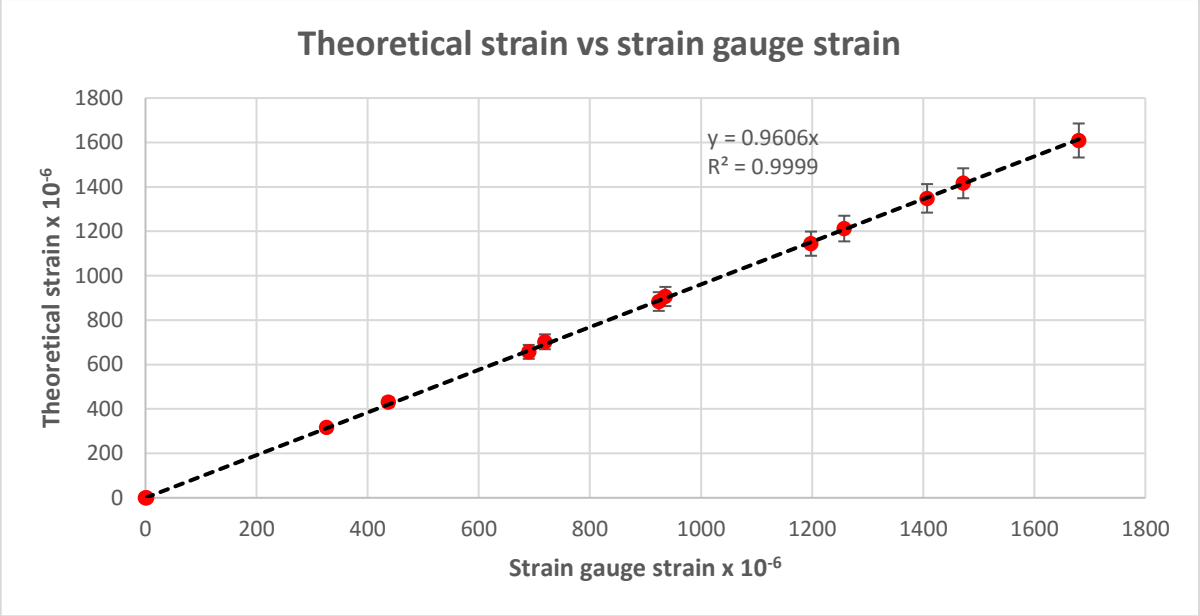

Figure B20: Strain obtained for the third test (B2) (actual diameter)

Table B16: Theoretical strain derived from the first test (B2) (nominal diameter)

strain gauge x 10^{-6}	F (kN)	σ (N/mm²)	theoretical εx10^{-6}	theoretical Δεx10^{-6}	error between theoretical and experimental value (%)	max error(%) E = 220 GPa	min error(%) E = 200 GPa
0	0	0.00	0	0	-	-	-
493	42	93.49	445	21	10.74	16.28	5.71
852	72	160.27	763	36	11.64	17.22	6.56
1233	104	231.50	1102	52	11.85	17.44	6.77
1633	138	307.18	1463	70	11.64	17.22	6.56
1733	146	324.99	1548	74	11.98	17.58	6.89
1525	130	289.37	1378	66	10.67	16.20	5.64
1146	98	218.14	1039	49	10.32	15.84	5.31
950	81	180.30	859	41	10.65	16.18	5.62
535	46	102.39	488	23	9.72	15.21	4.74
2	0	0.00	0	0	-	-	-

Table B17: Theoretical strain derived from the second test (B2) (nominal diameter)

strain gauge x 10^{-6}	F (kN)	σ (N/mm^2)	theoretical εx10^{-6}	theoretical Δεx10^{-6}	error between theoretical and experimental value (%)	max error(%) E = 220 GPa	min error(%) E = 200 GPa
2	0	0.00	0	0	-	-	-
320	27	60.10	286	14	11.81	17.40	6.73
716	60	133.56	636	30	12.58	18.21	7.46
965	81	180.30	859	41	12.40	18.02	7.29
1225	103	229.27	1092	52	12.20	17.81	7.10
1436	121	269.34	1283	61	11.96	17.56	6.87
1648	139	309.40	1473	70	11.85	17.45	6.77
1341	114	253.76	1208	58	10.98	16.53	5.93
1194	102	227.05	1081	51	10.44	15.96	5.42
944	81	180.30	859	41	9.95	15.45	4.95
473	41	91.26	435	21	8.84	14.28	3.89
0	0	0.00	0	0	-	-	-

Table B18: Theoretical strain derived from the third test (B2) (nominal diameter)

strain gauge x 10^{-6}	F (kN)	σ (N/mm^2)	theoretical εx10^{-6}	theoretical Δεx10^{-6}	error between theoretical and experimental value (%)	max error(%) E = 220 GPa	min error(%) E = 200 GPa
0	0	0.00	0	0	-	-	-
326	28	62.33	297	14	9.84	15.33	4.85
690	58	129.10	615	29	12.24	17.85	7.13
924	78	173.62	827	39	11.76	17.35	6.68
1198	101	224.82	1071	51	11.90	17.50	6.82
1407	119	264.89	1261	60	11.55	17.12	6.48
1680	142	316.08	1505	72	11.62	17.20	6.54
1472	125	278.24	1325	63	11.10	16.65	6.05
1258	107	238.17	1134	54	10.92	16.46	5.88
936	80	178.07	848	40	10.38	15.90	5.36
719	62	138.01	657	31	9.41	14.88	4.43
437	38	84.59	403	19	8.49	13.92	3.56
2	0	0.00	0	0	-	-	-

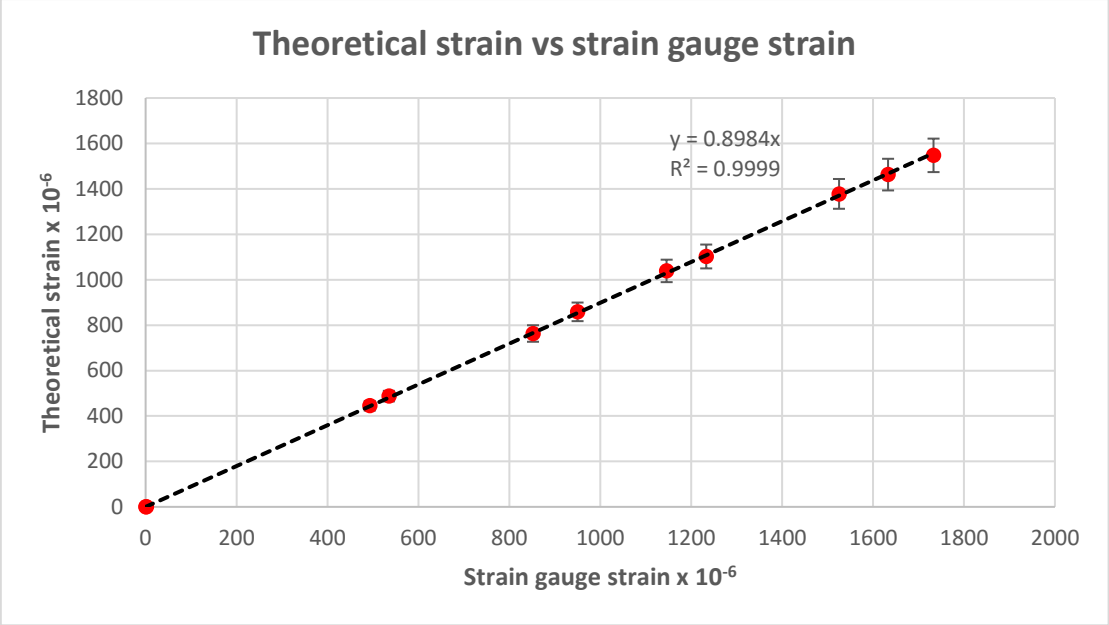

Figure B21: Strain obtained for the first test (B2) (nominal diameter)

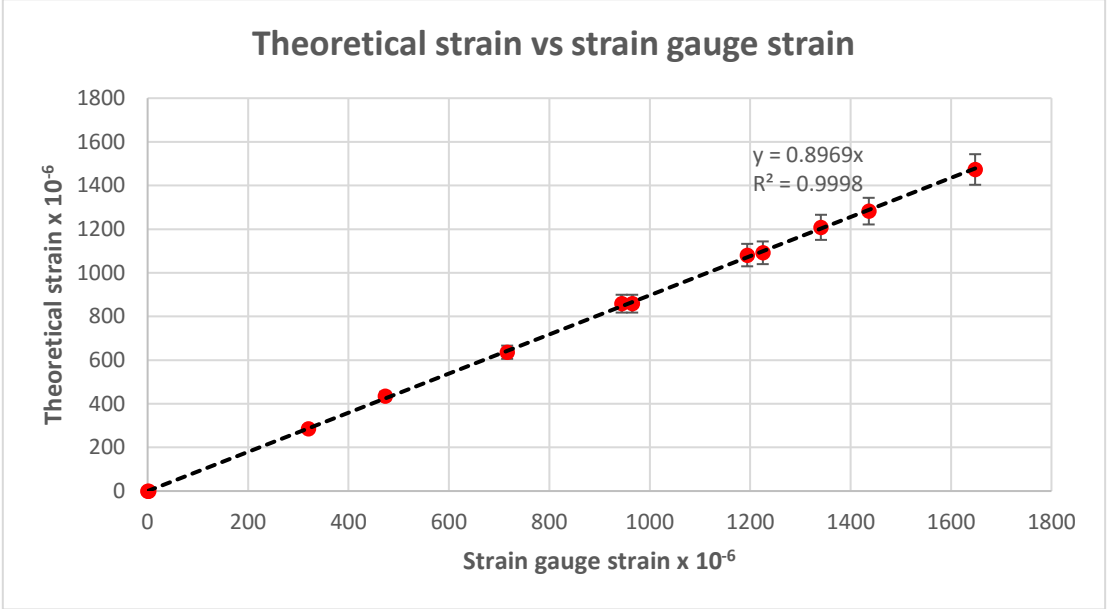

Figure B22: Strain obtained for the second test (B2) (nominal diameter)

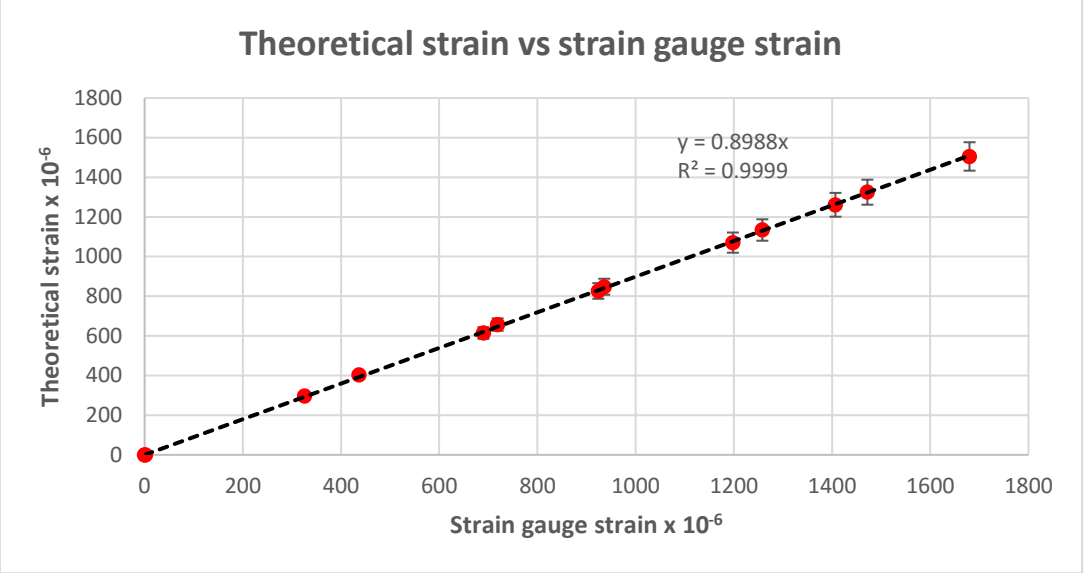

Figure B23: Strain obtained for the third test (B2) (nominal diameter)

Table B19: Theoretical strain derived from the first test (B2) (maximum diameter)

strain gauge x 10^{-6}	F (kN)	σ (N/mm^2)	theoretical εx10^{-6}	theoretical Δεx10^{-6}	error between theoretical and experimental value (%)	min error(%) E = 200 Gpa	max error(%) E = 220 Gpa
0	0	0.00	0	0	-	-	-
493	42	87.23	415	20	18.68	13.29	24.62
852	72	149.54	712	34	19.65	14.21	25.63
1233	104	216.01	1029	49	19.87	14.42	25.87
1633	138	286.62	1365	65	19.65	14.21	25.63
1733	146	303.24	1444	69	20.01	14.56	26.02
1525	130	270.01	1286	61	18.61	13.22	24.54
1146	98	203.54	969	46	18.24	12.86	24.15
950	81	168.23	801	38	18.58	13.19	24.51
535	46	95.54	455	22	17.59	12.25	23.47
2	0	0.00	0	0	-	-	-

Table B20: Theoretical strain derived from the second test (B2) (maximum diameter)

strain gauge x 10^{-6}	F (kN)	σ (N/mm^2)	theoretical εx10^{-6}	theoretical Δεx10^{-6}	error between theoretical and experimental value (%)	min error(%) E = 200 Gpa	max error(%) E = 220 Gpa
0	0	0.00	0	0	-	-	-
320	27	56.08	267	13	19.83	14.39	25.82
716	60	124.62	593	28	20.66	15.17	26.69
965	81	168.23	801	38	20.46	14.98	26.48
1225	103	213.93	1019	49	20.25	14.78	26.26
1436	121	251.31	1197	57	19.99	14.54	25.99
1648	139	288.70	1375	65	19.88	14.43	25.87
1341	114	236.77	1127	54	18.94	13.53	24.88
1194	102	211.85	1009	48	18.36	12.98	24.27
944	81	168.23	801	38	17.84	12.48	23.73
473	41	85.16	406	19	16.64	11.34	22.48
0	0	0.00	0	0	-	-	-

Table B21: Theoretical strain derived from the third test (B2) (maximum diameter)

strain gauge x 10^{-6}	F (kN)	σ (N/mm^2)	theoretical εx10^{-6}	theoretical Δεx10^{-6}	error between theoretical and experimental value (%)	min error(%) E = 200 Gpa	max error(%) E = 220 Gpa
0	0	0.00	0	0	-	-	-
326	28	58.16	277	13	17.72	12.37	23.61
690	58	120.46	574	27	20.28	14.82	26.30
924	78	162.00	771	37	19.77	14.33	25.76
1198	101	209.77	999	48	19.93	14.48	25.93
1407	119	247.16	1177	56	19.55	14.11	25.52
1680	142	294.93	1404	67	19.62	14.18	25.60
1472	125	259.62	1236	59	19.07	13.65	25.02
1258	107	222.24	1058	50	18.87	13.47	24.82
936	80	166.16	791	38	18.30	12.92	24.21
719	62	128.77	613	29	17.25	11.92	23.12
437	38	78.92	376	18	16.28	10.99	22.09
2	0	0.00	0	0	-	-	-

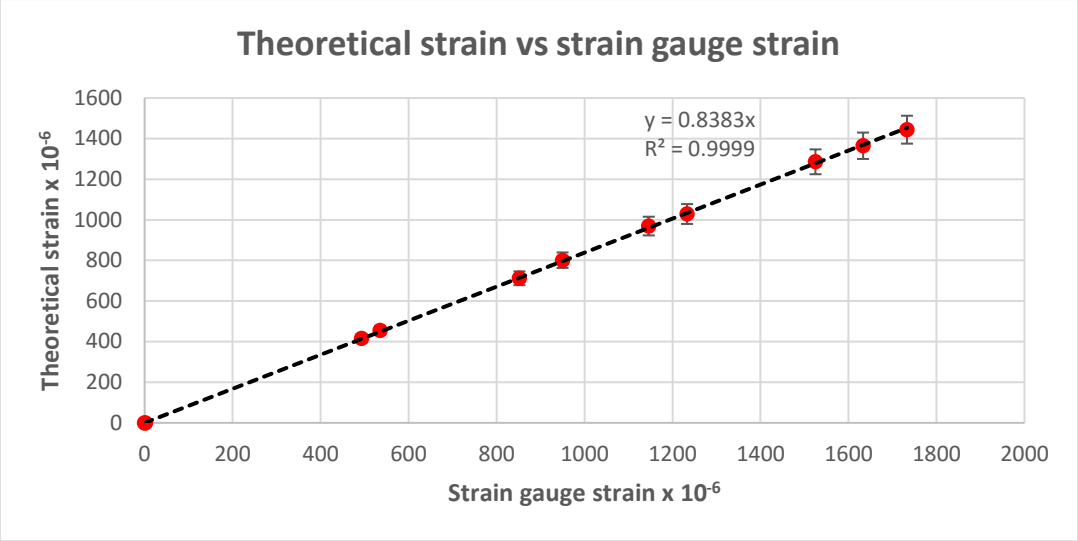

Figure B24: Strain obtained for the first test (B2) (maximum diameter)

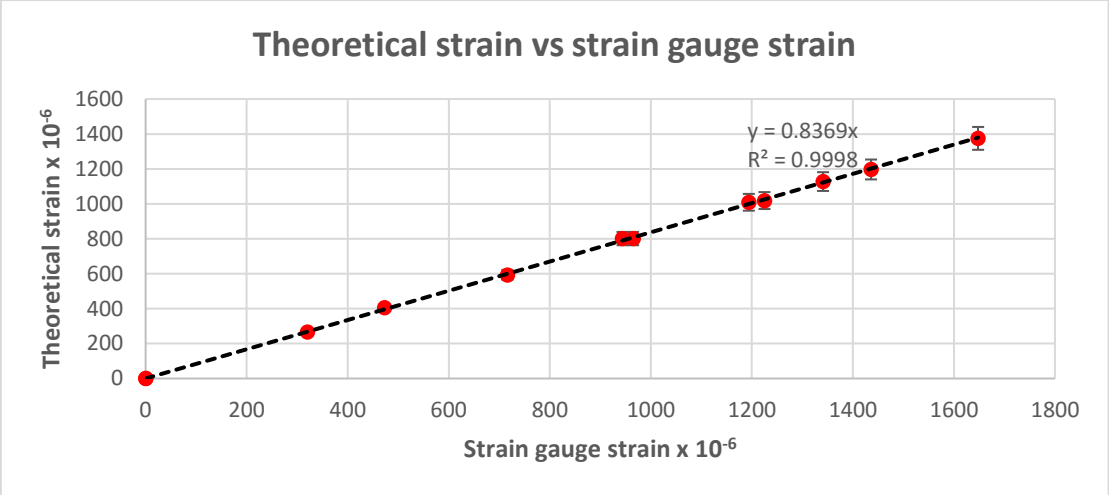

Figure B25: Strain obtained for the second test (B2) (maximum diameter)

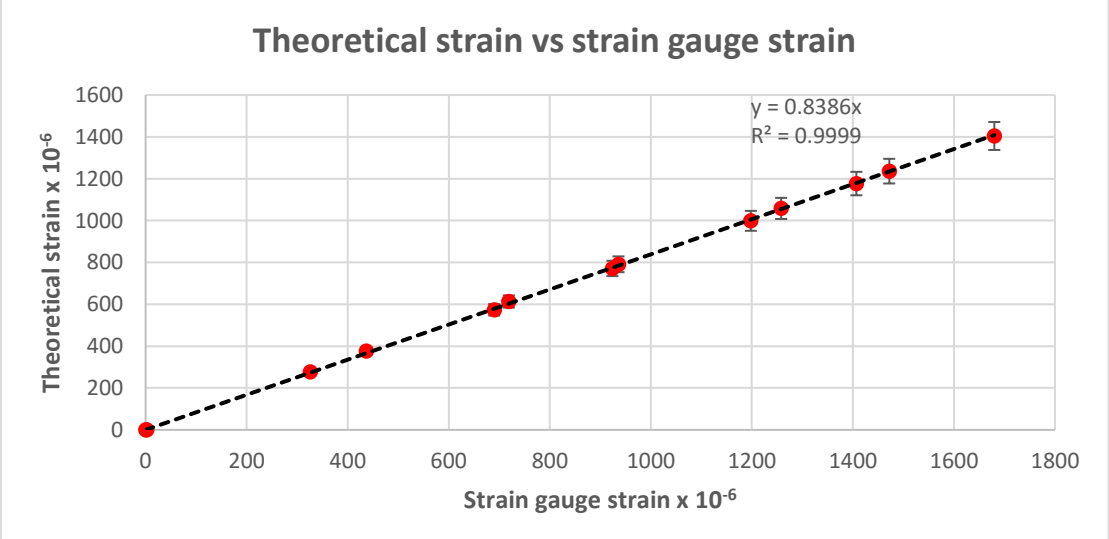

Figure B26: Strain obtained for the third test (B2) (maximum diameter)

Table B22: Theoretical strain derived from the first test (B2) (minimum diameter)

strain gauge x 10^{-6}	F (kN)	σ (N/mm^2)	theoretical εx10^{-6}	theoretical Δεx10^{-6}	error between theoretical and experimental value (%)	min error(%) E = 200 Gpa	max error(%) E = 220 Gpa
0	0	0.00	0	0	-	-	-
493	42	100.45	478	23	3.07	-1.62	8.22
852	72	172.20	820	39	3.91	-0.82	9.10
1233	104	248.73	1184	56	4.10	-0.63	9.31
1633	138	330.04	1572	75	3.91	-0.82	9.10
1733	146	349.17	1663	79	4.23	-0.51	9.44
1525	130	310.91	1481	71	3.00	-1.68	8.15
1146	98	234.38	1116	53	2.68	-1.99	7.81
950	81	193.72	922	44	2.98	-1.70	8.13
535	46	110.01	524	25	2.12	-2.52	7.23
2	0	0.00	0	0	-	-	-

Table B23: Theoretical strain derived from the second test (B2) (minimum diameter)

strain gauge x 10^{-6}	F (kN)	σ (N/mm^2)	theoretical εx10^{-6}	theoretical Δεx10^{-6}	error between theoretical and experimental value (%)	min error(%) E = 200 Gpa	max error(%) E = 220 Gpa
0	0	0.00	0	0	-	-	-
320	27	64.57	307	15	4.07	-0.66	9.27
716	60	143.50	683	33	4.78	0.02	10.02
965	81	193.72	922	44	4.61	-0.15	9.84
1225	103	246.33	1173	56	4.43	-0.32	9.65
1436	121	289.38	1378	66	4.21	-0.53	9.42
1648	139	332.43	1583	75	4.11	-0.63	9.31
1341	114	272.64	1298	62	3.29	-1.41	8.45
1194	102	243.94	1162	55	2.79	-1.89	7.93
944	81	193.72	922	44	2.33	-2.32	7.45
473	41	98.06	467	22	1.30	-3.30	6.36
0	0	0.00	0	0	-	-	-

Table B24: Theoretical strain derived from the third test (B2) (minimum diameter)

strain gauge x 10^{-6}	F (kN)	σ (N/mm^2)	theoretical εx10^{-6}	theoretical Δεx10^{-6}	error between theoretical and experimental value (%)	min error(%) E = 200 Gpa	max error(%) E = 220 Gpa
0	0	0.00	0	0	-	-	-
326	28	66.96	319	15	2.23	-2.41	7.34
690	58	138.71	661	31	4.46	-0.29	9.68
924	78	186.54	888	42	4.02	-0.71	9.22
1198	101	241.55	1150	55	4.15	-0.58	9.36
1407	119	284.60	1355	65	3.82	-0.90	9.01
1680	142	339.61	1617	77	3.88	-0.84	9.08
1472	125	298.95	1424	68	3.40	-1.30	8.57
1258	107	255.90	1219	58	3.24	-1.46	8.40
936	80	191.33	911	43	2.73	-1.94	7.87
719	62	148.28	706	34	1.83	-2.80	6.92
437	38	90.88	433	21	0.98	-3.61	6.03
2	0	0.00	0	0	-	-	-

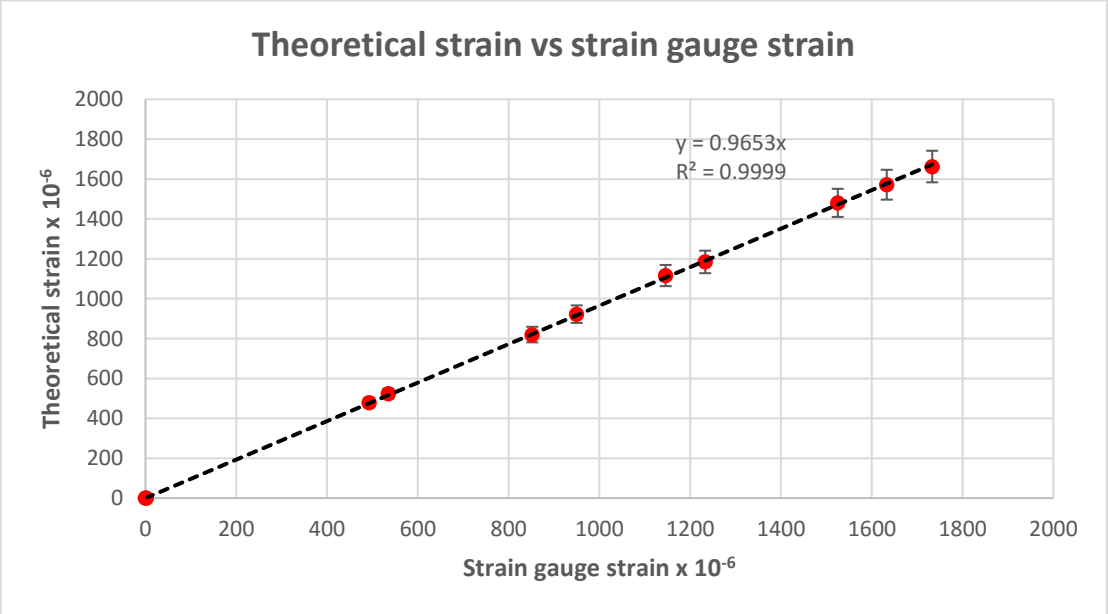

Figure B27: Strain obtained for the first test (B2) (minimum diameter)

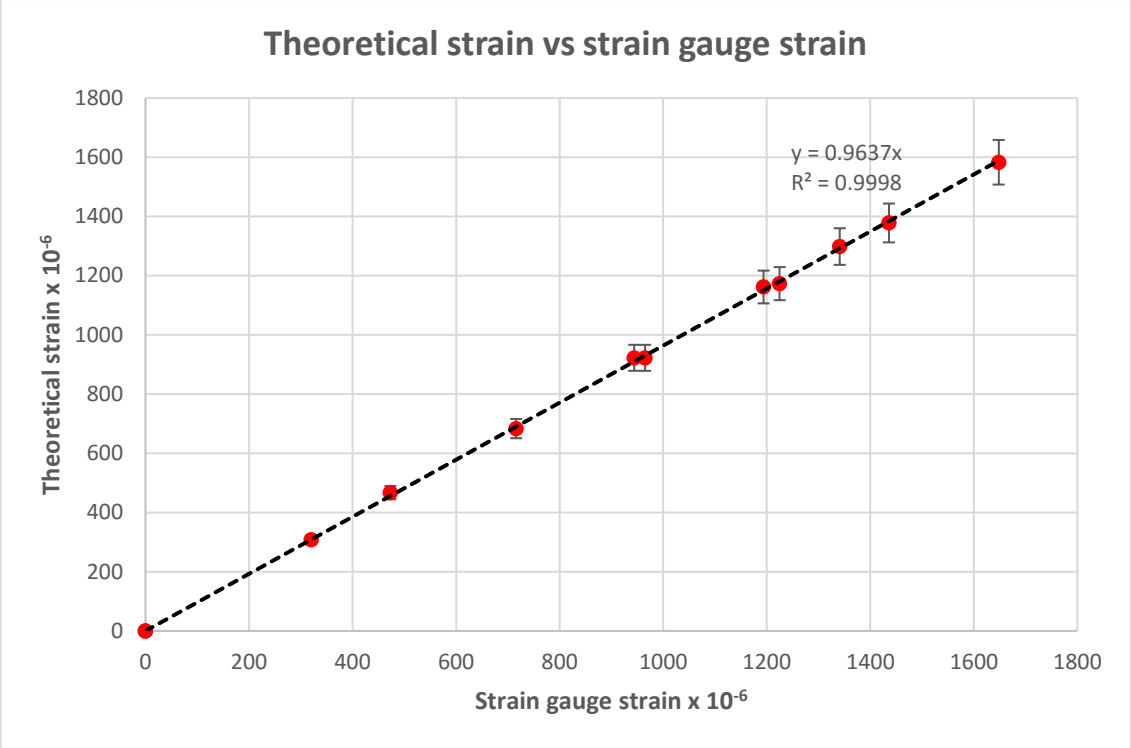

Figure B28: Strain obtained for the second test (B2) (minimum diameter)

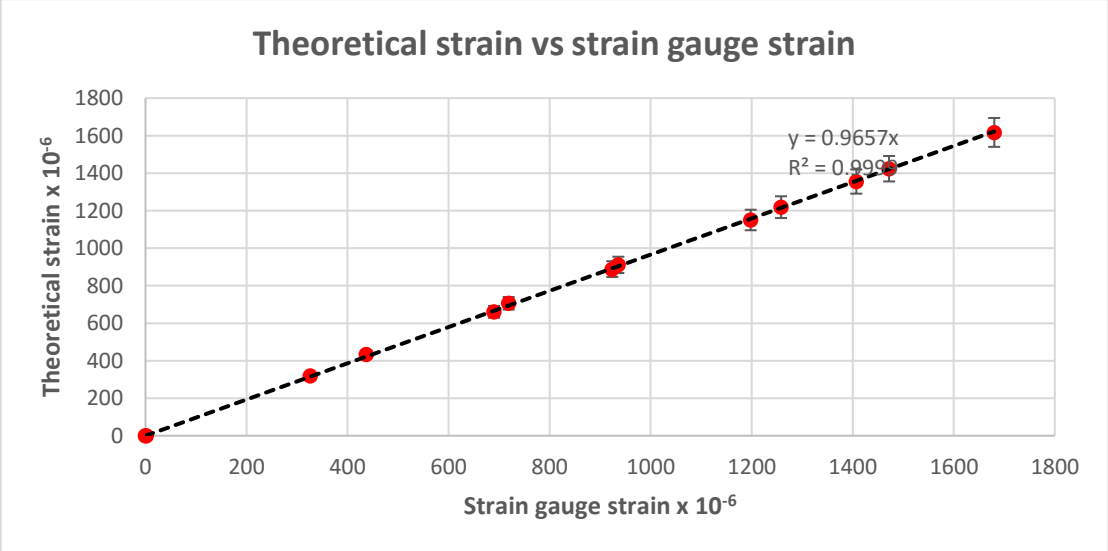

Figure B29: Strain obtained for the third test (B2) (minimum diameter)

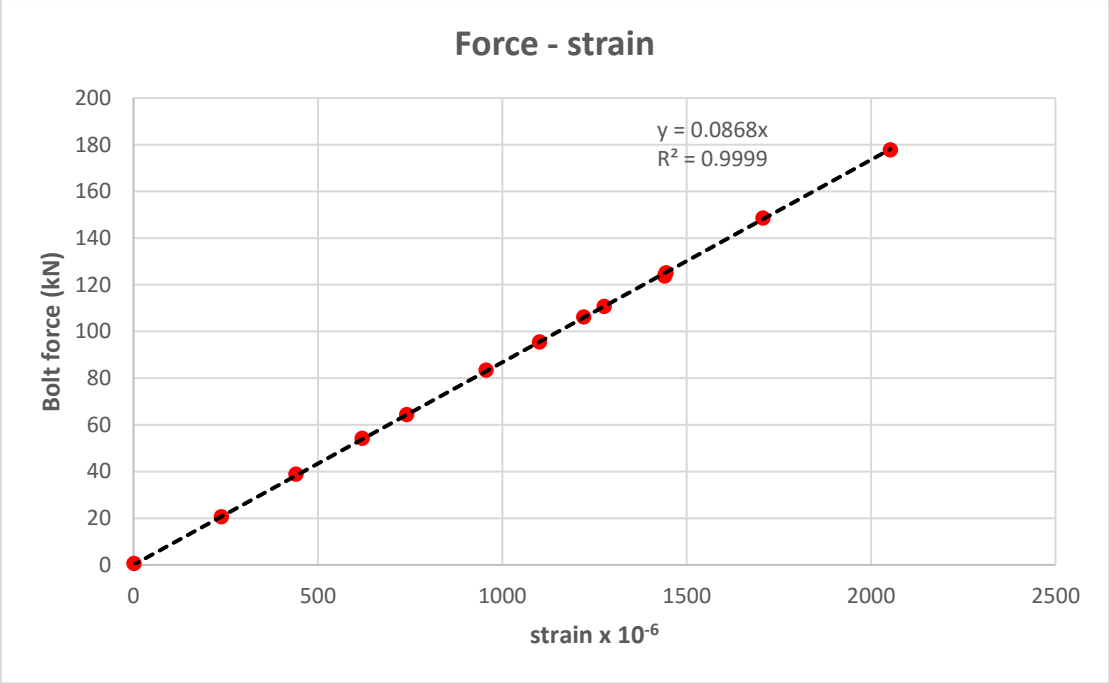

Figure B30: Force-strain diagram obtained for the first test (B3)

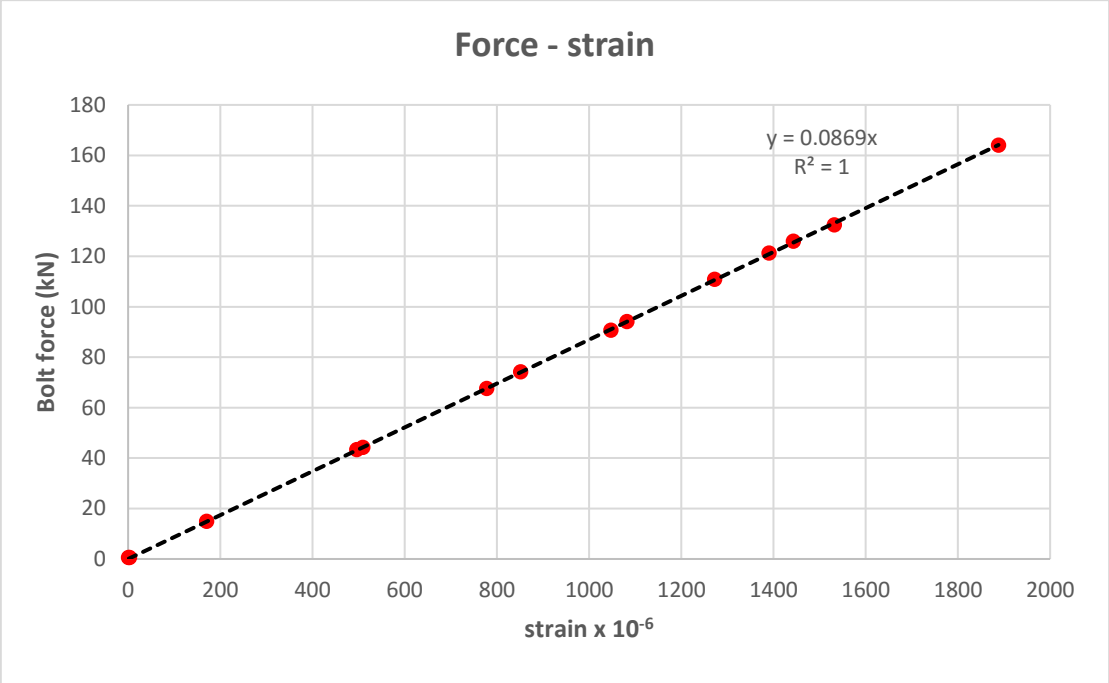

Figure B31: Force-strain diagram obtained for the second test (B3)

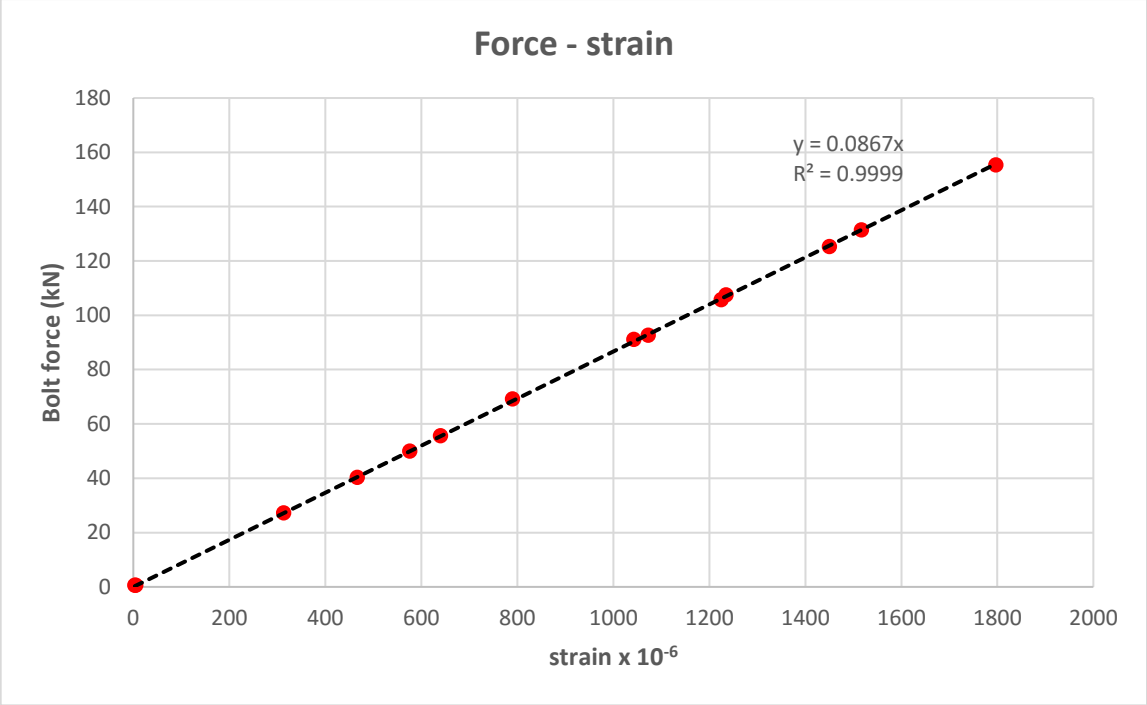

Figure B32: Force-strain diagram obtained for the third test (B3)

Table B25: Theoretical strain derived from the first test (B3) (actual diameter)

strain gauge $\varepsilon x10^{-6}$	F (kN)	σ (N/mm^2)	theoretical $\varepsilon x10^{-6}$	theoretical $\Delta\varepsilon x10^{-6}$	error between theoretical and experimental value (%)	min error(%) E = 200 Gpa	max error(%) E = 220 GPa
-5	0	0.00	0	0	-	-	-
238	21	47.06	224	11	6.21	1.38	11.52
741	64	143.42	683	33	8.50	3.57	13.92
1101	96	215.13	1024	49	7.47	2.59	12.85
1276	111	248.75	1185	56	7.72	2.83	13.11
1444	125	280.12	1334	64	8.25	3.33	13.67
1707	149	333.90	1590	76	7.36	2.48	12.73
2052	178	398.89	1899	90	8.03	3.12	13.43
1440	124	277.88	1323	63	8.82	3.88	14.27
1221	106	237.54	1131	54	7.94	3.04	13.34
956	83	186.00	886	42	7.94	3.03	13.33
620	54	121.01	576	27	7.59	2.70	12.97
440	39	87.40	416	20	5.72	0.92	11.01
1	0	0.00	0	0	-	-	-

Table B26: Theoretical strain derived from the second test (B3) (actual diameter)

strain gauge $\varepsilon x10^{-6}$	F (kN)	σ (N/mm^2)	theoretical $\varepsilon x10^{-6}$	theoretical $\Delta\varepsilon x10^{-6}$	error between theoretical and experimental value (%)	min error(%) E = 200 Gpa	max error(%) E = 220 GPa
1	0	0.00	0	0	-	-	-
170	15	33.61	160	8	6.21	1.38	11.52
509	44	98.60	470	22	8.41	3.48	13.83
851	74	165.83	790	38	7.77	2.87	13.16
1082	94	210.65	1003	48	7.87	2.96	13.26
1272	111	248.75	1185	56	7.39	2.51	12.76
1443	126	282.36	1345	64	7.32	2.44	12.69
1888	164	367.52	1750	83	7.88	2.98	13.28
1532	132	295.80	1409	67	8.76	3.82	14.20
1390	121	271.15	1291	61	7.65	2.76	13.03
1047	91	203.93	971	46	7.82	2.92	13.21
778	68	152.38	726	35	7.22	2.34	12.58
496	43	96.36	459	22	8.09	3.18	13.50
3	0	0.00	0	0	-	-	-

Table B27: Theoretical strain derived from the third test (B3) (actual diameter)

strain gauge $\varepsilon x10^{-6}$	F (kN)	σ (N/mm^2)	theoretical $\varepsilon x10^{-6}$	theoretical $\Delta\varepsilon x10^{-6}$	error between theoretical and experimental value (%)	min error(%) E = 200 Gpa	max error(%) E = 220 GPa
3	0	0.00	0	0	-	-	-
313	27	60.51	288	14	8.63	3.70	14.07
640	56	125.49	598	28	7.10	2.23	12.45
790	69	154.63	736	35	7.29	2.41	12.66
1043	91	203.93	971	46	7.41	2.52	12.78
1235	108	242.02	1152	55	7.16	2.29	12.52
1517	131	293.56	1398	67	8.52	3.59	13.94
1797	155	347.35	1654	79	8.64	3.71	14.08
1450	125	280.12	1334	64	8.70	3.76	14.14
1225	106	237.54	1131	54	8.30	3.37	13.71
1073	93	208.41	992	47	8.12	3.21	13.53
576	50	112.05	534	25	7.95	3.05	13.35
467	40	89.64	427	20	9.41	4.43	14.88
5	0	0.00	0	0	-	-	-

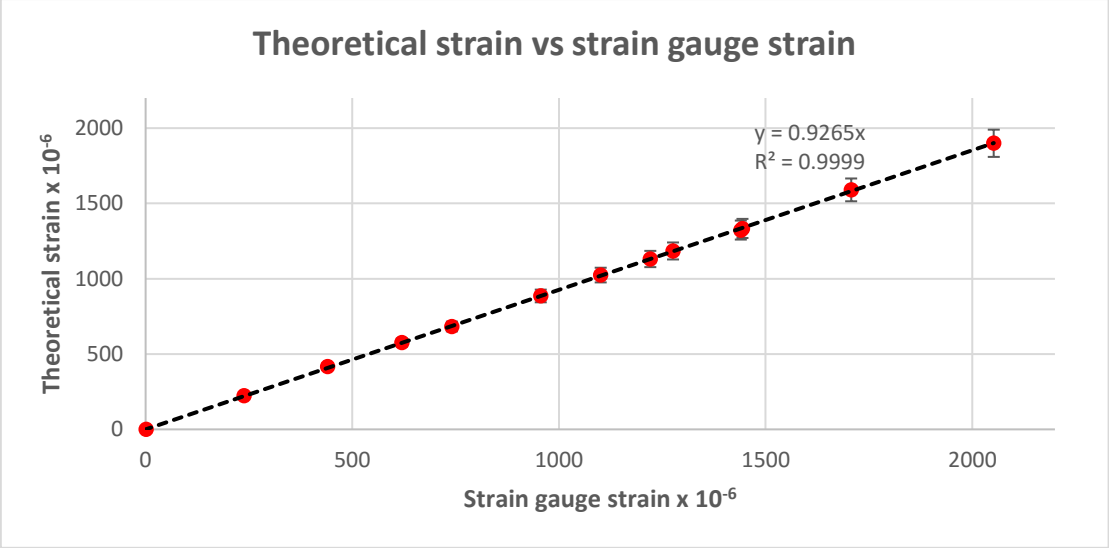

Figure B33: Strain obtained for the first test (B3) (actual diameter)

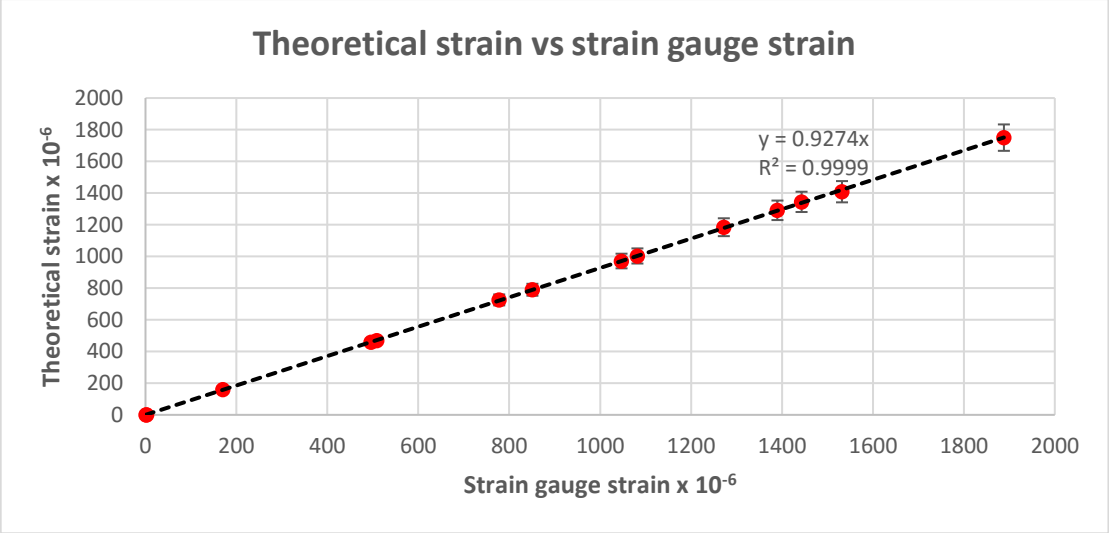

Figure B34: Strain obtained for the second test (B3) (actual diameter)

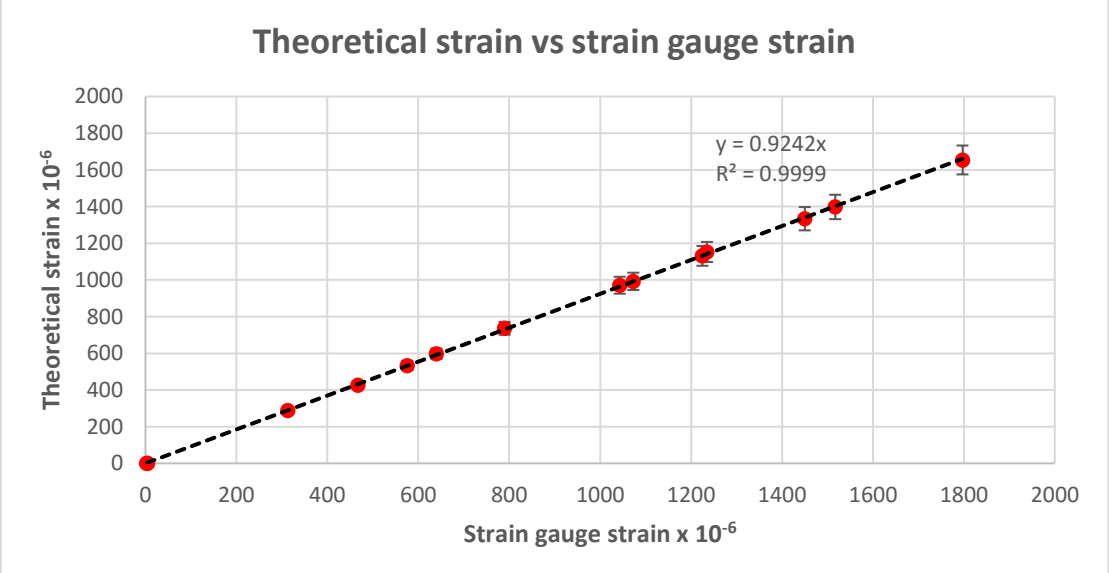

Figure B35: Strain obtained for the third test (B3)

Table B28: Theoretical strain derived from the first test (B3) (nominal diameter)

strain gauge $\varepsilon x10^{-6}$	F (kN)	σ (N/mm^2)	theoretical $\varepsilon x10^{-6}$	theoretical $\Delta\varepsilon x10^{-6}$	error between theoretical and experimental value (%)	min error(%) E = 200 Gpa	max error(%) E = 220 Gpa
-5	0	0.00	0	0	-	-	-
238	21	46.74	223	11	6.92	2.06	12.27
741	64	142.46	678	32	9.23	4.27	14.69
1101	96	213.69	1018	48	8.20	3.28	13.61
1276	111	247.08	1177	56	8.45	3.52	13.87
1444	125	278.24	1325	63	8.98	4.03	14.43
1707	149	331.66	1579	75	8.08	3.17	13.49
2052	178	396.22	1887	90	8.76	3.82	14.20
1440	124	276.02	1314	63	9.56	4.58	15.04
1221	106	235.95	1124	54	8.67	3.73	14.11
956	83	184.75	880	42	8.66	3.73	14.10
620	54	120.20	572	27	8.32	3.40	13.74
440	39	86.81	413	20	6.44	1.60	11.76
1	0	0.00	0	0	-	-	-

Table B29: Theoretical strain derived from the second test (B3) (nominal diameter)

strain gauge $\varepsilon x10^{-6}$	F (kN)	σ (N/mm^2)	theoretical $\varepsilon x10^{-6}$	theoretical $\Delta\varepsilon x10^{-6}$	error between theoretical and experimental value (%)	min error(%) E = 200 Gpa	max error(%) E = 220 Gpa
1	0	0.00	0	0	-	-	-
170	15	33.39	159	8	6.92	2.06	12.27
509	44	97.94	466	22	9.14	4.18	14.59
851	74	164.72	784	37	8.49	3.56	13.92
1082	94	209.24	996	47	8.59	3.66	14.02
1272	111	247.08	1177	56	8.11	3.20	13.52
1443	126	280.47	1336	64	8.04	3.13	13.45
1888	164	365.05	1738	83	8.61	3.67	14.04
1532	132	293.82	1399	67	9.49	4.52	14.97
1390	121	269.34	1283	61	8.38	3.45	13.80
1047	91	202.56	965	46	8.55	3.61	13.97
778	68	151.36	721	34	7.94	3.03	13.34
496	43	95.72	456	22	8.82	3.88	14.26
3	0	0.00	0	0	-	-	-

Table B30: Theoretical strain derived from the third test (B3) (nominal diameter)

strain gauge $\varepsilon x10^{-6}$	F (kN)	σ (N/mm^2)	theoretical $\varepsilon x10^{-6}$	theoretical $\Delta\varepsilon x10^{-6}$	error between theoretical and experimental value (%)	min error(%) E = 200 Gpa	max error(%) E = 220 Gpa
3	0	0.00	0	0	-	-	-
313	27	60.10	286	14	9.37	4.40	14.84
640	56	124.65	594	28	7.82	2.92	13.21
790	69	153.59	731	35	8.02	3.11	13.42
1043	91	202.56	965	46	8.13	3.22	13.54
1235	108	240.40	1145	55	7.88	2.98	13.28
1517	131	291.60	1389	66	9.25	4.28	14.71
1797	155	345.02	1643	78	9.38	4.40	14.85
1450	125	278.24	1325	63	9.44	4.46	14.91
1225	106	235.95	1124	54	9.03	4.07	14.48
1073	93	207.01	986	47	8.85	3.90	14.29
576	50	111.30	530	25	8.68	3.74	14.12
467	40	89.04	424	20	10.14	5.14	15.65
5	0	0.00	0	0	-	-	-

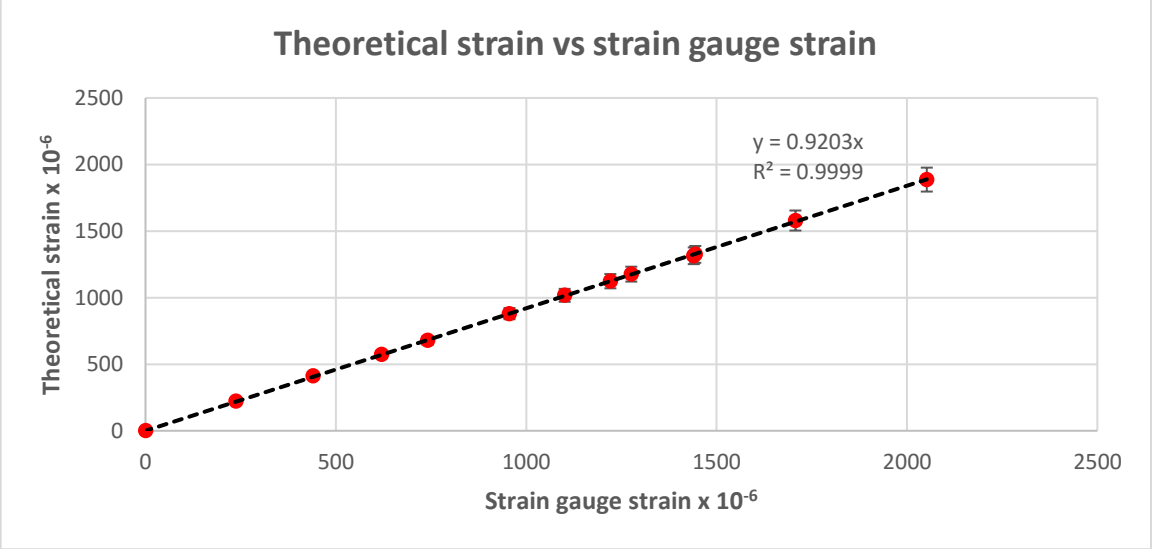

Figure B36: Strain obtained for the first test (B3) (nominal diameter)

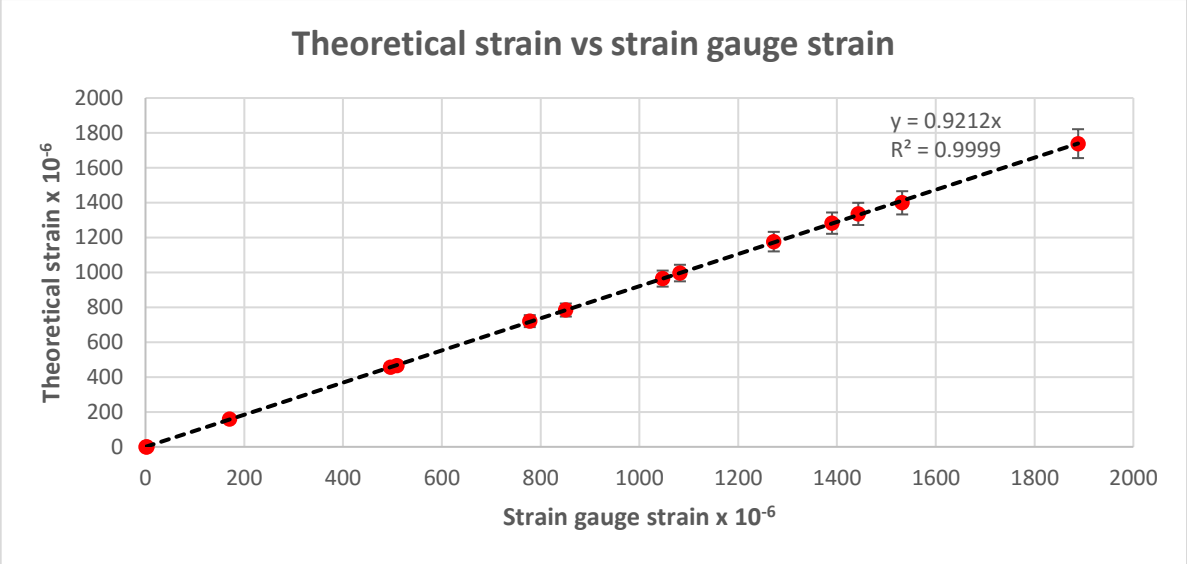

Figure B37: Strain obtained for the second test (B3) (nominal diameter)

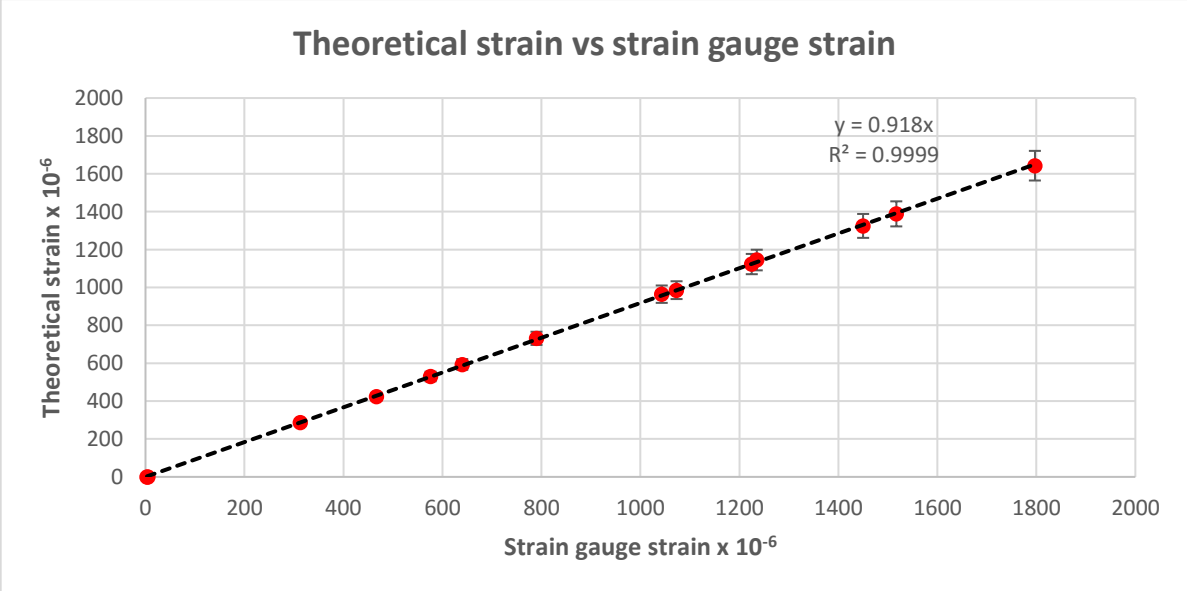

Figure B38: Strain obtained for the third test (B3) (nominal diameter)

Table B31: Theoretical strain derived from the first test (B3) (maximum diameter)

strain gauge $\varepsilon x10^{-6}$	F (kN)	σ (N/mm^2)	theoretical $\varepsilon x10^{-6}$	theoretical $\Delta\varepsilon x10^{-6}$	error between theoretical and experimental value (%)	min error(%) E = 200 Gpa	max error(%) E = 220 Gpa
-5	0	0.00	0	0	-	-	-
238	21	43.62	208	10	14.59	9.38	20.32
741	64	132.93	633	30	17.06	11.74	22.92
1101	96	199.39	949	45	15.96	10.69	21.76
1276	111	230.54	1098	52	16.23	10.95	22.04
1444	125	259.62	1236	59	16.80	11.49	22.64
1707	149	309.47	1474	70	15.83	10.57	21.63
2052	178	369.70	1760	84	16.56	11.26	22.39
1440	124	257.54	1226	58	17.42	12.08	23.29
1221	106	220.16	1048	50	16.47	11.17	22.29
956	83	172.39	821	39	16.46	11.16	22.28
620	54	112.16	534	25	16.09	10.81	21.89
440	39	81.00	386	18	14.07	8.89	19.77
1	0	0.00	0	0	-	-	-

Table B32: Theoretical strain derived from the second test (B3) (maximum diameter)

strain gauge $\varepsilon x10^{-6}$	F (kN)	σ (N/mm^2)	theoretical $\varepsilon x10^{-6}$	theoretical $\Delta\varepsilon x10^{-6}$	error between theoretical and experimental value (%)	min error(%) E = 200 Gpa	max error(%) E = 220 Gpa
1	0	0.00	0	0	-	-	-
170	15	31.15	148	7	14.59	9.38	20.32
509	44	91.39	435	21	16.96	11.65	22.81
851	74	153.70	732	35	16.28	10.99	22.09
1082	94	195.24	930	44	16.38	11.09	22.20
1272	111	230.54	1098	52	15.87	10.60	21.66
1443	126	261.70	1246	59	15.79	10.53	21.58
1888	164	340.62	1622	77	16.40	11.11	22.22
1532	132	274.16	1306	62	17.35	12.01	23.21
1390	121	251.31	1197	57	16.15	10.87	21.96
1047	91	189.00	900	43	16.33	11.04	22.15
778	68	141.23	673	32	15.68	10.42	21.46
496	43	89.31	425	20	16.63	11.33	22.46
3	0	0.00	0	0	-	-	-

Table B33: Theoretical strain derived from the third test (B3) (maximum diameter)

strain gauge $\varepsilon x10^{-6}$	F (kN)	σ (N/mm^2)	theoretical $\varepsilon x10^{-6}$	theoretical $\Delta\varepsilon x10^{-6}$	error between theoretical and experimental value (%)	min error(%) E = 200 Gpa	max error(%) E = 220 Gpa
3	0	0.00	0	0	-	-	-
313	27	56.08	267	13	17.21	11.88	23.07
640	56	116.31	554	26	15.55	10.30	21.33
790	69	143.31	682	32	15.76	10.50	21.55
1043	91	189.00	900	43	15.89	10.62	21.68
1235	108	224.31	1068	51	15.62	10.36	21.40
1517	131	272.08	1296	62	17.09	11.76	22.94
1797	155	321.93	1533	73	17.22	11.89	23.08
1450	125	259.62	1236	59	17.29	11.95	23.15
1225	106	220.16	1048	50	16.85	11.54	22.69
1073	93	193.16	920	44	16.66	11.35	22.49
576	50	103.85	495	24	16.48	11.18	22.30
467	40	83.08	396	19	18.04	12.68	23.95
5	0	0.00	0	0	-	-	-

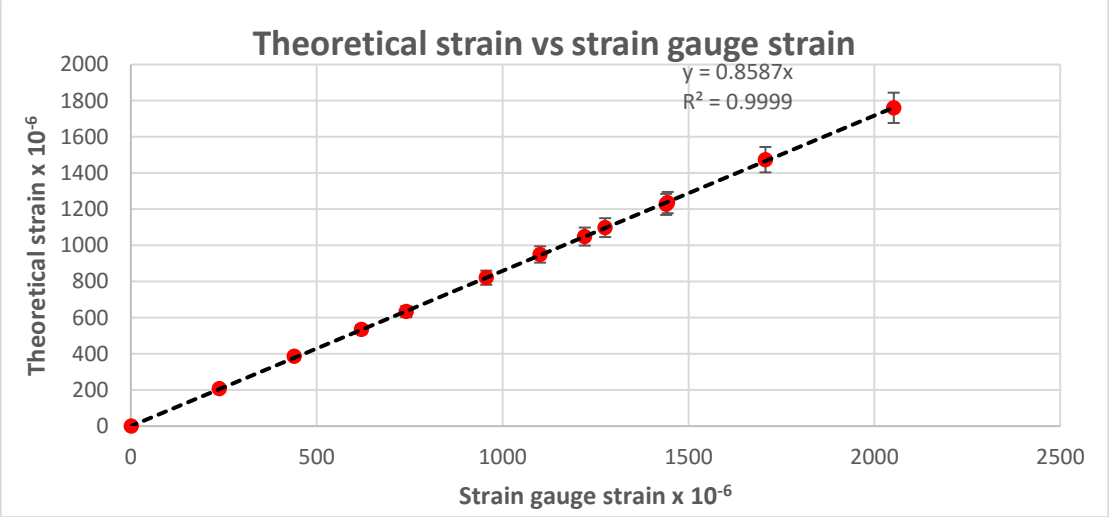

Figure B39: Strain obtained for the first test (B3) (maximum diameter)

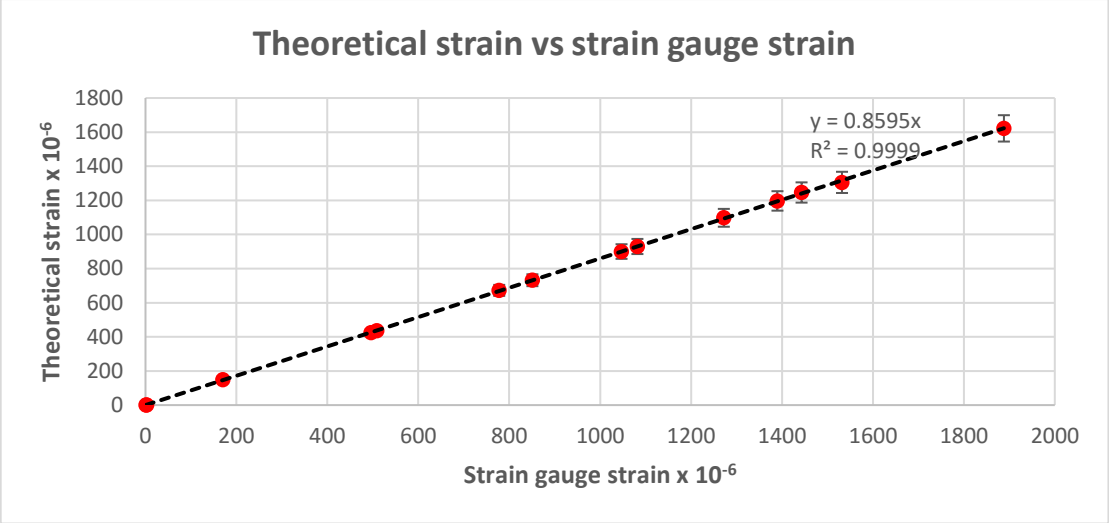

Figure B40: Strain obtained for the second test (B3) (maximum diameter)

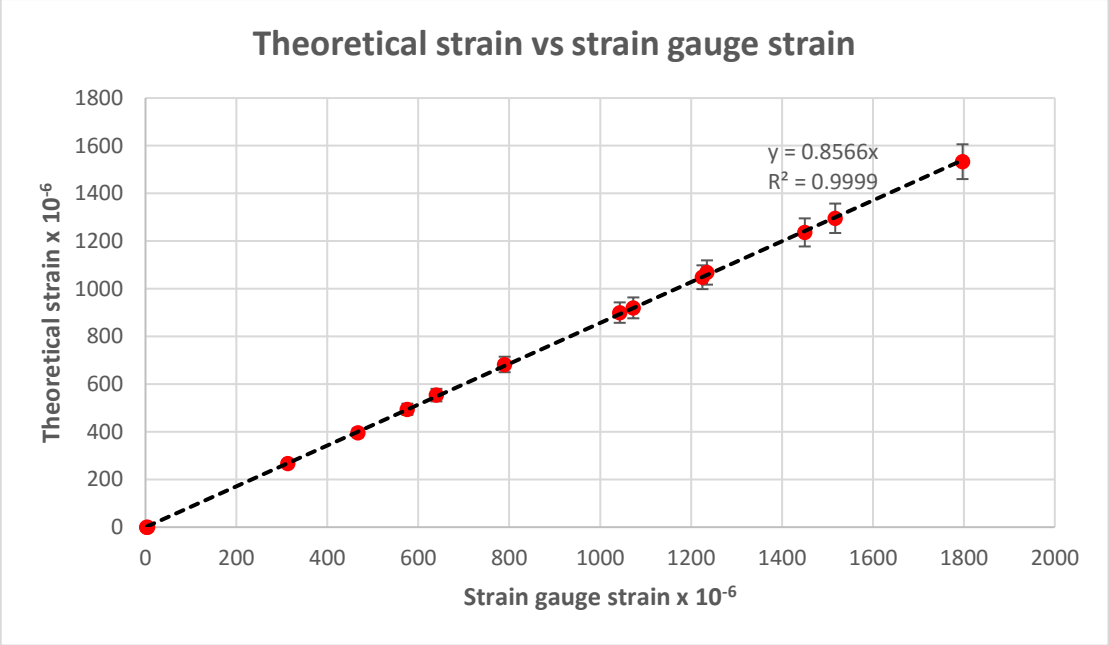

Figure B41: Strain obtained for the third test (B3) (maximum diameter)

Table B34: Theoretical strain derived from the first test (B3) (minimum diameter)

strain gauge $\varepsilon x10^{-6}$	F (kN)	σ (N/mm^2)	theoretical $\varepsilon x10^{-6}$	theoretical $\Delta\varepsilon x10^{-6}$	error between theoretical and experimental value (%)	min error(%) E = 200 Gpa	max error(%) E = 220 Gpa
-5	0	0.00	0	0	-	-	-
238	21	50.22	239	11	-0.49	-5.01	4.49
741	64	153.06	729	35	1.66	-2.96	6.75
1101	96	229.59	1093	52	0.70	-3.87	5.74
1276	111	265.47	1264	60	0.94	-3.65	5.99
1444	125	298.95	1424	68	1.43	-3.18	6.51
1707	149	356.35	1697	81	0.60	-3.98	5.63
2052	178	425.70	2027	97	1.23	-3.38	6.29
1440	124	296.56	1412	67	1.97	-2.67	7.07
1221	106	253.51	1207	57	1.14	-3.45	6.20
956	83	198.50	945	45	1.14	-3.46	6.19
620	54	129.15	615	29	0.82	-3.77	5.86
440	39	93.27	444	21	-0.94	-5.44	4.02
1	0	0.00	0	0	-	-	-

Table B35: Theoretical strain derived from the second test (B3) (minimum diameter)

strain gauge $\varepsilon x10^{-6}$	F (kN)	σ (N/mm^2)	theoretical $\varepsilon x10^{-6}$	theoretical $\Delta\varepsilon x10^{-6}$	error between theoretical and experimental value (%)	min error(%) E = 200 Gpa	max error(%) E = 220 Gpa
1	0	0.00	0	0	-	-	-
170	15	35.87	171	8	-0.49	-5.01	4.49
509	44	105.23	501	24	1.58	-3.04	6.66
851	74	176.98	843	40	0.98	-3.61	6.03
1082	94	224.81	1071	51	1.07	-3.52	6.13
1272	111	265.47	1264	60	0.62	-3.95	5.65
1443	126	301.34	1435	68	0.56	-4.01	5.59
1888	164	392.22	1868	89	1.09	-3.51	6.14
1532	132	315.69	1503	72	1.91	-2.72	7.01
1390	121	289.38	1378	66	0.87	-3.72	5.91
1047	91	217.64	1036	49	1.03	-3.57	6.08
778	68	162.63	774	37	0.46	-4.10	5.48
496	43	102.84	490	23	1.28	-3.32	6.35
3	0	0.00	0	0	-	-	-

Table B36: Theoretical strain derived from the third test (B3) (minimum diameter)

strain gauge $\varepsilon x10^{-6}$	F (kN)	σ (N/mm^2)	theoretical $\varepsilon x10^{-6}$	theoretical $\Delta\varepsilon x10^{-6}$	error between theoretical and experimental value (%)	min error(%) E = 200 Gpa	max error(%) E = 220 Gpa
3	0	0.00	0	0	-	-	-
313	27	64.57	307	15	1.79	-2.84	6.88
640	56	133.93	638	30	0.35	-4.21	5.37
790	69	165.02	786	37	0.53	-4.04	5.56
1043	91	217.64	1036	49	0.64	-3.93	5.67
1235	108	258.29	1230	59	0.41	-4.15	5.43
1517	131	313.30	1492	71	1.68	-2.94	6.77
1797	155	370.70	1765	84	1.80	-2.83	6.89
1450	125	298.95	1424	68	1.86	-2.77	6.95
1225	106	253.51	1207	57	1.48	-3.14	6.55
1073	93	222.42	1059	50	1.31	-3.30	6.37
576	50	119.58	569	27	1.15	-3.44	6.21
467	40	95.66	456	22	2.52	-2.14	7.64
5	0	0.00	0	0	-	-	-

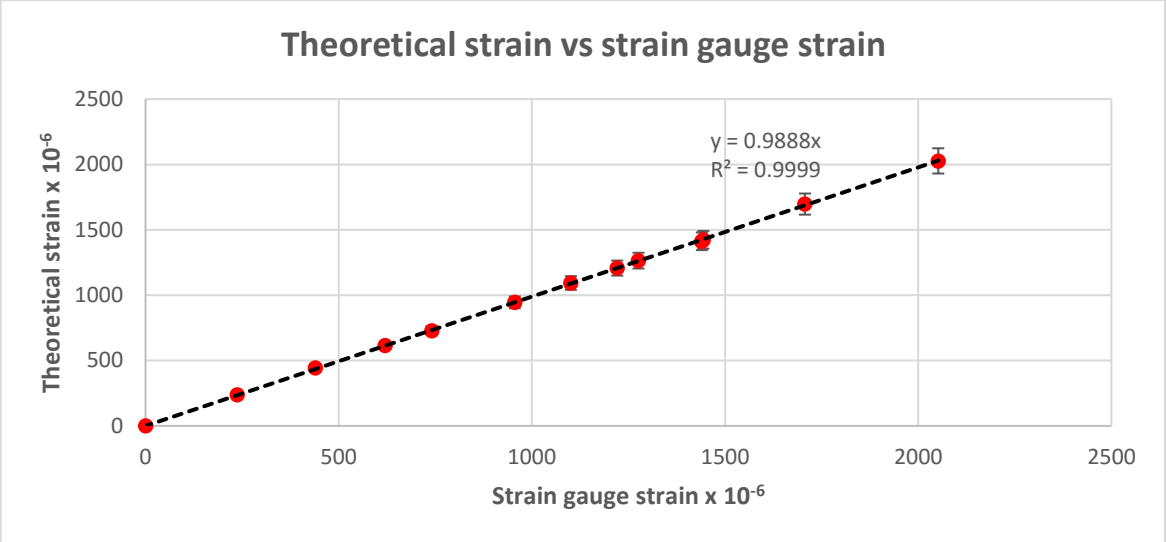

Figure B42: Strain obtained for the first test (B3) (minimum diameter)

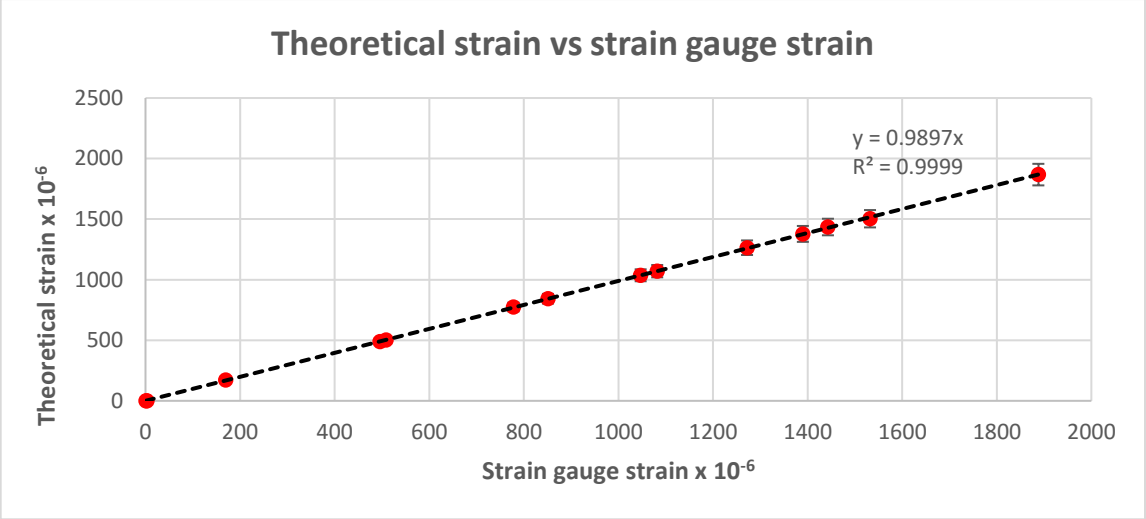

Figure B43: Strain obtained for the second test (B3) (minimum diameter)

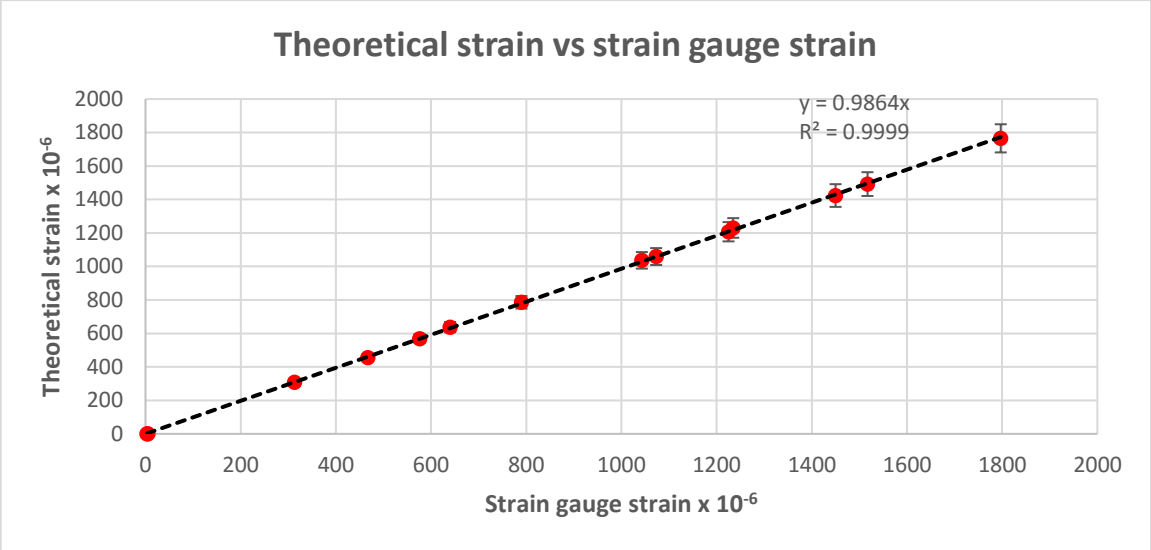

Figure B44: Strain obtained for the third test (B3) (minimum diameter)

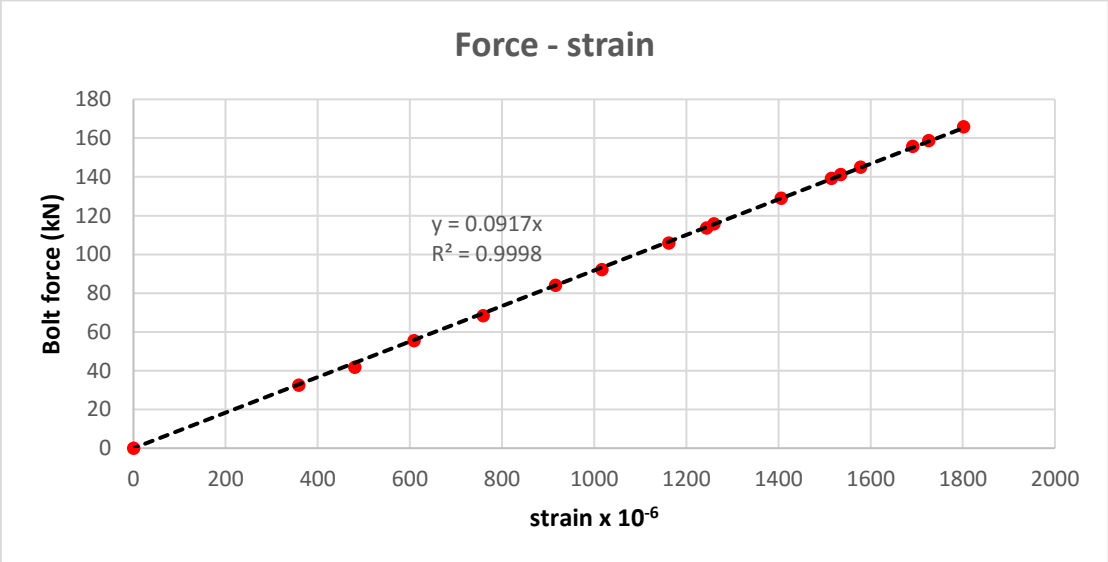

Figure B45: Force-strain diagram obtained for the first test (B4)

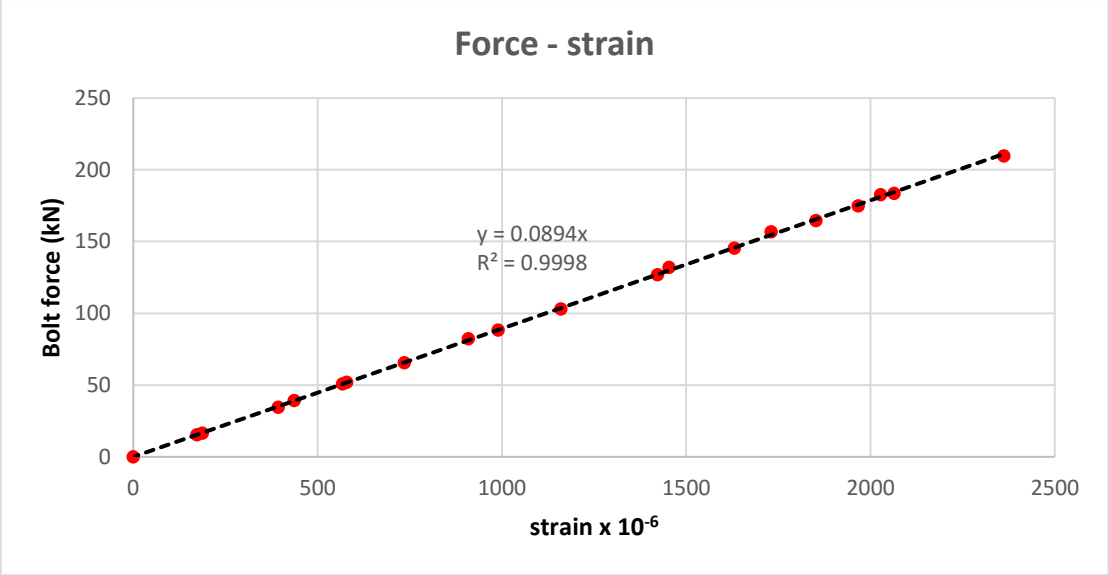

Figure B46: Force-strain diagram obtained for the second test (B4)

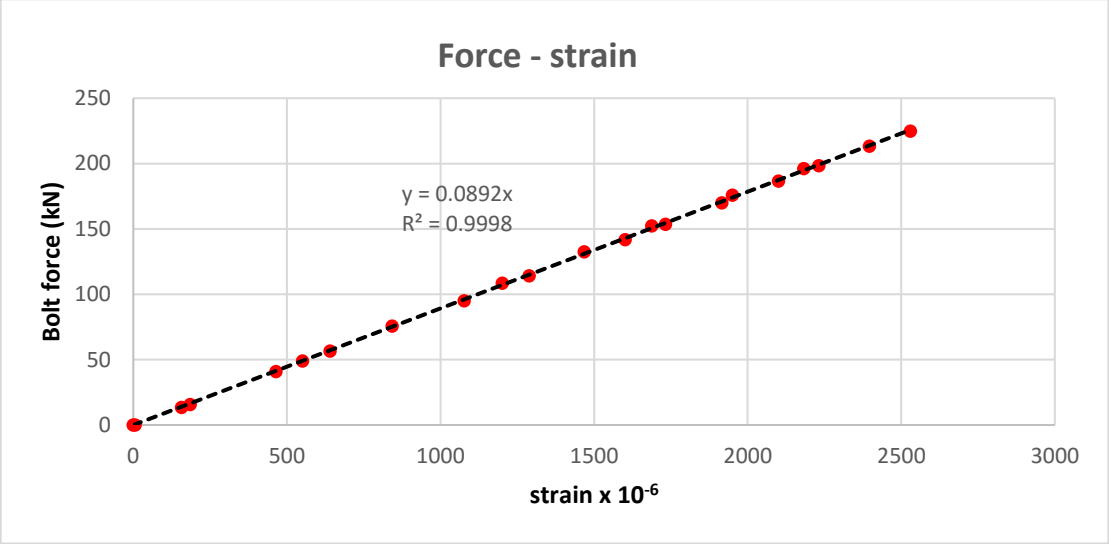

Figure B47: Force-strain diagram obtained for the third test (B4)

Table B37: Theoretical strain derived from the first test (B4) (actual diameter)

strain gauge x 10^{-6}	F (kN)	σ (N/mm^2)	theoretical $\varepsilon x10^{-6}$	theoretical $\Delta\varepsilon x10^{-6}$	error between theoretical and experimental value (%)	min error(%) E = 200 Gpa	max error(%) E = 220 Gpa
0	0	0.00	0	0	-	-	-
480	42	90.28	430	20	11.63	6.67	17.07
759	68	146.17	696	33	9.05	4.12	14.48
1017	92	197.76	942	45	7.96	3.04	13.38
1162	106	227.85	1085	52	7.10	2.20	12.49
1244	114	245.05	1167	56	6.60	1.72	11.97
1406	129	277.29	1320	63	6.52	1.66	11.85
1535	141	303.08	1443	69	6.38	1.52	11.72
1578	145	311.68	1484	71	6.33	1.48	11.68
1691	156	335.33	1597	76	5.89	1.08	11.18
1802	166	356.82	1699	81	6.06	1.24	11.37
1726	159	341.77	1627	77	6.08	1.29	11.35
1515	139	298.78	1423	68	6.47	1.61	11.81
1260	116	249.34	1187	57	6.15	1.29	11.50
916	84	180.56	860	41	6.51	1.66	11.84
609	56	120.37	573	27	6.28	1.50	11.54
359	33	70.93	338	16	6.21	1.41	11.49
-7	0	0.00	0	0	-	-	-

Table B38: Theoretical strain derived from the second test (B4) (actual diameter)

strain gauge $\varepsilon x10^{-6}$	F (kN)	σ (N/mm^2)	theoretical $\varepsilon x10^{-6}$	theoretical $\Delta\varepsilon x10^{-6}$	error between theoretical and experimental value (%)	min error(%) E = 200 Gpa	max error(%) E = 220 Gpa
-7	0	0.00	0	0	-	-	-
173	15	32.24	154	7	12.34	7.45	17.69
437	39	83.83	399	19	9.52	4.55	15.00
568	51	109.63	522	25	8.81	3.84	14.29
735	66	141.87	676	32	8.73	3.81	14.13
990	88	189.16	901	43	9.88	4.87	15.38
1160	103	221.40	1054	50	10.06	5.07	15.54
1422	127	272.99	1300	62	9.38	4.41	14.86
1631	145	311.68	1484	71	9.91	4.89	15.43
1852	165	354.67	1689	80	9.65	4.69	15.10
1967	175	376.17	1791	85	9.83	4.85	15.30
2064	184	395.51	1883	90	9.61	4.61	15.11
2362	210	451.40	2150	102	9.86	4.88	15.33
2028	183	393.36	1873	89	8.28	3.36	13.68
1731	157	337.47	1607	77	7.72	2.79	13.14
1454	132	283.74	1351	64	7.62	2.76	12.98
909	82	176.26	839	40	8.34	3.41	13.77
579	52	111.78	532	25	8.83	3.95	14.20
393	35	75.23	358	17	9.78	4.80	15.25
187	17	36.54	174	8	7.47	2.75	12.65
0	0	0.00	0	0	-	-	-

Table B39: Theoretical strain derived from the third test (B4) (actual diameter)

strain gauge $\varepsilon x10^{-6}$	F (kN)	σ (N/mm^2)	theoretical $\varepsilon x10^{-6}$	theoretical $\Delta\varepsilon x10^{-6}$	error between theoretical and experimental value (%)	min error(%) E = 200 Gpa	max error(%) E = 220 Gpa
0	0	0.00	0	0	-	-	-
157	14	30.09	143	7	9.79	4.67	15.44
465	41	88.13	420	20	10.71	5.68	16.25
641	57	122.52	583	28	9.95	4.91	15.50
1077	95	204.20	972	46	10.80	5.80	16.31
1289	114	245.05	1167	56	10.45	5.40	16.02
1602	142	305.23	1453	69	10.25	5.26	15.75
1733	154	331.03	1576	75	9.96	4.97	15.46
1916	170	365.42	1740	83	10.11	5.10	15.63
2101	187	401.96	1914	91	9.77	4.79	15.25
2232	198	425.61	2027	97	10.11	5.08	15.65
2397	213	457.85	2180	104	9.95	4.95	15.46
2530	225	483.64	2303	110	9.86	4.85	15.37
2183	196	421.31	2006	96	8.82	3.85	14.29
1951	176	378.32	1802	86	8.27	3.34	13.69
1688	152	326.73	1556	74	8.48	3.56	13.90
1468	133	285.89	1361	65	7.86	2.95	13.27
1201	109	234.30	1116	53	7.62	2.74	12.98
843	76	163.36	778	37	8.35	3.44	13.77
551	49	105.33	502	24	9.76	4.75	15.27
185	16	34.39	164	8	12.80	7.56	18.59
6	0	0.00	0	0	-	-	-

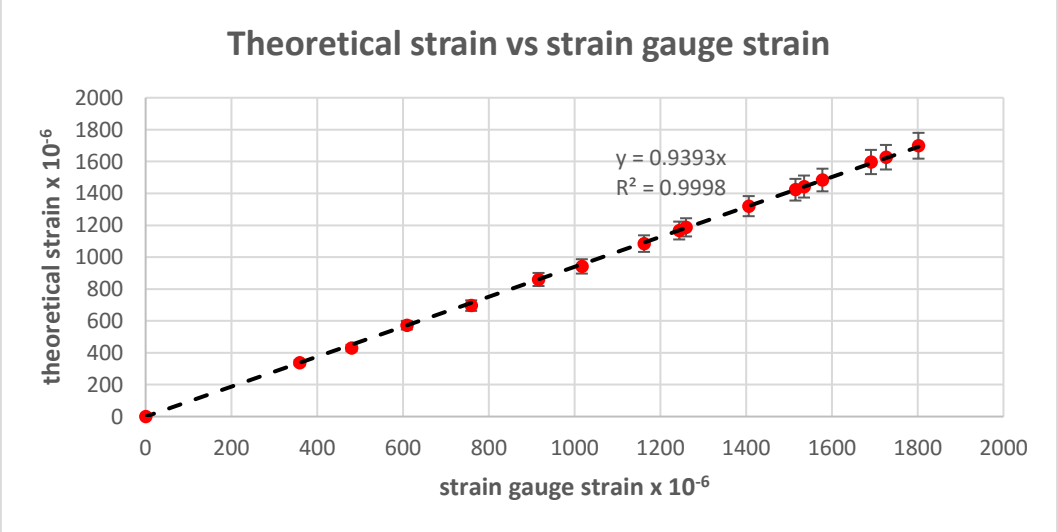

Figure B48: Strain obtained for the third test (B4) (actual diameter)

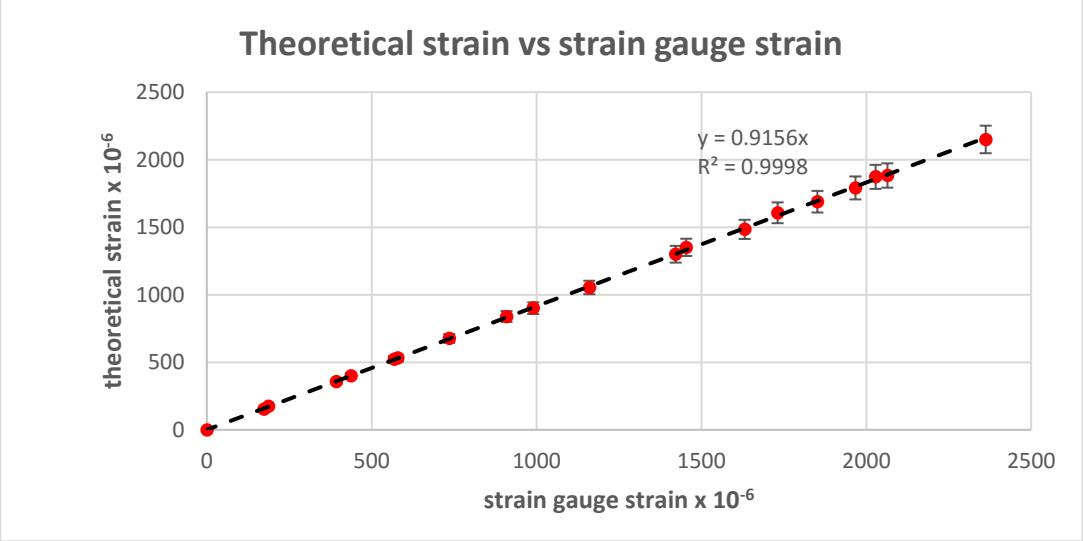

Figure B49: Strain obtained for the third test (B4) (actual diameter)

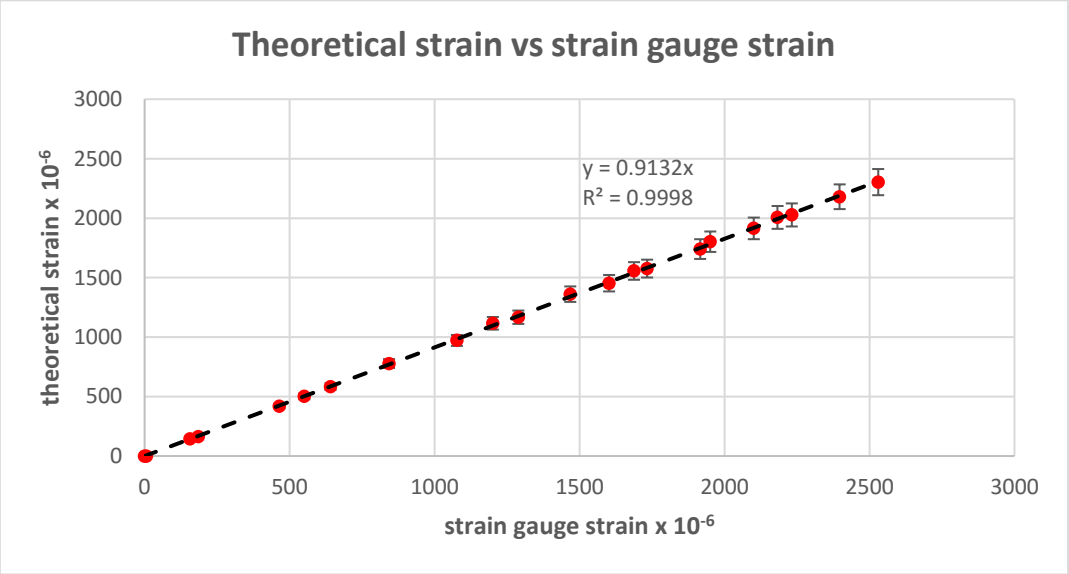

Figure B50: Strain obtained for the third test (B4) (actual diameter)

Table B40: Theoretical strain derived from the first test (B4) (nominal diameter)

strain gauge x 10^{-6}	F (kN)	σ (N/mm^2)	theoretical $\varepsilon x10^{-6}$	theoretical $\Delta\varepsilon x10^{-6}$	error between theoretical and experimental value (%)	min error(%) E = 200 Gpa	max error(%) E = 220 Gpa
0	0	0.00	0	0	-	-	-
480	42	93.49	445	21	7.87	3.00	13.21
759	68	151.36	721	34	5.27	0.53	10.48
1017	92	204.79	975	46	4.31	-0.39	9.47
1162	106	235.95	1124	54	3.38	-1.36	8.60
1244	114	253.76	1208	58	2.98	-1.74	8.17
1406	129	287.15	1367	65	2.85	-1.82	7.99
1535	141	313.86	1495	71	2.68	-1.98	7.79
1578	145	322.76	1537	73	2.67	-1.99	7.79
1691	156	347.25	1654	79	2.24	-2.42	7.37
1802	166	369.51	1760	84	2.39	-2.28	7.52
1726	159	353.92	1685	80	2.43	-2.21	7.54
1515	139	309.41	1473	70	2.85	-1.81	7.98
1260	116	258.21	1230	59	2.44	-2.25	7.60
916	84	186.98	890	42	2.92	-1.72	8.02
609	56	124.65	594	28	2.53	-2.09	7.60
359	33	73.46	350	17	2.57	-2.18	7.81
-7	0	0.00	0	0	-	-	-

Table B41: Theoretical strain derived from the second test (B4) (nominal diameter)

strain gauge $\varepsilon x10^{-6}$	F (kN)	σ (N/mm^2)	theoretical $\varepsilon x10^{-6}$	theoretical $\Delta\varepsilon x10^{-6}$	error between theoretical and experimental value (%)	min error(%) E = 200 Gpa	max error(%) E = 220 Gpa
-7	0	0.00	0	0	-	-	-
173	15	33.39	159	8	8.81	3.59	14.57
437	39	86.81	413	20	5.81	0.92	11.20
568	51	113.52	541	26	4.99	0.18	10.29
735	66	146.91	700	33	5.00	0.27	10.19
990	88	195.88	933	44	6.11	1.33	11.36
1160	103	229.27	1092	52	6.23	1.40	11.54
1422	127	282.69	1346	64	5.65	0.85	10.92
1631	145	322.76	1537	73	6.12	1.30	11.41
1852	165	367.28	1749	83	5.89	1.09	11.16
1967	175	389.54	1855	88	6.04	1.24	11.32
2064	184	409.57	1950	93	5.85	1.03	11.15
2362	210	467.45	2226	106	6.11	1.29	11.42
2028	183	407.35	1940	92	4.54	-0.20	9.74
1731	157	349.47	1664	79	4.03	-0.69	9.21
1454	132	293.82	1399	67	3.93	-0.82	9.16
909	82	182.53	869	41	4.60	-0.11	9.78
579	52	115.75	551	26	5.08	0.35	10.29
393	35	77.91	371	18	5.93	1.03	11.33
187	17	37.84	180	9	3.89	-1.06	9.36
0	0	0.00	0	0	-	-	-

Table B42: Theoretical strain derived from the third test (B4) (nominal diameter)

strain gauge $\varepsilon x10^{-6}$	F (kN)	σ (N/mm^2)	theoretical $\varepsilon x10^{-6}$	theoretical $\Delta\varepsilon x10^{-6}$	error between theoretical and experimental value (%)	min error(%) E = 200 Gpa	max error(%) E = 220 Gpa
0	0	0.00	0	0	-	-	-
157	14	31.16	148	7	6.08	1.29	11.35
465	41	91.26	435	21	6.90	1.97	12.32
641	57	126.88	604	29	6.13	1.26	11.48
1077	95	211.46	1007	48	6.95	2.09	12.30
1289	114	253.76	1208	58	6.71	1.82	12.09
1602	142	316.08	1505	72	6.45	1.59	11.79
1733	154	342.80	1632	78	6.19	1.35	11.52
1916	170	378.41	1802	86	6.33	1.48	11.66
2101	187	416.25	1982	94	6.00	1.20	11.28
2232	198	440.74	2099	100	6.34	1.50	11.66
2397	213	474.13	2258	108	6.16	1.31	11.49
2530	225	500.84	2385	114	6.08	1.24	11.40
2183	196	436.28	2078	99	5.05	0.28	10.31
1951	176	391.77	1866	89	4.56	-0.20	9.79
1688	152	338.34	1611	77	4.78	0.00	10.04
1468	133	296.05	1410	67	4.11	-0.61	9.31
1201	109	242.63	1155	55	3.98	-0.74	9.18
843	76	169.17	806	38	4.59	-0.12	9.77
551	49	109.07	519	25	6.17	1.29	11.54
185	16	35.62	170	8	8.82	3.93	14.20
6	0	0.00	0	0	-	-	-

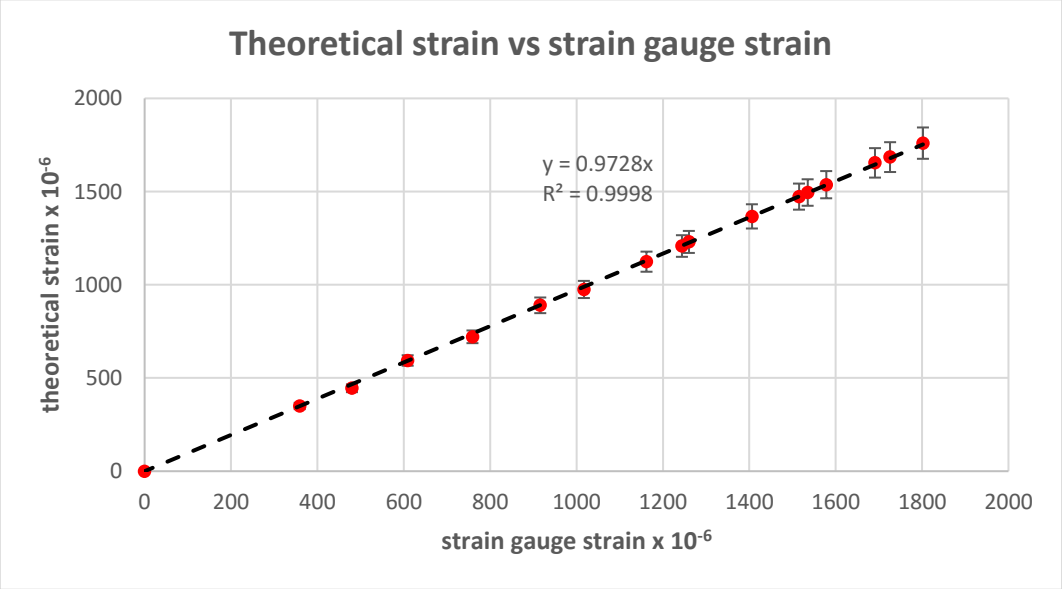

Figure B51: Strain obtained for the first test (B4) (nominal diameter)

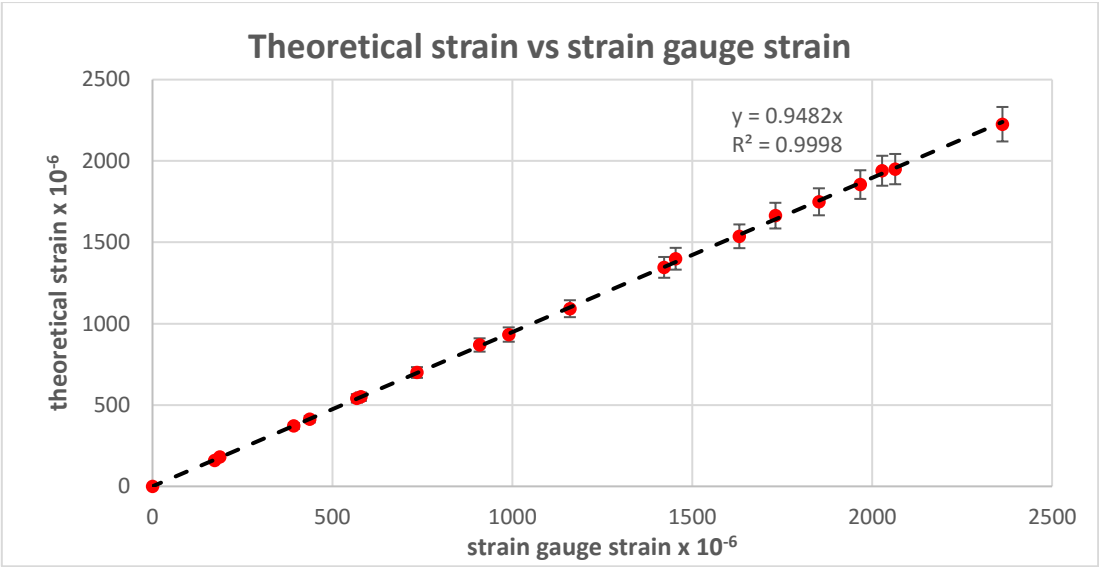

Figure B52: Strain obtained for the second test (B4) (nominal diameter)

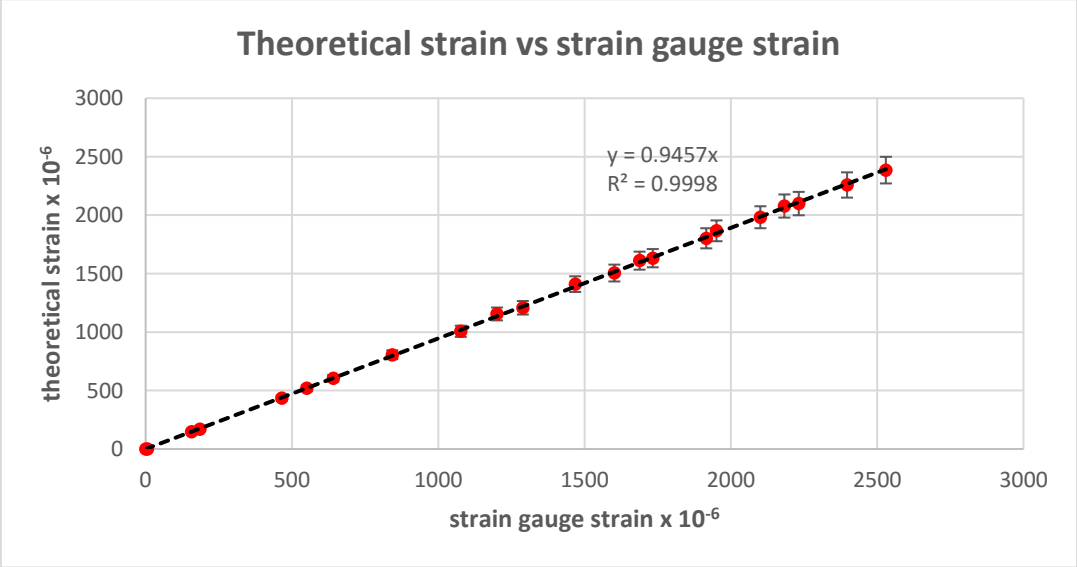

Figure B53: Strain obtained for the third test (B4) (nominal diameter)

Table B43: Theoretical strain derived from the first test (B4) (maximum diameter)

strain gauge x 10^{-6}	F (kN)	σ (N/mm^2)	theoretical $\varepsilon x10^{-6}$	theoretical $\Delta\varepsilon x10^{-6}$	error between theoretical and experimental value (%)	min error(%) E = 200 Gpa	max error(%) E = 220 Gpa
0	0	0.00	0	0	-	-	-
480	42	87.23	415	20	15.66	10.34	21.52
759	68	141.23	673	32	12.78	7.66	18.41
1017	92	191.08	910	43	11.76	6.72	17.30
1162	106	220.16	1048	50	10.88	5.83	16.43
1244	114	236.78	1128	54	10.28	5.25	15.83
1406	129	267.93	1276	61	10.19	5.16	15.72
1535	141	292.85	1395	66	10.04	5.07	15.50
1578	145	301.16	1434	68	10.04	5.06	15.52
1691	156	324.01	1543	73	9.59	4.64	15.03
1802	166	344.78	1642	78	9.74	4.77	15.22
1726	159	330.24	1573	75	9.73	4.73	15.22
1515	139	288.70	1375	65	10.18	5.21	15.65
1260	116	240.93	1147	55	9.85	4.83	15.38
916	84	174.47	831	40	10.23	5.17	15.80
609	56	116.31	554	26	9.93	5.00	15.34
359	33	68.54	326	16	10.12	4.97	15.81
-7	0	0.00	0	0	-	-	-

Table B44: Theoretical strain derived from the second test (B4) (maximum diameter)

strain gauge x 10^{-6}	F (kN)	σ (N/mm^2)	theoretical $\varepsilon x10^{-6}$	theoretical $\Delta\varepsilon x10^{-6}$	error between theoretical and experimental value (%)	min error(%) E = 200 Gpa	max error(%) E = 220 Gpa
-7	0	0.00	0	0	-	-	-
173	15	31.15	148	7	16.89	11.61	22.70
437	39	81.00	386	18	13.21	8.17	18.75
568	51	105.93	504	24	12.70	7.58	18.33
735	66	137.08	653	31	12.56	7.46	18.17
990	88	182.77	870	41	13.79	8.67	19.42
1160	103	213.93	1019	49	13.84	8.61	19.59
1422	127	263.78	1256	60	13.22	8.05	18.90
1631	145	301.16	1434	68	13.74	8.59	19.40
1852	165	342.70	1632	78	13.48	8.30	19.18
1967	175	363.47	1731	82	13.63	8.49	19.28
2064	184	382.16	1820	87	13.41	8.23	19.10
2362	210	436.16	2077	99	13.72	8.55	19.41
2028	183	380.09	1810	86	12.04	6.96	17.63
1731	157	326.09	1553	74	11.46	6.39	17.04
1454	132	274.16	1306	62	11.33	6.29	16.88
909	82	170.31	811	39	12.08	6.94	17.75
579	52	108.00	514	24	12.65	7.62	18.16
393	35	72.69	346	16	13.58	8.56	19.09
187	17	35.31	168	8	11.31	6.25	16.88
0	0	0.00	0	0	-	-	-

Table B45: Theoretical strain derived from the third test (B4) (maximum diameter)

strain gauge x 10^{-6}	F (kN)	σ (N/mm^2)	theoretical $\varepsilon x10^{-6}$	theoretical $\Delta\varepsilon x10^{-6}$	error between theoretical and experimental value (%)	min error(%) E = 200 Gpa	max error(%) E = 220 Gpa
0	0	0.00	0	0	-	-	-
157	14	29.08	138	7	13.77	8.28	19.85
465	41	85.16	406	19	14.53	9.41	20.16
641	57	118.39	564	27	13.65	8.46	19.37
1077	95	197.31	940	45	14.57	9.34	20.34
1289	114	236.78	1128	54	14.27	9.05	20.02
1602	142	294.93	1404	67	14.10	8.91	19.82
1733	154	319.85	1523	73	13.79	8.58	19.52
1916	170	353.09	1681	80	13.98	8.80	19.68
2101	187	388.39	1849	88	13.63	8.47	19.31
2232	198	411.24	1958	93	13.99	8.82	19.68
2397	213	442.40	2107	100	13.76	8.61	19.43
2530	225	467.32	2225	106	13.71	8.54	19.40
2183	196	407.09	1939	92	12.58	7.48	18.19
1951	176	365.55	1741	83	12.06	6.96	17.67
1688	152	315.70	1503	72	12.31	7.17	17.96
1468	133	276.24	1315	63	11.63	6.53	17.25
1201	109	226.39	1078	51	11.41	6.38	16.94
843	76	157.85	752	36	12.10	6.98	17.74
551	49	101.77	485	23	13.61	8.46	19.26
185	16	33.23	158	8	17.09	11.45	23.33
6	0	0.00	0	0	-	-	-

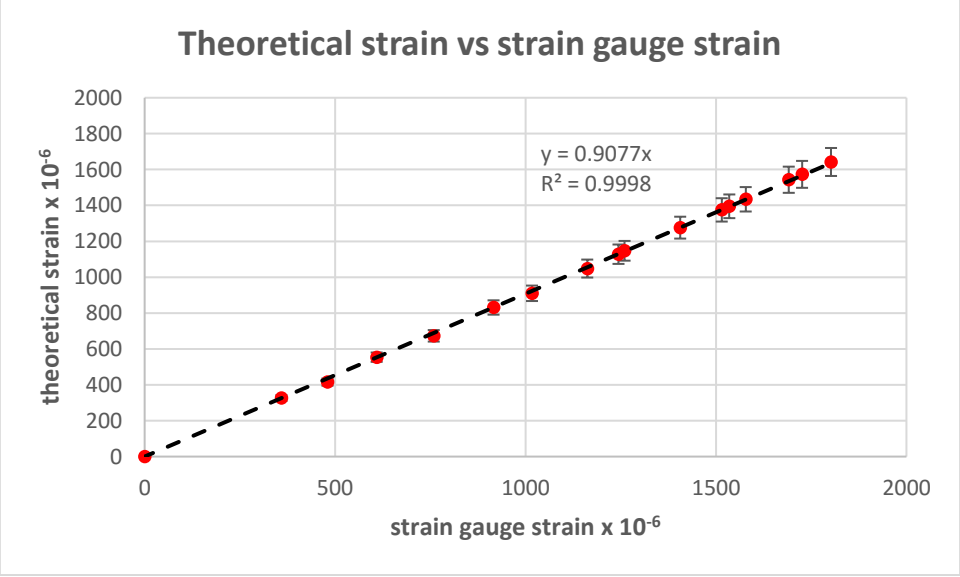

Figure B54: Strain obtained for the first test (B4) (maximum diameter)

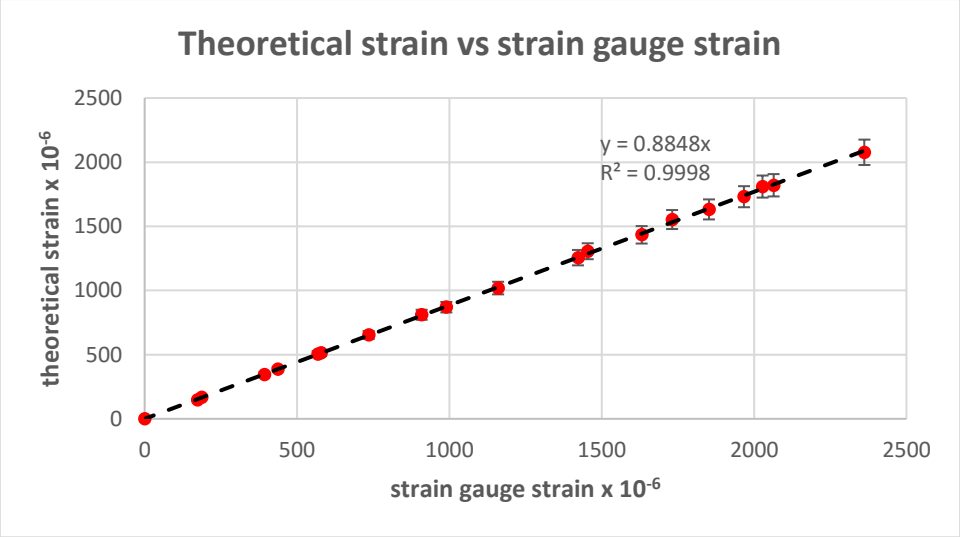

Figure B55: Strain obtained for the second test (B4) (maximum diameter)

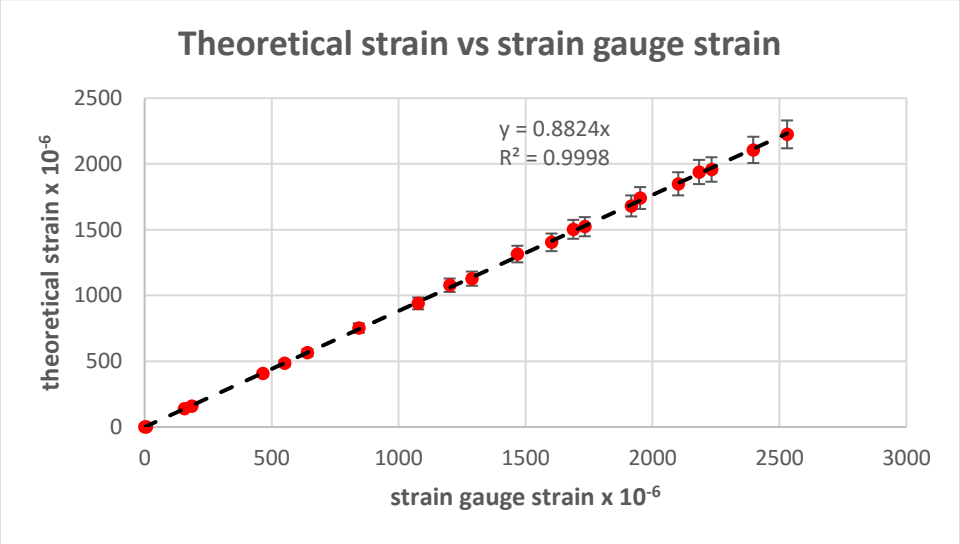

Figure B56: Strain obtained for the third test (B4) (maximum diameter)

Table B46: Theoretical strain derived from the first test (B4) (minimum diameter)

strain gauge x 10^{-6}	F (kN)	σ (N/mm^2)	theoretical $\varepsilon x10^{-6}$	theoretical $\Delta\varepsilon x10^{-6}$	error between theoretical and experimental value (%)	max error(%) E = 200 Gpa	min error(%) E = 220 Gpa
0	0	0.00	0	0	-	-	-
480	42	100.45	478	23	0.42	-4.19	5.49
759	68	162.63	774	37	-1.94	-6.41	2.99
1017	92	220.02	1048	50	-2.96	-7.38	1.90
1162	106	253.51	1207	57	-3.73	-8.07	1.04
1244	114	272.64	1298	62	-4.16	-8.53	0.65
1406	129	308.51	1469	70	-4.29	-8.64	0.50
1535	141	337.21	1606	76	-4.42	-8.74	0.33
1578	145	346.78	1651	79	-4.42	-8.79	0.38
1691	156	373.09	1777	85	-4.84	-9.18	-0.06
1802	166	397.00	1890	90	-4.66	-8.99	0.11
1726	159	380.26	1811	86	-4.69	-9.01	0.06
1515	139	332.43	1583	75	-4.30	-8.62	0.46
1260	116	277.42	1321	63	-4.62	-8.96	0.16
916	84	200.89	957	46	-4.28	-8.67	0.55
609	56	133.93	638	30	-4.55	-8.83	0.16
359	33	78.92	376	18	-4.52	-8.88	0.28
-7	0	0.00	0	0	-	-	-

Table B47: Theoretical strain derived from the second test (B4) (minimum diameter)

strain gauge x 10^{-6}	F (kN)	σ (N/mm^2)	theoretical $\varepsilon x10^{-6}$	theoretical $\Delta\varepsilon x10^{-6}$	error between theoretical and experimental value (%)	max error(%) E = 200 Gpa	min error(%) E = 220 Gpa
-7	0	0.00	0	0	-	-	-
173	15	35.87	171	8	1.17	-3.35	6.13
437	39	93.27	444	21	-1.58	-6.02	3.31
568	51	121.97	581	28	-2.24	-6.73	2.71
735	66	157.84	752	36	-2.26	-6.73	2.65
990	88	210.46	1002	48	-1.20	-5.71	3.77
1160	103	246.33	1173	56	-1.11	-5.61	3.85
1422	127	303.73	1446	69	-1.66	-6.14	3.27
1631	145	346.78	1651	79	-1.21	-5.72	3.75
1852	165	394.61	1879	89	-1.44	-5.89	3.46
1967	175	418.53	1993	95	-1.30	-5.80	3.64
2064	184	440.05	2095	100	-1.48	-5.97	3.46
2362	210	502.23	2392	114	-1.25	-5.75	3.69
2028	183	437.66	2084	99	-2.69	-7.10	2.17
1731	157	375.48	1788	85	-3.19	-7.58	1.64
1454	132	315.69	1503	72	-3.26	-7.68	1.61
909	82	196.11	934	44	-2.68	-7.06	2.13
579	52	124.36	592	28	-2.20	-6.61	2.66
393	35	83.71	399	19	-1.50	-5.98	3.42
187	17	40.66	194	9	-3.61	-7.88	1.08
0	0	0.00	0	0	-	-	-

Table B48: Theoretical strain derived from the third test (B4) (minimum diameter)

strain gauge x 10^{-6}	F (kN)	σ (N/mm^2)	theoretical $\varepsilon x10^{-6}$	theoretical $\Delta\varepsilon x10^{-6}$	error between theoretical and experimental value (%)	max error(%) E = 200 Gpa	min error(%) E = 220 Gpa
0	0	0.00	0	0	-	-	-
157	14	33.48	159	8	-1.26	-5.99	3.97
465	41	98.05	467	22	-0.43	-4.91	4.49
641	57	136.32	649	31	-1.23	-5.74	3.72
1077	95	227.20	1082	52	-0.46	-5.03	4.56
1289	114	272.64	1298	62	-0.69	-5.22	4.29
1602	142	339.60	1617	77	-0.93	-5.43	4.03
1733	154	368.30	1754	84	-1.20	-5.71	3.77
1916	170	406.57	1936	92	-1.03	-5.52	3.90
2101	187	447.22	2130	101	-1.36	-5.83	3.55
2232	198	473.53	2255	107	-1.02	-5.50	3.91
2397	213	509.41	2426	116	-1.20	-5.70	3.77
2530	225	538.10	2562	122	-1.25	-5.74	3.69
2183	196	468.75	2232	106	-2.20	-6.63	2.68
1951	176	420.92	2004	95	-2.64	-7.05	2.20
1688	152	363.52	1731	82	-2.48	-6.89	2.37
1468	133	318.08	1515	72	-3.10	-7.50	1.73
1201	109	260.68	1241	59	-3.22	-7.62	1.61
843	76	181.76	866	41	-2.66	-7.06	2.18
551	49	117.19	558	27	-1.25	-5.81	3.77
185	16	38.27	182	9	1.65	-3.14	6.94
6	0	0.00	0	0	-	-	-

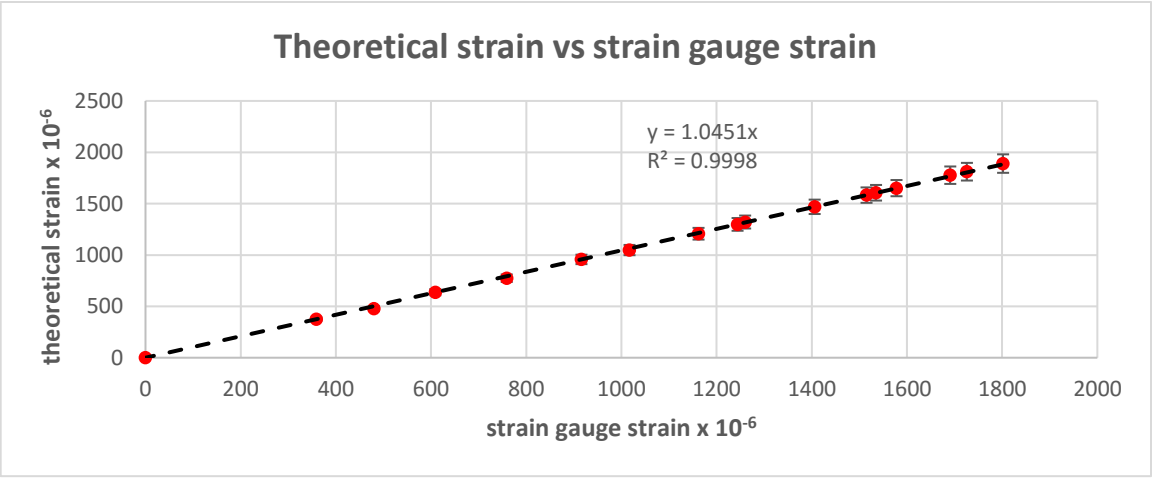

Figure B57: Strain obtained for the first test (B4) (minimum diameter)

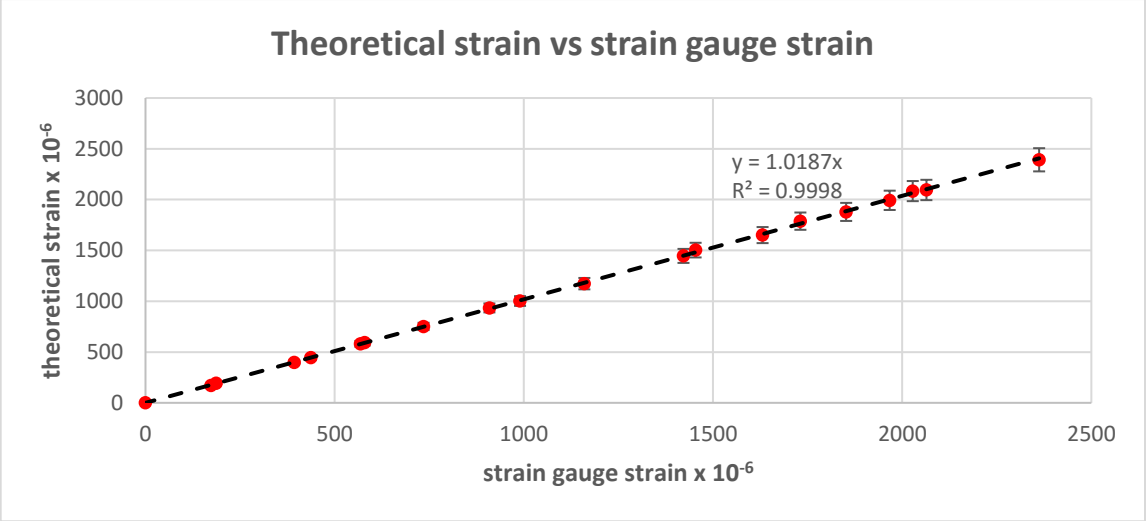

Figure B58: Strain obtained for the second test (B4) (minimum diameter)

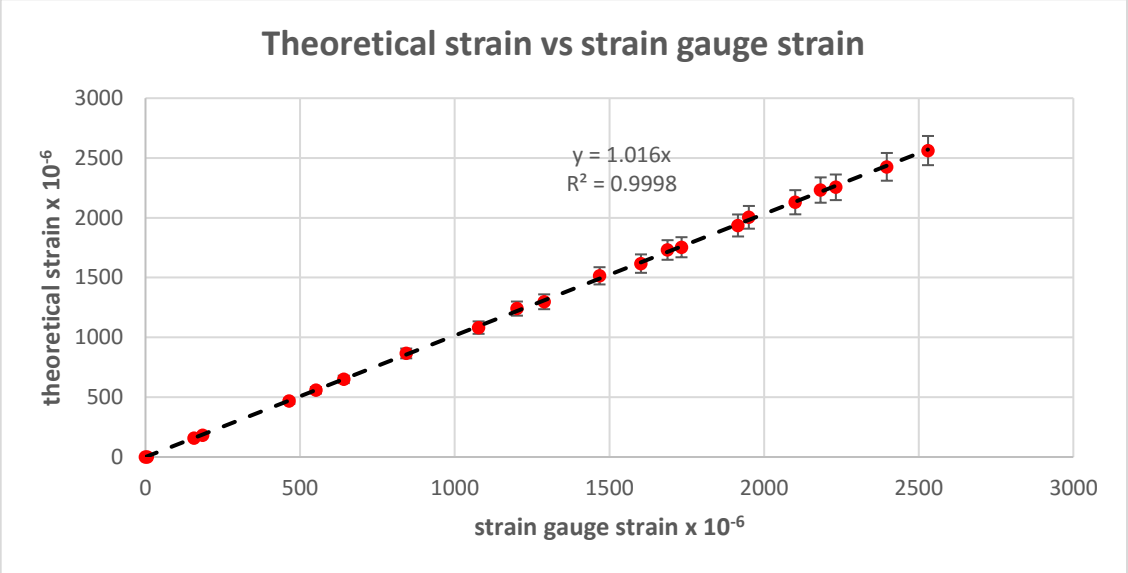

Figure B59: Strain obtained for the third test (B4) (minimum diameter)

APPENDIX C

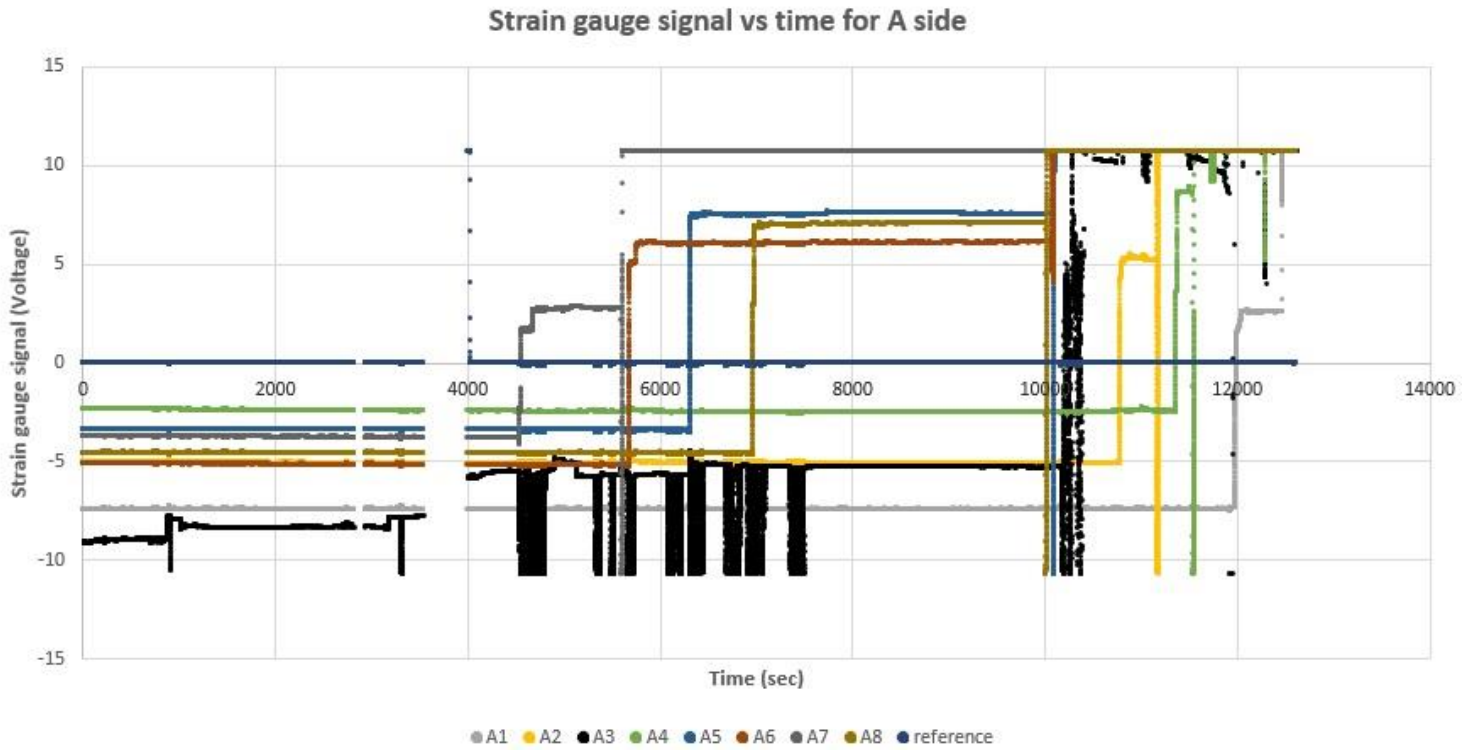

Figure C1: Strain gauge signals, A side

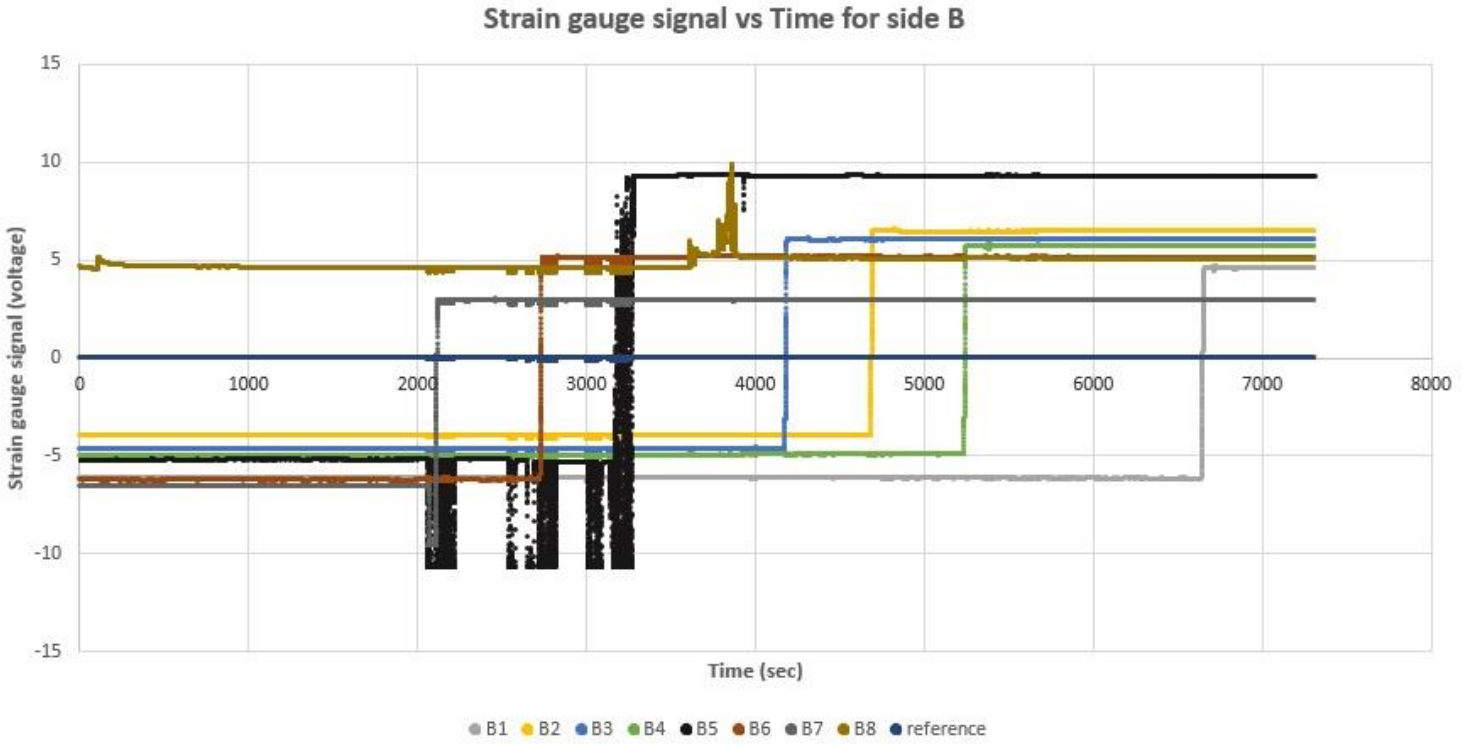

Figure C2: Strain gauge signals, B side

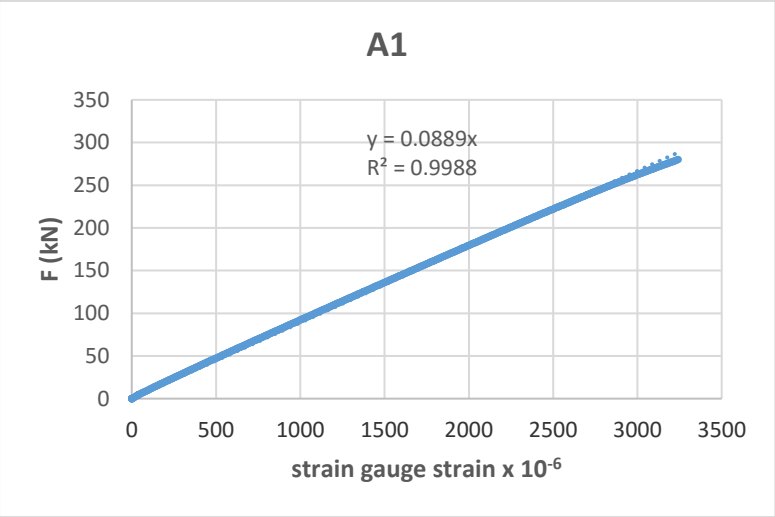

Figure C3: Calibration line of bolt A1

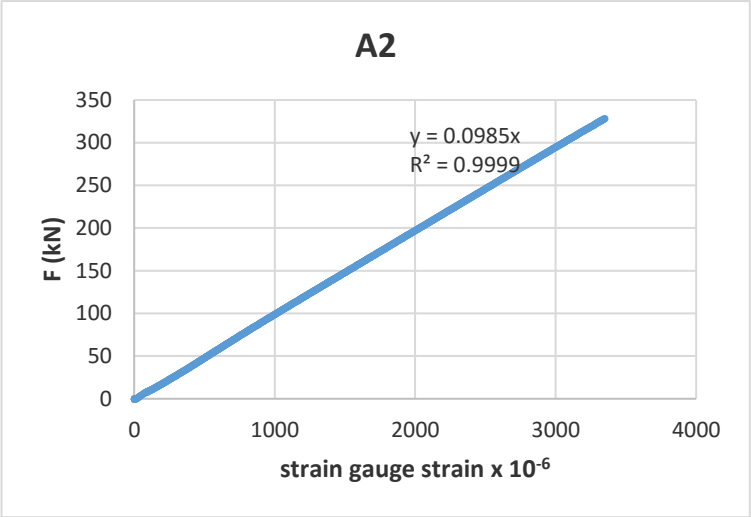

Figure C4: Calibration line of bolt A2

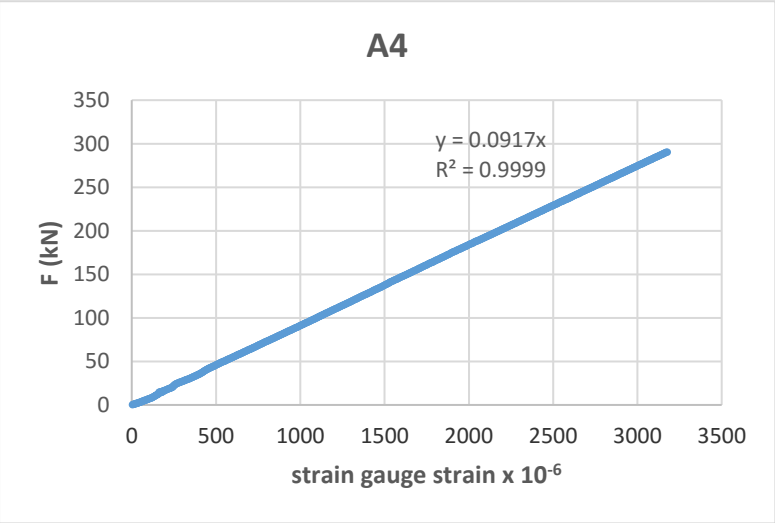

Figure C5: Calibration line of bolt A4

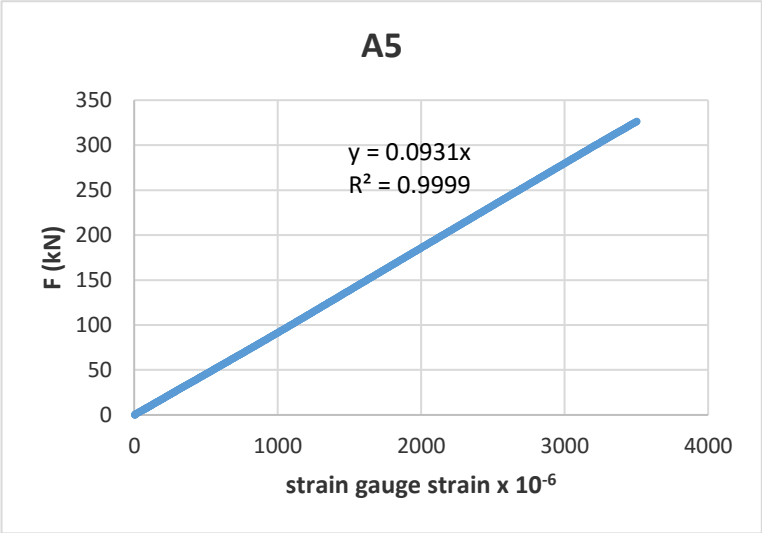

Figure C6: Calibration line of bolt A5

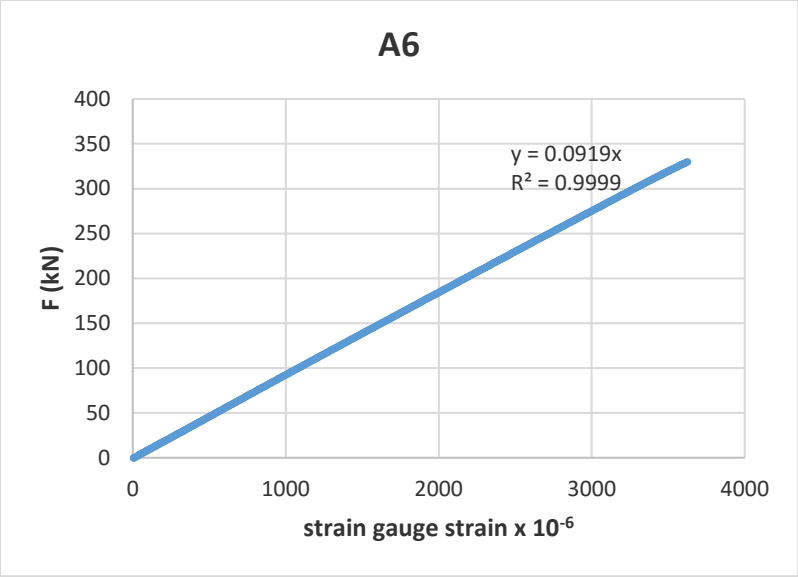

Figure C7: Calibration line of bolt A6

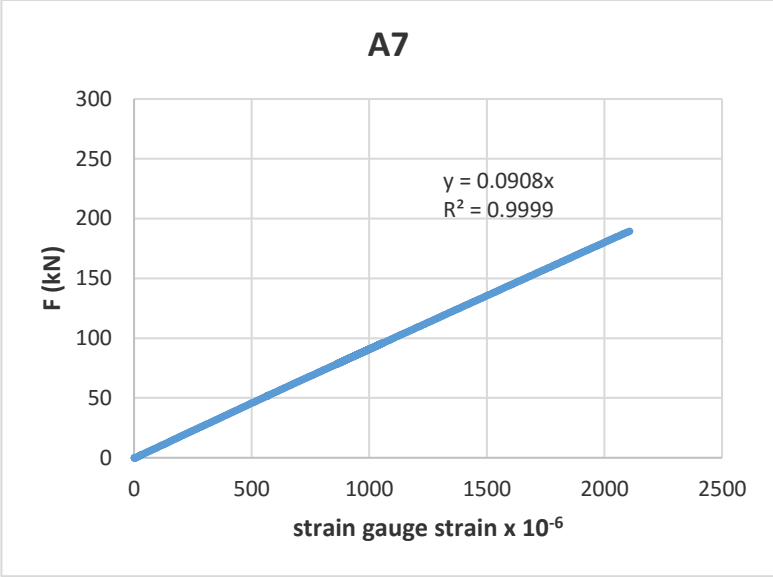

Figure C8: Calibration line of bolt A7

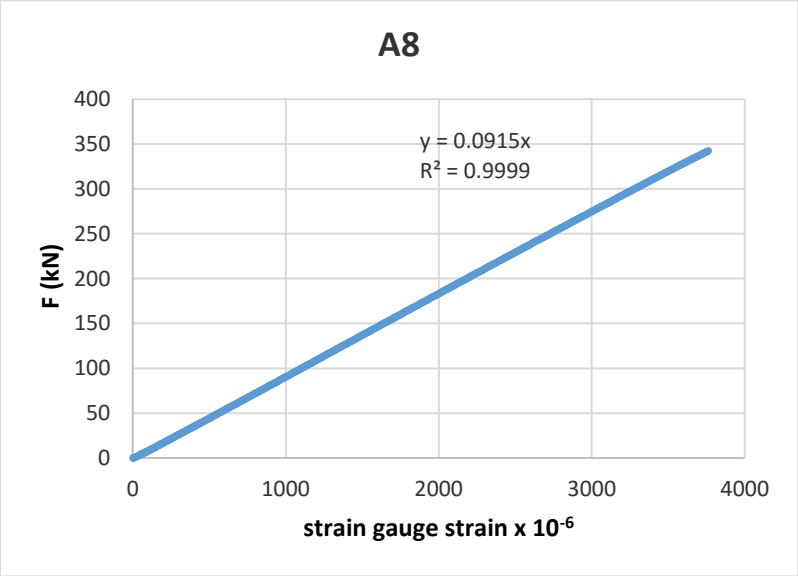

Figure C9: Calibration line of bolt A8

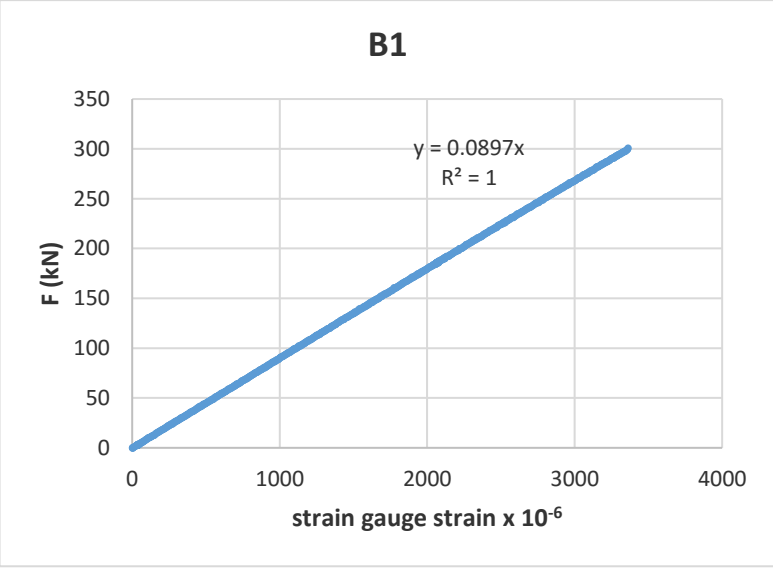

Figure C10: Calibration line of bolt B1

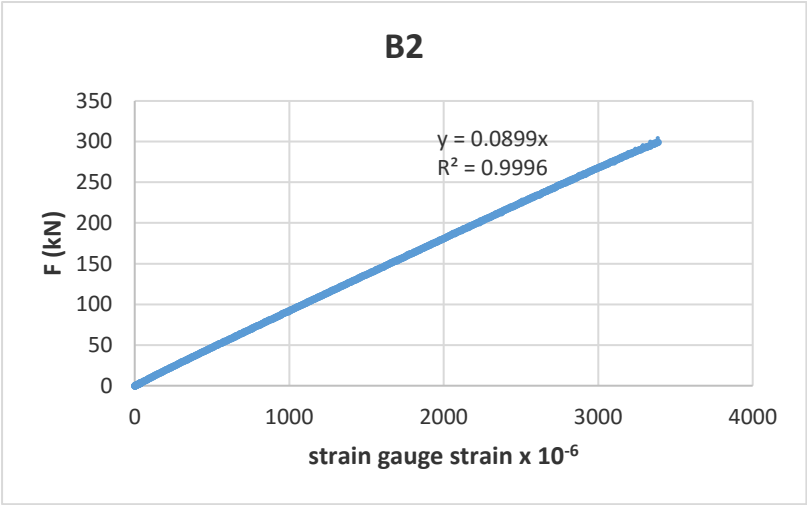

Figure C11: Calibration line of bolt B2

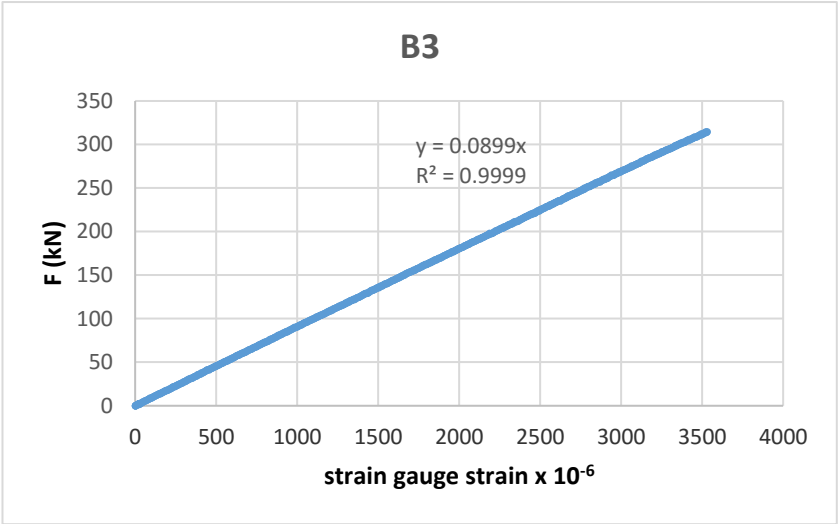

Figure C12: Calibration line of bolt B3

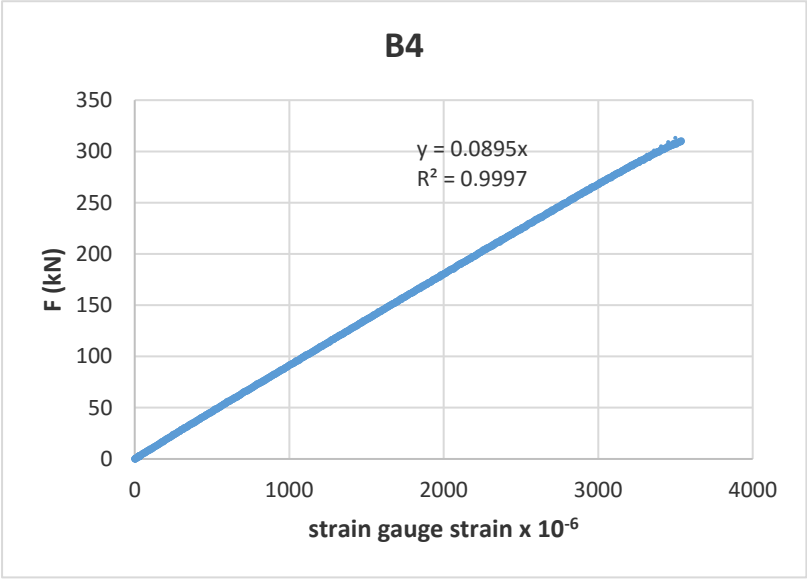

Figure C13: Calibration line of bolt B4

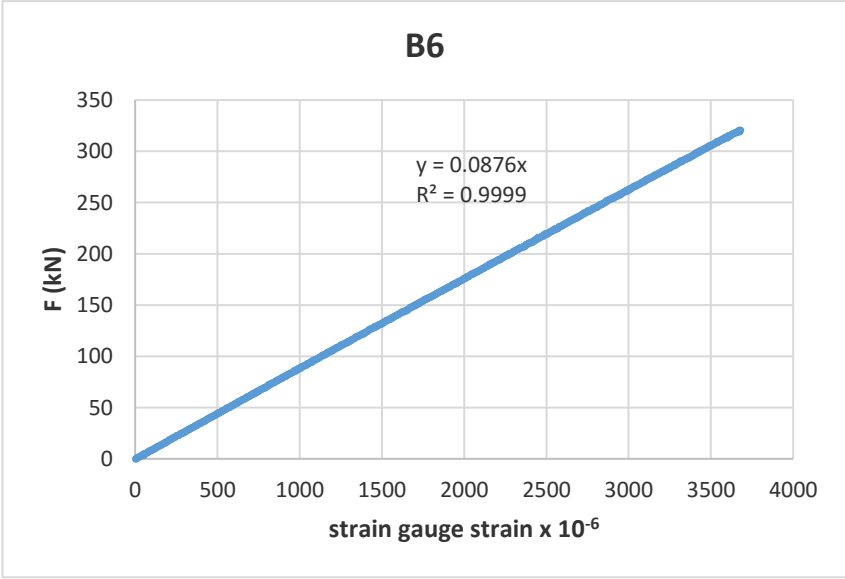

Figure C14: Calibration line of bolt B6

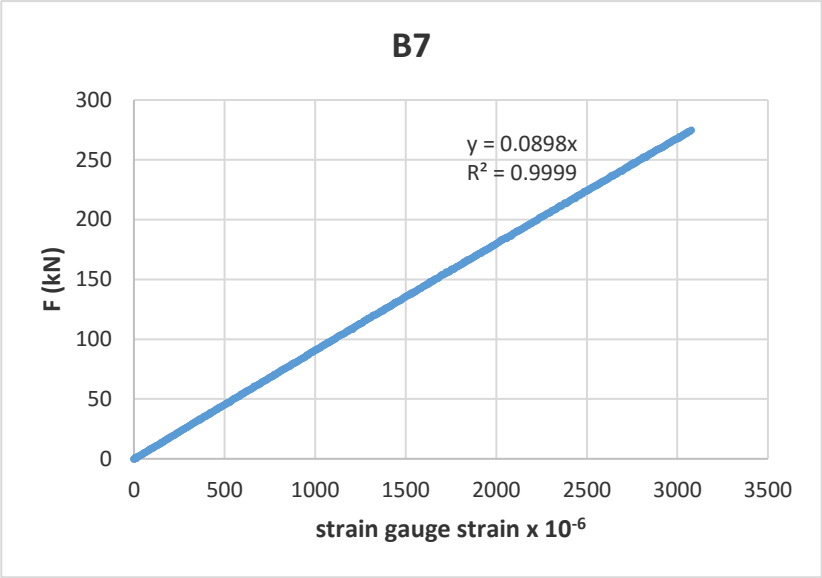

Figure C15: Calibration line of bolt B7

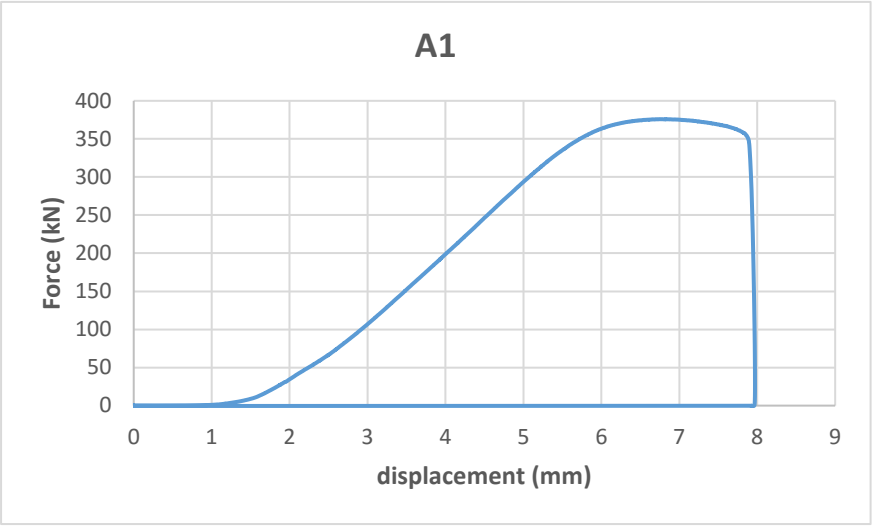

Figure C16: Force – displacement for bolt A1

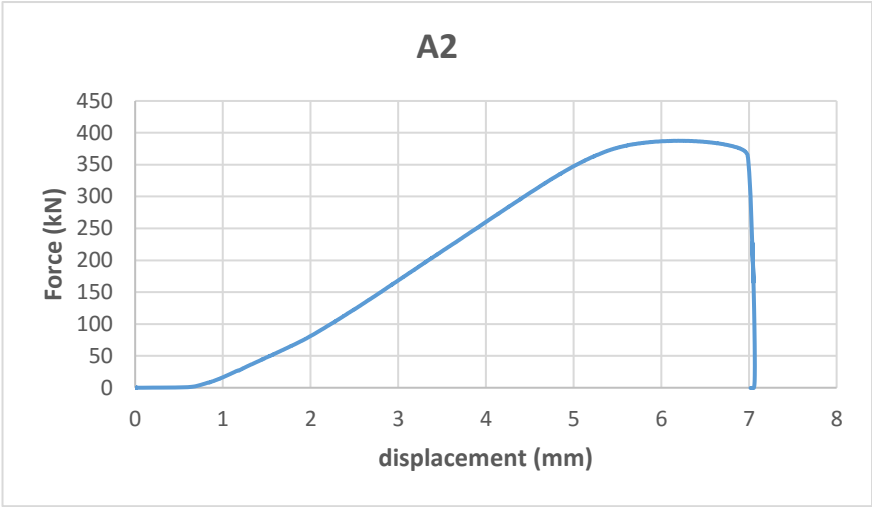

Figure C17: Force – displacement for bolt A2

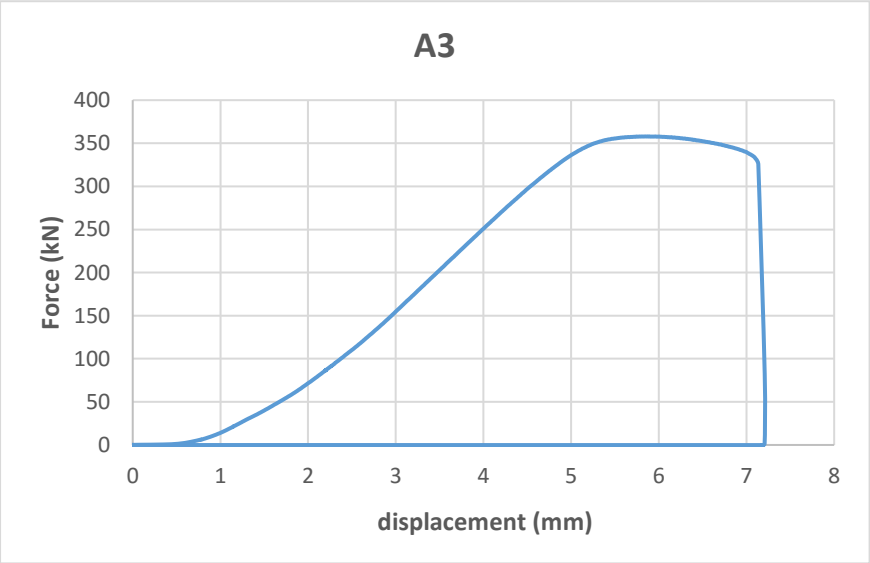

Figure C18: Force – displacement for bolt A3

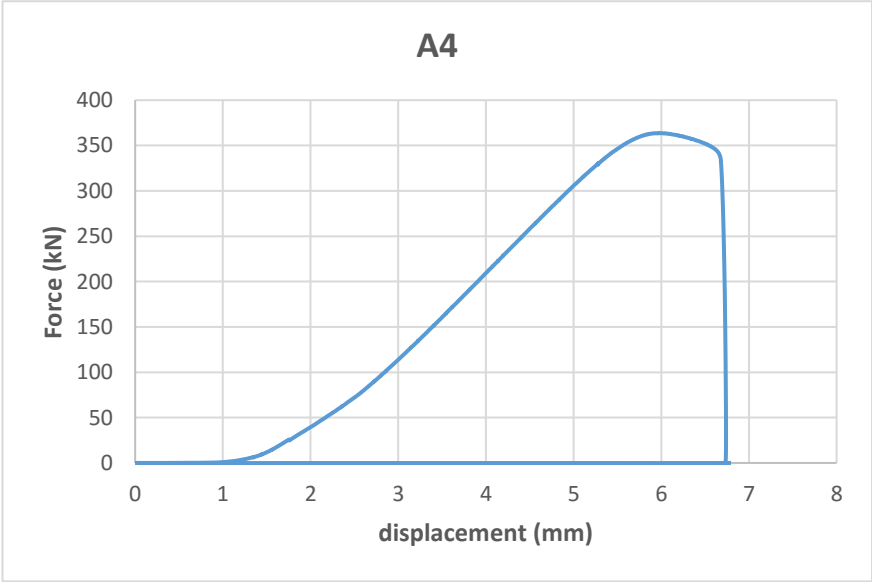

Figure C19: Force – displacement for bolt A4

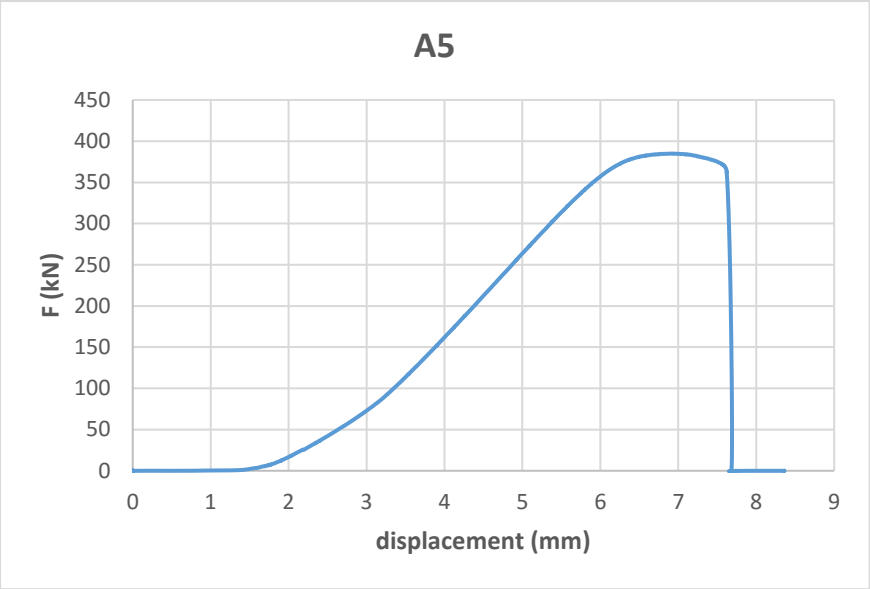

Figure C20: Force – displacement for bolt A5

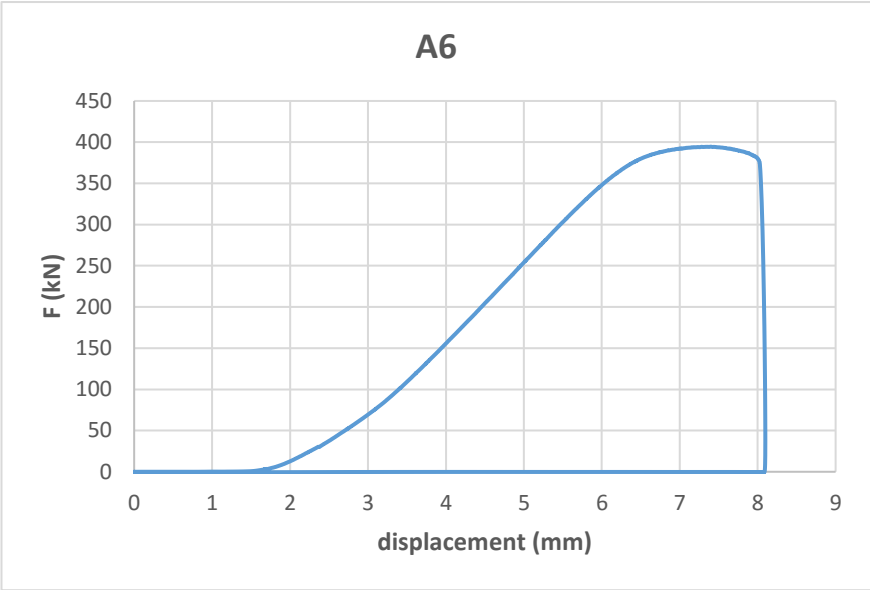

Figure C21: Force – displacement for bolt A6

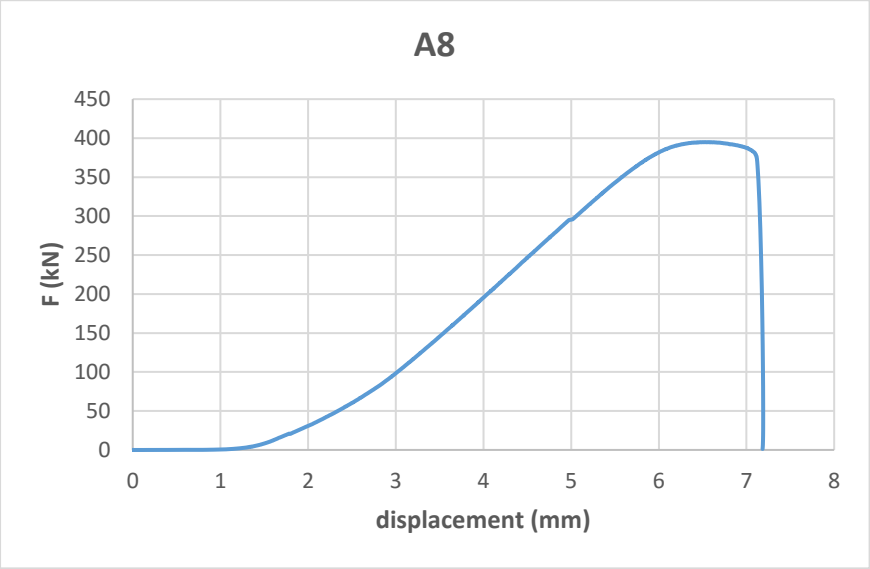

Figure C22: Force – displacement for bolt A8

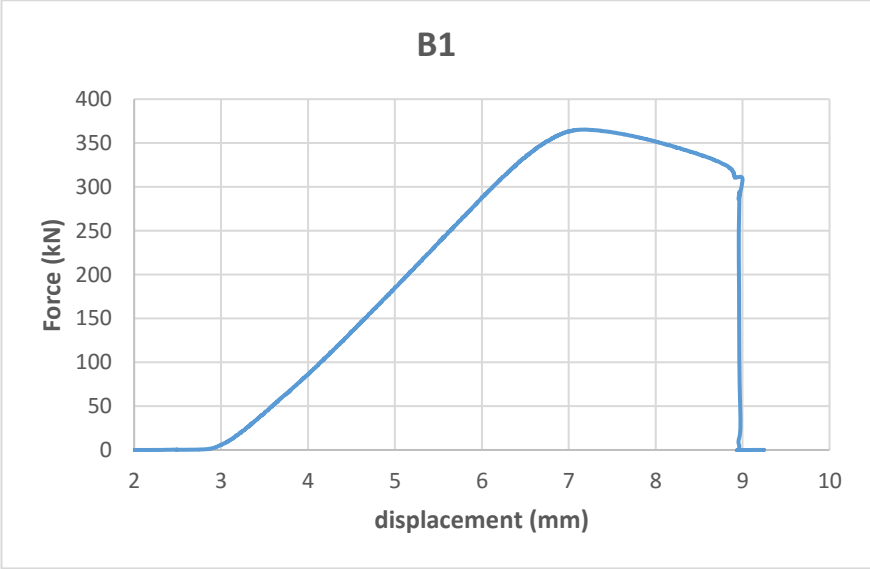

Figure C23: Force – displacement for bolt B1

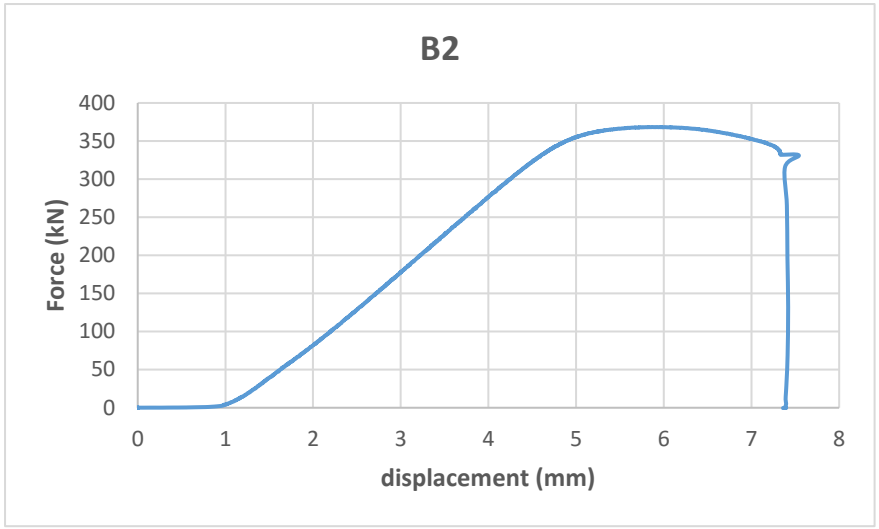

Figure C24: Force – displacement for bolt B2

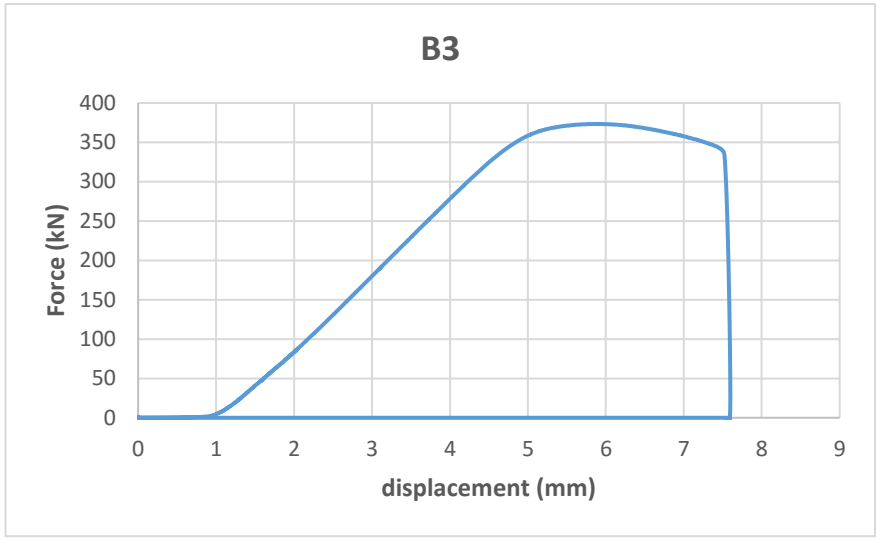

Figure C25: Force – displacement for bolt B3

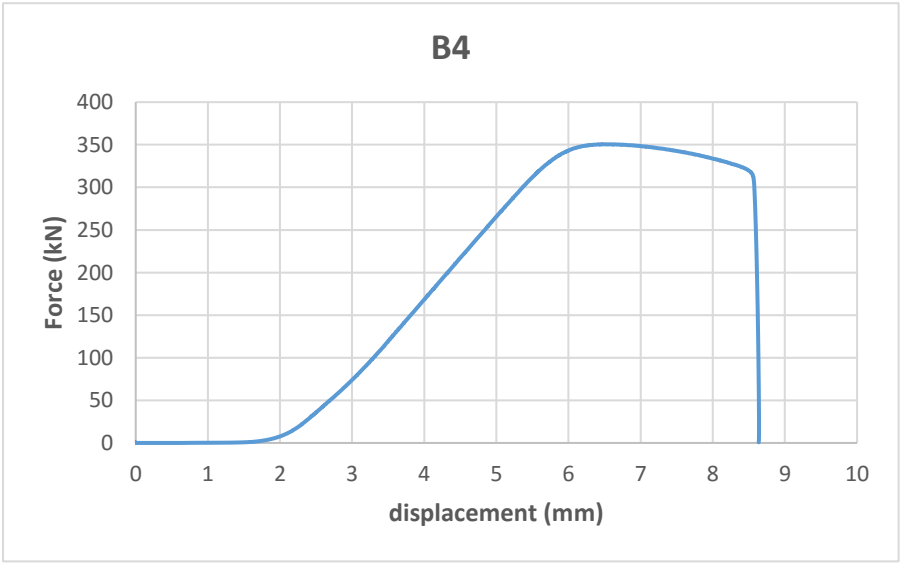

Figure C26: Force – displacement for bolt B4

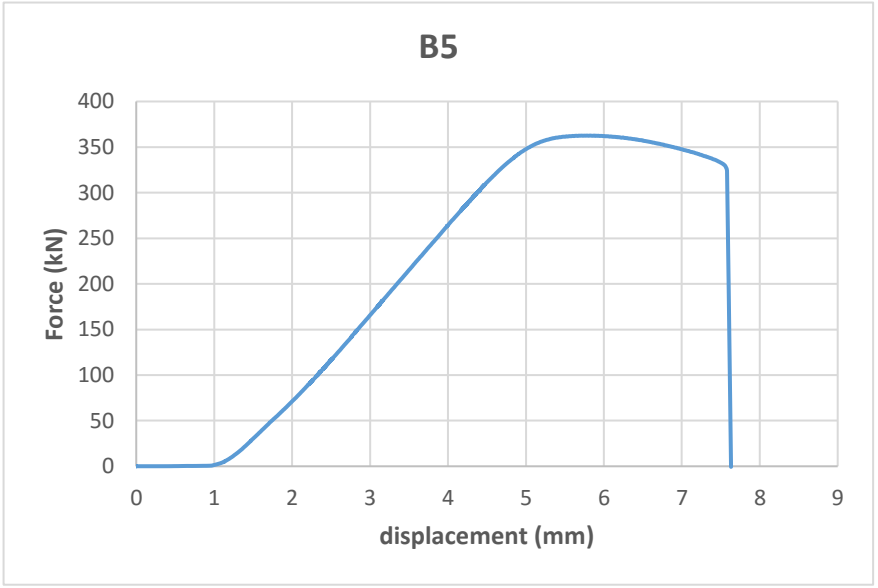

Figure C27: Force – displacement for bolt B5

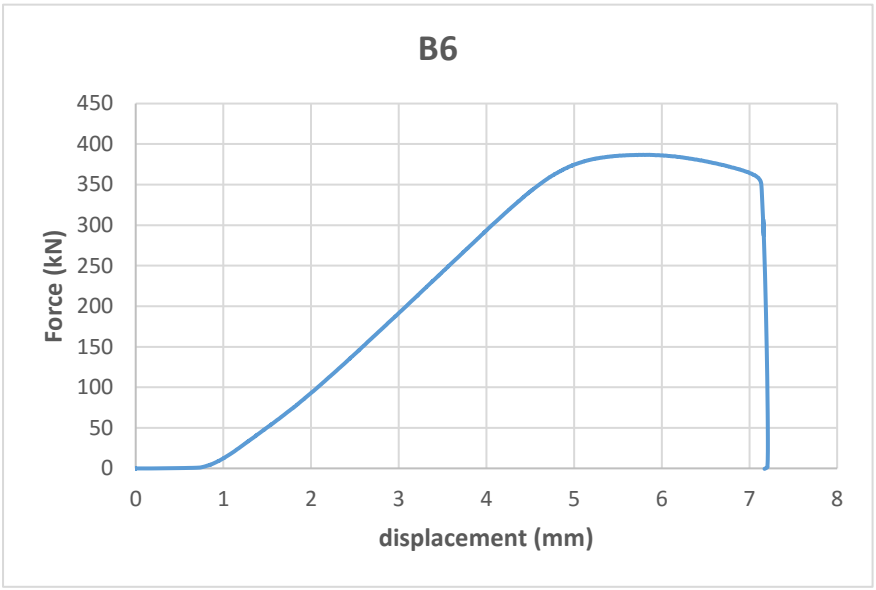

Figure C28: Force – displacement for bolt B6

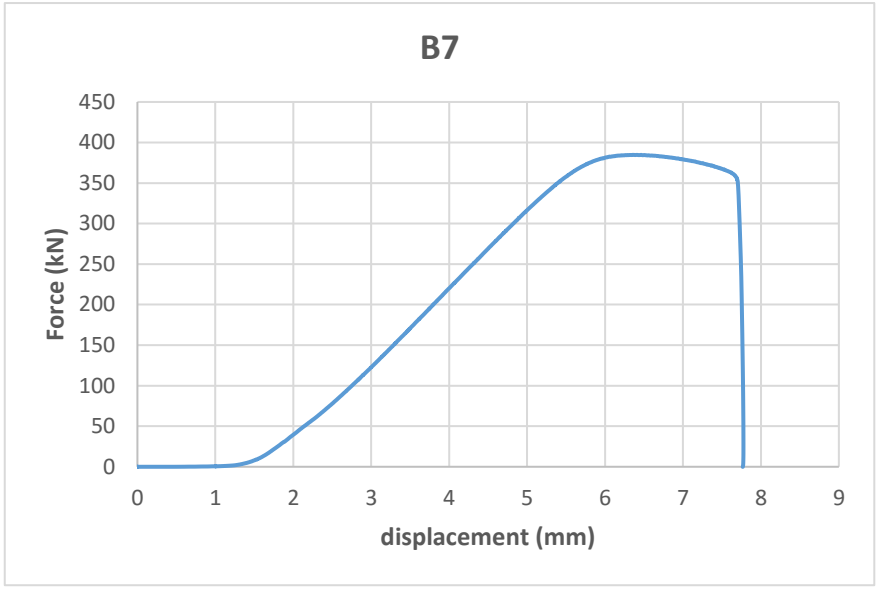

Figure C29: Force – displacement for bolt B7

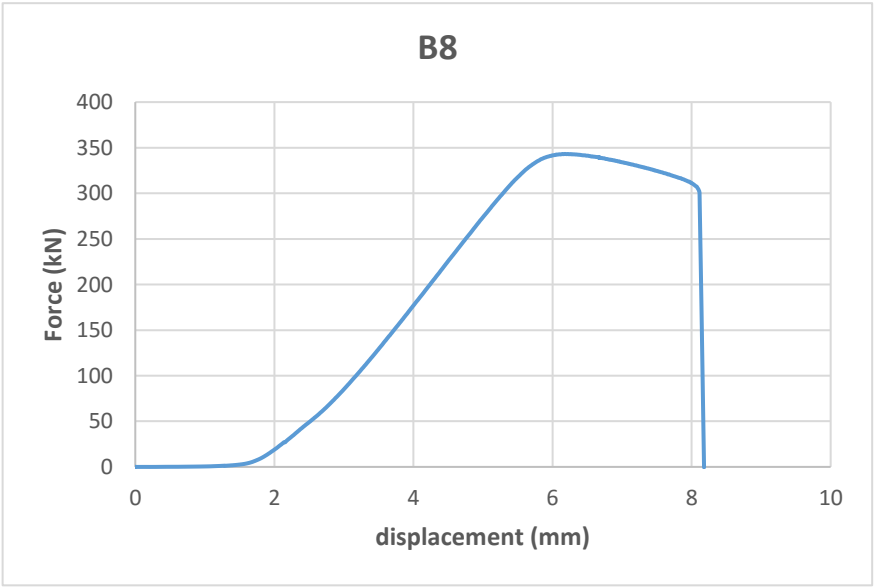

Figure C30: Force – displacement for bolt B8

APPENDIX D

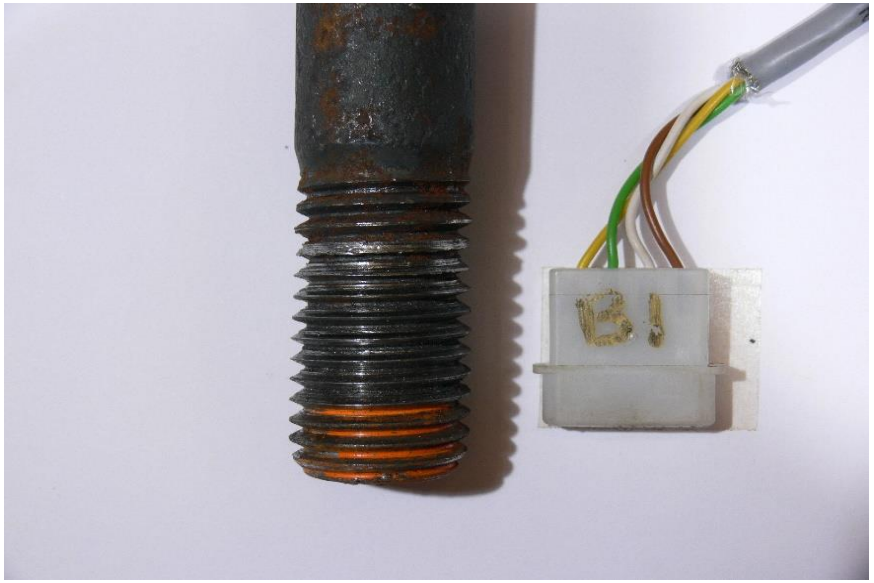

Figure D1: Threads of bolt B1

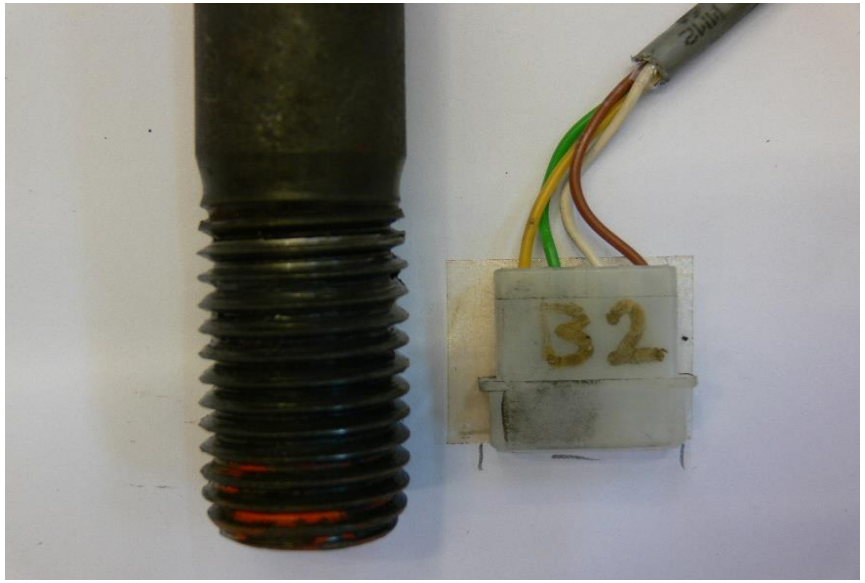

Figure D2: Threads of bolt B2

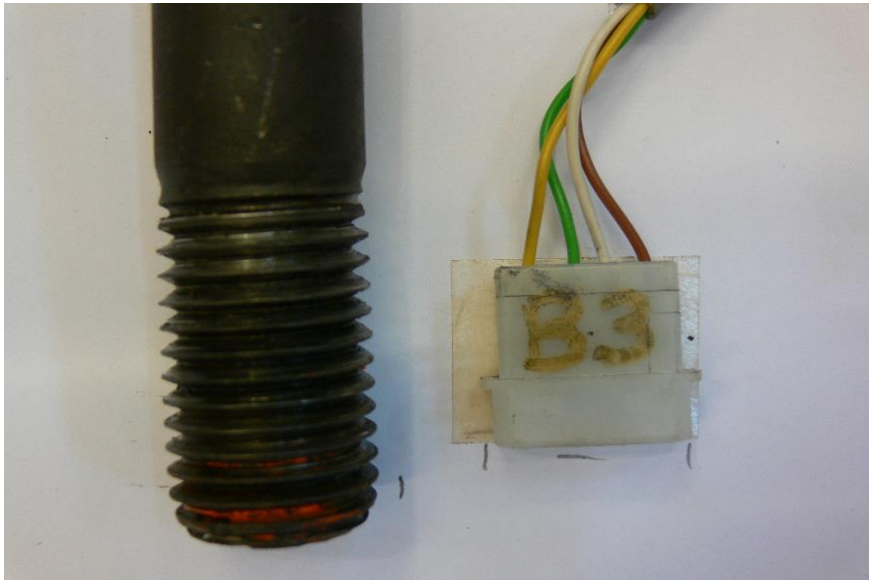

Figure D3: Threads of bolt B3

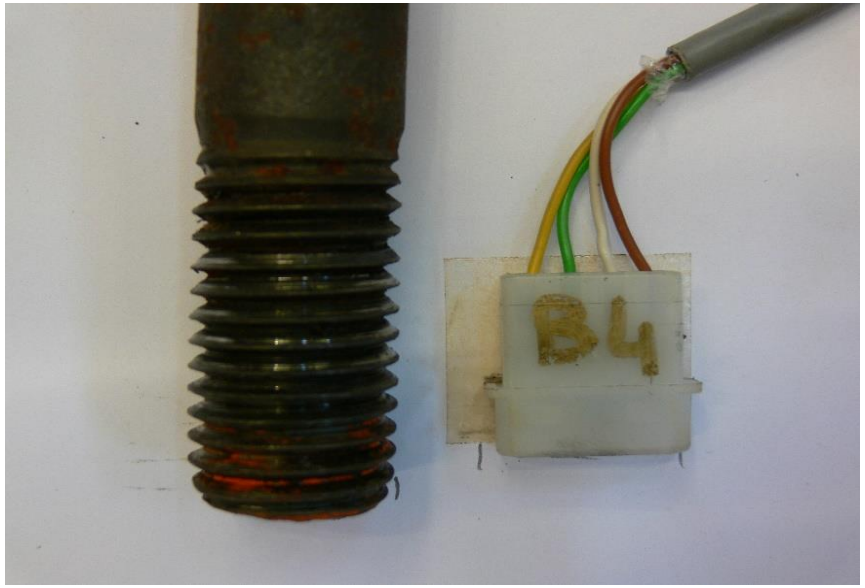

Figure D4: Threads of bolt B4

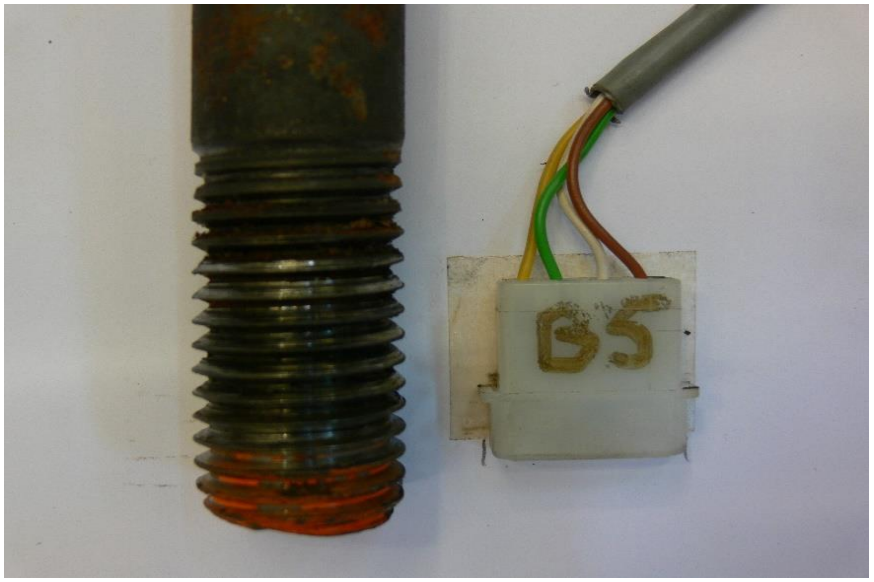

Figure D5: Threads of bolt B5

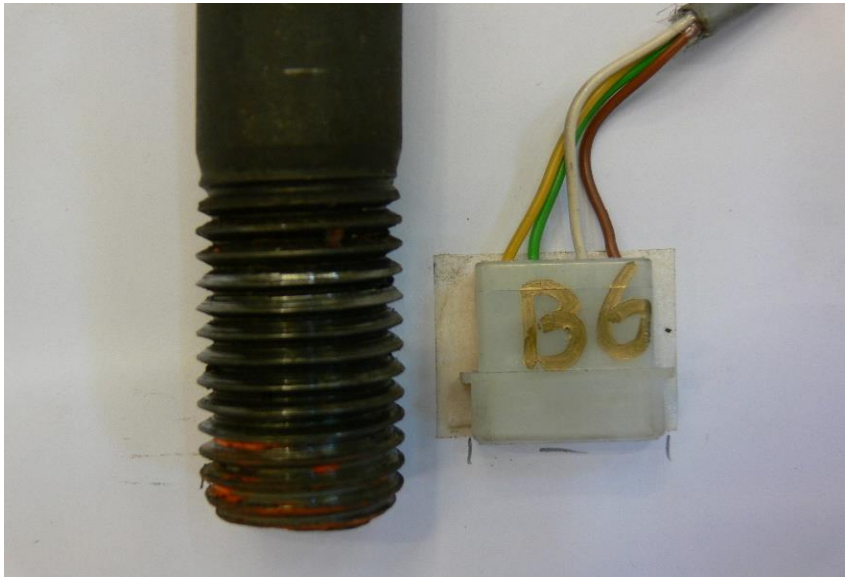

Figure D6: Threads of bolt B6

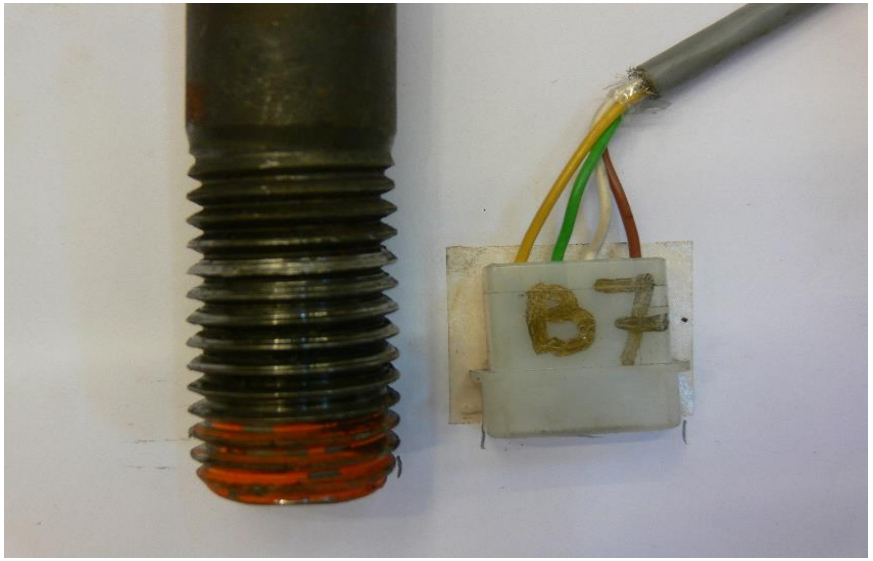

Figure D7: Threads of bolt B7

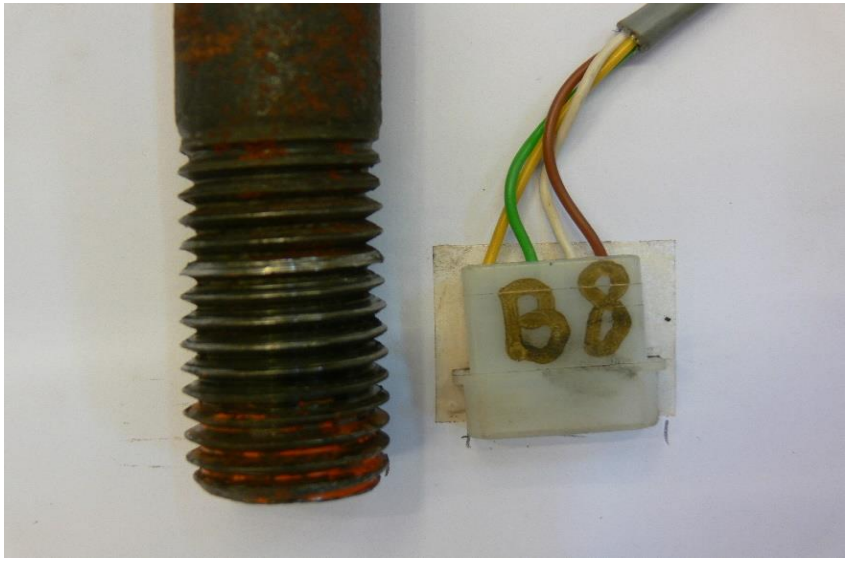

Figure D8: Threads of bolt B8

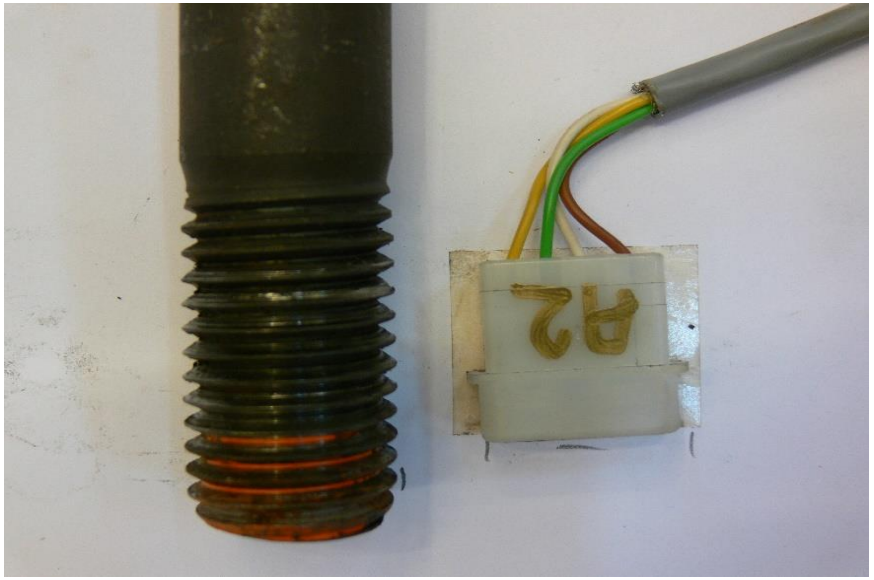

Figure D9: Threads of bolt A2

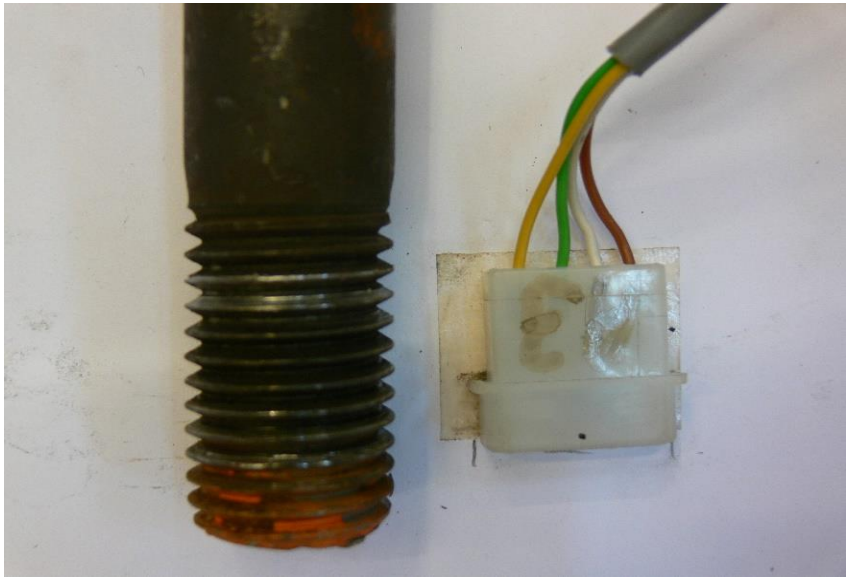

Figure D10: Threads of bolt A3

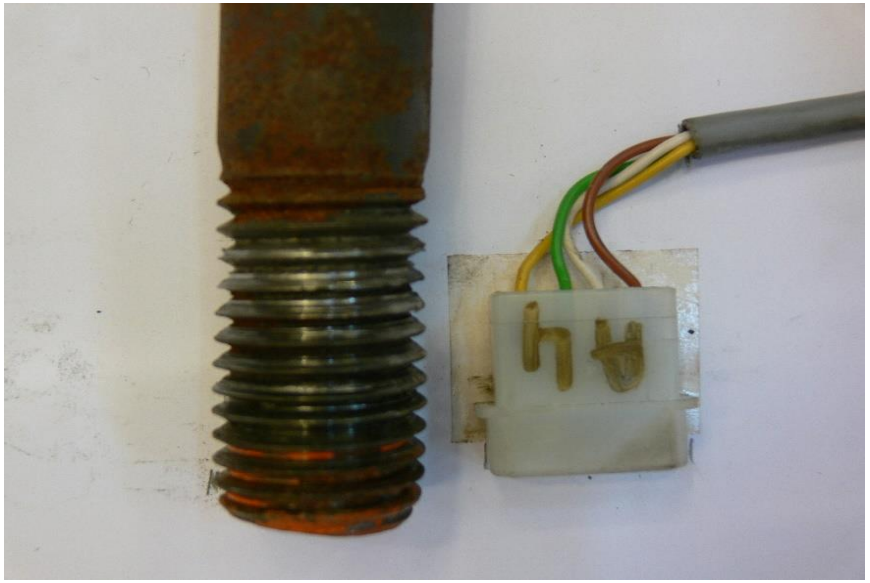

Figure D11: Threads of bolt A4

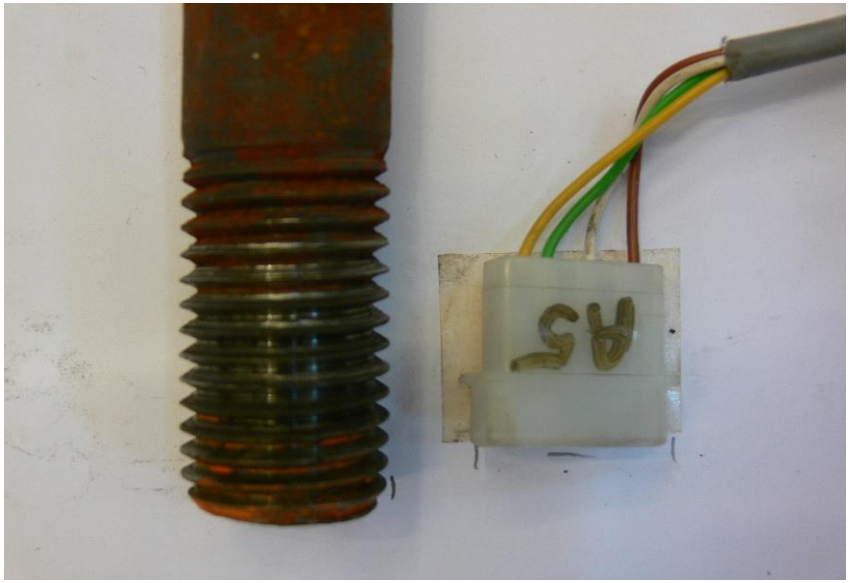

Figure D12: Threads of bolt A5

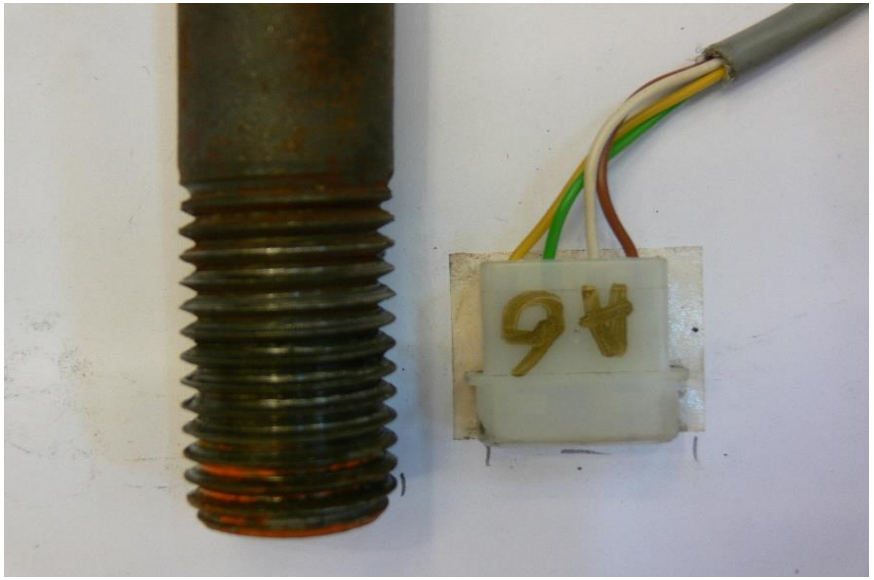

Figure D13: Threads of bolt A6

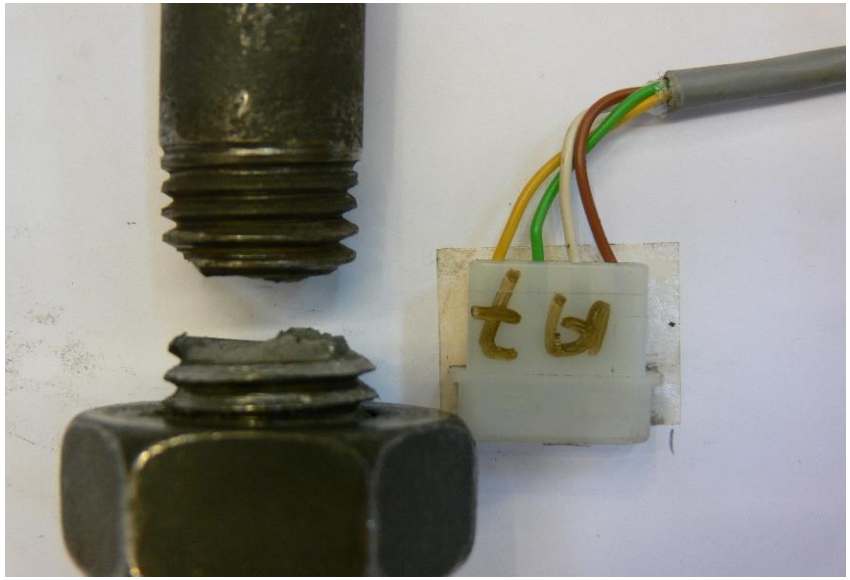

Figure D14: Threads of bolt A7

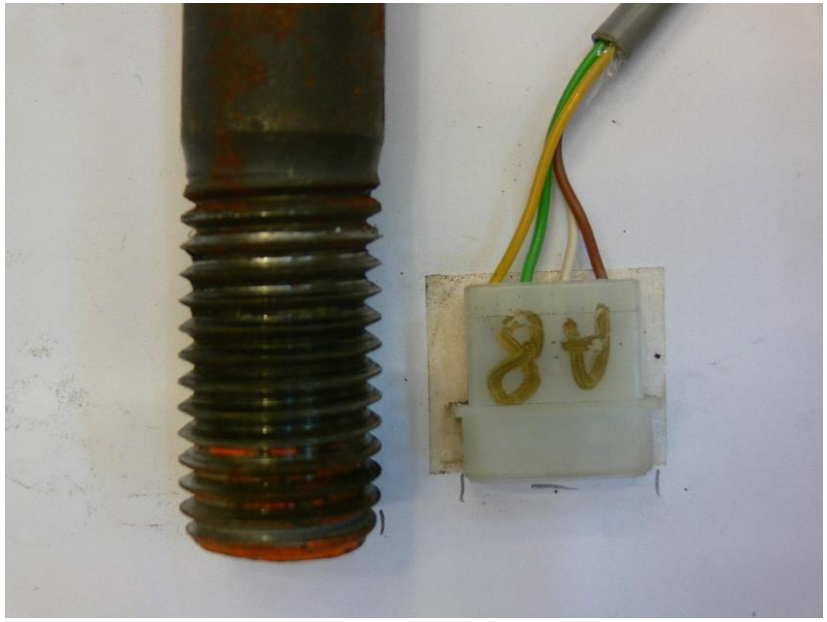

Figure D15: Threads of bolt A8

APPENDIX E

Table E1: Diameters of A series

Bolts	d (mm)
A1	23.50
A2	23.92
A3	24.01
A4	23.71
A5	23.89
A6	23.76
A7	23.70
A8	23.71

Table E2: Diameters of B series

Bolts	d (mm)
B1	23.61
B2	23.67
B3	23.63
B4	23.62
B5	23.66
B6	23.50
B7	23.62
B8	23.61

Table E3: Model forces based on actual diameter for E = 210 GPa (A series)

Bolts	A1	A2	A3	A4	A5	A6	A7	A8
$A_{net}(mm^2)$	430.59	446.11	449.62	438.38	445.11	440.25	438.01	438.38
$E(N/mm^2)$	210000	210000	210000	210000	210000	210000	210000	210000
EA(N)	90425	93683	94421	92060	93473	92451	91982	92060
$\varepsilon \times 10^{-6}$	3239	3346	-	3579	3502	3625	2104	3754
F_{model}	293	313	-	330	327	335	193	346
$F_{calibration}$	280	328	-	337	326	330	189	342
difference (%)	-4.62	4.42	-	2.22	-0.4	-1.54	-2.38	-1.05

Table E4: Model forces based on actual diameter for E = 210 GPa (B series)

Bolts	B1	B2	B3	B4	B5	B6	B7	B8
$A_{net}(mm^2)$	434.74	436.89	435.41	434.91	436.52	430.59	435.04	434.66
$E(N/mm^2)$	210000	210000	210000	210000	210000	210000	210000	210000
EA(N)	91295	91747	91435	91331	91669	90425	91357	91280
$\varepsilon \times 10^{-6}$	3466	3385	3531	3537	-	3676	3074	-
F_{model}	316	311	323	323	-	332	281	-
$F_{calibration}$	308	299	317	313	-	320	271	-
difference (%)	-2.74	-3.87	-1.84	-3.21	-	-3.89	-3.64	-

Table E5: Model forces based on d_{max} = 24.84 mm for E = 210 GPa (A series)

	A1	A2	A3	A4	A5	A6	A7	A8
$A_{net}(mm^2)$	481.47	481.47	481.47	481.47	481.47	481.47	481.47	481.47
$E(N/mm^2)$	210000	210000	210000	210000	210000	210000	210000	210000
EA(N)	101109	101109	101109	101109	101109	101109	101109	101109
$\varepsilon \times 10^{-6}$	3239	3346	-	3579	3502	3625	2104	3754
F_{model}	328	338	-	362	354	366	213	380
$F_{calibration}$	280	328	-	337	326	330	189	342
difference (%)	16.98	3.15	-	7.39	8.60	11.05	12.53	10.98

Table E6: Model forces based on d_{max} = 24.84 mm for E = 210 GPa (B series)

Bolts	B1	B2	B3	B4	B5	B6	B7	B8
$A_{net}(mm^2)$	481.47	481.47	481.47	481.47	481.47	481.47	481.47	481.47
$E(N/mm^2)$	210000	210000	210000	210000	210000	210000	210000	210000
EA(N)	101109	101109	101109	101109	101109	101109	101109	101109
ε x 10-6	3466	3385	3531	3537	-	3676	3074	-
F_{model}	350	342	357	358	-	372	311	-
$F_{calibration}$	308	299	317	313	-	320	271	-
difference (%)	13.64	14.38	12.62	14.38	-	16.25	14.76	-

Table E7: Model forces based on d_{min} = 23.16 mm for E = 210 GPa (A series)

Bolts	A1	A2	A3	A4	A5	A6	A7	A8
$A_{net}(mm^2)$	418.13	418.13	418.13	418.13	418.13	418.13	418.13	418.13
$E(N/mm^2)$	210000	210000	210000	210000	210000	210000	210000	210000
EA(N)	87808	87808	87808	87808	87808	87808	87808	87808
$\varepsilon \times 10^{-6}$	3239	3346	-	3579	3502	3625	2104	3754
F_{model}	284	294	-	314	307	318	185	330
$F_{calibration}$	280	328	-	337	326	330	189	342
difference (%)	1.59	-10.42	-	-6.74	-5.68	-3.56	-2.27	-3.62

Table E8: Model forces based on d_{min} = 23.16 mm for E = 210 GPa (B series)

Bolts	B1	B2	B3	B4	B5	B6	B7	B8
$A_{net}(mm^2)$	418.13	418.13	418.13	418.13	418.13	418.13	418.13	418.13
$E(N/mm^2)$	210000	210000	210000	210000	210000	210000	210000	210000
EA(N)	87808	87808	87808	87808	87808	87808	87808	87808
$\varepsilon \times 10^{-6}$	3466	3385	3531	3537	-	3676	3074	-
F_{model}	304	297	310	311	-	323	270	-
$F_{calibration}$	308	299	317	313	-	320	271	-
difference (%)	-1.19	-0.59	-2.20	-0.77	-	0.88	-0.38	-

Table E9: Model forces based on actual diameter for E = 220 GPa (A series)

Bolts	A1	A2	A3	A4	A5	A6	A7	A8
$A_{net}(mm^2)$	430.59	446.11	449.62	438.38	445.11	440.25	438.01	438.38
$E(N/mm^2)$	220000	220000	220000	220000	220000	220000	220000	220000
EA(N)	94731	98145	98917	96444	97924	96854	96362	96444
$\varepsilon \times 10^{-6}$	3239	3346	-	3579	3502	3625	2104	3754
F_{model}	307	328	-	345	343	351	203	362
$F_{calibration}$	280	328	-	337	326	330	189	342
difference (%)	-9.60	-0.13	-	-2.43	-5.18	-6.38	-7.25	-5.86

Table E10: Model forces based on actual diameter for E = 220 GPa (B series)

Bolts	B1	B2	B3	B4	B5	B6	B7	B8
$A_{net}(mm^2)$	434.74	436.89	435.41	434.91	436.52	430.59	435.04	434.66
$E(N/mm^2)$	220000	220000	220000	220000	220000	220000	220000	220000
EA(N)	95643	96116	95789	95681	96035	94731	95708	95626
$\varepsilon \times 10^{-6}$	3466	3385	3531	3537	-	3676	3074	-
F_{model}	331	325	338	338	-	348	294	-
$F_{calibration}$	308	299	317	313	-	320	271	-
difference (%)	-7.63	-8.82	-6.69	-8.13	-	-8.83	-8.58	-

Table E11: Model forces based on d_{max} = 24.84 mm for E = 220 GPa (A series)

Bolts	A1	A2	A3	A4	A5	A6	A7	A8
$A_{net}(mm^2)$	481.47	481.47	481.47	481.47	481.47	481.47	481.47	481.47
$E(N/mm^2)$	220000	220000	220000	220000	220000	220000	220000	220000
EA(N)	105923	105923	105923	105923	105923	105923	105923	105923
$\varepsilon \times 10^{-6}$	3239	3346	-	3579	3502	3625	2104	3754
F_{model}	343	354	-	379	371	384	223	398
$F_{calibration}$	280	328	-	337	326	330	189	342
difference (%)	22.55	8.06	-	12.50	13.77	16.34	17.89	16.27

Table E12: Model forces based on d_{max} = 24.84 mm for E = 220 GPa (B series)

Bolts	B1	B2	B3	B4	B5	B6	B7	B8
$A_{net}(mm^2)$	481.47	481.47	481.47	481.47	481.47	481.47	481.47	481.47
$E(N/mm^2)$	220000	220000	220000	220000	220000	220000	220000	220000
EA(N)	105923	105923	105923	105923	105923	105923	105923	105923
$\varepsilon \times 10^{-6}$	3466	3385	3531	3537	-	3676	3074	-
F_{model}	367	359	374	375	-	389	326	-
$F_{calibration}$	308	299	317	313	-	320	271	-
difference (%)	19.20	19.92	17.98	19.70	-	21.69	20.17	-

Table E13: Model forces based on d_{min} = 23.16 mm for E = 220 GPa (A series)

Bolts	A1	A2	A3	A4	A5	A6	A7	A8
$A_{net}(mm^2)$	418.13	418.13	418.13	418.13	418.13	418.13	418.13	418.13
$E(N/mm^2)$	220000	220000	220000	220000	220000	220000	220000	220000
EA(N)	91990	91990	91990	91990	91990	91990	91990	91990
$\varepsilon \times 10^{-6}$	3239	3346	-	3579	3502	3625	2104	3754
F_{model}	298	308	-	329	322	333	194	345
$F_{calibration}$	280	328	-	337	326	330	189	342
difference (%)	6.43	-6.15	-	-2.30	-1.19	1.04	2.38	0.97

Table E14: Model forces based on d_{min} = 23.16 mm for E = 220 GPa (B series)

Bolts	B1	B2	B3	B4	B5	B6	B7	B8
$A_{net}(mm^2)$	418.13	418.13	418.13	418.13	418.13	418.13	418.13	418.13
$E(N/mm^2)$	220000	220000	220000	220000	220000	220000	220000	220000
EA(N)	91990	91990	91990	91990	91990	91990	91990	91990
$\varepsilon \times 10^{-6}$	3466	3385	3531	3537	-	3676	3074	-
F_{model}	319	311	325	325	-	338	283	-
$F_{calibration}$	308	299	317	313	-	320	271	-
difference (%)	3.52	4.15	2.46	3.96	-	5.68	4.36	-

Table E15: Model forces based on actual diameter for E = 200 GPa (A series)

Bolts	A1	A2	A3	A4	A5	A6	A7	A8
$A_{net}(mm^2)$	430.59	446.11	449.62	438.38	445.11	440.25	438.01	438.38
$E(N/mm^2)$	200000	200000	200000	200000	200000	200000	200000	200000
EA(N)	86119	89222	89925	87676	89022	88049	87602	87676
$\varepsilon \times 10^{-6}$	3239	3346	-	3579	3502	3625	2104	3754
F_{model}	279	299	-	314	312	319	184	329
$F_{calibration}$	280	328	-	337	326	330	189	342
difference (%)	0.36	8.97	-	6.88	4.38	3.29	2.50	3.76

Table E16: Model forces based on actual diameter for E = 200 GPa (B series)

Bolts	B1	B2	B3	B4	B5	B6	B7	B8
$A_{net}(mm^2)$	434.74	436.89	435.41	434.91	436.52	430.59	435.04	434.66
$E(N/mm^2)$	200000	200000	200000	200000	200000	200000	200000	200000
EA(N)	86948	87379	87081	86982	87304	86119	87007	86933
$\varepsilon \times 10^{-6}$	3466	3385	3531	3537	-	3676	3074	-
F_{model}	301	296	307	308	-	317	267	-
$F_{calibration}$	308	299	317	313	-	320	271	-
difference (%)	2.16	1.08	3.01	1.70	-	1.06	1.29	-

Table E17: Model forces based on d_{max} = 24.84 mm for E = 200 GPa (A series)

Bolts	A1	A2	A3	A4	A5	A6	A7	A8
$A_{net}(mm^2)$	481.47	481.47	481.47	481.47	481.47	481.47	481.47	481.47
$E(N/mm^2)$	200000	200000	200000	200000	200000	200000	200000	200000
EA(N)	96294	96294	96294	96294	96294	96294	96294	96294
$\varepsilon \times 10^{-6}$	3239	3346	-	3579	3502	3625	2104	3754
F_{model}	312	322	-	345	337	349	203	361
$F_{calibration}$	280	328	-	337	326	330	189	342
difference (%)	11.41	-1.76	-	2.27	3.43	5.77	7.17	5.70

Table E18: Model forces based on d_{max} = 24.84mm for E = 200 GPa (B series)

Bolts	B1	B2	B3	B4	B5	B6	B7	B8
$A_{net}(mm^2)$	481.47	481.47	481.47	481.47	481.47	481.47	481.47	481.47
$E(N/mm^2)$	200000	200000	200000	200000	200000	200000	200000	200000
EA(N)	96294	96294	96294	96294	96294	96294	96294	96294
$\varepsilon \times 10^{-6}$	3466	3385	3531	3537	-	3676	3074	-
F_{model}	334	326	340	341	-	354	296	-
$F_{calibration}$	308	299	317	313	-	320	271	-
difference (%)	8.36	9.02	7.25	8.82	-	10.63	9.24	-

Table E19: Model forces based on d_{min} = 23.16 mm for E = 200 GPa (A series)

Bolts	A1	A2	A3	A4	A5	A6	A7	A8
$A_{net}(mm^2)$	418.13	418.13	418.13	418.13	418.13	418.13	418.13	418.13
$E(N/mm^2)$	200000	200000	200000	200000	200000	200000	200000	200000
EA(N)	83627	83627	83627	83627	83627	83627	83627	83627
$\varepsilon \times 10^{-6}$	3239	3346	-	3579	3502	3625	2104	3754
F_{model}	271	280	-	299	293	303	176	314
$F_{calibration}$	280	328	-	337	326	330	189	342
difference (%)	-3.25	-14.68	-	-11.18	-10.18	-8.15	-6.92	-8.20

Table E20: Model forces based on d_{min} = 23.16 mm for E = 20 GPa (B series)

Bolts	B1	B2	B3	B4	B5	B6	B7	B8
$A(mm^2)$	418.13	418.13	418.13	418.13	418.13	418.13	418.13	418.13
$E(N/mm^2)$	200000	200000	200000	200000	200000	200000	200000	200000
EA(N)	83627	83627	83627	83627	83627	83627	83627	83627
$\varepsilon \times 10^{-6}$	3466	3385	3531	3537	-	3676	3074	-
F_{model}	290	283	295	296	-	307	257	-
$F_{calibration}$	308	299	317	313	-	320	271	-
difference (%)	-5.89	-5.32	-6.86	-5.49	-	-3.92	-5.13	-

APPENDIX F

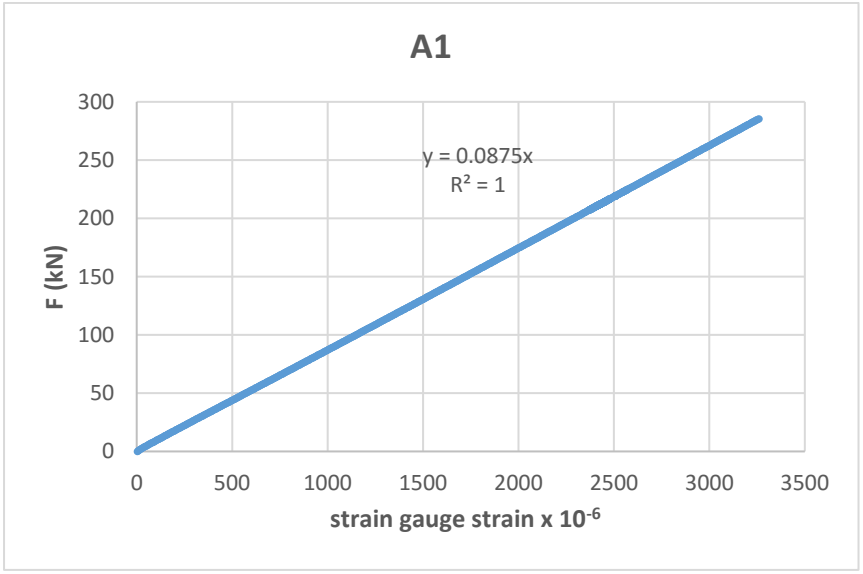

Figure F1: Calibration line of bolt A1

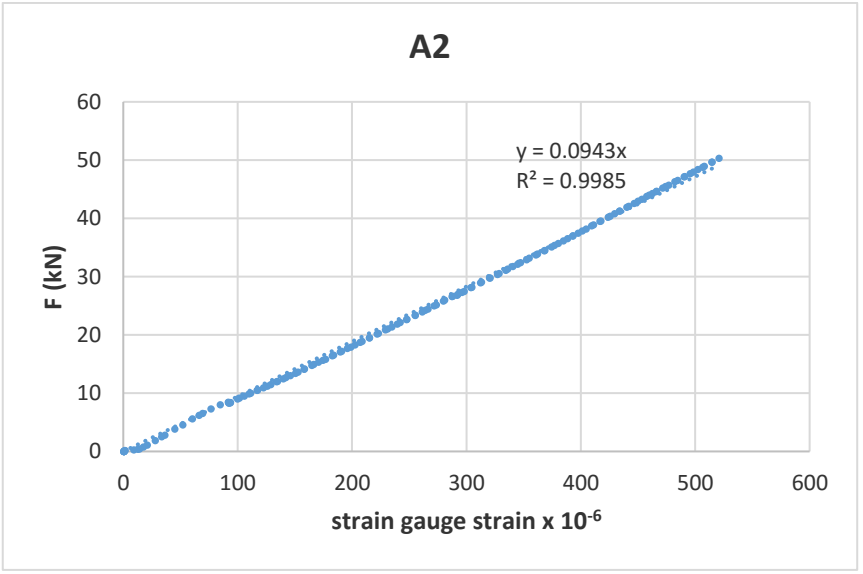

Figure F2: Calibration line of bolt A2

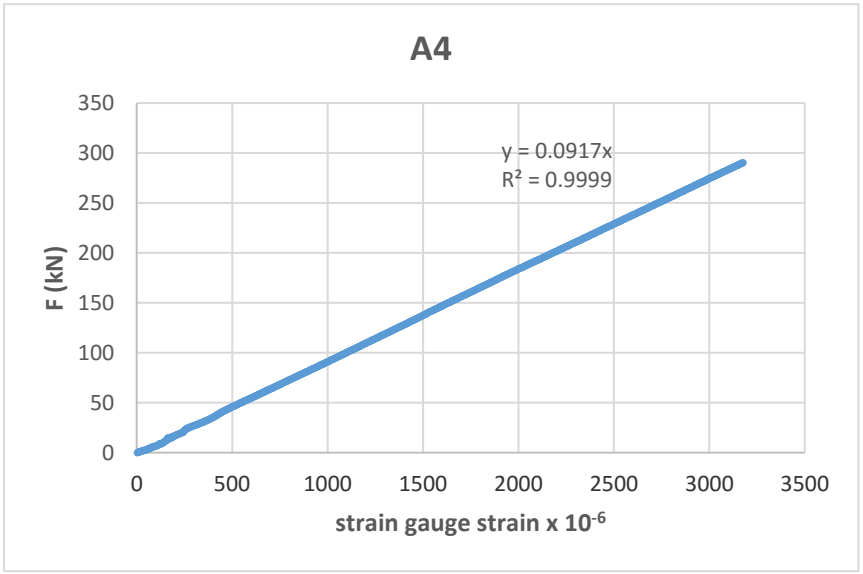

Figure F3: Calibration line of bolt A4

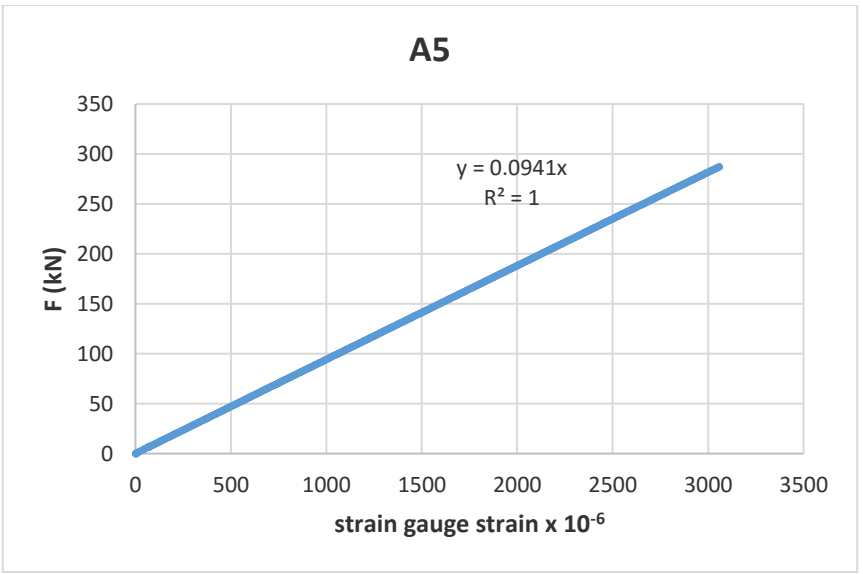

Figure F4: Calibration line of bolt A5

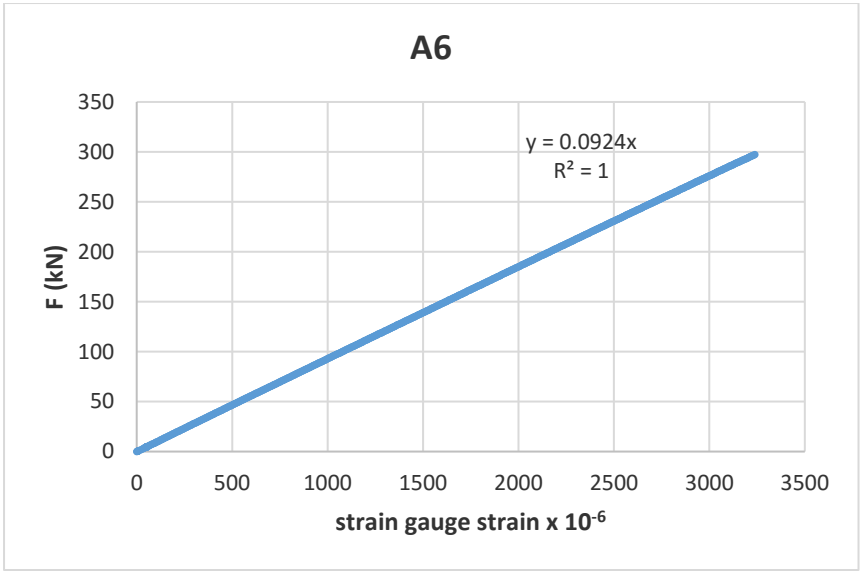

Figure F5: Calibration line of bolt A6

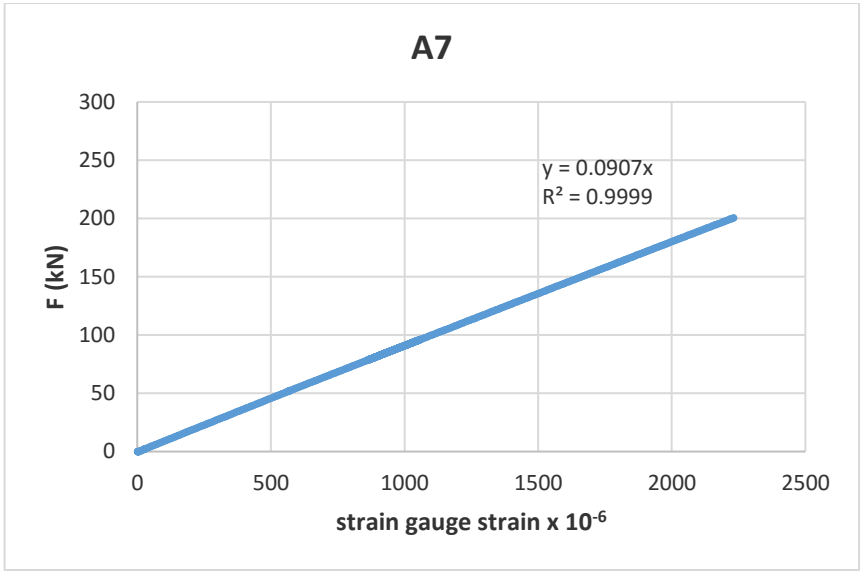

Figure F6: Calibration line of bolt A7

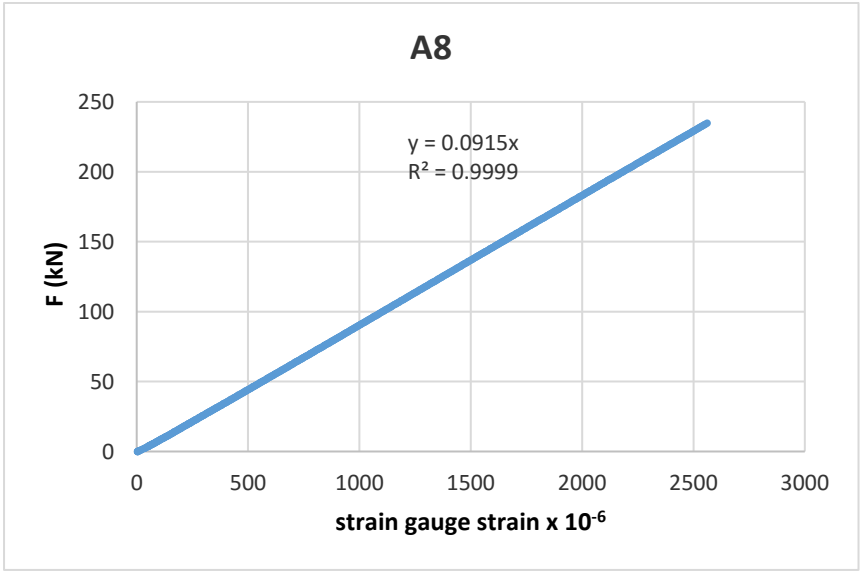

Figure F7: Calibration line of bolt A8

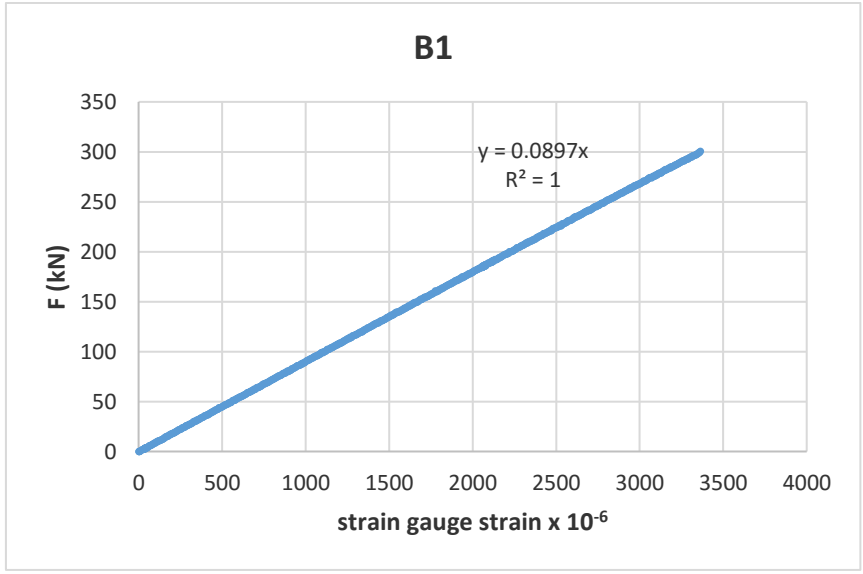

Figure F8: Calibration line of bolt B1

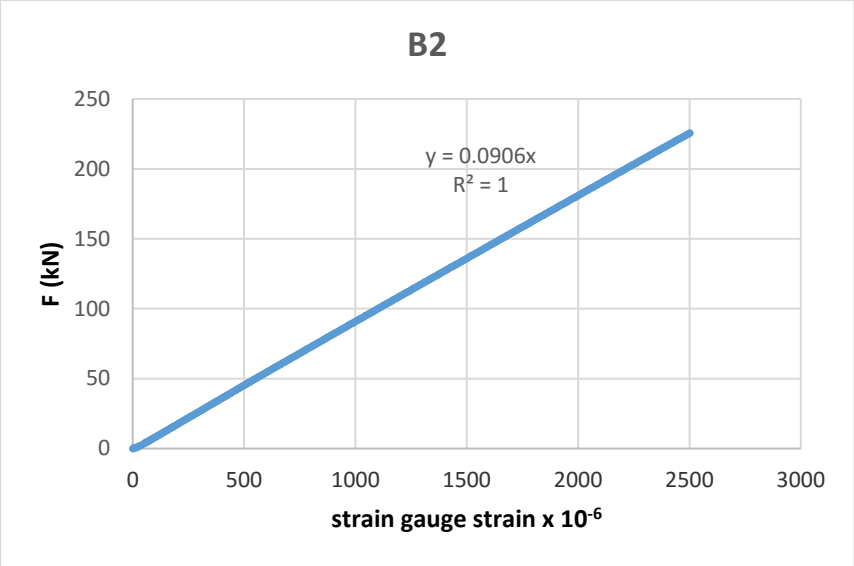

Figure F9: Calibration line of bolt B2

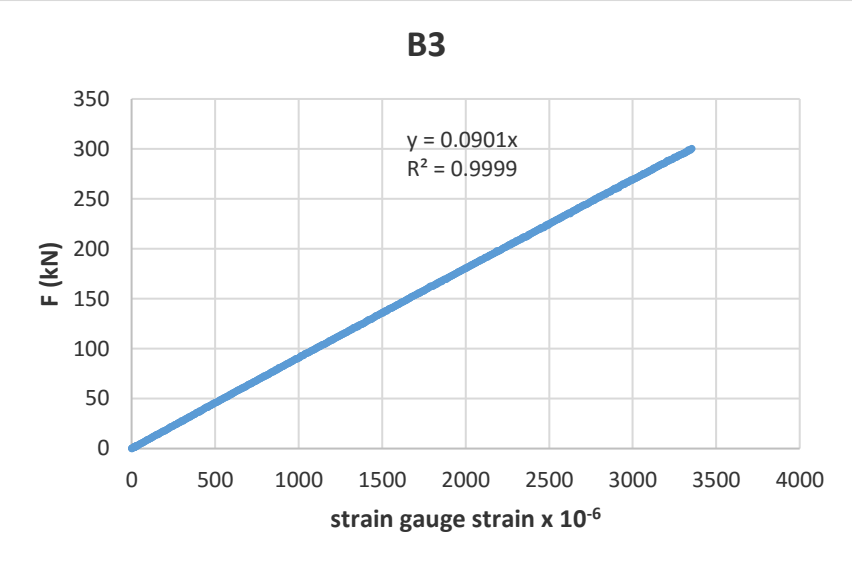

Figure F10: Calibration line of bolt B3

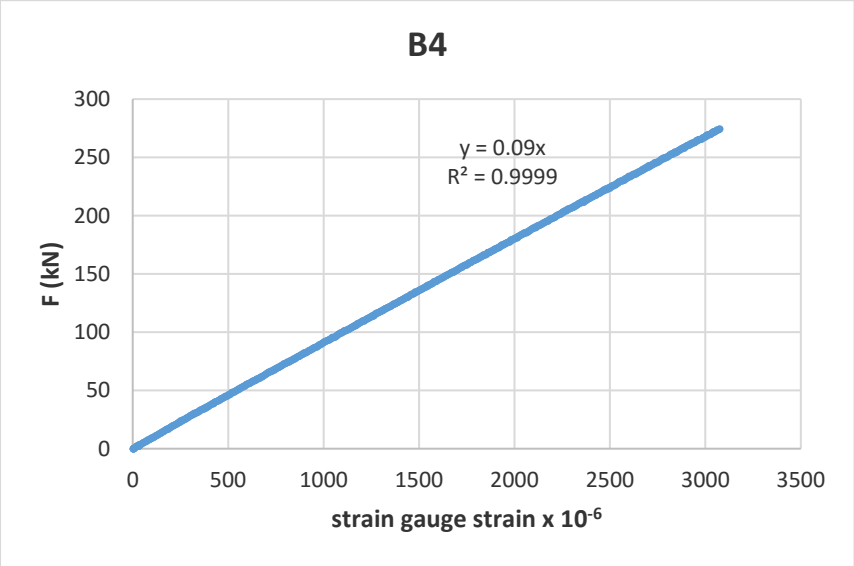

Figure F11: Calibration line of bolt B4

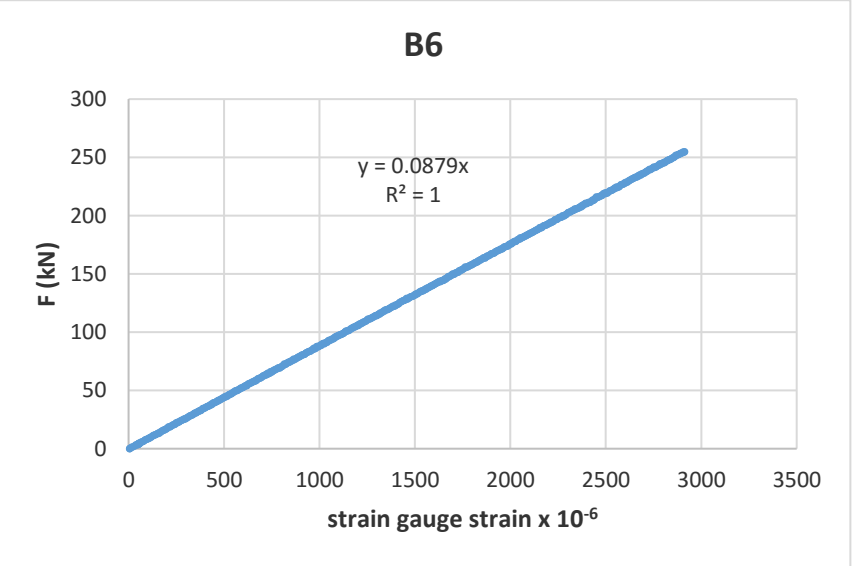

Figure F12: Calibration line of bolt B6

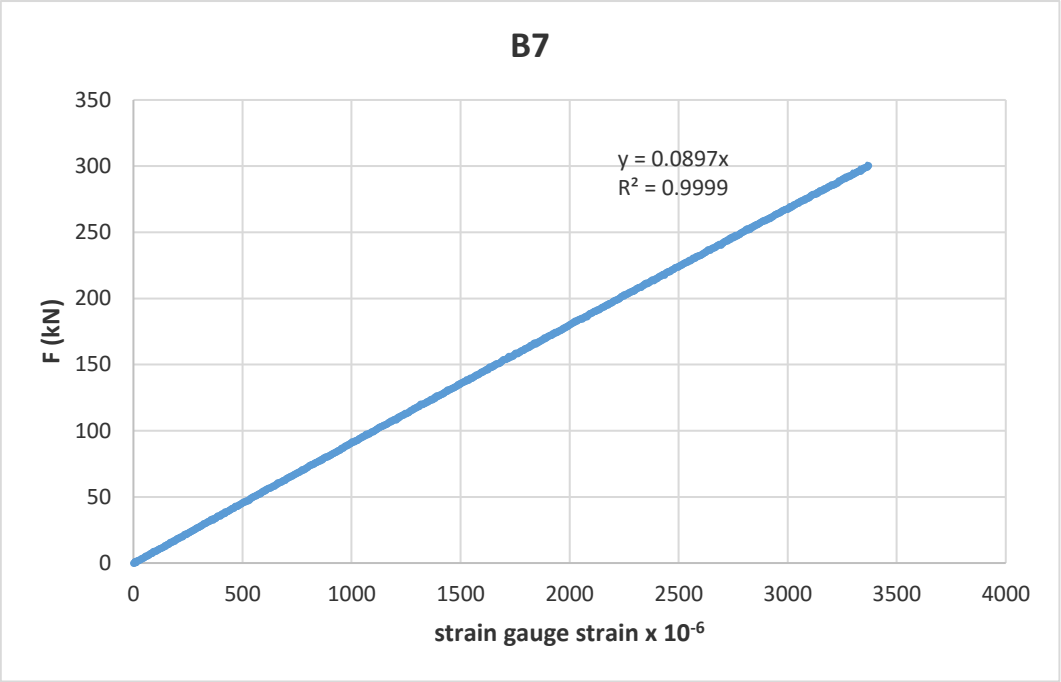

Figure F13: Calibration line of bolt B7

Table F14: Residual preloads based on corrected calibration line of A1

A1												
Bolts	**A2**	**A4**	**A5**	**A6**	**A7**	**A8**	**B1**	**B2**	**B3**	**B4**	**B6**	**B7**
EAi	0.0907	0.0891	0.0904	0.0895	0.089	0.0891	0.088	0.0888	0.0885	0.0884	0.0875	0.0884
ε x 10^{-6}	3346	3579	3502	3625	2104	3754	3466	3385	3531	3537	3676	3074
F_{model}	303	319	317	324	187	334	306	301	312	313	322	272
$F_{calibration}$	328	337	326	330	189	342	308	299	317	313	320	271
difference (%)	7.62	5.34	2.76	1.82	1.06	2.34	0.65	0.67	1.58	0	0.63	0.37

Table F15: Residual preloads based on corrected calibration line of A2

A2												
Bolts	**A1**	**A4**	**A5**	**A6**	**A7**	**A8**	**B1**	**B2**	**B3**	**B4**	**B6**	**B7**
EAi	0.091	0.0927	0.0941	0.0931	0.0926	0.0927	0.092	0.0924	0.092	0.0919	0.091	0.092
ε x 10^{-6}	3239	3579	3502	3625	2104	3754	3466	3385	3531	3537	3676	3074
F_{model}	295	332	329	337	195	348	319	313	325	325	335	283
$F_{calibration}$	280	337	326	330	189	342	308	299	317	313	320	271
difference (%)	-5.36	1.48	-0.92	-2.12	-3.17	-1.75	-3.57	-4.68	-2.52	-3.83	-4.69	-4.43

Table F16: Residual preloads based on corrected calibration line of A4

A4												
Bolts	**A1**	**A2**	**A5**	**A6**	**A7**	**A8**	**B1**	**B2**	**B3**	**B4**	**B6**	**B7**
EAi	0.0901	0.0933	0.0931	0.0921	0.0916	0.0917	0.091	0.0914	0.0911	0.091	0.0901	0.091
ε x 10^{-6}	3239	3346	3502	3625	2104	3754	3466	3385	3531	3537	3676	3074
F_{model}	292	312	326	334	193	344	315	309	322	322	331	280
$F_{calibration}$	280	328	326	330	189	342	308	299	317	313	320	271
difference (%)	-4.29	4.88	0	-1.21	-2.12	-0.58	-2.27	-3.34	-1.58	-2.88	-3.44	-3.32

Table F17: Residual preloads based on corrected calibration line of A5

A5												
Bolts	**A1**	**A2**	**A4**	**A6**	**A7**	**A8**	**B1**	**B2**	**B3**	**B4**	**B6**	**B7**
EAi	0.091	0.0943	0.0927	0.0931	0.0926	0.0927	0.092	0.0924	0.092	0.0919	0.091	0.092
ε x 10^{-6}	3239	3346	3579	3625	2104	3754	3466	3385	3531	3537	3676	3074
F_{model}	295	316	332	337	195	348	319	313	325	325	335	283
$F_{calibration}$	280	328	337	330	189	342	308	299	317	313	320	271
difference (%)	-5.36	3.66	1.48	-2.12	-3.17	-1.75	-3.57	-4.68	-2.52	-3.83	-4.69	-4.43

Table F18: Residual preloads based on corrected calibration line of A6

A6												
Bolts	**A1**	**A2**	**A4**	**A5**	**A7**	**A8**	**B1**	**B2**	**B3**	**B4**	**B6**	**B7**
EAi	0.0904	0.0936	0.092	0.0934	0.0919	0.092	0.091	0.0917	0.0914	0.0913	0.0904	0.0913
ε x 10^{-6}	3239	3346	3579	3502	2104	3754	3466	3385	3531	3537	3676	3074
F_{model}	293	313	329	327	193	345	316	310	323	323	332	281
$F_{calibration}$	280	328	337	326	189	342	308	299	317	313	320	271
difference (%)	-4.64	4.57	2.37	-0.31	-2.12	-0.88	-2.6	-3.68	-1.89	-3.19	-3.75	-3.69

Table F19: Residual preloads based on corrected calibration line of A7

A7												
Bolts	**A1**	**A2**	**A4**	**A5**	**A6**	**A8**	**B1**	**B2**	**B3**	**B4**	**B6**	**B7**
EAi	0.0892	0.0924	0.0908	0.0922	0.0912	0.0908	0.09	0.0905	0.0902	0.0901	0.0892	0.0901
ε x 10^{-6}	3239	3346	3579	3502	3625	3754	3466	3385	3531	3537	3676	3074
F_{model}	289	309	325	323	330	341	312	306	318	319	328	277
$F_{calibration}$	280	328	337	326	330	342	308	299	317	313	320	271
difference (%)	-3.21	5.79	3.56	0.92	0	0.29	-1.3	-2.34	-0.32	-1.92	-2.5	-2.21

Table F20: Residual preloads based on corrected calibration line of A8

A8												
Bolts	**A1**	**A2**	**A4**	**A5**	**A6**	**A7**	**B1**	**B2**	**B3**	**B4**	**B6**	**B7**
EAi	0.0899	0.0931	0.0915	0.0929	0.0919	0.0914	0.091	0.0912	0.0909	0.0908	0.0899	0.0908
ε x 10^{-6}	3239	3346	3579	3502	3625	2104	3466	3385	3531	3537	3676	3074
F_{model}	291	312	327	325	333	192	315	309	321	321	330	279
$F_{calibration}$	280	328	337	326	330	189	308	299	317	313	320	271
difference (%)	-3.93	4.88	2.97	0.31	-0.91	-1.59	-2.27	-3.34	-1.26	-2.56	-3.13	-2.95

Table F21: Residual preloads based on corrected calibration line of B1

B1												
Bolts	**A1**	**A2**	**A4**	**A5**	**A6**	**A7**	**A8**	**B2**	**B3**	**B4**	**B6**	**B7**
EAi	0.0888	0.092	0.0905	0.0918	0.0908	0.0904	0.09	0.0897	0.0901	0.0898	0.0897	0.0888
ε x 10^{-6}	3239	3346	3579	3502	3625	2104	3754	3385	3531	3537	3676	3074
F_{model}	288	308	324	322	329	190	340	304	318	318	330	273
$F_{calibration}$	280	328	337	326	330	189	342	299	317	313	320	271
difference (%)	-2.86	6.1	3.86	1.23	0.3	-0.53	0.58	-1.67	-0.32	-1.6	-3.13	-0.74

Table F22: Residual preloads based on corrected calibration line of B2

B2												
Bolts	**A1**	**A2**	**A4**	**A5**	**A6**	**A7**	**A8**	**B1**	**B3**	**B4**	**B6**	**B7**
EAi	0.0893	0.0925	0.0909	0.0923	0.0913	0.0908	0.091	0.0902	0.0903	0.0902	0.0893	0.0902
ε x 10^{-6}	3239	3346	3579	3502	3625	2104	3754	3466	3531	3537	3676	3074
F_{model}	289	310	325	323	331	191	341	312	319	319	328	277
$F_{calibration}$	280	328	337	326	330	189	342	308	317	313	320	271
difference (%)	-3.21	5.49	3.56	0.92	-0.3	-1.06	0.29	-1.3	-0.63	-1.92	-2.5	-2.21

Table F23: Residual preloads based on corrected calibration line of B3

B3												
Bolts	**A1**	**A2**	**A4**	**A5**	**A6**	**A7**	**A8**	**B1**	**B2**	**B4**	**B6**	**B7**
EAi	0.0891	0.0923	0.0907	0.0921	0.0911	0.0906	0.091	0.09	0.0904	0.09	0.0891	0.09
ε x 10^{-6}	3239	3346	3579	3502	3625	2104	3754	3466	3385	3537	3676	3074
F_{model}	289	309	325	323	330	191	341	312	306	318	328	277
$F_{calibration}$	280	328	337	326	330	189	342	308	299	313	320	271
difference (%)	-3.21	5.79	3.56	0.92	0	-1.06	0.29	-1.3	-2.34	-1.6	-2.5	-2.21

Table F24: Residual preloads based on corrected calibration line of B4

B4												
Bolts	**A1**	**A2**	**A4**	**A5**	**A6**	**A7**	**A8**	**B1**	**B2**	**B3**	**B6**	**B7**
EAi	0.0891	0.0923	0.0907	0.0921	0.0911	0.0906	0.091	0.09	0.0904	0.0901	0.0891	0.09
ε x 10^{-6}	3239	3346	3579	3502	3625	2104	3754	3466	3385	3531	3676	3074
F_{model}	289	309	325	323	330	191	341	312	306	318	328	277
$F_{calibration}$	280	328	337	326	330	189	342	308	299	317	320	271
difference (%)	-3.21	5.79	3.56	0.92	0	-1.06	0.29	-1.3	-2.34	-0.32	-2.5	-2.21

Table F25: Residual preloads based on corrected calibration line of B6

B6												
Bolts	**A1**	**A2**	**A4**	**A5**	**A6**	**A7**	**A8**	**B1**	**B2**	**B3**	**B4**	**B7**
EAi	0.0879	0.0911	0.0895	0.0909	0.0899	0.0894	0.089	0.0887	0.0892	0.0889	0.0888	0.0888
ε x 10^{-6}	3239	3346	3579	3502	3625	2104	3754	3466	3385	3531	3537	3074
F_{model}	285	305	320	318	326	188	336	308	302	314	314	273
$F_{calibration}$	280	328	337	326	330	189	342	308	299	317	313	271
difference (%)	-1.79	7.01	5.04	2.45	1.21	0.53	1.75	0	-1	0.95	-0.32	-0.74

Table F26: Residual preloads based on corrected calibration line of B7

B7												
Bolts	**A1**	**A2**	**A4**	**A5**	**A6**	**A7**	**A8**	**B1**	**B2**	**B3**	**B4**	**B6**
EAi	0.087	0.0901	0.0886	0.0899	0.089	0.0885	0.089	0.0878	0.0883	0.088	0.0879	0.087
ε x 10^{-6}	3239	3346	3579	3502	3625	2104	3754	3466	3385	3531	3537	3676
F_{model}	282	302	317	315	322	186	333	304	299	311	311	320
$F_{calibration}$	280	328	337	326	330	189	342	308	299	317	313	320
difference (%)	-0.71	7.93	5.93	3.37	2.42	1.59	2.63	1.3	0	1.89	0.64	0

Table F27: Residual preloads based on calibration line of A1

A1												
Bolts	**A2**	**A4**	**A5**	**A6**	**A7**	**A8**	**B1**	**B2**	**B3**	**B4**	**B6**	**B7**
EAi	0.0908	0.0908	0.0908	0.0908	0.0908	0.0908	0.0908	0.0908	0.0908	0.0908	0.0908	0.0908
ε x 10^{-6}	3346	3579	3502	3625	2104	3754	3466	3385	3531	3537	3676	3074
F_{model}	304	325	318	329	191	341	315	307	321	321	334	279
$F_{calibration}$	328	337	326	330	189	342	308	299	317	313	320	271
difference (%)	7.32	3.56	2.45	0.3	-1.06	0.29	-2.27	-2.68	-1.26	-2.56	-4.38	-2.95

Table F28: Residual preloads based on calibration line of A2

A2												
Bolts	**A1**	**A4**	**A5**	**A6**	**A7**	**A8**	**B1**	**B2**	**B3**	**B4**	**B6**	**B7**
EAi	0.0943	0.0943	0.0943	0.0943	0.0943	0.0943	0.0943	0.0943	0.0943	0.0943	0.0943	0.0943
ε x 10^{-6}	3239	3579	3502	3625	2104	3754	3466	3385	3531	3537	3676	3074
F_{model}	305	337	330	342	198	354	327	319	333	334	347	290
$F_{calibration}$	280	337	326	330	189	342	308	299	317	313	320	271
difference (%)	-8.93	0	-1.23	-3.64	-4.76	-3.51	-6.17	-6.69	-5.05	-6.71	-8.44	-7.01

Table F29: Residual preloads based on calibration line of A4

A4												
Bolts	**A1**	**A2**	**A5**	**A6**	**A7**	**A8**	**B1**	**B2**	**B3**	**B4**	**B6**	**B7**
EAi	0.0917	0.0917	0.0917	0.0917	0.0917	0.0917	0.0917	0.0917	0.0917	0.0917	0.0917	0.0917
ε x 10^{-6}	3239	3346	3502	3625	2104	3754	3466	3385	3531	3537	3676	3074
F_{model}	297	307	321	332	193	344	318	310	324	324	337	282
$F_{calibration}$	280	328	326	334	189	342	308	299	317	313	320	271
difference (%)	-6.07	6.4	1.53	0.6	-2.12	-0.58	-3.25	-3.68	-2.21	-3.51	-5.31	-4.06

Table F30: Residual preloads based on calibration line of A5

A5												
Bolts	**A1**	**A2**	**A4**	**A6**	**A7**	**A8**	**B1**	**B2**	**B3**	**B4**	**B6**	**B7**
EAi	0.0941	0.0941	0.0941	0.0941	0.0941	0.0941	0.0941	0.0941	0.0941	0.0941	0.0941	0.0941
ε x 10^{-6}	3239	3346	3579	3625	2104	3754	3466	3385	3531	3537	3676	3074
F_{model}	305	315	337	341	198	353	326	319	332	333	346	289
$F_{calibration}$	280	328	337	334	189	342	308	299	317	313	320	271
difference (%)	-8.93	3.96	0	-2.1	-4.76	-3.22	-5.84	-6.69	-4.73	-6.39	-8.13	-6.64

Table F31: Residual preloads based on calibration line of A6

A6												
Bolts	**A1**	**A2**	**A4**	**A5**	**A7**	**A8**	**B1**	**B2**	**B3**	**B4**	**B6**	**B7**
EAi	0.0924	0.0924	0.0924	0.0924	0.0924	0.0924	0.0924	0.0924	0.0924	0.0924	0.0924	0.0924
ε x 10^{-6}	3239	3346	3579	3502	2104	3754	3466	3385	3531	3537	3676	3074
F_{model}	299	309	331	324	194	347	320	313	326	327	340	284
$F_{calibration}$	280	328	337	326	189	342	308	299	317	313	320	271
difference (%)	-6.79	5.79	1.78	0.61	-2.65	-1.46	-3.9	-4.68	-2.84	-4.47	-6.25	-4.8

Table F32: Residual preloads based on calibration line of A7

A7												
Bolts	**A1**	**A2**	**A4**	**A5**	**A6**	**A8**	**B1**	**B2**	**B3**	**B4**	**B6**	**B7**
EAi	0.0907	0.0907	0.0907	0.0907	0.0907	0.0907	0.0907	0.0907	0.0907	0.0907	0.0907	0.0907
ε x 10^{-6}	3239	3346	3579	3502	3625	3754	3466	3385	3531	3537	3676	3074
F_{model}	294	303	325	318	329	340	314	307	320	321	333	279
$F_{calibration}$	280	328	337	326	334	342	308	299	317	313	320	271
difference (%)	-5	7.62	3.56	2.45	1.5	0.58	-1.95	-2.68	-0.95	-2.56	-4.06	-2.95

Table F33: Residual preloads based on calibration line of A8

A8												
Bolts	**A1**	**A2**	**A4**	**A5**	**A6**	**A7**	**B1**	**B2**	**B3**	**B4**	**B6**	**B7**
EAi	0.0915	0.0915	0.0915	0.0915	0.0915	0.0915	0.0915	0.0915	0.0915	0.0915	0.0915	0.0915
ε x 10^{-6}	3239	3346	3579	3502	3625	2104	3466	3385	3531	3537	3676	3074
F_{model}	296	306	327	320	332	193	317	310	323	324	336	281
$F_{calibration}$	280	328	337	326	334	189	308	299	317	313	320	271
difference (%)	-5.71	6.71	2.97	1.84	0.6	-2.12	-2.92	-3.68	-1.89	-3.51	-5	-3.69

Table F34: Residual preloads based on calibration line of B1

B1												
Bolts	**A1**	**A2**	**A4**	**A5**	**A6**	**A7**	**A8**	**B2**	**B3**	**B4**	**B6**	**B7**
EAi	0.0897	0.0897	0.0897	0.0897	0.0897	0.0897	0.0897	0.0897	0.0897	0.0897	0.0897	0.0897
ε x 10^{-6}	3239	3346	3579	3502	3625	2104	3754	3385	3531	3537	3676	3074
F_{model}	291	300	321	314	325	189	337	304	317	317	330	276
$F_{calibration}$	280	328	337	326	334	189	342	299	317	313	320	271
difference (%)	-3.93	8.54	4.75	3.68	2.69	0	1.46	-1.67	0	-1.28	-3.13	-1.85

Table F35: Residual preloads based on calibration line of B2

B2												
Bolts	**A1**	**A2**	**A4**	**A5**	**A6**	**A7**	**A8**	**B1**	**B3**	**B4**	**B6**	**B7**
EAi	0.0906	0.0906	0.0906	0.0906	0.0906	0.0906	0.0906	0.0906	0.0906	0.0906	0.0906	0.0906
ε x 10^{-6}	3239	3346	3579	3502	3625	2104	3754	3466	3531	3537	3676	3074
F_{model}	293	303	324	317	328	191	340	314	320	320	333	279
$F_{calibration}$	280	328	337	326	334	189	342	308	317	313	320	271
difference (%)	-4.64	7.62	3.86	2.76	1.8	-1.06	0.58	-1.95	-0.95	-2.24	-4.06	-2.95

Table F36: Residual preloads based on calibration line of B3

B3												
Bolts	**A1**	**A2**	**A4**	**A5**	**A6**	**A7**	**A8**	**B1**	**B2**	**B4**	**B6**	**B7**
EAi	0.0901	0.0901	0.0901	0.0901	0.0901	0.0901	0.0901	0.0901	0.0901	0.0901	0.0901	0.0901
ε x 10^{-6}	3239	3346	3579	3502	3625	2104	3754	3466	3385	3537	3676	3074
F_{model}	292	301	322	316	327	190	338	312	305	319	331	277
$F_{calibration}$	280	328	337	326	334	189	342	308	299	313	320	271
difference (%)	-4.29	8.23	4.45	3.07	2.1	-0.53	1.17	-1.3	-2.01	-1.92	-3.44	-2.21

Table F37: Residual preloads based on calibration line of B4

B4												
Bolts	**A1**	**A2**	**A4**	**A5**	**A6**	**A7**	**A8**	**B1**	**B2**	**B3**	**B6**	**B7**
EAi	0.09	0.09	0.09	0.09	0.09	0.09	0.09	0.09	0.09	0.09	0.09	0.09
ε x 10^{-6}	3239	3346	3579	3502	3625	2104	3754	3466	3385	3531	3676	3074
F_{model}	292	301	322	315	326	189	338	312	305	318	331	277
$F_{calibration}$	280	328	337	326	334	189	342	308	299	317	320	271
difference (%)	-4.29	8.23	4.45	3.37	2.4	0	1.17	-1.3	-2.01	-0.32	-3.44	-2.21

Table F38: Residual preloads based on calibration line of B6

B6												
Bolts	**A1**	**A2**	**A4**	**A5**	**A6**	**A7**	**A8**	**B1**	**B2**	**B3**	**B4**	**B7**
EAi	0.0879	0.0879	0.0879	0.0879	0.0879	0.0879	0.0879	0.0879	0.0879	0.0879	0.0879	0.0879
ε x 10^{-6}	3239	3346	3579	3502	3625	2104	3754	3466	3385	3531	3537	3074
F_{model}	285	294	315	308	319	185	330	305	298	310	311	270
$F_{calibration}$	280	328	337	326	334	189	342	308	299	317	313	271
difference (%)	-1.79	10.37	6.53	5.52	4.49	2.12	3.51	0.97	0.33	2.21	0.64	0.37

Table F39: Residual preloads based on calibration line of B7

B7												
Bolts	**A1**	**A2**	**A4**	**A5**	**A6**	**A7**	**A8**	**B1**	**B2**	**B3**	**B4**	**B6**
EAi	0.0879	0.0879	0.0879	0.0879	0.0879	0.0879	0.0879	0.0879	0.0879	0.0879	0.0879	0.0879
ε x 10^{-6}	3239	3346	3579	3502	3625	2104	3754	3466	3385	3531	3537	3676
F_{model}	285	294	315	308	319	185	330	305	298	310	311	323
$F_{calibration}$	280	328	337	326	334	189	342	308	299	317	313	320
difference (%)	-1.79	10.37	6.53	5.52	4.49	2.12	3.51	0.97	0.33	2.21	0.64	-0.94

Table F40: Residual preloads based on calibration line of A1

A1 corrected												
Bolts	**A2**	**A4**	**A5**	**A6**	**A7**	**A8**	**B1**	**B2**	**B3**	**B4**	**B6**	**B7**
EAi	0.0899	0.0899	0.0899	0.0899	0.0899	0.0899	0.0899	0.0899	0.0899	0.0899	0.0899	0.0899
ε x 10^{-6}	3346	3579	3502	3625	2104	3754	3466	3385	3531	3537	3676	3074
F_{model}	301	322	315	326	189	337	312	304	317	318	330	276
$F_{calibration}$	328	337	326	330	189	342	308	299	317	313	320	271
difference (%)	8.23	4.45	3.37	1.21	0	1.46	-1.3	-1.67	0	-1.6	-3.13	-1.85

Table F41: Residual preloads based on calibration line of A2

A2 corrected												
Bolts	**A1**	**A4**	**A5**	**A6**	**A7**	**A8**	**B1**	**B2**	**B3**	**B4**	**B6**	**B7**
EAi	0.0934	0.0934	0.0934	0.0934	0.0934	0.0934	0.0934	0.0934	0.0934	0.0934	0.0934	0.0934
ε x 10^{-6}	3239	3579	3502	3625	2104	3754	3466	3385	3531	3537	3676	3074
F_{model}	302	334	327	338	196	350	324	316	330	330	343	287
$F_{calibration}$	280	337	326	330	189	342	308	299	317	313	320	271
difference (%)	-7.86	0.89	-0.31	-2.42	-3.7	-2.34	-5.19	-5.69	-4.1	-5.43	-7.19	-5.9

Table F42: Residual preloads based on calibration line of A4

A4 corrected												
Bolts	**A1**	**A2**	**A5**	**A6**	**A7**	**A8**	**B1**	**B2**	**B3**	**B4**	**B6**	**B7**
EAi	0.0908	0.0908	0.0908	0.0908	0.0908	0.0908	0.0908	0.0908	0.0908	0.0908	0.0908	0.0908
ε x 10^{-6}	3239	3346	3502	3625	2104	3754	3466	3385	3531	3537	3676	3074
F_{model}	294	304	318	329	191	341	315	307	321	321	334	279
$F_{calibration}$	280	328	326	334	189	342	308	299	317	313	320	271
difference (%)	-5	7.32	2.45	1.5	-1.06	0.29	-2.27	-2.68	-1.26	-2.56	-4.38	-2.95

Table F43: Residual preloads based on calibration line of A5

A5 corrected												
Bolts	**A1**	**A2**	**A4**	**A6**	**A7**	**A8**	**B1**	**B2**	**B3**	**B4**	**B6**	**B7**
EAi	0.0932	0.0932	0.0932	0.0932	0.0932	0.0932	0.0932	0.0932	0.0932	0.0932	0.0932	0.0932
ε x 10^{-6}	3239	3346	3579	3625	2104	3754	3466	3385	3531	3537	3676	3074
F_{model}	302	312	333	338	196	350	323	315	329	329	342	286
$F_{calibration}$	280	328	337	334	189	342	308	299	317	313	320	271
difference (%)	-7.86	4.88	1.19	-1.2	-3.7	-2.34	-4.87	-5.35	-3.79	-5.11	-6.88	-5.54

Table F44: Residual preloads based on calibration line of A6

A6 corrected												
Bolts	**A1**	**A2**	**A4**	**A5**	**A7**	**A8**	**B1**	**B2**	**B3**	**B4**	**B6**	**B7**
EAi	0.0915	0.0915	0.0915	0.0915	0.0915	0.0915	0.0915	0.0915	0.0915	0.0915	0.0915	0.0915
ε x 10^{-6}	3239	3346	3579	3502	2104	3754	3466	3385	3531	3537	3676	3074
F_{model}	296	306	327	320	192	343	317	310	323	324	336	281
$F_{calibration}$	280	328	337	326	189	342	308	299	317	313	320	271
difference (%)	-5.71	6.71	2.97	1.84	-1.59	-0.29	-2.92	-3.68	-1.89	-3.51	-5	-3.69

Table F45: Residual preloads based on calibration line of A7

A7 corrected												
Bolts	**A1**	**A2**	**A4**	**A5**	**A6**	**A8**	**B1**	**B2**	**B3**	**B4**	**B6**	**B7**
EAi	0.0898	0.0898	0.0898	0.0898	0.0898	0.0898	0.0898	0.0898	0.0898	0.0898	0.0898	0.0898
ε x 10^{-6}	3239	3346	3579	3502	3625	3754	3466	3385	3531	3537	3676	3074
F_{model}	291	300	321	314	325	337	311	304	317	318	330	276
$F_{calibration}$	280	328	337	326	334	342	308	299	317	313	320	271
difference (%)	-3.93	8.54	4.75	3.68	2.69	1.46	-0.97	-1.67	0	-1.6	-3.13	-1.85

Table F46: Residual preloads based on calibration line of A8

A8 corrected												
Bolts	**A1**	**A2**	**A4**	**A5**	**A6**	**A7**	**B1**	**B2**	**B3**	**B4**	**B6**	**B7**
EAi	0.0906	0.0906	0.0906	0.0906	0.0906	0.0906	0.0906	0.0906	0.0906	0.0906	0.0906	0.0906
ε x 10^{-6}	3239	3346	3579	3502	3625	2104	3466	3385	3531	3537	3676	3074
F_{model}	293	303	324	317	328	191	314	307	320	320	333	278
$F_{calibration}$	280	328	337	326	334	189	308	299	317	313	320	271
difference (%)	-4.64	7.62	3.86	2.76	1.8	-1.06	-1.95	-2.68	-0.95	-2.24	-4.06	-2.58

Table F47: Residual preloads based on calibration line of B1

B1 corrected												
Bolts	**A1**	**A2**	**A4**	**A5**	**A6**	**A7**	**A8**	**B2**	**B3**	**B4**	**B6**	**B7**
EAi	0.0888	0.0888	0.0888	0.0888	0.0888	0.0888	0.0888	0.0888	0.0888	0.0888	0.0888	0.0888
ε x 10^{-6}	3239	3346	3579	3502	3625	2104	3754	3385	3531	3537	3676	3074
F_{model}	288	297	318	311	322	187	333	301	314	314	326	273
$F_{calibration}$	280	328	337	326	334	189	342	299	317	313	320	271
difference (%)	-2.86	9.45	5.64	4.6	3.59	1.06	2.63	-0.67	0.95	-0.32	-1.88	-0.74

Table F48: Residual preloads based on calibration line of B2

B2 corrected												
Bolts	**A1**	**A2**	**A4**	**A5**	**A6**	**A7**	**A8**	**B1**	**B3**	**B4**	**B6**	**B7**
EAi	0.0897	0.0897	0.0897	0.0897	0.0897	0.0897	0.0897	0.0897	0.0897	0.0897	0.0897	0.0897
ε x 10^{-6}	3239	3346	3579	3502	3625	2104	3754	3466	3531	3537	3676	3074
F_{model}	291	300	321	314	325	189	337	311	317	317	330	276
$F_{calibration}$	280	328	337	326	334	189	342	308	317	313	320	271
difference (%)	-3.93	8.54	4.75	3.68	2.69	0	1.46	-0.97	0	-1.28	-3.13	-1.85

Table F49: Residual preloads based on calibration line of B3

B3 corrected												
Bolts	**A1**	**A2**	**A4**	**A5**	**A6**	**A7**	**A8**	**B1**	**B2**	**B4**	**B6**	**B7**
EAi	0.0892	0.0892	0.0892	0.0892	0.0892	0.0892	0.0892	0.0892	0.0892	0.0892	0.0892	0.0892
ε x 10^{-6}	3239	3346	3579	3502	3625	2104	3754	3466	3385	3537	3676	3074
F_{model}	289	298	319	312	323	188	335	309	302	315	328	274
$F_{calibration}$	280	328	337	326	334	189	342	308	299	313	320	271
difference (%)	-3.21	9.15	5.34	4.29	3.29	0.53	2.05	-0.32	-1	-0.64	-2.5	-1.11

Table F50: Residual preloads based on calibration line of B4

B4 corrected												
Bolts	**A1**	**A2**	**A4**	**A5**	**A6**	**A7**	**A8**	**B1**	**B2**	**B3**	**B6**	**B7**
EAi	0.0891	0.0891	0.0891	0.0891	0.0891	0.0891	0.0891	0.0891	0.0891	0.0891	0.0891	0.0891
ε x 10^{-6}	3239	3346	3579	3502	3625	2104	3754	3466	3385	3531	3676	3074
F_{model}	289	298	319	312	323	187	334	309	302	315	328	274
$F_{calibration}$	280	328	337	326	334	189	342	308	299	317	320	271
difference (%)	-3.21	9.15	5.34	4.29	3.29	1.06	2.34	-0.32	-1	0.63	-2.5	-1.11

Table F51: Residual preloads based on calibration line of B6

B6 corrected												
Bolts	**A1**	**A2**	**A4**	**A5**	**A6**	**A7**	**A8**	**B1**	**B2**	**B3**	**B4**	**B7**
EAi	0.087	0.087	0.087	0.087	0.087	0.087	0.087	0.087	0.087	0.087	0.087	0.087
ε x 10^{-6}	3239	3346	3579	3502	3625	2104	3754	3466	3385	3531	3537	3074
F_{model}	282	291	311	305	315	183	327	302	295	307	308	267
$F_{calibration}$	280	328	337	326	334	189	342	308	299	317	313	271
difference (%)	-0.71	11.28	7.72	6.44	5.69	3.17	4.39	1.95	1.34	3.15	1.6	1.48

Table F52: Residual preloads based on calibration line of B7

B7 corrected												
Bolts	**A1**	**A2**	**A4**	**A5**	**A6**	**A7**	**A8**	**B1**	**B2**	**B3**	**B4**	**B6**
EAi	0.087	0.087	0.087	0.087	0.087	0.087	0.087	0.087	0.087	0.087	0.087	0.087
ε x 10^{-6}	3239	3346	3579	3502	3625	2104	3754	3466	3385	3531	3537	3676
F_{model}	282	291	311	305	315	183	327	302	295	307	308	320
$F_{calibration}$	280	328	337	326	334	189	342	308	299	317	313	320
difference (%)	-0.71	11.28	7.72	6.44	5.69	3.17	4.39	1.95	1.34	3.15	1.6	0

Table F53: Residual preloads based on calibration line of A1 (correction B)

A1 corrected (correction B)												
Bolts	**A2**	**A4**	**A5**	**A6**	**A7**	**A8**	**B1**	**B2**	**B3**	**B4**	**B6**	**B7**
EAi	0.0881	0.0881	0.0881	0.0881	0.0881	0.0881	0.0881	0.0881	0.0881	0.0881	0.0881	0.0881
ε x 10^{-6}	3346	3579	3502	3625	2104	3754	3466	3385	3531	3537	3676	3074
F_{model}	295	315	308	319	185	331	305	298	311	312	324	271
$F_{calibration}$	328	337	326	330	189	342	308	299	317	313	320	271
difference (%)	10.06	6.53	5.52	3.33	2.12	3.22	0.97	0.33	1.89	0.32	-1.25	0

Table F54: Residual preloads based on calibration line of A2 (correction B)

A2 corrected (correction B)												
Bolts	**A1**	**A4**	**A5**	**A6**	**A7**	**A8**	**B1**	**B2**	**B3**	**B4**	**B6**	**B7**
EAi	0.0915	0.0915	0.0915	0.0915	0.0915	0.0915	0.0915	0.0915	0.0915	0.0915	0.0915	0.0915
ε x 10^{-6}	3239	3579	3502	3625	2104	3754	3466	3385	3531	3537	3676	3074
F_{model}	296	327	320	332	192	343	317	310	323	324	336	281
$F_{calibration}$	280	337	326	330	189	342	308	299	317	313	320	271
difference (%)	-5.71	2.97	1.84	-0.61	-1.59	-0.29	-2.92	-3.68	-1.89	-3.51	-5	-3.69

Table F55: Residual preloads based on calibration line of A4 (correction B)

A4 corrected (correction B)												
Bolts	**A1**	**A2**	**A5**	**A6**	**A7**	**A8**	**B1**	**B2**	**B3**	**B4**	**B6**	**B7**
EAi	0.089	0.089	0.089	0.089	0.089	0.089	0.089	0.089	0.089	0.089	0.089	0.089
ε x 10^{-6}	3239	3346	3502	3625	2104	3754	3466	3385	3531	3537	3676	3074
F_{model}	288	298	312	322	187	334	308	301	314	315	327	273
$F_{calibration}$	280	328	326	334	189	342	308	299	317	313	320	271
difference (%)	-2.86	9.15	4.29	3.59	1.06	2.34	0	-0.67	0.95	-0.64	-2.19	-0.74

Table F56: Residual preloads based on calibration line of A5 (correction B)

A5 corrected (correction B)												
Bolts	**A1**	**A2**	**A4**	**A6**	**A7**	**A8**	**B1**	**B2**	**B3**	**B4**	**B6**	**B7**
EAi	0.0913	0.0913	0.0913	0.0913	0.0913	0.0913	0.0913	0.0913	0.0913	0.0913	0.0913	0.0913
ε x 10^{-6}	3239	3346	3579	3625	2104	3754	3466	3385	3531	3537	3676	3074
F_{model}	296	305	327	331	192	343	316	309	322	323	336	281
$F_{calibration}$	280	328	337	334	189	342	308	299	317	313	320	271
difference (%)	-5.71	7.01	2.97	0.9	-1.59	-0.29	-2.6	-3.34	-1.58	-3.19	-5	-3.69

Table F57: Residual preloads based on calibration line of A6 (correction B)

A6 corrected (correction B)												
Bolts	**A1**	**A2**	**A4**	**A5**	**A7**	**A8**	**B1**	**B2**	**B3**	**B4**	**B6**	**B7**
EAi	0.0896	0.0896	0.0896	0.0896	0.0896	0.0896	0.0896	0.0896	0.0896	0.0896	0.0896	0.0896
ε x 10^{-6}	3239	3346	3579	3502	2104	3754	3466	3385	3531	3537	3676	3074
F_{model}	290	300	321	314	189	336	311	303	316	317	329	276
$F_{calibration}$	280	328	337	326	189	342	308	299	317	313	320	271
difference (%)	-3.57	8.54	4.75	3.68	0	1.75	-0.97	-1.34	0.32	-1.28	-2.81	-1.85

Table F58: Residual preloads based on calibration line of A7 (correction B)

A7 corrected (correction B)												
Bolts	**A1**	**A2**	**A4**	**A5**	**A6**	**A8**	**B1**	**B2**	**B3**	**B4**	**B6**	**B7**
EAi	0.088	0.088	0.088	0.088	0.088	0.088	0.088	0.088	0.088	0.088	0.088	0.088
ε x 10^{-6}	3239	3346	3579	3502	3625	3754	3466	3385	3531	3537	3676	3074
F_{model}	285	294	315	308	319	330	305	298	311	311	323	270
$F_{calibration}$	280	328	337	326	334	342	308	299	317	313	320	271
difference (%)	-1.79	10.37	6.53	5.52	4.49	3.51	0.97	0.33	1.89	0.64	-0.94	0.37

Table F59: Residual preloads based on calibration line of A8 (correction B)

A8 corrected (correction B)												
Bolts	**A1**	**A2**	**A4**	**A5**	**A6**	**A7**	**B1**	**B2**	**B3**	**B4**	**B6**	**B7**
EAi	0.0888	0.0888	0.0888	0.0888	0.0888	0.0888	0.0888	0.0888	0.0888	0.0888	0.0888	0.0888
ε x 10^{-6}	3239	3346	3579	3502	3625	2104	3466	3385	3531	3537	3676	3074
F_{model}	287	297	318	311	322	187	308	300	313	314	326	273
$F_{calibration}$	280	328	337	326	334	189	308	299	317	313	320	271
difference (%)	-2.5	9.45	5.64	4.6	3.59	1.06	0	-0.33	1.26	-0.32	-1.88	-0.74

Table F60: Residual preloads based on calibration line of B1 (correction B)

B1 corrected (correction B)												
Bolts	**A1**	**A2**	**A4**	**A5**	**A6**	**A7**	**A8**	**B2**	**B3**	**B4**	**B6**	**B7**
EAi	0.087	0.087	0.087	0.087	0.087	0.087	0.087	0.087	0.087	0.087	0.087	0.087
ε x 10^{-6}	3239	3346	3579	3502	3625	2104	3754	3385	3531	3537	3676	3074
F_{model}	282	291	311	305	315	183	327	295	307	308	320	267
$F_{calibration}$	280	328	337	326	334	189	342	299	317	313	320	271
difference (%)	-0.71	11.28	7.72	6.44	5.69	3.17	4.39	1.34	3.15	1.6	0	1.48

Table F61: Residual preloads based on calibration line of B2 (correction B)

B2 corrected (correction B)												
Bolts	**A1**	**A2**	**A4**	**A5**	**A6**	**A7**	**A8**	**B1**	**B3**	**B4**	**B6**	**B7**
EAi	0.0879	0.0879	0.0879	0.0879	0.0879	0.0879	0.0879	0.0879	0.0879	0.0879	0.0879	0.0879
ε x 10^{-6}	3239	3346	3579	3502	3625	2104	3754	3466	3531	3537	3676	3074
F_{model}	285	294	315	308	319	185	330	305	310	311	323	270
$F_{calibration}$	280	328	337	326	334	189	342	308	317	313	320	271
difference (%)	-1.79	10.37	6.53	5.52	4.49	2.12	3.51	0.97	2.21	0.64	-0.94	0.37

Table F62: Residual preloads based on calibration line of B3 (correction B)

B3 corrected (correction B)												
Bolts	**A1**	**A2**	**A4**	**A5**	**A6**	**A7**	**A8**	**B1**	**B2**	**B4**	**B6**	**B7**
EAi	0.0874	0.0874	0.0874	0.0874	0.0874	0.0874	0.0874	0.0874	0.0874	0.0874	0.0874	0.0874
ε x 10^{-6}	3239	3346	3579	3502	3625	2104	3754	3466	3385	3537	3676	3074
F_{model}	283	292	313	306	317	184	328	303	296	309	321	269
$F_{calibration}$	280	328	337	326	334	189	342	308	299	313	320	271
difference (%)	-1.07	10.98	7.12	6.13	5.09	2.65	4.09	1.62	1	1.28	-0.31	0.74

Table F63: Residual preloads based on calibration line of B4 (correction B)

B4 corrected (correction B)												
Bolts	**A1**	**A2**	**A4**	**A5**	**A6**	**A7**	**A8**	**B1**	**B2**	**B3**	**B6**	**B7**
EAi	0.0873	0.0873	0.0873	0.0873	0.0873	0.0873	0.0873	0.0873	0.0873	0.0873	0.0873	0.0873
ε x 10^{-6}	3239	3346	3579	3502	3625	2104	3754	3466	3385	3531	3676	3074
F_{model}	283	292	312	306	316	184	328	303	296	308	321	268
$F_{calibration}$	280	328	337	326	334	189	342	308	299	317	320	271
difference (%)	-1.07	10.98	7.42	6.13	5.39	2.65	4.09	1.62	1	2.84	-0.31	1.11

Table F64: Residual preloads based on calibration line of B6 (correction B)

B6 corrected (correction B)												
Bolts	**A1**	**A2**	**A4**	**A5**	**A6**	**A7**	**A8**	**B1**	**B2**	**B3**	**B4**	**B7**
EAi	0.0853	0.0853	0.0853	0.0853	0.0853	0.0853	0.0853	0.0853	0.0853	0.0853	0.0853	0.0853
ε x 10^{-6}	3239	3346	3579	3502	3625	2104	3754	3466	3385	3531	3537	3074
F_{model}	276	285	305	299	309	179	320	296	289	301	302	262
$F_{calibration}$	280	328	337	326	334	189	342	308	299	317	313	271
difference (%)	1.43	13.11	9.5	8.28	7.49	5.29	6.43	3.9	3.34	5.05	3.51	3.32

Table F65: Residual preloads based on calibration line of B7 (correction B)

B7 corrected (correction B)												
Bolts	**A1**	**A2**	**A4**	**A5**	**A6**	**A7**	**A8**	**B1**	**B2**	**B3**	**B4**	**B6**
EAi	0.0853	0.0853	0.0853	0.0853	0.0853	0.0853	0.0853	0.0853	0.0853	0.0853	0.0853	0.0853
ε x 10^{-6}	3239	3346	3579	3502	3625	2104	3754	3466	3385	3531	3537	3676
F_{model}	276	285	305	299	309	179	320	296	289	301	302	313
$F_{calibration}$	280	328	337	326	334	189	342	308	299	317	313	320
difference (%)	1.43	13.11	9.5	8.28	7.49	5.29	6.43	3.9	3.34	5.05	3.51	2.19

Table F66: Residual preloads based on calibration line of A1 corrected based on average diameter

A1 mean												
Bolts	**A2**	**A4**	**A5**	**A6**	**A7**	**A8**	**B1**	**B2**	**B3**	**B4**	**B6**	**B7**
EAi	0.0921	0.0921	0.0921	0.0921	0.0921	0.0921	0.0921	0.0921	0.0921	0.0921	0.0921	0.0921
ε x 10^{-6}	3346	3579	3502	3625	2104	3754	3466	3385	3531	3537	3676	3074
F_{model}	308	330	323	334	194	346	319	312	325	326	339	283
$F_{calibration}$	328	337	326	330	189	342	308	299	317	313	320	271
difference (%)	6.1	2.08	0.92	-1.21	-2.65	-1.17	-3.57	-4.35	-2.52	-4.15	-5.94	-4.43

Table F67: Residual preloads based on calibration line of A2 corrected based on average diameter

A2 mean												
Bolts	**A1**	**A4**	**A5**	**A6**	**A7**	**A8**	**B1**	**B2**	**B3**	**B4**	**B6**	**B7**
EAi	0.0924	0.0924	0.0924	0.0924	0.0924	0.0924	0.0924	0.0924	0.0924	0.0924	0.0924	0.0924
ε x 10^{-6}	3239	3579	3502	3625	2104	3754	3466	3385	3531	3537	3676	3074
F_{model}	299	331	323	335	194	347	320	313	326	327	339	284
$F_{calibration}$	280	337	326	330	189	342	308	299	317	313	320	271
difference (%)	-6.79	1.78	0.92	-1.52	-2.65	-1.46	-3.9	-4.68	-2.84	-4.47	-5.94	-4.8

Table F68: Residual preloads based on calibration line of A4 corrected based on average diameter

A4 mean												
Bolts	**A1**	**A2**	**A5**	**A6**	**A7**	**A8**	**B1**	**B2**	**B3**	**B4**	**B6**	**B7**
EAi	0.0914	0.0914	0.0914	0.0914	0.0914	0.0914	0.0914	0.0914	0.0914	0.0914	0.0914	0.0914
ε x 10^{-6}	3239	3346	3502	3625	2104	3754	3466	3385	3531	3537	3676	3074
F_{model}	296	306	320	331	192	343	317	309	323	323	336	281
$F_{calibration}$	280	328	326	334	189	342	308	299	317	313	320	271
difference (%)	-5.71	6.71	1.84	0.9	-1.59	-0.29	-2.92	-3.34	-1.89	-3.19	-5	-3.69

Table F69: Residual preloads based on calibration line of A5 corrected based on average diameter

A5 mean												
Bolts	**A1**	**A2**	**A4**	**A6**	**A7**	**A8**	**B1**	**B2**	**B3**	**B4**	**B6**	**B7**
EAi	0.0924	0.0924	0.0924	0.0924	0.0924	0.0924	0.0924	0.0924	0.0924	0.0924	0.0924	0.0924
ε x 10^{-6}	3239	3346	3579	3625	2104	3754	3466	3385	3531	3537	3676	3074
F_{model}	299	309	331	335	194	347	320	313	326	327	340	284
$F_{calibration}$	280	328	337	334	189	342	308	299	317	313	320	271
difference (%)	-6.79	5.79	1.78	-0.3	-2.65	-1.46	-3.9	-4.68	-2.84	-4.47	-6.25	-4.8

Table F70: Residual preloads based on calibration line of A6 corrected based on average diameter

A6 mean												
Bolts	**A1**	**A2**	**A4**	**A5**	**A7**	**A8**	**B1**	**B2**	**B3**	**B4**	**B6**	**B7**
EAi	0.0917	0.0917	0.0917	0.0917	0.0917	0.0917	0.0917	0.0917	0.0917	0.0917	0.0917	0.0917
ε x 10^{-6}	3239	3346	3579	3502	2104	3754	3466	3385	3531	3537	3676	3074
F_{model}	297	307	328	321	193	344	318	310	324	324	337	282
$F_{calibration}$	280	328	337	326	189	342	308	299	317	313	320	271
difference (%)	-6.07	6.4	2.67	1.53	-2.12	-0.58	-3.25	-3.68	-2.21	-3.51	-5.31	-4.06

Table F71: Residual preloads based on calibration line of A7 corrected based on average diameter

A7 mean												
Bolts	**A1**	**A2**	**A4**	**A5**	**A6**	**A8**	**B1**	**B2**	**B3**	**B4**	**B6**	**B7**
EAi	0.0905	0.0905	0.0905	0.0905	0.0905	0.0905	0.0905	0.0905	0.0905	0.0905	0.0905	0.0905
ε x 10^{-6}	3239	3346	3579	3502	3625	3754	3466	3385	3531	3537	3676	3074
F_{model}	293	303	324	317	328	340	314	306	319	320	333	278
$F_{calibration}$	280	328	337	326	334	342	308	299	317	313	320	271
difference (%)	-4.64	7.62	3.86	2.76	1.8	0.58	-1.95	-2.34	-0.63	-2.24	-4.06	-2.58

Table F72: Residual preloads based on calibration line of A8 corrected based on average diameter

A8 mean												
Bolts	**A1**	**A2**	**A4**	**A5**	**A6**	**A7**	**B1**	**B2**	**B3**	**B4**	**B6**	**B7**
EAi	0.0912	0.0912	0.0912	0.0912	0.0912	0.0912	0.0912	0.0912	0.0912	0.0912	0.0912	0.0912
ε x 10^{-6}	3239	3346	3579	3502	3625	2104	3466	3385	3531	3537	3676	3074
F_{model}	295	305	326	319	331	192	316	309	322	323	335	280
$F_{calibration}$	280	328	337	326	334	189	308	299	317	313	320	271
difference (%)	-5.36	7.01	3.26	2.15	0.9	-1.59	-2.6	-3.34	-1.58	-3.19	-4.69	-3.32

Table F73: Residual preloads based on calibration line of B1 corrected based on average diameter

B1 mean												
Bolts	**A1**	**A2**	**A4**	**A5**	**A6**	**A7**	**A8**	**B2**	**B3**	**B4**	**B6**	**B7**
EAi	0.0901	0.0901	0.0901	0.0901	0.0901	0.0901	0.0901	0.0901	0.0901	0.0901	0.0901	0.0901
ε x 10^{-6}	3239	3346	3579	3502	3625	2104	3754	3385	3531	3537	3676	3074
F_{model}	292	302	323	316	327	190	338	305	318	319	331	277
$F_{calibration}$	280	328	337	326	334	189	342	299	317	313	320	271
difference (%)	-4.29	7.93	4.15	3.07	2.1	-0.53	1.17	-2.01	-0.32	-1.92	-3.44	-2.21

Table F74: Residual preloads based on calibration line of B2 corrected based on average diameter

B2 mean												
Bolts	**A1**	**A2**	**A4**	**A5**	**A6**	**A7**	**A8**	**B1**	**B3**	**B4**	**B6**	**B7**
EAi	0.0906	0.0906	0.0906	0.0906	0.0906	0.0906	0.0906	0.0906	0.0906	0.0906	0.0906	0.0906
ε x 10^{-6}	3239	3346	3579	3502	3625	2104	3754	3466	3531	3537	3676	3074
F_{model}	293	303	324	317	328	191	340	314	320	320	333	279
$F_{calibration}$	280	328	337	326	334	189	342	308	317	313	320	271
difference (%)	-4.64	7.62	3.86	2.76	1.8	-1.06	0.58	-1.95	-0.95	-2.24	-4.06	-2.95

Table F75: Residual preloads based on calibration line of B3 corrected based on average diameter

B3 mean												
Bolts	**A1**	**A2**	**A4**	**A5**	**A6**	**A7**	**A8**	**B1**	**B2**	**B4**	**B6**	**B7**
EAi	0.0904	0.0904	0.0904	0.0904	0.0904	0.0904	0.0904	0.0904	0.0904	0.0904	0.0904	0.0904
ε x 10^{-6}	3239	3346	3579	3502	3625	2104	3754	3466	3385	3537	3676	3074
F_{model}	293	303	324	317	328	190	339	313	306	320	332	278
$F_{calibration}$	280	328	337	326	334	189	342	308	299	313	320	271
difference (%)	-4.64	7.62	3.86	2.76	1.8	-0.53	0.88	-1.62	-2.34	-2.24	-3.75	-2.58

Table F76: Residual preloads based on calibration line of B4 corrected based on average diameter

B4 mean												
Bolts	**A1**	**A2**	**A4**	**A5**	**A6**	**A7**	**A8**	**B1**	**B2**	**B3**	**B6**	**B7**
EAi	0.0904	0.0904	0.0904	0.0904	0.0904	0.0904	0.0904	0.0904	0.0904	0.0904	0.0904	0.0904
ε x 10^{-6}	3239	3346	3579	3502	3625	2104	3754	3466	3385	3531	3676	3074
F_{model}	293	303	324	317	328	190	339	313	306	319	332	278
$F_{calibration}$	280	328	337	326	334	189	342	308	299	317	320	271
difference (%)	-4.64	7.62	3.86	2.76	1.8	-0.53	0.88	-1.62	-2.34	-0.63	-3.75	-2.58

Table F77: Residual preloads based on calibration line of B6 corrected based on average diameter

B6 mean												
Bolts	**A1**	**A2**	**A4**	**A5**	**A6**	**A7**	**A8**	**B1**	**B2**	**B3**	**B4**	**B7**
EAi	0.0892	0.0892	0.0892	0.0892	0.0892	0.0892	0.0892	0.0892	0.0892	0.0892	0.0892	0.0892
ε x 10^{-6}	3239	3346	3579	3502	3625	2104	3754	3466	3385	3531	3537	3074
F_{model}	289	298	319	312	323	188	335	309	302	315	315	274
$F_{calibration}$	280	328	337	326	334	189	342	308	299	317	313	271
difference (%)	-3.21	9.15	5.34	4.29	3.29	0.53	2.05	-0.32	-1	0.63	-0.64	-1.11

Table F78: Residual preloads based on calibration line of B7 corrected based on average diameter

B7 mean												
Bolts	**A1**	**A2**	**A4**	**A5**	**A6**	**A7**	**A8**	**B1**	**B2**	**B3**	**B4**	**B6**
EAi	0.0883	0.0883	0.0883	0.0883	0.0883	0.0883	0.0883	0.0883	0.0883	0.0883	0.0883	0.0883
ε x 10^{-6}	3239	3346	3579	3502	3625	2104	3754	3466	3385	3531	3537	3676
F_{model}	286	295	316	309	320	186	331	306	299	312	312	325
$F_{calibration}$	280	328	337	326	334	189	342	308	299	317	313	320
difference (%)	-2.14	10.06	6.23	5.21	4.19	1.59	3.22	0.65	0	1.58	0.32	-1.56

Table F79: Influence of corrections on the highest and lowest boundaries of the force

correction	$-6 \cdot 0.005 d_i$	$-5 \cdot 0.005 d_i$	$-4 \cdot 0.005 d_i$	$-3 \cdot 0.005 d_i$	$-1 \cdot 0.005 d_i$	$1 \cdot 0.005 d_i$	$3 \cdot 0.005 d_i$	$4 \cdot 0.005 d_i$
average error/underestimated force (%)	5.38	4.66	4.19	3.93	3.67	2.89	2.55	2.45
max error/underestimated force (%)	7.01	6.05	5.37	4.77	4.67	3.87	3.61	3.74
min error/underestimated force (%)	3.75	3.27	3.01	3.09	2.7	1.91	1.49	1.16
average error/overestimated force (%)	0.21	0.44	0.75	1.23	2.21	3.69	5.18	5.9
max error/overestimated force (%)	0.62	1.13	1.65	2.16	3.59	5.23	6.98	7.79
min error/overestimated force (%)	0.2	0.25	0.15	0.3	0.83	2.15	3.38	4.01